

# Lawrence Berkeley National Laboratory

## Recent Work

### **Title**

STATIC EQUILIBRIA OF THE INTERSTELLAR GAS IN THE PRESENCE OF MAGNETIC AND GRAVITATIONAL FIELDS

### **Permalink**

<https://escholarship.org/uc/item/3s71x11h>

### **Author**

Mouschovias, Telemachos Charalambous.

### **Publication Date**

1975

RECEIVED  
BERKELEY LABORATORY

LBL-3602

c.1

JUL 21 1975

LIBRARY AND  
DOCUMENTS SECTION

STATIC EQUILIBRIA OF THE INTERSTELLAR GAS IN THE  
PRESENCE OF MAGNETIC AND GRAVITATIONAL FIELDS

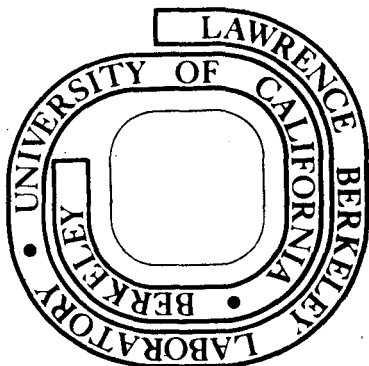
Telemachos Charalambous Mouschovias  
(Ph. D. thesis)

January 1975

Prepared for the U. S. Energy Research and  
Development Administration under Contract W-7405-ENG-48

**For Reference**

Not to be taken from this room



LBL-3602

c.1

## **DISCLAIMER**

This document was prepared as an account of work sponsored by the United States Government. While this document is believed to contain correct information, neither the United States Government nor any agency thereof, nor the Regents of the University of California, nor any of their employees, makes any warranty, express or implied, or assumes any legal responsibility for the accuracy, completeness, or usefulness of any information, apparatus, product, or process disclosed, or represents that its use would not infringe privately owned rights. Reference herein to any specific commercial product, process, or service by its trade name, trademark, manufacturer, or otherwise, does not necessarily constitute or imply its endorsement, recommendation, or favoring by the United States Government or any agency thereof, or the Regents of the University of California. The views and opinions of authors expressed herein do not necessarily state or reflect those of the United States Government or any agency thereof or the Regents of the University of California.

0 0 0 4 3 0 0 5 8

-ii-

LBL-3602

To Margarita and Charalambos

## FORWARD

This work concerns itself with some basic physical processes pertinent to the interstellar medium. Its assumptions are guided by observational evidence to the extent possible. If a simplifying assumption becomes necessary, it is adopted only if a more realistic one is not expected to alter the qualitative nature of our conclusions.

The internal structure and, in particular, the relative length of the sections of this dissertation is determined by three objectives.

First, the work must be sufficiently self-contained. This is mainly for the benefit of a student of physics beginning his research on large-scale interstellar phenomena involving the magnetic field. It accounts for the relatively lengthy but critical review of the literature in § I through IV and in § VI.

Second, all arguments presented must be related to the central theme (namely, the formation, equilibrium, and stability of interstellar clouds), which in turn bears on the process of star formation. It is hoped that this will render the manuscript a coherent exposition.

Finally, enough original results must be explained clearly to provide stimulation for the specialist (theorist and observer) for further study of the subject matter (§ V and § VII). A special effort is made to interpret physically all formalism, assumptions, and conclusions.

## TABLE OF CONTENTS

	<u>Page</u>
ABSTRACT	ix
I. INTRODUCTION	
A. Motivation.....	1
B. Background and Perspective.....	2
II. FORMATION AND EQUILIBRIUM OF NON-GRAVITATING INTERSTELLAR CLOUDS: SMALL-SCALE CONDENSATIONS.	
A. Thermal Instability	
1. A steady-state model.....	5
2. A time-dependent model.....	7
3. Criticism.....	8
B. A Statistical Model.....	10
III. EVIDENCE FOR THE INTERSTELLAR MAGNETIC FIELD	
A. Synchrotron Radiation.....	13
B. Polarization of Starlight.....	15
C. Faraday Rotation.....	16
D. The Zeeman Effect.....	20
IV. THEORETICAL DESCRIPTION OF LARGE-SCALE PHENOMENA IN THE INTER- STELLAR MEDIUM.	
A. The Dynamical Equations	
1. A system of thermal gas, magnetic fields, and gravitational fields.....	24
2. The system with cosmic rays included.....	26
3. Approximations of the energy equation.....	30
B. Implications of Flux-Freezing	
1. Two-dimensional geometry.....	31
2. Three-dimensional geometry with axial symmetry: a poloidal field.....	32

TABLE OF CONTENTS - contd.

	<u>Page</u>
V. FORMATION AND EQUILIBRIUM OF NON-GRAVITATING INTERSTELLAR CLOUDS: LARGE-SCALE CONDENSATIONS	
A. The Magnetic Rayleigh-Taylor (or, Magnetogravitational) Instability	
1. The basic physics of the instability.....	34
2. Retrospect.....	38
B. Final States for the Magnetogravitational Instability	
1. Do final states really exist?.....	40
2. Some features of the final states.....	42
a. Scale height	
i. Gas .....	43
ii. Magnetic field.....	44
b. Gas density.....	45
c. The ratio ( $\alpha$ ) of the magnetic pressure to the gas pressure.....	47
3. Dependence on the assumed initial state.....	48
4. Comparison with observations.....	49
5. Refinements.....	51
a. A gravitational field varying with altitude....	51
b. Alpha larger than unity.....	53
c. A non-isothermal equation of state.....	55
d. The effect of cosmic rays	
i. Modification of the instability criterion...	57
ii. Formulation of an equilibrium problem.....	58
e. A non-equilibrium initial state.....	67

## TABLE OF CONTENTS - contd.

	<u>Page</u>
VI. SELF-GRAVITATING INTERSTELLAR CLOUDS	
A. Non-Magnetic Clouds: A Summary.....	74
B. Flux-Freezing in Dense Clouds.....	78
C. Magnetic Clouds: Background	
1. The Problem of Angular Momentum and Magnetic Braking.....	80
2. Non-Equilibrium Calculations	
a. Mestel's Spherical Model.....	84
b. Strittmatter's Spheroidal Model.....	86
c. A Comment on the Virial Theorem.....	88
3. Equilibrium Calculations.....	89
a. A Thin Disk with a Magnetic Field Parallel to its Axis.....	90
b. An Infinite Cylinder Aligned with the Magnetic Field.....	91
c. An Axisymmetric Model Without Flux- Freezing.....	93
VII. NONHOMOLOGOUS CONTRACTION AND EQUILIBRIA OF SELF-GRAVITATING INTERSTELLAR CLOUDS EMBEDDED IN AN INTERCLOUD MEDIUM: FLUX-FREEZING	
A. Formulation of the Problem	
1. The Equilibrium Equations.....	97
2. Calculation of the Functions $q_k(\phi)$ , $k = 1, 2$ .	100
3. Approximate Description of the Intercloud Medium.....	101
4. Continuity Conditions Across the Cloud Boundary	
a. Gravitational Field.....	102
b. Gas Pressure.....	104
c. Magnetic Field.....	104
d. The Function $q(\phi)$ .....	105



TABLE OF CONTENTS - contd.

	<u>Page</u>
5. Boundary Conditions.....	106
B. A Reference (Non-Equilibrium) State.....	108
C. The Dimensionless Problem.....	110
1. The Basic Equations.....	111
2. Boundary Conditions.....	112
3. The Reference State.....	112
4. Free Parameters.....	113
D. Method of Solution.....	114
E. Equilibrium States	
1. A Preview of the Results.....	116
2. Dependence on $R_1$ .....	119
3. Dependence on $P_0$ .....	123
4. Dependence on $\alpha_1$ .....	126
F. Discussion of Results and Comparison with Observations.....	128
1. Some General Conclusions.....	129
a. The Slope of $\log B_c$ versus $\log \rho_c$ .....	129
b. Correlation between the External Pressure and the Central Density.....	133
c. The Ratio $\rho_c/\rho_S$ .....	135
d. Critical States.....	137
2. Returning to the World of Dimensional Quantities.	138
3. Line Widths in Dense Clouds.....	144
4. Why is Star Formation Inefficient?.....	149
VIII. EQUILIBRIUM CALCULATIONS AND STAR FORMATION.....	151
ACKNOWLEDGEMENTS.....	153

## TABLE OF CONTENTS - contd.

	<u>Page</u>
TABLE.....	154
REFERENCES.....	155
LEGENDS FOR FIGURES.....	163
FIGURES.....	167
APPENDIX A: METHOD OF SOLUTION.....	197
APPENDIX B: PAPER I (reprint).....	204

Static Equilibria of the Interstellar Gas  
in the Presence of Magnetic and Gravitational Fields

by

Telemachos Charalambous Mouschovias

ABSTRACT

No exact self-consistent equilibrium calculations exist for (any model of) the system of the interstellar gas and the frozen-in magnetic field. On a large scale ( $\sim 1$  kpc) this system is affected by the vertical galactic gravitational field, while on a small scale ( $\sim 1$  pc) the self-gravitation of the gas comes into play and is responsible for the collapse of some clouds to form stars. We determine accessible equilibrium states for the gas-field system on both of these scales. In each case our main conclusions are summarized as follows.

(i) Final equilibrium states of the gas-field system in the galactic gravitational field can be reached after a magnetic Rayleigh-Taylor instability develops. We show that the tension of the field lines will eventually stop their inflation. Even though we solve a time-independent problem, we connect a final state with the stratified initial equilibrium state by conserving the mass-to-flux ratio in each flux tube of the system. A transition in time can therefore be made between them through continuous deformations of the field lines.

Final states are lower in total energy than corresponding initial states. Their properties depend quantitatively on the

horizontal (but not so much on the vertical) wavelength of the initial perturbation. A striking feature of the final states is that the scale height of the gas increases (decreases) where the gas density increases (decreases). The characteristics of our final states are in agreement with observations in both our Galaxy and in M 81.

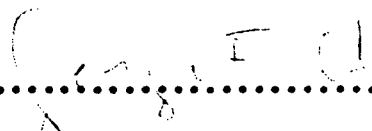
(ii) We determine equilibrium states for massive interstellar clouds, whose electrical conductivity is extremely high. Self-gravity and the pressure of the hot and tenuous intercloud medium bind them, in general, against the disruptive effects of their internal pressure and magnetic stresses. The surface of a cloud is a free boundary determined by the requirement that there exist pressure balance across it. We find that a cloud becomes oblate with its major axis normal to the field lines. For a fixed mass (external pressure) the flattening increases as either the magnetic field or the external pressure (mass) increases. For a given magnetic flux threading the cloud and a given mass (external pressure), no equilibrium solutions exist if the external pressure (mass) exceeds some critical value. For example, for a background field of 3.54 microgauss and an intercloud pressure of  $1800 \text{ k deg/cm}^3$ , an H I cloud of temperature equal to  $50^\circ \text{K}$  will collapse if its mass exceeds about 1320 solar masses. In this critical state, the surface density through the center of the cloud is in the range  $10.6 \times 10^{-3} - 23.5 \times 10^{-3} \text{ grams/cm}^2$  depending on the orientation of the line of sight.

We determine the exponent  $\kappa$  in the relation  $B_c \propto \rho_c^\kappa$  between the magnetic field and the gas density at the cloud cen-

ter. It depends on the ratio of the magnetic and gas pressures in the cloud. It is certainly smaller than  $2/3$  (isotropic contraction) and it decreases further the stronger the magnetic field. It is likely to be less than  $1/2$  for much of the life time of a cloud.

An alternative mechanism capable of explaining large line widths in molecular clouds consists of oscillations of a (magnetic) cloud as a whole about equilibrium states such as the ones which we have calculated.

We also discuss problems related to the formation of interstellar clouds as well as star formation. Most significantly, we suggest that the observed inefficiency of the star formation process cannot be attributed to the birth of an O 7, or an earlier type star within a collapsing cloud, but can naturally be explained by magnetic effects in a contracting and, therefore, nonuniform cloud.

  
.....  
(Signature)

Professor George B. Field  
Dissertation Chairman

## I. INTRODUCTION

### A. Motivation

Undisputed observational evidence indicates a strong correlation in space between young stars and relatively dense concentrations of interstellar matter (Baade 1944). This led to the hypothesis that stars are in fact born out of the surrounding matter. Since young stars are also seen to form predominantly in groups, it follows that they form either out of a single, massive condensation of interstellar matter that fragments while collapsing, or out of small-scale, low-mass structures within a large-scale condensation that undergo collapse almost simultaneously. The two processes need not be mutually exclusive, especially since observations show a hot and tenuous interstellar medium in which there exist both cold "clouds" ranging in mass from several to a few thousand solar masses, as well as "cloud complexes" whose mass, combined with the mass of the embedded young stars, may be as large as  $10^6 M_{\odot}$ . Thus, if an interstellar cloud is presumed to be the entity that gives birth to stars, a theory of star formation must ultimately answer the following questions:

- i) How do individual interstellar clouds (with such a wide range of masses) and cloud complexes form?
- ii) Given a set of physical parameters sufficient to describe an interstellar cloud and its environment, what are the equilibrium states, if any, accessible to the cloud?
- iii) Under what conditions does an interstellar cloud evolve away from (or avoid altogether) its accessible equilibrium state(s), and can these conditions be met in the interstellar medium?

Although this is not a complete set of questions whose answers a theory

of star formation must provide, it is nevertheless a fundamental set insofar as it aims at an understanding of the basic mechanical forces that govern the behavior of the interstellar medium as it relates to star formation.

The interstellar medium is a complex system far from thermodynamic equilibrium. In it thermal, turbulent and ordered motions, radiation, cosmic rays, magnetic and gravitational fields store energies in comparable densities, thus rendering a detailed dynamical description a formidable task. The apparent complexities of the physical system necessitate idealizations in any theoretical description. Seemingly important features of the interstellar medium are isolated, abstracted and used as assumptions in mathematical models, whose predictions are then compared with observations. Discrepancies between predictions and observations lead to improvements of the original assumptions and, consequently, to a more accurate representation of the physical system. Models for the interstellar medium have gone through many such iterations. Yet, the above three fundamental questions concerning the formation, equilibrium, and stability of interstellar clouds and, ultimately, the process of star formation remain unanswered.

#### B. Background and Perspective

This paper undertakes to decipher the nonlinear interaction among gravitational, pressure, and magnetic forces under typical interstellar conditions. The gravitational instability of a uniform (non-equilibrium) gas was studied early in the twentieth century (Jeans 1928). The investigation of the equilibrium of an isothermal sphere, bounded by a constant external pressure and supported by internal pressure gradients against self-gravitation, provided us with much quantitative information such as the largest ("critical") mass that may still exist in equilibrium

at a given internal temperature and a fixed external pressure (Ebert 1955, 1957; Bonnor 1956; McCrea 1957). Studies of the equilibrium in a direction parallel to the axis of symmetry of a gaseous, self-gravitating disk (Spitzer 1942; Ledoux 1951) were extended to include the effect of rotation and the growth of perturbations in the plane of the disk (Fricke 1954; Safranov 1960a, 1960b; Goldreich and Lynden-Bell 1965). But it was only recently that theorists paid due attention to the interstellar magnetic field, which for many years had been considered as an undesirable impediment to the processes of cloud collapse and star formation. At about the same time that E. N. Parker (1966) was demonstrating that the interstellar gas, which is partially supported by magnetic and cosmic-ray pressures against the galactic gravitational field, could be subject to a magnetic Rayleigh-Taylor instability that tends to accumulate the gas into clumps, Mestel (1966) and Strittmatter (1966) were obtaining criteria for the collapse of a cold, self-gravitating, magnetic cloud in a direction perpendicular to the field. Thus, the role of the magnetic field in the formation, equilibrium and stability of interstellar clouds was brought to the foreground. The determination of equilibrium states for the highly conducting interstellar gas has been restricted to models mathematically tractable (Lerche 1967; E. N. Parker 1968a; D. A. Parker 1973), rather than models preserving the essential features of the interstellar medium not the least consequential of which is a magnetic field "frozen-in" the matter.

In pursuit of an understanding of the interplay among gravitational, pressure and magnetic forces that may produce observable entities such as clouds and stars, we proceed on two fronts. First, we study these forces on a large scale. E. N. Parker's suggestion, that interstellar clouds may be nothing more than clumps of gas held in magnetic field



"valleys" by the vertical gravitational field of the Galaxy, is a reasonable possibility especially since (i) self-gravitation for most interstellar clouds is several orders of magnitude weaker than that required for binding, and (ii) observations show an intimate association between the interstellar gas and field. We, therefore, seek final equilibrium states for the gas-field-gravity system that Parker (1966) showed to be unstable. Our choice is between a brute-force numerical solution of the magnetohydrodynamic (MHD) equations and an elegant reduction and solution of the magnetohydrostatic (MHS) equations. We follow the latter path. It rewards us with an insight into the basic physics of the problem. The challenge is to incorporate the assumption of flux-freezing in a time-independent problem; and then to solve the resulting equation(s) and compare the results with observations [see Mouschovias 1973, 1974 (Paper I); reprint attached]. Here, we shall extend the formalism of Paper I to include the cosmic-ray gas. Contrary to previous expectations (Parker 1968b), the cosmic rays may not inflate the field lines forever, that is, an equilibrium state of the gas-field-gravity system may still be possible in the presence of cosmic rays. Second, we study the same forces on a (relatively) small scale--that of an individual interstellar cloud, held in a delicate balance by its internal pressure and a frozen-in field against self-gravitation and an external pressure, exerted by a hot and tenuous intercloud medium; the magnetic field threads both media, which are highly conducting. Presumably, such a cloud would give birth to stars upon collapse and fragmentation. We, therefore, obtain equilibrium states for a wide range of pertinent physical parameters and we determine "critical" values for them. Our endeavors on these fronts carry us a significant step forward in our quest for answers to the aforementioned three fundamental questions. In both, our large-scale and small-scale studies, we discuss possible refinements of our work.

## II. FORMATION AND EQUILIBRIUM OF NON-GRAVITATING INTERSTELLAR CLOUDS: SMALL-SCALE CONDENSATIONS

### A. Thermal Instability

#### 1. A Steady-State Model

Spitzer's (1951) suggestion that the cold and dense interstellar clouds are in pressure equilibrium with a hot and tenuous intercloud medium gained new impetus because of important theoretical and observational developments. On theoretical grounds, Hayakawa, Nishimura and Takayanagi (1961) concluded that, if a sufficient flux of low-energy (1 - 100 Mev) cosmic rays is present, it can ionize and heat (by the produced secondary electrons) the interstellar clouds up to the observed temperatures. Field (1962) showed that a low-density, neutral intercloud medium can be maintained at a high temperature ( $\sim 10^4$  °K) by cosmic-ray heating, thus providing the pressure necessary for confining the interstellar clouds. On the other hand, Heiles (1968) found evidence for an intercloud medium with a density of  $0.2 \text{ cm}^{-3}$  and a velocity dispersion of 6 km/sec (implying an upper limit on its temperature of several thousand degrees). Subsequent work by Pikel'ner (1967), Field, Goldsmith, and Habing (1969), and Spitzer and Scott (1969) established that two thermally stable, nearly isothermal phases can exist in pressure equilibrium in the interstellar medium: a hot, tenuous intercloud medium ( $n \sim 0.2 \text{ cm}^{-3}$ ,  $T \sim 10^4$  °K) and cool, dense clouds ( $n \sim 10^2 \text{ cm}^{-3}$ ,  $T \sim 20$  °K). What is crucial to the theoretical establishment of the possibility of the existence of two stable phases is a heating mechanism directly proportional to the gas density [for example, low-energy cosmic rays; soft X-rays (Bergeron and Souffrin 1971; Habing and Goldsmith 1971)] and a cooling mechanism proportional to the second power of the gas density (for example, collisional excitation followed by radiative de-excitation in spectral lines at which the medium

is optically thin).

In this steady-state, two-phase picture of the interstellar medium, matter "condenses" from the intercloud to the cloud phase if the density of the nearly isothermal intercloud gas increases beyond some critical value, thus causing a rise in pressure that cannot be maintained. The critical point marks the onset of a thermal instability (Field 1965) that proceeds almost isobarically and effects the transition from the tenuous to the dense phase. This transition (assumed to take place at a fixed degree of ionization) relieves the excess pressure so that the ambient pressure is maintained at the critical value (Field et al. 1969). If the actual pressure of the intercloud medium is below the calculated value, all interstellar matter must exist in the rarefied phase according to this model. Since 21-cm observations have established the existence of cold, dense clouds (for example, Clark 1965; Hughes, Thompson, and Colvin 1971; Radhakrishnan et al. 1971) one must postulate that the intercloud pressure is at the critical point. Under this postulate and the assumption of hydrostatic equilibrium in the vertical gravitational field of the Galaxy, Field et al. (1969) estimate that 75 percent of the gas must be in the dense phase.

As a "phase transition" occurs it is possible for electrons to recombine onto hydrogen ions. Schatzman (1958) had studied an instability resulting from a reduction in pressure that accompanies the recombination process. Goldsmith (1970) and Defouw (1970), working independently, extended Field's thermal-instability criterion to account for a varying degree of ionization. Goldsmith followed the instability numerically (in one space dimension) and observed the details of the transition from the tenuous to the dense phase of this model of the interstellar medium.

Once again there exists a critical value of the gas density. Beyond this density, efficient radiative recombination of electrons onto protons causes a rapid decline in the equilibrium temperature. Cosmic-ray heating cannot keep pace with the rapid losses, and the pressure drops below its ambient value while the density continues to increase. Although the new degree of freedom, that is, recombination, has altered the details of the process, the net result is a transition from the tenuous to the dense phase, as before.

## 2. A Time-Dependent Model

A thermal instability may also develop in a cooling (rather than a nearly isothermal) medium regardless of the particular value of the ambient pressure. The criterion for this instability was derived by Field (1965). If the interstellar medium is heated by sporadic supernova bursts, its subsequent cooling may be conducive to the formation of condensations. This idea is the basis of what is known as the time-dependent model of the interstellar medium (McCray and Schwarz 1971). Schwarz, McCray, and Stein (1972) worked out the details and pointed out the differences of this model from the steady-state one. They emphasize that, because the instability criterion depends on physical parameters (for example, cooling rate) which are functions of time in this case, the possibility arises that an initially growing perturbation may be damped at a later time, and vice versa. This is confirmed by their numerical calculations, in which they follow the time development of the instability in one space dimension. Mansfield (1973) followed the instability in a spherical geometry as well, having included heating due to ultraviolet photo-emission of electrons from grains (Watson 1972). He also studied in a crude fashion the effect of a uniform magnetic field on the condensation

process. He found what Field (1965) and Goldsmith (1970) had already concluded, that is, even a moderate magnetic field ( $\approx 1 \mu\text{gauss}$ ) renders the thermal instability ineffective in all but one direction (parallel to the field).

### 3. Criticism

The truth or falsity of their assumptions aside, and other agreement or disagreement with observations notwithstanding, under the most favorable of conditions both the steady-state and the time-dependent models of the interstellar medium produce condensations with sizes ( $\sim 0.01 \text{ pc}$  to  $\sim 0.1 \text{ pc}$ )<sup>1</sup> two to four orders of magnitude smaller than the sizes of most of the observed interstellar clouds. Moreover, the predicted "cloud" masses fall short of the observed ones by at least as many orders of magnitude. Why condensations predicted by these models continue to be referred to as "typical" interstellar clouds (for example, Mansfield 1973) remains a puzzle to this author.

A serious difficulty with the time-dependent model within its own assumptions was pointed out by Goldsmith (1972): if each region of the interstellar medium is indeed heated by a supernova explosion once every  $10^6$  years, within this time interval, density contrasts of less than four are produced because the longer wavelengths of a perturbation cool nearly isochorically. This is a direct consequence of the short cooling times typical of the interstellar medium (see below).

In spite of their differences the two models are similar in that they employ a thermal instability for the formation of cool, dense sheets of

---

1. Field (1970) recognized this difficulty: "If clouds actually form by thermal instability, it appears that small ones are initially favored".

gas in an otherwise uniform interstellar medium. This is the reason for which they cannot account for interstellar clouds such as the observed ones. Although perturbations with a broad range of wavelengths may grow at almost the maximum growth rate, these wavelengths have an upper bound determined by the fact (consistent with the force equation) that the "condensation mode" (Field 1965) evolves almost isobarically. This means that the upper bound on the fastest-growing wavelengths of a perturbation is approximately that distance within which a sound wave can establish pressure equilibrium in a time not exceeding the cooling time of the medium. Typical cooling times for the intercloud medium are less than  $10^6$  years and become shorter as the gas density increases (Spitzer 1968a; Jura and Dalgarno 1972). Therefore, with a sound speed smaller than  $10 \text{ km sec}^{-1}$ , the wavelengths that can grow at a rate near maximum will be less than 10 pc. Since the density of the intercloud gas is approximately  $0.2 \text{ atoms cm}^{-3}$ , the resulting condensation must have a size of about 0.01 pc if it is to reproduce the observed cloud densities ( $\geq 30 \text{ atoms cm}^{-3}$ ) by one-dimensional compression along the magnetic field.

Aiming at obtaining larger condensations, Goldsmith (1970) considered the growth of perturbations with wavelengths considerably larger than the fastest-growing ones. He chose  $\lambda = 300 \text{ pc}$  (corresponding to an e-folding time of about  $10^7$  years); but even so, the final condensation had an extent of only 0.13 pc (at  $T \sim 20 \text{ }^\circ\text{k}$ ) - still a dwarf cloud. At any rate, as we have already mentioned, shorter wavelengths that correspond to growth rates near the maximum one are favored by the instability. In addition, the thermal instability for a perturbation with a large enough wavelength to involve a sufficiently large mass will evolve more slowly than the magnetic Rayleigh-Taylor instability (see below), in which the magnetic field is instrumental (rather than a nuisance) in the formation of large

condensations.

Schwarz et al. (1972) raised the point that inertial effects will maintain the flow and, therefore, a condensation will continue to grow for a long time after the instability shuts off. Valid as this point may be, it nevertheless is the case that the final size of a condensation does not usually exceed 1/2 of the wavelength of the perturbation that initiated the instability. Since the observed dimensions of clouds (for example, Heiles and Jenkins 1973, Heiles 1973) are often larger than the wavelengths which can grow with an e-folding time less than  $10^7$  years, and since  $n \gtrsim 30 \text{ cm}^{-3}$ , the thermal instability will not account for the formation of these condensations even if inertial effects are included.

#### B. A Statistical Model

The complexity of the interstellar medium and the apparent randomness in the motion of clouds and in their distribution in space led Oort (1954) to suggest that a theoretical description of the interstellar medium must be statistical in nature. Once some low-mass clouds form, it is postulated that they collide inelastically and coalesce to form larger clouds. The process continues until a critical mass, corresponding to gravitational instability, is reached. The collapsing cloud presumably fragments and forms stars, the brightest of which ionize the remaining gas, thus generating conditions assumed to be appropriate for the formation of second-generation, low-mass clouds. Field and Saslaw (1965) formulated these statistical ideas into a mathematical model. They made the following assumptions. (i) Only small clouds of the same ("unit") mass are created. (ii) All clouds have the same cross section and the same speed and are isotropically distributed in velocity. (iii) All collisions between clouds are inelastic, so that agglomeration is the

inevitable outcome.

Despite the simplicity of its assumptions, the statistical model predicts a mass spectrum for clouds ( $m^{-3/2}$ ) in rough agreement with observations. Because it invokes a binary collision process ultimately leading to star formation, the model provides a theoretical basis for Schmidt's (1959) empirical law, which states that the rate of depletion of gas because of star formation varies approximately as the second power of the gas density. [For an alternative theoretical foundation of a similar dependence of star formation on the gas density, see Mouschovias, Shu, and Woodward (1974), Paper II.] Another statistical calculation by Penston et al. (1969) predicts a maxwellian velocity distribution for clouds and a mean speed varying as  $m^{-1/2}$ . For the purpose of this discussion, the important point is that the statistical model does account for a wide range of cloud masses provided, however, that upon its formation a "unit" cloud has mass of the order of  $10 M_{\odot}$ . This implies that a thermal instability cannot be responsible for its formation in the presence of the interstellar magnetic field ( $\approx 3 \mu\text{gauss}$ ) because the instability can develop only along field lines -- see § IIA2 above.

Heiles (1973) questions the very foundations of the statistical model. He points to observational evidence that cloud velocities "are highly organized with respect to the [interstellar] magnetic field," and that "one gains the impression that the gas is moving along the magnetic field." He also questions, on observational grounds, the random distribution of clouds in space assumed by the statistical model. Clouds are often found in cloud complexes [see, for instance, Raimond (1966); Kerr (1968) and references therein], and long filamentary structures aligned with the magnetic field are prominent features of the interstellar medium. It may



be, however, that the cloud model is valid within the cloud complexes themselves (van Woerden 1967), although Heiles doubts even that.

Overwhelming observational evidence demonstrates not only that interstellar magnetic fields exist, but also suggests that magnetic forces are comparable to gravitational and pressure forces. Hence, it should not be surprising that models ignoring magnetic effects run into difficulties sooner or later. Before we discuss the role of the magnetic field in the formation, equilibrium, and stability of interstellar clouds, we turn to a critical review of the evidence for its existence.

### III. EVIDENCE FOR THE INTERSTELLAR MAGNETIC FIELD

With very few exceptions, our knowledge of astrophysical objects and processes stems from analyses of radiation received at the earth. The interstellar magnetic field does not belong to the exceptions. It may be instrumental in the production of radiation, or it may modify radiation propagating through the region where the field exists.

#### A. Synchrotron Radiation

Synchrotron radiation is produced by highly relativistic electrons gyrating in a magnetic field. It is highly directional about the instantaneous electron velocity, so that the line of sight must lie in the plane of the electron's orbit if the radiation is to be observed at all. The radiation from an ensemble of electrons can be recognized by its power-law spectrum and by its high degree of linear polarization, with the electric field normal to the plane defined by the magnetic field and the line of sight (Ginzburg and Syrovatskii 1965; also, Bless 1968). On these grounds and on independent evidence for the existence of cosmic-ray electrons with energies around 1 GeV (see review by Meyer 1969), the synchrotron mechanism accounts for a major fraction of the background radio continuum emission in our galaxy (for example, Spitzer 1968a and references therein; compilation of observations from 10 MHz to 400 MHz by Daniel and Stephens 1970).

Observations of synchrotron radiation establish the existence of an interstellar magnetic field. But to deduce the magnitude of the field, one needs to introduce a number of dubious assumptions, the most common of which is equipartition between the energies stored in magnetic fields and in cosmic-ray protons. [At a given energy per particle, the number of cosmic-ray electrons is only about 2% that of the protons (Earl 1961;

Meyer and Vogt 1961).] Additional uncertainties enter in estimating the size of the emitting region. For instance, the extent of the emitting region at high Galactic latitude is still controversial, with some authors claiming that the background radio continuum is produced in a disk of 2 kpc thickness, and others preferring a radio "halo" having a diameter of 20 kpc or so (see discussion by Woltjer 1965). Others yet speak of a thin-disk and a fat-disk component of the nonthermal radiation (Mathewson, van der Kruit, and Brouw 1972). Even if the size of the emitting region is known, however, additional assumptions concerning its internal structure are necessary in order to estimate the strength of the magnetic field. [The measured intensity of the radiation at some frequency is proportional to the line integral (along the line of sight) of the product of the number density of relativistic electrons and some power of the perpendicular (to the line of sight) component of the magnetic field - this exponent is usually around 1.8.]

Under the specter of the above uncertainties, large-scale magnetic fields ranging from 10  $\mu$ gauss to 50  $\mu$ gauss are deduced (Woltjer 1965; Davis and Berge 1968). Daniel and Stephens (1970) used the fluxes of cosmic-ray electrons and synchrotron radiation observed at the earth to deduce an energy spectrum for electrons with energies  $\lesssim$  5 GeV (because the observed one has been modulated by the solar wind) and to show that this spectrum joins smoothly with the observed spectrum above 5 GeV (which does not suffer solar modulation) only if the magnetic field is in the range 6 - 9  $\mu$ gauss. They assumed, however, that the region of emission was homogeneous. Their method will give larger fields if the size of the region of emission is reduced. There is evidence for enhancement of the synchrotron emission associated with spiral arms (for example, see Price 1974 and references therein). On the other hand, since regions of strong

fields are overweighted if the cosmic-ray density is nearly uniform, the background interstellar field may actually be weaker than the one deduced by Daniel and Stephens. Weaker fields are supported by observations of Faraday rotation (see below).

B. Polarization of Starlight

The polarization of light from distant stars (Hall 1949; Hiltner 1949) and its correlation with interstellar reddening led to the generally accepted hypothesis that it is produced by elongated dust grains aligned dynamically due to the presence of a magnetic field (Davis and Greenstein 1951; Davis 1958; Miller 1962). The grains are presumed to be paramagnetic and to have a complex index of refraction. Jones and Spitzer (1967) used statistical ideas to arrive at the same conclusions. We reproduce the essence of their arguments here.

In the absence of a magnetic field a prolate grain in kinetic equilibrium with the surrounding gas will have equal rotational kinetic energies about each of its principal axes. Since the angular momentum about each principal axis is proportional to the square root of the moment of inertia about that axis, a grain will tend to rotate mainly about an axis perpendicular to the axis of symmetry. In the presence of a magnetic field, the axis of rotation will tend to align with the direction of the field; otherwise dissipation of angular momentum due to magnetic torques will ensue. Thus, the axis of symmetry (major axis) of the prolate grains will tend to be perpendicular to the magnetic field. It is essential in these considerations that the grain temperature be less than the gas temperature, so that the system will not be in thermodynamic equilibrium, that would destroy the alignment through collisions with gas atoms. The magnetic field needed to sufficiently orient the grains is of the order of 10  $\mu$ gauss

although a weaker field (1  $\mu$ gauss) would do if the grains were ferromagnetic (Jones and Spitzer 1967).

As starlight propagates through interstellar space, the component of the electric field which is perpendicular to the major axis of the grains (and, therefore, more or less parallel to the magnetic field) is less efficiently absorbed by these particles. Consequently, a map of the observed polarization vectors will also reveal the topology of the interstellar magnetic field. In order to obtain the magnitude of the field from extinction and polarization measurements, one must know the gas temperature and density and, in addition, such uncertain quantities as the shape, composition and temperature of the grains. Although our understanding of the nature and evolution of interstellar grains is increasing rapidly (see review by Aannestad and Purcell 1973), it is wise to settle for obtaining the general topology, rather than the magnitude of the field by this method. We consider it very revealing that the field lines, as unveiled by polarization measurements, exhibit an orderly large-scale behavior, but have "waves" or "arches" over distances of a few hundred parsecs (Mathewson and Ford 1970; Davis and Berge 1968). Serkowski (1973), however, observed a field fluctuation over a scale of 0.3 pc in the direction of the star cluster Stock 2. On the other hand, reports of fields with magnitude as large as 1 mgauss (Beichman and Chaisson 1974) should be regarded as tentative until confirmed or refuted by some other method of measurement — especially since they depend on scaling laws relating the magnetic field and the gas density which our work shows to be incorrect (see § VB2c).

### C. Faraday Rotation

It is well known that a tenuous plasma becomes optically active (or,

birefringent) in the presence of a magnetic field. Faraday rotation refers to the rotation of the plane of polarization of a linearly-polarized electromagnetic wave, or to the rotation of the major axis of an elliptically-polarized wave passing through such a medium. The angle of rotation over a distance  $L$  is given by (Spitzer 1968a, p. 51)

$$\Delta\theta = R_m \lambda^2 \equiv (0.81 \int_0^L ds n_e B \cos\phi) \lambda^2 \text{ rad}, \quad (1)$$

where the wavelength ( $\lambda$ ) is measured in meters, the electron density ( $n_e$ ) in  $\text{cm}^{-3}$ , the magnetic field ( $B$ ) in  $\mu\text{gauss}$ , and the distance along the line of sight ( $s$ ) in parsecs. The angle between  $\vec{B}$  and the propagation vector,  $\vec{k}$ , is denoted by  $\phi$ . The sign convention is such that  $\Delta\theta$  is positive for right-hand rotation along the direction of propagation. The rotation measure is denoted by  $R_m$ .

Since typical rotation measures for the interstellar medium fall in the range  $1 - 100 \text{ rad m}^{-2}$ , it is clear that Faraday rotation is negligible for optical wavelengths. In principle one can use optical polarization to establish a standard and then measure  $\Delta\theta$  for radio waves. Unfortunately, not many radio sources emit in the optical portion of the electromagnetic spectrum. To obtain  $R_m$  (see discussion by Davis and Berge 1968) one is forced to measure  $\Delta\theta$  for a least two radio wavelengths. However, because of the indistinguishability of rotation angles differing by  $\pi$ , and because the position angle of the plane of polarization at the source is not usually known, one must measure  $\Delta\theta$  at several wavelengths, plotting the observed position angles as a function of  $\lambda^2$  and fitting a straight line through the points. In principle, several points differing by multiples of  $\pi$  must be plotted for each observation, and that set must be selected which fits a straight line best. The slope of the line gives  $R_m$ , and its extrapolation to  $\lambda^2 = 0$  gives the position angle at the source.

Once the rotation measure is known, one may obtain the mean value of the magnetic field along the line of sight to the observed radio source only if the distance to the source and the interstellar electron density are known. To obtain the latter would have been very difficult without the discovery of pulsars. Regular signals from pulsars reaching the earth exhibit a dispersion effect (that is, a difference in the arrival time of the left-handed and right-handed circularly polarized modes) that can be precisely measured. This is given by

$$\Delta t = \left( \frac{e^2}{2 \pi m_e c^3} \int_0^L ds n_e \right) \lambda^2, \quad (2)$$

where all units are in cgs. The dispersion measure,  $D_m \equiv \int_0^L ds n_e$ , is obtained from a single measurement and it constitutes a direct measure of the column density of electrons along the line of sight. If  $R_m$  and  $D_m$  are measured for the same source, one can obtain the mean value of the magnetic field along the line of sight,  $\langle B_{\parallel} \rangle$ . This is weighted by the electron density in the region between the source and the observer. (The contribution of the earth's ionosphere is taken into consideration.) Also, reversals in the direction of the magnetic field would produce cancellations in  $\Delta\theta$ , so that the measured  $\langle B_{\parallel} \rangle$  would be smaller than the general interstellar field. Such irregularities in the field may be detected, however, if measurements of starlight polarization and Faraday rotation are combined, since the two methods measure two mutually orthogonal components of the magnetic field.

Faraday rotation measures have also been obtained and analyzed for many extragalactic radio sources (Morris and Berge 1964; Gardner and Davies 1966; Gardner, Morris, and Whiteoak 1969; Wright 1973). These observations yield  $\langle n_e B_{\parallel} \rangle$  rather than  $\langle B_{\parallel} \rangle$  itself, since an independent determination of  $\langle n_e \rangle$  is not usually made. But the product

$\langle n_e B_{\parallel} \rangle$  is very useful especially since extragalactic radio sources are distributed all over the celestial sphere.

Wright (1973) recently analyzed the rotation measures from 354 extragalactic radio sources, and Manchester (1974) did the same for 38 pulsars. Their results are in good agreement, indicating a large-scale magnetic field directed toward  $l \approx 90^\circ$  (both above and below the Galactic plane). The direction of the field is in fair agreement with that determined by Appenzeller (1968) from interstellar polarization observations for stars near the south Galactic pole. He found that the mean direction of the polarization vectors was  $l \approx 80^\circ$ . According to these workers, the local helical field, which was suggested in order to explain the starlight polarization data (Hornby 1966; Mathewson 1968; Mathewson and Nicholls 1968; Mathewson 1969), is in conflict with the Faraday rotation observations. This resolves a long-standing theoretical dilemma: a nonvanishing magnetic field in the Galactic plane, having opposite directions above and below, implies that there exists a current sheet in the plane.

The magnitude of the field determined from Faraday rotation measurements lies in the range 1 - 3  $\mu$ gauss. Superposed on the general background field, both Wright and Manchester find field "irregularities" with field strength comparable to that of the background field. The typical scale of the "irregularities" appears to be a few hundred parsecs. This is significant when combined with the interpretation of data on rotation measures of extragalactic radio sources given by Gardner, Whiteoak, and Morris (1967). They found it necessary to assume that magnetic field lines protruded from spiral arms at least at some regions. However, they suggested that gas flow was responsible for pulling the field lines away from the Galactic plane. In Paper I we attributed the arches in the



field lines observed in the solar neighborhood to the development of the magnetic Rayleigh-Taylor instability, and we argued that field lines are inflated only because gas is drained from their raised portions.

#### D. The Zeeman Effect

The splitting of the 21-cm line into three components in the presence of a weak (on laboratory standards) magnetic field raises the possibility of studying the interstellar magnetic field in the most direct manner. The frequency separation between the two shifted, or  $\sigma$ , components of the line depends only on the component of the magnetic field in the direction of propagation, and is given by

$$\Delta\nu \equiv \Delta\nu_{+1} - \Delta\nu_{-1} = \frac{e B \cos\phi}{2 \pi m_e c} \quad (3)$$

The notation is the conventional one. If we neglect terms of order  $m_e/m_p = 1/1836 \ll 1$ , the split of the hyperfine-structure energy levels due to a weak magnetic field,  $B$ , is given by  $\Delta\mathcal{E} = \mu_B g_F m'_F B$ , where  $\mu_B = e\hbar/2m_e c$  is the Bohr magneton,  $m'_F$  is the azimuthal quantum number, and  $g_F$  is the Landé  $g$  factor. The orbital angular momentum vanishes in the ground state ( $l' = 0$ ), and  $g_F = [f'(f' + 1) + j'(j' + 1) - i'(i' + 1)] / f'(f' + 1) \approx 1$  because  $j' = i' = 1/2$ . Since  $m'_F = 0, \pm 1$ , eq. (3) follows. The subscripts  $+1$  and  $-1$  in eq. (3) refer to values of  $m'_F$ . Numerically, the split  $\Delta\nu$  is equal to 2.8 Hz per  $\mu$ gauss for propagation along the field ( $\phi = 0$ ). Since line widths are typically measured in kHz, observations of the Zeeman effect in hydrogen are very difficult, and special techniques become necessary. [See Davis and Berge (1968, pp. 762-765) for an excellent discussion and for the reason why the transverse Zeeman effect is even more difficult to detect.] As in the case of Faraday rotation, only the mean field along the line of sight is measured. However, fields measured through Zeeman observations may be indicative of conditions within

interstellar clouds rather than representative of the ambient interstellar fields (see below).

Among the many attempts to observe the Zeeman effect in interstellar clouds, only few produced positive detections. Most measurements put only upper limits on the magnetic field, leaving even the direction of the field undetermined. Although observers and theorists generally agree that our knowledge of the interstellar field that resulted from Zeeman measurements is meager, we take much interest in the fact that both the few positive detections and the upper limits reveal fields consistently weaker than those expected on theoretical grounds. The usual argument is that, under the assumption that the magnetic field is frozen in the matter,<sup>2</sup> the background interstellar field would be enhanced by a factor  $(n_c/n_{ic})^{2/3}$  during the formation of clouds (of density  $n_c$ ) through spherical contraction and condensation of the intercloud medium (of density  $n_{ic}$ ). It follows that clouds with densities  $30 - 1000 \text{ cm}^{-3}$  should have fields in the range  $85 - 300 \text{ } \mu\text{gauss}$ , with  $100 \text{ } \mu\text{gauss}$  being a rather typical value. No such fields have been observed (see Verschuur 1971 and references therein). The few positive detections are summarized in Table 1, which is taken from Verschuur (1974).

Spherical, isotropic contraction has been taken so seriously that a straight line with slope equal to  $2/3$  has been frequently forced through points of  $\log B$  versus  $\log n_c$  plots (for example, Verschuur 1970a), even

---

2. The conductivity of the interstellar medium is given by  $\sigma \sim 10^7 T^{3/2}$  (Spitzer 1962), where  $T$  is the temperature. The dissipation time for the magnetic field over a characteristic scale  $L$  is  $\tau = 4 \pi \sigma L^2/c^2$ . Since  $T \approx 50-10^4 \text{ }^\circ\text{K}$  and  $L \approx 10 \text{ pc}$ , then  $\tau > 10^{21}$  years! Therefore, flux-freezing is an excellent assumption. However, the motion of ions (and the field) through neutrals must be considered (Spitzer 1968a) for densities larger than  $\sim 10^8 \text{ cm}^{-3}$  (Nakano and Tademaru 1972) -- see discussion in § VI below.

though a line with a slope of 1/3 would fit the (uncertain) data at least as well. We shall show in §VII that weak fields must be the rule rather than the exception, thus removing the discrepancy between observations and theoretical expectations.

Atomic hydrogen is believed to be converted to molecular hydrogen in the densest clouds, in which many molecules were discovered (see reviews by Heiles 1971; Rank, Townes, and Welch 1971; Solomon 1973; Zuckerman and Palmer 1974). The magnetic field within the molecular (or, dust) clouds is expected to be relatively high, since the gas density often exceeds  $10^3 \text{ cm}^{-3}$ . The field may be measured through Zeeman observations on the 18-cm line of OH. One such measurement by Turner and Verschuur (1970) yielded an upper limit of about  $10^2 \text{ } \mu\text{gauss}$ , which Heiles (1971) finds rather small compared to (popular) expectations. This contrasts sharply with the upper limit of  $5 \text{ } \mu\text{gauss}$  obtained for another dust cloud (Verschuur 1970b) when the measurement was performed on the 21-cm line, which is seen in self-absorption. To reconcile the two, Heiles (1971) suggests that the hydrogen exists in a thin shell around the molecular cloud, so that the 21-cm result does not reflect the physical conditions inside the dust cloud. This point is well taken. Yet, it is our view that the smaller field, even uncorrected for projection effects, may not be inconsistent with theoretical expectations based on our calculations of equilibria of self-gravitating, magnetic clouds.

There are additional, indirect methods for obtaining the interstellar magnetic field (see Woltjer 1965; van de Hulst 1967; Davis and Berge 1968), but they yield such uncertain estimates that their discussion here is not warranted. They are based mainly on the virial theorem (for example, see Biermann and Davis 1960) applied to various regions of, or the entire inter-

stellar medium. We shall discuss some of the shortcomings of the virial theorem in § VI (see also Mestel 1965).

#### IV. THEORETICAL DESCRIPTION OF LARGE-SCALE PHENOMENA IN THE INTERSTELLAR MEDIUM

##### A. The Dynamical Equations

##### 1. A System of Thermal Gas, Magnetic Fields, and Gravitational Fields.

We mentioned in § I that the interstellar medium is such a complex system that a complete theoretical description is impossible at present. However, the range and relative magnitude of some physical parameters of the system are such that the framework of a useful theoretical description may be specified. First, as we have already noted, the electrical conductivity of the medium is so high ( $10^9 - 10^{13} \text{ sec}^{-1}$ ) and the scales of interest are so large ( $10^{19} - 10^{22} \text{ cm}$ ) that we may assume that the magnetic field is frozen in the ionized matter. Furthermore, the excellent coupling between electrons and ions on the one hand [ $\omega_{\text{coll. (e-i)}} \sim 10^{-7} \text{ sec}^{-1}$ ] and between ions and atoms on the other [ $\omega_{\text{coll. (i-a)}} \sim 10^{-9} \text{ sec}^{-1}$ ] permits us to treat the three-component gas as a single, compressible fluid.

When the phenomena of interest occur on relatively large scales (for example, formation of interstellar clouds, motion of clouds through the intercloud medium, cloud-cloud collisions, cloud collapse), one may specialize to very long-wavelength hydromagnetic disturbances. In this regime, in which an electron collides many times before it is forced to reverse its direction by the oscillating electric field of the disturbance, collective plasma effects become unimportant ( $\omega_p \sim 10^3 \text{ sec}^{-1}$ ). Although collision frequencies are relatively large (compared to the frequency of the hydromagnetic wave,  $\omega \sim 10^{-14} \text{ sec}^{-1}$ ), they are nevertheless much smaller than gyrofrequencies ( $\omega_c \sim 10 \text{ sec}^{-1}$  for electrons). Hence, diffusion across the field (which would result from collisions between

opposite charges before a gyration is completed) may be neglected. In summary, we have the inequalities

$$\omega_p \gg \omega_c \gg \omega_{\text{coll.}} \gg \omega. \quad (4)$$

For scales much larger than collision mean free paths we may also neglect viscosity and thermal conduction, and we may write the magnetohydrodynamic (MHD) equations appropriate for our system.

We consider a conducting gas of density  $\rho$ , pressure  $P$ , and temperature  $T$  embedded in a magnetic field  $\vec{B}$  and a gravitational field  $\vec{g}$ , derivable from a potential  $\psi$ . Both the gas and the stars, whose density ( $\rho_*$ ) is known from observations, may contribute to  $\psi$ . The gas has a bulk velocity  $\vec{v}$ . A current density  $\vec{j}$  maintains the frozen-in field, which is derivable from a vector potential  $\vec{A}$ . The entropy per gram of matter is denoted by  $S$ , and  $\mathcal{L}$  represents the net rate of energy loss (losses minus gains) per gram of matter. The MHD equations are

$$\text{mass conservation:} \quad \frac{d\rho}{dt} + \rho \nabla \cdot \vec{v} = 0 \quad (5)$$

$$\text{force equation:} \quad \rho \frac{d\vec{v}}{dt} = -\vec{\nabla}P - \rho \vec{\nabla}\psi + \frac{\vec{j}}{c} \times \vec{B} \quad (6)$$

$$\text{energy equation:} \quad \rho T \frac{dS}{dt} = -\rho \mathcal{L}(\rho, T) \quad (7)$$

$$\text{ideal-gas law:} \quad P = \frac{\rho}{\bar{m}} k T \quad (8)$$

$$\text{flux-freezing:} \quad \frac{\partial \vec{B}}{\partial t} = \vec{\nabla} \times (\vec{v} \times \vec{B}) \quad (9)$$

$$\text{Poisson equation:} \quad \nabla^2 \psi = 4\pi G (\rho_* + \rho) \quad (10)$$

$$\text{Ampere's law:} \quad \vec{\nabla} \times \vec{B} = \frac{4\pi}{c} \vec{j} \quad (11)$$

$$\text{definitions:} \quad \vec{g} = -\vec{\nabla}\psi \quad (12)$$

$$\vec{B} = \vec{\nabla} \times \vec{A} \quad (13)$$

$$S = \frac{1}{\gamma-1} \frac{k}{\bar{m}} \ln(P \rho^{-\gamma}) + \text{const.} \quad (14)$$

In the above equations  $\bar{m}$  is the mean mass per particle;  $k$  is the Boltzmann constant;  $c$  is the speed of light in vacuum; and  $\gamma = 5/3$ . The comoving time derivative is defined by  $d/dt \equiv \partial/\partial t + \vec{v} \cdot \vec{\nabla}$ . Spitzer (1962) gives a detailed discussion of some fine points in the assumptions behind the MHD equations. References already cited in § IIA discuss the loss function in the energy equation.

## 2. The System with Cosmic Rays Included

The dynamical effects of cosmic rays in the Galaxy have been the subject of intensive investigation for several years. A long series of important papers discuss the conditions under which cosmic rays, considered as a very hot, collisionless plasma, may be described in the MHD approximation. Three excellent reviews (Parker 1968b, 1969a; Lerche 1969) point out what phenomena are excluded when such a description is adopted, but they argue that the MHD description is the proper one for cosmic rays in the Galactic environment. Our new approach to magnetohydrostatic (MHS) equilibrium configurations will shed light on the assumptions, on which some previously derived consequences of the existence of cosmic rays in interstellar space are based. In particular, the conclusion that cosmic rays will inflate the interstellar magnetic field indefinitely (Parker 1965a, 1968b) will be discussed critically in §VB5d. Here we draw from the reviews mentioned above and we summarize the MHD description of the cosmic-ray gas.

In the absence of a magnetic field, the cosmic-ray pressure is maintained isotropic to within  $\sim 1\%$  by various rapidly growing ( $\tau \sim 10^3$  years) relativistic micro-instabilities (for example, see Lerche 1969). In introducing the magnetic field, we shall restrict our attention to very long-wavelength (much larger than gyroradii) hydromagnetic waves. In this

regime and for slow bulk motions ( $v_{cr}^2 \ll c^2$ ), Parker argues that an isotropic cosmic-ray pressure is a fair approximation in most astrophysical situations even in the presence of a magnetic field. It follows from this and the first law of thermodynamics that, under adiabatic conditions,

$$\frac{d\rho_{cr}}{dt} + \left( \rho_{cr} + \frac{P_{cr}}{c^2} \right) \vec{\nabla} \cdot \vec{v}_{cr} = 0. \tag{15}$$

The quantity  $\rho_{cr}$  denotes the mass density of cosmic rays. (The rate of change of the total energy of cosmic rays in a volume element  $\delta V$  is  $d(\rho_{cr} c^2 \delta V)/dt = -P_{cr} d(\delta V)/dt$ . One then uses the relation  $d(\delta V)/dt = \delta V \vec{\nabla} \cdot \vec{v}_{cr}$  to derive eq. [15].) A relation between  $P_{cr}$  and  $\rho_{cr}$  is not simple if a collection of relativistic particles is considered, because each particle contributes to the speed of sound,

$$C_{cr} \equiv (d P_{cr} / d\rho_{cr})^{1/2}, \tag{16}$$

in a manner that depends on its own Lorentz factor,  $\gamma_L \equiv \mathcal{E}/m_0 c^2$ . But in the extreme relativistic case, we have the relation

$$P_{cr} = \frac{1}{3} \rho_{cr} c^2 \equiv \rho_{cr} C_{cr}^2. \tag{17}$$

Then, it follows that

$$\frac{d \ln P_{cr}}{dt} = \frac{d \ln \rho_{cr}}{dt} = \frac{4}{3} \frac{d \ln n_{cr}}{dt}. \tag{18}$$

Because the cosmic rays and the thermal gas are tied to the magnetic field, their bulk velocities  $\vec{v}_{cr}$  and  $\vec{v}$  ( $v_{cr}^2, v^2 \ll c^2$ ) will have equal components in a direction perpendicular to the field. In the long-wavelength limit, the electric field ( $\vec{E}$ ) in a frame with respect to which the thermal gas and the cosmic rays have velocities  $\vec{v}$  and  $\vec{v}_{cr}$ , respectively,



is given by

$$\vec{E} = -\frac{\vec{v}}{c} \times \vec{B} = -\frac{\vec{v}_{cr}}{c} \times \vec{B}. \quad (19)$$

Thus, an equation identical to (9), with  $\vec{v}$  replaced by  $\vec{v}_{cr}$ , holds for the cosmic-ray gas as well.

If the motion of the cosmic-ray gas along field lines is completely decoupled from that of the thermal gas (cf. Kulsrud and Pearce 1969), one may write the force equation for cosmic rays in a direction parallel to the field as

$$\left( \rho_{cr} + \frac{P_{cr}}{c^2} \right) \left( \frac{d(\vec{v}_{cr})}{dt} \right)_{\parallel} = -\vec{v}_{\parallel} P_{cr} - \rho_{cr} \vec{v}_{\parallel} \psi. \quad (20)$$

Actually, gravitational forces on cosmic rays are negligible and the last term may be left out of equation (20). To show this, we may compare the magnitudes of the last two terms of equation (20) and make use of equation (17):

$$\frac{|\rho_{cr} \vec{v}_{\parallel} \psi|}{|\vec{v}_{\parallel} P_{cr}|} = \frac{\rho_{cr} |\vec{v}_{\parallel} \psi|}{C_{cr}^2 |\vec{v}_{\parallel} \rho_{cr}|} \approx \frac{|\Delta\psi|}{C_{cr}^2} \approx \frac{v_{\text{escape}}^2}{C_{cr}^2} \ll 1.$$

The presence of cosmic rays introduces a "suprathermal mode" (Parker 1965b) in addition to the usual fast and slow hydromagnetic modes. It represents a sound wave in the cosmic-ray gas propagating along field lines with speed  $C_{cr}$  (see eq. [17]). The suprathermal mode is independent of the two hydromagnetic modes except for propagation nearly normal to the field, in which case the fast mode collapses to zero and the suprathermal mode takes over.

The nearly instantaneous communication of cosmic rays along field lines establishes pressure equilibrium in the cosmic-ray gas over

a distance  $L$  in a time  $L/C_{cr} \approx L/c$ . If  $L$  is as large as 1 kpc, this time is  $\approx 10^{11}$  sec. This is much smaller than the time scale of the hydro-magnetic phenomena of interest to us here which is  $\approx 10^{14}$  sec. We may therefore ignore the inertial effects of the cosmic-ray gas and we may write that

$$\vec{\nabla}_{\parallel} P_{cr} \equiv \vec{B} \cdot \vec{\nabla} P_{cr} / B = 0 \quad (21a)$$

as a further approximation to equation (20). Equation (21a) states that the cosmic-ray pressure is constant on a field line, but it does not determine its value, which is different for different field lines. In §VB5d we shall show how to calculate  $P_{cr}$  at the position of any field line without reference to equations (15) and (17). For now, we note that equation (21a) will be exact at equilibrium insofar as the hot ( $T_{cr} \sim 10^{13}$  °K) and tenuous ( $n_{cr} \sim 10^{-10}$  cm<sup>-3</sup>) cosmic-ray gas is not affected by the galactic gravitational field ( $g \sim 10^{-9}$  cm/sec<sup>2</sup>).

It remains to specify how cosmic rays will modify the force equation (6) in a direction normal to  $\vec{B}$ . Once this is done, the system of MHD equations including cosmic rays will be closed. We write the force equation for cosmic rays in a direction normal to the field by neglecting the gravitational term because of the reason given above:

$$\left( \rho_{cr} + \frac{P_{cr}}{c^2} \right) \left( \frac{d(\vec{v}_{cr})}{dt} \right)_{\perp} = - \vec{\nabla}_{\perp} P_{cr} + \vec{j}_{cr} \times \vec{B}/c, \quad (21b)$$

where  $\vec{j}_{cr}$  is the current density due to cosmic rays alone. Because of eq. (21a), the term  $-\vec{\nabla}_{\perp} P_{cr}$  may be replaced by  $-\vec{\nabla} P_{cr}$  in eq. (21b). The resulting equation must be combined with eq. (6) - the left-hand sides of the two equations must be added together, and so must the right-hand sides. We note, however, that  $\rho_{cr} = 3 P_{cr}/c^2$  (see eq. [17]) is much

smaller than  $\rho$ ; in a typical HI region  $\rho_{\text{cr}}/\rho \sim 10^{-10}$ . Hence, we may neglect the inertial term in eq. (21b), which is combined with (6) to yield

$$\rho \frac{d\vec{v}}{dt} = -\vec{\nabla}P - \vec{\nabla}P_{\text{cr}} - \rho\vec{\nabla}\psi + (\vec{j} + \vec{j}_{\text{cr}}) \times \vec{B}/c. \quad (21c)$$

Finally, eq. (11) undergoes the obvious modification

$$\vec{\nabla} \times \vec{B} = (4\pi/c) (\vec{j} + \vec{j}_{\text{cr}}). \quad (21d)$$

The approximation expressed by eq. (21a) was also used by Shu (1974), who asserted that eq. (21a) is sufficient to categorize the cosmic-ray gas and that the system of MHD equations is closed without reference to eqs. (15), (17), and (18). In view of our remark above, namely, that equation (21a) states that  $P_{\text{cr}}$  is constant on a field line without specifying its value, it is clear that eqs. (15) - (18), which specify how  $P_{\text{cr}}$  changes in time, are also needed in order to close the system of MHD equations.

### 3. Approximations of the Energy Equation

We have already noted that virtually all information received from the Galactic and extragalactic space comes in the form of photons. It is natural, therefore, that the energy equation is the most exhaustively studied one in astrophysics. In our work we shall focus on Newton's laws as supplemented by Maxwell's equations. The force equation, and in particular magnetic, pressure, and gravitational forces, will be the subject of our studies. All thermodynamics will be dumped into an equation of state  $P = P(\rho)$ . We shall assume an isothermal equation of state frequently and then we shall generalize our formalism to the case  $P = P(\rho)$  without actually solving the more general problem. In view of the meager theoretical (as well as observational) understanding

of the phenomena which we shall study, we offer no apologies for this procedure. We shall discuss the priorities in refining our work at the end.

We begin with the derivation of some (known) implications of flux freezing (eq. [9]), upon which we shall call later.

## B. Implications of Flux-Freezing

### 1. Two-dimensional Geometry

If  $\vec{v}$  and  $\vec{B}$  are confined to a plane (x,y) and all quantities are assumed independent of z, we may set  $A_x = A_y = 0$  without loss of generality. Then we have that

$$\vec{A} = \hat{e}_z A_z(x,y) \equiv \hat{e}_z A(x,y). \quad (22)$$

Since  $\vec{B}$  may be written as

$$\vec{B} = -\hat{e}_z \times \vec{\nabla} A, \quad (23)$$

it follows that

$$\vec{B} \cdot \vec{\nabla} A = 0, \quad (24)$$

so that  $A(x,y)$  is constant on a field line. Moreover, we may write eq. (9) in terms of  $\vec{A}$  as

$$\frac{\partial \vec{A}}{\partial t} = \vec{v} \times \vec{B} + \vec{\nabla} \xi, \quad (25)$$

where  $\xi$  is an arbitrary scalar function of x and y. Both  $\vec{A}$  and  $\vec{v} \times \vec{B}$  have z-components only. Therefore,  $\vec{\nabla} \xi$  must vanish.

By using (23) in (25) and expanding the vector triple product, we obtain

$$\frac{\partial \vec{A}}{\partial t} = -\hat{a}_z (\vec{v} \cdot \vec{\nabla} A) + \vec{\nabla} A (\hat{e}_z \cdot \vec{v}).$$

Since  $\hat{e}_z \cdot \vec{v} = 0$ , we make use of (22) to find

$$\hat{e}_z \frac{dA}{dt} \equiv \hat{e}_z \left( \frac{\partial A}{\partial t} + \vec{v} \cdot \vec{\nabla} A \right) = 0. \quad (26)$$

Hence, in addition to being constant on field lines, A is also a constant of the motion. In this geometry, the magnetic flux between two neighboring field lines, characterized by A and A + δA, is equal to δA. So eq. (26) is a statement of conservation of magnetic flux through any surface co-moving with the fluid.

## 2. Three-dimensional Geometry with Axial Symmetry: A Poloidal Field

Conclusions similar to those described by eqs. (24) and (26) may also be derived in the case of a three-dimensional geometry with axial symmetry (all functions assumed independent of φ). We let r be the (cylindrical) radial coordinate. Once again, eq. (25) follows. Now  $\vec{A}$  and  $\vec{v} \times \vec{B}$  are in the azimuthal direction. Hence,  $\vec{\nabla} \xi = 0$ . We write

$$\begin{aligned} \vec{v} \times \vec{B} &\equiv \vec{v} \times (\vec{\nabla} \times \vec{A}) \\ &= \vec{\nabla} \cdot (\vec{v} \cdot \vec{A}) - (\vec{v} \cdot \vec{\nabla})\vec{A} - (\vec{A} \cdot \vec{\nabla})\vec{v} - \vec{A} \times (\vec{\nabla} \times \vec{v}). \end{aligned} \quad (27)$$

Since  $\vec{v}$  is in the (r,z) plane and  $\vec{A}$  has only a φ-component, the first term on the right-hand side of eq. (27) vanishes. The third term may be written as

$$\begin{aligned} (\vec{A} \cdot \vec{\nabla})\vec{v} &= A_\phi r^{-1} \frac{\partial}{\partial \phi} (\hat{e}_r v_r + \hat{e}_z v_z) \\ &= \hat{e}_\phi r^{-1} A_\phi v_r. \end{aligned} \quad (28)$$

The last term in (27) vanishes because  $\vec{\nabla} \times \vec{v}$  is in the φ-direction. Altogether, then, we have

$$\frac{\partial \vec{A}}{\partial t} = -(\vec{v} \cdot \vec{\nabla})\vec{A} - r^{-1} \vec{A} v_r,$$

or

$$\begin{aligned} r \frac{d\vec{A}}{dt} &= -\vec{A} v_r \\ &= -\vec{A} \frac{dr}{dt}. \end{aligned}$$

We, therefore, conclude that

$$\frac{d(rA)}{dt} \equiv \frac{d\phi}{dt} = 0, \tag{29}$$

where  $A \equiv A_\phi$ . Eq. (29) is a statement of flux conservation in the present geometry. It is easily shown directly that the magnetic flux through a contour, described by the equation  $r = \text{constant}$ , is equal to  $2 \pi \phi$ . Direct calculation also shows, by using eq. (13), that

$$\vec{B} \cdot \vec{\nabla} \phi = 0, \tag{30}$$

so that  $\phi$  is constant on a magnetic surface. We see that flux-freezing in a three-dimensional geometry with axial symmetry implies relations similar to those in the two-dimensional rectangular geometry, except that  $\phi \equiv rA$  replaces  $A$ .

V. FORMATION AND EQUILLIBRIUM OF NON-GRAVITATING INTERSTELLAR CLOUDS: LARGE-SCALE CONDENSATIONS

A. The Magnetic Rayleigh-Taylor (or, Magnetogravitational) Instability

1. The Basic Physics of the Instability

Parker (1966) argued on the basis of the virial theorem that the interstellar magnetic field is confined to the galactic disk only by the weight of the highly conducting interstellar gas. As long as the field lines are parallel to the galactic plane, an equilibrium state is possible. At any distance from the axis of galactic rotation, a gas element is acted upon by a centripetal force appropriate to that distance; this is the only force necessary to keep the gas element in orbit about the galactic center. In a direction perpendicular to the galactic plane, the gas is distributed in such a manner that, at each altitude, the forces due to its pressure gradients, aided by the magnetic-pressure gradients, balance the vertical gravitational forces. Self-gravitation of the gas is neglected in this picture because the mass in the form of gas is only a few percent of the mass in stars.

Mathematical simplicity and observational evidence that the magnetic field is more or less parallel to the local spiral arm suggest the study of the nature of the equilibrium of the gas-field-gravity system in two dimensions. Horizontal distance is measured in a nearly azimuthal direction (x-axis), and the y-axis extends perpendicular to the galactic plane. All quantities are then assumed independent of z, the distance along a radial direction in the galaxy. Some interesting effects appear when proper consideration is paid to the third (z) dimension (see Parker 1967a, 1967b; Shu 1974), but they do not alter the basic conclusions of the two-dimensional calculations even when new physics, such as differential rotation, is

introduced.

In this two-dimensional geometry, Parker's stratified equilibrium state is symmetric about the x-axis because the galactic gravitational field exhibits such symmetry:

$$\vec{g} \equiv -\vec{\nabla}\psi = -\hat{e}_y g(y), \quad (31)$$

where Parker assumed that

$$g(y) = -g(-y) = \text{a positive constant.} \quad (32)$$

One, then, considers only the upper half plane. The magnetic field,  $\vec{B}$ , is assumed to point in the +x-direction everywhere. [The essence of the conclusions (see below) does not change when one considers the case in which  $g$  is a linear function of  $y$  (Parker 1966).] Parker also assumed that the ratio,  $\alpha$ , of the magnetic pressure to the gas pressure,  $P$ , is fixed in the initial state, that is,

$$\alpha \equiv B^2/8\pi P = \text{a constant.} \quad (33)$$

In fact, Parker (1969a) argued on observational grounds that  $\alpha$  is very nearly equal to unity. We shall return to this point below.

The equation of state is taken as

$$P = \rho C^2, \quad (34)$$

where  $C$  is the isothermal speed of sound in the gas. The force equation is nontrivial only in the  $y$ -direction, and it is written as

$$(1 + \alpha) \frac{dP}{dy} = -\rho g. \quad (35)$$

Its solution (for  $y \geq 0$ ) is

$$P(y) \equiv \frac{B^2(y)}{8\pi\alpha} \equiv \frac{[-A(y)]^2}{32\pi\alpha H^2} = \rho(0) C^2 \exp(-y/H), \quad (36)$$

where  $\rho(0)$  is the value of the gas density at  $y = 0$ , and the scale height  $H$



is defined by

$$H \equiv (1 + \alpha) C^2/g. \quad (37)$$

Parker (1966) introduces perturbations with wavelengths  $\lambda_x$  and  $\lambda_y$  in the x- and y-directions, respectively, and requires that the field line originally coinciding with the x-axis remain undeformed, as well as that the perturbations be bounded at infinity. A representative perturbation is written as

$$\delta A = -\mu_1 A(y) \sin(2\pi y/\lambda_y) \cos(2\pi x/\lambda_x). \quad (38)$$

The quantity  $\mu_1$  is a positive constant much less than unity. He solves the linearized MHD equations and finds that the stratified ("initial") state is unstable, provided only that  $\lambda_x$  and  $\lambda_y$  simultaneously exceed some critical values,  $\Lambda_x$  and  $\Lambda_y$ , respectively (see eqs. [31] and [32] of Paper I). The existence of a lower limit on  $\lambda_x$  for instability to develop is understood on simple physical grounds. If  $\lambda_x$  is very large, the curvature of the field lines is small, and so is the tension. The vertical galactic gravitational field acquires a component along a deformed field line that induces gas motions, tending to drain matter from the raised portion of the field line. As gas gets "unloaded" from the inflated portion, the magnetic-pressure gradient remains unopposed there (where the tension is small) and, therefore, it causes an additional rise of the already inflated part. Hence, the situation is unstable.

The physical origin of a critical wavelength in the y-direction is more obscure and, as far as we know, this point has not been discussed elsewhere. Parker's dispersion relation shows that if  $\lambda_y < \Lambda_y$ , the initial stratified state is stable even if  $\lambda_x > \Lambda_x$ . To understand why this is so, we proceed as follows. First, we note that if  $\lambda_y < \infty$  there

is always a set of field lines that are left undeformed by the perturbation (38). They are located at  $y = n \lambda_y / 2$ ,  $n = 1, 2, 3, \dots$ . Above and below each of these special field lines, the rest of the field lines, that is, the deformed ones, curve in an opposite sense (see Fig. 1). As the instability progresses, this "symmetry" implies that the undeformed field lines will retain their special status. (Rigorously,  $\delta v_y$  has the same  $y$ -dependence as the perturbation  $\delta A$ ; hence, it vanishes at the position of the special field lines.) Consider, then, the first undeformed field line, at  $y = \lambda_y / 2$ . It acts as a natural "lid" to the system below it which, in fact, contains most of the mass and energy of the entire system. Now, we recall that the instability is driven by (i) the galactic gravitational field that causes the gas to slide down the deformed field lines; and by (ii) the magnetic-pressure gradients at the position of the "unloaded" portions of the field lines. The instability is opposed by (i) the increase in the field strength due to the compression that takes place at the position of the "valleys" of the field lines; and by (ii) the tension of the curved field lines. The gas-pressure gradients are neglected for the purpose of this argument.<sup>3</sup> If the first undeformed field line is too low, that is, if  $\lambda_y$  is too small, the instability cannot develop because the volume available for the field lines to expand is restricted. As a matter of fact, if field lines do inflate in the usual manner, they will "pile up" close to the first undeformed field line in the region where inflation occurs. Consequently, the magnetic field will increase there, tending to suppress rather than to aid the instability.

---

3. See Paper I § IV and § VIb for a more complete discussion of the energetics in the case of an isothermal transition. Pressure forces are important in determining final equilibrium states; after all, they are the only forces available to oppose the galactic gravitational field along field lines.

If  $\lambda_y$  is large enough, the effects just described will remain the same qualitatively. But, because the "pile-up" of field lines occurs at a much higher altitude than before, the magnetic field was much weaker there in the first place. Therefore, the increase in the field due to the "pile-up" is not sufficient to suppress the expansionist tendencies of the magnetic-pressure gradients below, which remain virtually unopposed because of gas drainage from the inflated portions of field lines. On the basis of energy considerations, the increase in the magnetic energy due to the compression at the "lid" is considerably smaller than the decrease in magnetic energy resulting from the inflation of field lines, which originate from much lower altitudes. Incidentally, these considerations provide a physical explanation for the fact that, for a given (unstable)  $\lambda_x$  the growth-rate of the instability is maximum if  $\lambda_y = \infty$ . Clearly, if the first undeformed field line occurs at infinity (where  $B = 0$ ), the magnetic field by itself does not initially act in the region of expansion so as to prevent the instability, which proceeds at a rate faster than it would if in this part of the system the field were acting so as to suppress it.

## 2. Retrospect

Altogether, the magnetogravitational instability involves motions tending to accumulate the gas into clumps at the position of valleys of the field lines. This led Parker (1966) to suggest that interstellar clouds form in this manner, and they are suspended by the field at the position of the valleys. Whether, in fact, these condensations will resemble the observed interstellar clouds can be decided only if the final states for the instability are known. And these can be determined only by solving the nonlinear MHS equations with appropriate boundary conditions. In

Paper I we found such final states. In the process, we had to tackle several interesting theoretical questions. (i) How does one include the assumption that the magnetic field is frozen in the matter in a time-independent problem, so that a connection between initial and final states may be made? Our method for doing this has potential and direct applications in such diverse research areas as pulsar magnetospheres, equilibria of high-beta plasmas, and steady (but non-uniform) fluid flow in the absence of magnetic fields if vorticity is conserved in the same sense that magnetic flux is. It is well known that vorticity (or, circulation) is conserved for barotropic fluids (Bjerknes' theorem). (ii) What is the appropriate "potential energy" of an isothermal ( $\gamma = 1$ ) plasma? Without an expression for the effective potential energy one would not know whether the calculated equilibrium states are higher or lower in energy than the initial (unstable) state. Finally, we developed an original procedure for solving the reduced MHS equations since neither analytical nor numerical methods for solving the equations were known.

A question asked frequently is: Why should one seek equilibrium states for (any model of) the interstellar medium, especially since one knows in advance that this system is a highly complex dynamical one? First, for the practically-minded skeptic, we point out that the e-folding time for the magnetogravitational instability ( $\sim 10^7$  years) is smaller than other relevant time scales, such as the passage through two successive spiral shock waves ( $\sim 10^8$  years). Our equilibrium states, then, are referred to as "final" in the sense that they can persist for almost  $10^8$  years -- before they might be modified by the general decompression that takes place downstream from a galactic shock (see Paper II). If the instability is triggered regularly (for example, by spiral density shock

waves), one may hope to observe such configurations in the interstellar medium of our own, as well as of other, spiral galaxies. On the other hand, if the instability is active today, one might observe gas motions consistent with the final states. There are more general theoretical reasons for which a knowledge of equilibrium states of any system is very useful, but these are best dealt with in the context of self-gravitating interstellar clouds (see § VIII).

We now summarize the main features and predictions of our equilibrium solutions, after we settle an important question bearing on the very existence of final equilibrium states.

## B. Final States for the Magnetogravitational Instability

### 1. Do Final States Really Exist?

We could offer our calculated final states as a proof of the existence of such states for the idealized system under consideration. We would nevertheless prefer to understand their existence on the basis of first principles. After all, it has been argued in the literature on intuitive grounds that such states should not exist! What prevents the field lines from expanding indefinitely while the gas slides down into every thinner clumps of matter at the position of the valleys? In answering this question we distinguish two cases.

a.  $\lambda_y < \infty$ . A finite vertical wavelength of the initial perturbation implies that a set of field lines is left undeformed. In particular, the first undeformed field line acts as a natural "lid" on the part of the system below. The "lid" by itself would prevent the unlimited expansion of the field lines. For this reasoning to be correct it must be verified that the  $y$ -component of the velocity always (not just initially) vanishes at the undeformed field lines. This calculation has not been attempted.

But it seems reasonable that, once the field lines have deformed in an opposite sense above and below each undeformed field line, it would take a finite amount of energy to reverse that trend. In the absence of a continuing source of agitation this may happen only if a flow of energy occurs from the shorter to the longer vertical wavelengths of the spectrum of the initial perturbation. Eventually, then, that state will prevail that is characterized by  $\lambda_y = \infty$ . For, if this "mode mixing" ceases at some  $\lambda_y < \infty$ , we would have illustrated the point that a final state with a finite  $\lambda_y$  is possible. So, we turn to the second case.

b.  $\lambda_y = \infty$ . Will the field lines inflate forever in this case?

We suggest that they will not. The increasing curvature of the field lines, both at the position of the valleys and at the "wings" (where inflation occurs) of a condensation, will eventually stop the expansion. To show this, we consider two initially neighboring field lines characterized by  $A$  and  $A + \Delta A$ . Since the field lines are held down at the position of the valleys by the weight of the gas, we focus our attention at the peaks of the two field lines (points  $a$  and  $b$  of fig. 2). Specifically, we consider them after they have moved further apart because of the general inflation of the field lines. We denote by  $h$  the distance between points  $a$  and  $b$ . Since  $\Delta A$  is fixed by flux conservation, the mean magnetic field in the space between  $a$  and  $b$  varies as

$$\bar{B} = \bar{B}_x \propto h^{-1}. \quad (39)$$

The expansive tendencies of the magnetic field are due to the pressure force  $-\vec{\nabla}_\perp B^2/8\pi$  acting in the  $+y$ -direction in this region. Since  $\partial/\partial y \sim h^{-1}$ , it follows that

$$|\vec{\nabla}_\perp B^2| \approx |B_x \frac{\partial B_x}{\partial y}| \propto h^{-3}. \quad (40)$$

We must now compare the variation of the disruptive force given by eq. (40) with the variation of the confining force (tension) due to the curvature of the field lines. The tension is  $+B^2(\partial\hat{s}/\partial s)/4\pi$ , where  $\hat{s}$  is a unit vector tangent to a field line. We also have that  $|\partial\hat{s}/\partial s| = (\text{radius of curvature})^{-1} \approx \lambda_x^{-1}$  for highly deformed field lines. Therefore, in the space between a and b we obtain the relation

$$|B^2(\partial\hat{s}/\partial s)| \approx \bar{B}^2 \lambda_x^{-1} \propto h^{-2}. \quad (41)$$

A comparison between eqs. (40) and (41) reveals that the magnetic-pressure gradients (disruptive) decrease with altitude faster than the tension of the field lines (confining). Hence, the inflation of field lines will eventually stop.

The gas, of course, contributes its share in limiting the inflation of the field lines. This is done both by holding the field lines down with its weight at the position of the valleys and by resisting unlimited compression along field lines due to its finite temperature. At equilibrium, the gas density varies with altitude,  $y$ , as  $\exp[-g y(x,A)/C^2]$  along a field line characterized by the value  $A$  of the magnetic potential. Thus, the field does not turn into an exact vacuum field at any finite altitude.

## 2. Some Features of the Final States

In Paper I we presented three final states having the same vertical but different horizontal wavelengths, and we discussed their features in detail. We had taken  $\alpha = 1$  in the initial state, a value which Parker (1969a) finds reasonable on observational grounds. We suggested that final states represented "large-scale" condensations of the interstellar gas in valleys of the field lines. The scale, of course, is determined from Parker's (1966) instability criterion, if the interstellar medium has ever existed in the stratified state. But Parker had suggested that

horizontal wavelengths as small as 10 pc and as large as 1000 pc could grow. The critical wavelength in the horizontal direction is given by

$$\Lambda_x = \frac{4 \pi H}{(2\alpha + 1)^{1/2}}, \quad \alpha > 0. \quad (42)$$

Therefore,  $\Lambda_x$  is expected to be several times larger than the initial scale height  $H$ , which is about half the scale height of a typical final state. Since observations reveal a scale height  $\sim 10^2$  pc today, wavelengths smaller than a few hundred parsecs will not grow, even when cosmic rays are included (see § VB5d below), unless  $\alpha$  is unusually large. This is the origin of our terminology "large-scale condensations".

The following are some of the main characteristics and implications of our final states.

a. Scale Height

i. Gas.

Compared with that of the corresponding initial state, the scale height of the gas in a final state increases at the position of the valleys, where the field is compressed (see isodensity contours of figs. 2a, 2b and 2c of Paper I). This is so because matter accumulates in the valleys mainly due to motions along field lines rather than due to a vertical compression. On the other hand, the scale height of the gas decreases at the wings of the condensations. For wavelengths within  $\pm 20\%$  of the wavelength corresponding to the maximum growth rate, the scale height of the gas at the valleys is 1.5-2.7 times that at the wings. The observed "high latitude gas" in the Galaxy may be nothing more than the high altitude matter indicated by the rise in the isodensity contours of figures 2a, 2b and 2c of Paper I. This is in contrast with the traditional interpretation of the high latitude gas as



matter raised by inflated field lines during the development of the magnetogravitational instability. A significant amount of matter is not raised by inflated field lines. Field lines inflate only because, (and only as fast as) gas can drain away from their raised portions. (When all is settled, at any point in the region where inflation occurred, the density in a final state is smaller than that in the initial state.) If the magnetic pressure gradient remained undiminished during the expansion process, it might be able to lift a significant amount of matter to higher altitudes. It is the case, however, that expansion takes place at the expense of the forces that initiated it; that is, magnetic energy is released during the expansion. Matter which was originally at large  $y$ 's travels down steeper field lines. It may, therefore, reveal itself as relatively rapidly falling gas above large-scale condensations in the interstellar medium. Since the e-folding time of the magnetogravitational instability is  $\sim 10^7$  years, the high altitude gas would be depleted by now unless some mechanism replenishes it. We shall suggest that the mechanism which periodically triggers the instability may also be responsible for replenishing the high altitude gas (see § VB5e below). No additional assumptions are necessary.

ii. Magnetic Field.

Fig. 3 exhibits the variation of the field,  $B_f(x,y)$ , with  $y$  at  $x = 0$  (valley) and at  $x = X \equiv \lambda_x/2 = 15 C^2/g$  (wing) of the final state of fig. 2c of Paper I (hereafter referred to as state c). On the same graph we plotted the field of the initial state,  $B_i(y)$ , for comparison. All values are normalized to  $B_i(y = 0)$ . It is evident that although the field at the valley,  $B_f(0,y)$ , starts out larger than the field at the wings,  $B_f(X,y)$ , it decreases more rapidly. For  $y \gtrsim 3 C^2/g$ , it becomes

smaller than  $B_i(y)$ . Also, for  $y \gtrsim 5 C^2/g$ , it is smaller than  $B_f(X,y)$ . The scale height of the field at the valley has decreased to about 2.9, and at the wings to about 3.5 compared to that of the stratified initial state, in which it was equal to 4.0 (units of  $C^2/g$ ). Thus, the individual scale heights of the gas and field change in the same direction at the wings of a condensation and in opposite directions at the valleys, where matter accumulates. Since observations of synchrotron radiation indicate a scale height of the field larger than that of the gas, our solutions suggest that the radiation may be produced mainly at the wings of the condensations. We shall return to this point when we consider cosmic rays (§ VB5d).

The above dependence of  $B_f(0,y)$  and  $B_f(X,y)$  on  $y$  is a direct consequence of flux conservation. The total magnetic flux between the  $x$ -axis and  $y = Y \equiv \lambda_y/2 \leq \infty$  is fixed. Therefore, the areas under the curves  $B_f(0,y)$  and  $B_f(X,y)$ ,  $0 \leq y \leq Y$ , must be equal. Since  $B_f(0,y)$  exceeds  $B_f(X,y)$  for small  $y$ , it must decrease below  $B_f(X,y)$  beyond some finite value of  $y$ .

b. Gas density.

The reflection symmetry about the galactic plane implies that the field line originally coinciding with the  $x$ -axis will always do so during the development of the instability. We recall that  $g$  has only a vertical component and that magnetic forces do not act along field lines. Consequently, the gas density will be uniform along the  $x$ -axis, even though its value will be different, in general, in the initial and final states. Will  $\rho_f(x,y=0)$  be much larger than  $\rho_i(0)$ ?

It has been a tacit assumption in all work on the magnetogravitational instability that the final central (that is,  $x = 0, y = 0$ ) density of a condensation will be much larger than  $\rho_i(0)$ . Even star formation resulting

from a very large increase in gas density at the valleys has been contemplated. Yet, our solutions show that the final density on the x-axis is smaller than, and within a few percent of, its value in the stratified initial state. This is so because if the density increases at the valleys, where vertical compression takes place, the resulting increase in pressure is unopposed along the x-axis. Therefore, matter has to move out of the compression region (along the x-axis) to relieve the pressure gradients. The fractional increase of the cross-section of a flux tube at  $y \sim 0$  is larger at the wings than the fractional decrease taking place at the valleys. Therefore, the mean gas density in the tube will drop. But since the density must be uniform on the x-axis, it will always be equal to the mean density there. Thus, the density on the x-axis in a final state will be smaller than that in the corresponding initial state. This decrease in density is very small because the deformation suffered by a field line neighboring the x-axis is small. This effect is seen clearly in fig. 4, which shows  $\rho_f(x=0,y)$  and  $\rho_f(x=\lambda,y)$  for state c, and  $\rho_i(y)$ .

The dependence of the density on  $y$  at any  $x$  is indicated by the isodensity contours of figs. 2a, 2b, and 2c of Paper I.

A directly observable quantity in those external galaxies which are seen nearly face-on is the column density of the gas if the gas is predominantly neutral, or the "emission measure" if the gas is mainly ionized. Our solutions predict a contrast between the maximum and minimum values of these quantities in the range 1.4 : 1 to 3.0 : 1 for wavelengths within  $\pm 20\%$  of the one corresponding to the maximum growth rate (see fig. 3, Paper I). (In the case of ionized gas, a fixed degree of ionization is assumed throughout the system.) The curves for the emission measure may represent those for the column density within at most 18%

because  $\rho_f$  varies nearly exponentially with  $y$  at a fixed  $x$ , at least for the first few scale heights, where most mass is found. Thus, the integrals  $N_H(x) \equiv \int dy \rho_f(x,y)$  and  $E_m(x) \equiv \int dy \rho_f^2(x,y)$ , normalized to those of the initial state, will (almost) differ by a multiplicative constant  $\approx 1$ .

c. The ratio ( $\alpha$ ) of the magnetic pressure to the gas pressure.

We assumed that  $\alpha = 1$  everywhere in the initial state and we determined final equilibrium states some of which were discussed in Paper I. Parker (1969a) interprets the observations as suggesting a value of  $\alpha$  close to unity. One uses the observed values of  $H$ ,  $C$ , and  $g$  in eq. (37) in order to obtain  $\alpha$ .<sup>4</sup> This is misleading conceptually. The e-folding time of the magnetogravitational instability is about  $10^7$  years. Therefore, observations carried out today will reveal values for  $H$  characteristic of some final state rather than of the assumed initial state. We have seen that the scale height of the gas varies typically by a factor of 2 in going from the midplane ( $x = 0$ ,  $y > 0$ ) to the wings of a condensation.

In a final state (for example, state c)  $\alpha$  varies considerably with position even though it was taken equal to unity everywhere in the initial state. At  $x = 0$ , it decreases rapidly with  $y$  from its maximum value of 2 (see fig. 5), while at  $x = X$ , the opposite is true. Such a quantity as an "average"  $\alpha$  is meaningless. Since observations may give only a mean value of the field and of the gas density along a line of sight, the most one may extract from observations is the quantity

$$\bar{\alpha} = \langle B \rangle^2 / 8 \pi \langle P \rangle. \quad (43)$$

---

4. If  $g$  is taken as a linear function of  $y$  (as is actually the case for the first one or two scale heights in our galaxy), the mean value of  $g$  over the first scale height must be used. If cosmic rays are included, eq. (37) is replaced by equation (50), with the quantity  $\beta$  given by eq. (48). The point of our argument does not change by these considerations.

Faraday rotation measurements give  $\langle B_{\parallel} \rangle$  weighted by the number density of thermal electrons along the line of sight. Observations of synchrotron radiation may give  $\langle B_{\perp}^{1.8} \rangle$  weighted by the number density of relativistic electrons. To obtain  $B$  itself, some assumption concerning the structure of the emitting region is necessary, [Note that  $\bar{\alpha}$  is not the same as the "average"  $\alpha$  defined by  $\langle \alpha \rangle = V^{-1} \int dV \alpha(x,y)$ , where  $dV$  is a volume element.] The quantity  $\bar{\alpha}$  (not  $\alpha$  itself) is near unity, indicating a large-scale "equipartition" between the energies in magnetic fields and in random motions of gas. Biermann and Schlüter (1951) advocated such large-scale equipartition on theoretical grounds (see also Parker 1969a, 1969b).

It should be unnecessary to remark that eq. (43) does not imply the relation  $B^2 \propto P$ ; unfortunately, this relation is often used and justified "on observational grounds." Neither observations nor our calculations (see fig. 5) imply that  $\alpha$  itself is constant in the interstellar medium today.

### 3. Dependence on the Assumed Initial State

We have used as an initial state the stratified state suggested by Parker (1966) in order to keep contact with previous work on the subject. We do not suggest that the interstellar medium must have existed in such a state. As emphasized in Paper I, our final states depend on the initial state only in that they have the same mass-to-flux ratio in their various flux tubes. If this ratio may be obtained from observations, our formalism and method of solution of the MHS equations can be used to determine equilibrium states of the gas and field in the galactic gravitational field without reference to any particular initial state and without reference to the magnetogravitational instability.

#### 4. Comparison with Observations

In Paper I we compared the calculated final states with observations in the solar neighborhood. We argued that the topology of the magnetic field, the distribution of the interstellar gas, and the observed gas motions can be understood in terms of, and can be taken as evidence for, the magnetogravitational instability. The sun is located at an estimated distance roughly equal to  $\lambda_x/3$  from the "center" of the large-scale condensation observed at  $l \approx 40^\circ$ . A second large-scale condensation is located at  $l \approx 250^\circ$  at a distance  $\sim 2 \lambda_x/3$  from the sun. The horizontal separation between the "centers" of these two condensations is  $\lambda_x \approx 1/2$  kpc.

The observed gas motions indicate that matter is still sliding down the deformed field lines. Note that if the sun's location were equidistant from the two condensations, zero velocities would be predicted at a latitude  $b \sim 90^\circ$  because a line of sight at  $b \sim 90^\circ$  would intersect all field lines at right angles. With the sun's position as described above, however, the maximum velocities are expected to be observed at  $b \sim 90^\circ$  because for these latitudes the line of sight forms the smallest attainable angle with highly deformed field lines. At intermediate and low latitudes, gas sliding toward a valley of the field lines from both sides will reveal itself in both positive and negative velocity (with respect to the velocity of the center of the condensation arising due to the rotation of the Galaxy as a whole). Because field lines close to the Galactic plane do not deform very much, low latitude local gas is expected to exhibit smaller velocities than the high latitude gas, which is falling freely through large distances.

Clearer evidence for the magnetogravitational instability is expected in spiral galaxies seen nearly face-on if spiral density shock waves

trigger the instability. Rots (1974) observed the column density of hydrogen along the spiral arms of M81 with a resolution of  $400 \times 800$  pc. As his figure 12 shows, the spiral arms are broken up into many clumps of matter at fairly regular intervals of about 1 kpc; this is in accordance with our expectations based on the development of the magnetogravitational instability in an interstellar medium in which  $\alpha \sim 1$  (see Paper II). Typically, the observed ratio of the maximum to the minimum column densities is somewhat less than 2, as predicted by fig. 3 of Paper I. Since the observations were performed along a theoretical spiral, rather than through the actual maxima of hydrogen emission, the full contrast in column densities between maxima and minima is not revealed in all cases. (Also, not all condensations are well resolved.) A repetition of the experiment with this particular point in mind and with a better resolution would be very useful.

To model a particular condensation one must know how its mass is distributed among its flux tubes. Until high resolution observations of the gas and field may yield information on that matter, any comparison with observations will, of necessity, be of a semi-quantitative nature. Our calculated final states predict that the interstellar medium, at least along spiral arms, would exhibit the following characteristics:

i) The gas will be broken up into clumps of matter at fairly regular intervals larger than a few hundred parsecs. For  $\alpha \sim 1$ , the most likely separation is in the range 500 pc - 1000 pc, the lower limit being allowed by the fact that the observed scale height may be twice that of the initial state.

ii) The contrast in column densities between maxima and minima will be roughly in the ratio 2 : 1. A similar contrast is expected

between maxima and minima of the emission measure if the gas is predominantly ionized.

iii) There will be an intimate association between the interstellar gas and field. Yet, the scale height of the gas is maximum where that of the field is minimum (that is, at the valleys) and vice versa.

Further consequences of the development of the magnetogravitational instability along spiral arms are discussed in Paper II. In particular, we suggest that cloud complexes, giant H II regions, and gravitationally unbound OB stellar associations may have their origin in the triggering of this instability by spiral density shock waves.

#### 5. Refinements

Although we formulated (and described a method for solving) a very general problem in Paper I, the particular solutions presented may be restricted by some simplifying assumptions made. First, the gravitational field of the galaxy was assumed independent of  $y$ , the altitude above the galactic plane. Second, the magnetic pressure was taken equal to the gas pressure (that is,  $\alpha = 1$ ) in the initial state. Third, the gas temperature in a final state was assumed to be the same as that of the corresponding initial state. Fourth, the initial state was taken as the (unstable) equilibrium state proposed by Parker (1966). Fifth, the effect of cosmic rays on the final equilibrium states was neglected. How would our final states be modified if each of these assumptions is relaxed? We argue that changes will be of a quantitative, rather than a qualitative, nature - contrary to Parker's (1968b) suggestion that cosmic rays preclude final equilibrium states.

##### a. A gravitational field varying with altitude.

The vertical component of the Galactic gravitational field,  $g(y)$ ,



deduced from observations of the motion of K giant stars, is plotted against  $y$  in fig. 6, taken from Oort (1965). For altitudes smaller than two scale heights,  $g(y)$  increases almost linearly from 0 to  $5 \times 10^{-9}$  cm/sec<sup>2</sup>. For the next 10 - 15 scale heights,  $g(y)$  increases only by an additional factor of 2. It must decrease as  $y^{-2}$  eventually. So, our solutions might be expected to change at least close to the Galactic plane and at very large altitudes because  $g(y)$  cannot be approximated by a constant there. In the region where  $g$  increases with  $y$ , one might expect the new final states to have field lines somewhat more deformed compared to those of the constant  $g$  case. This is so because a gas element is heavier the higher it is along a deformed field line, so that drainage of gas into valleys is likely to be more efficient. On the other hand, the almost vanishing  $g$  close to the Galactic plane will give rise to small gravitational forces that can be balanced by small pressure gradients along the slightly deformed field lines. Thus, gas drainage into valleys might be less efficient at small altitudes than it was in the constant  $g$  case.

The inverse-square dependence of  $g$  on  $y$  at very high altitudes indicates that the deformation of field lines in this region may be much less than before.

On the basis of these intuitive arguments one might speculate on the expected dependence of the magnetic field and the gas density on position; but one's intuition cannot substitute for quantitative calculations. We shall, therefore, refrain from further speculations. If and when observations allow the determination of the mass-to-flux ratio in the flux tubes of the system, solution of eqs. (10) and (12) of Paper I with a more realistic  $g$  will be necessary (and straightforward). Then a

detailed, quantitative comparison with observations would be possible.

b. Alpha larger than unity.

In Paper I and in § VB2 above, we pointed to observational evidence suggesting that the critical horizontal wavelength for the magneto-gravitational instability is a few (3 or 4) hundred parsecs. The horizontal wavelength corresponding to the maximum growth rate is about twice as large. Since the horizontal "width" of a condensation is in the range  $\lambda_x/4 - \lambda_x/2$  (see Paper I, § VIa), it is clear that the magneto-gravitational instability accounts most naturally only for condensations larger than  $10^2$  pc. Thus, we have two proposed mechanisms for cloud formation: (i) the thermal instability, which can account for dwarf clouds of dimension  $\lesssim 10^{-1}$  pc; and (ii) the magnetogravitational instability that can produce giant condensations of dimension  $\gtrsim 10^2$  pc. What, then, is responsible for clouds of intermediate [or, "standard" (see Spitzer 1968a)] size?

Equation (42) shows that, if  $\alpha \gg 1$ , the critical horizontal wavelength ( $\Lambda_x$ ) for the magnetogravitational instability becomes comparable to, or smaller than, the combined scale height (H) of the gas and field in the initial state. It might be tempting to suggest that this is the manner in which "standard" clouds form, namely, that the magnetogravitational instability develops in a cold gas for which  $\alpha \gg 1$ . There are some difficulties with this picture. First, Faraday rotation observations yield a large-scale magnetic field of a few microgauss. So, one does not have the freedom of achieving large  $\alpha$ 's by assuming a much stronger field. An additional restriction on  $\alpha$  and the gas temperature (T) is imposed by the requirement that H remain reasonably close to the scale height observed today. For H to remain nearly fixed while  $\alpha$  and T vary,

one must have the approximate proportionality (see eq. [37])

$$\alpha \propto C^{-2} \propto T^{-1}. \quad (44)$$

Since the magnetic field must also remain nearly fixed, we have the additional relation

$$\alpha \propto P^{-1}. \quad (45)$$

Combining relations (44) and (45), we obtain

$$P \propto T. \quad (46)$$

Equation (46) states that, in order for alpha to increase appreciably, the interstellar gas must cool nearly isochorically. In § IIA2, we discussed the possibility that standard clouds might form through the development of a thermal instability in an interstellar medium cooling isochorically. We concluded that much smaller condensations are favored for times less than  $\sim 10^7$  years. We now ask: if indeed large  $\alpha$ 's are achieved because of isochoric cooling, would the magnetogravitational instability account for standard clouds?

We may obtain a hint on the nature of the answer to this question if we compare the tension of the field lines with the galactic gravitational force exerted on the gas. Since wavelengths smaller than  $H$  are now favored (see eq. [42]) we may write for the radius of curvature of a typical field line  $R \sim \lambda_x = \kappa H$ , where  $\kappa$  is a positive constant smaller than unity. Then the ratio of the tension of the field lines to the gravitational force is

$$\frac{|B^2(\partial \hat{s}/\partial s)|}{4 \pi \rho g} \sim \frac{B^2}{4 \pi R} \frac{1}{\rho g} = \frac{B^2}{4 \pi \kappa H} \frac{C^2}{P g} \approx \frac{2}{\kappa}, \quad (47)$$

where we made use of the equation  $H \approx \alpha C^2/g$  for  $\alpha \gg 1$ . Equation (47)

suggests that, even if the horizontal wavelength is as large as the scale height (that is,  $\kappa = 1$ ), the tension of the field lines might prevent large deformations. Hence, final equilibrium states are expected to have field lines only slightly deformed. The deformation would be smaller for smaller wavelengths. As a consequence, the density contrast between the valleys and the wings of a condensation is unlikely to be very large, casting doubt on the original proposition that the case  $\alpha \gg 1$  might produce standard interstellar clouds. Yet, this possibility (and especially the case  $\alpha > 1$ ) should not be dismissed without an exact equilibrium calculation.

We note in passing that Heiles (1968) found an abnormally small number of clouds with masses 24 - 280  $M_{\odot}$ . This "gap" may not be unrelated to the gap in wavelengths that separates the realms of thermal and magneto-gravitational instabilities.

c. A non-isothermal equation of state.

The result discussed in § VB2b, that the gas density is uniform along the x-axis, might be a consequence of the assumption that the gas is isothermal. Suppose then that some other equation of state, such as  $P = P(\rho)$ , is used. The gas pressure must still be uniform along the x-axis because there are no other forces available to sustain any pressure gradients. We must, therefore, have that  $\vec{\nabla}_x P = (dP/d\rho) \vec{\nabla}_x \rho = 0$ . Clearly, the possibility now arises that there may be density variations along the x-axis. The necessary and sufficient condition is that  $dP/d\rho = 0$  for some ("critical") value of  $\rho$ ; that is, a "phase transition" (an increase in density at a constant pressure) must take place.

If such "phase transitions" (see also § IIA1) are permitted, two new effects may appear. The first one is that small elements of dense gas

may form (by a thermal instability) and be collected in the valleys because they "see" an external potential well (see Table 2, Paper I), into which they may fall by sliding along field lines. If small-scale condensations form, or pre-exist, in the interstellar medium in which the magnetogravitational instability develops, they will be accelerated along deformed field lines giving rise to ordered motions of interstellar matter. There exists observational evidence for such motions (see § IIB). The second effect that may appear due to a general equation of state is that forced (or, driven) "phase transitions" may occur as the gas accumulates in valleys of the field lines. Such transitions may not suffer from the limitations of the thermal instability. In particular, the (short) cooling time of the interstellar gas need not determine the range of most unstable wavelengths, which will be appropriate to the magnetogravitational rather than the thermal instability. The rate of forced "phase transitions" will be limited by the speed with which gas slides down the deformed field lines. This may be comparable to the speed of sound in the intercloud medium; that is, about 10 km/sec. Several hundred parsecs of intercloud medium may undergo such transition within a few times  $10^7$  years. Under these circumstances,  $\rho$  may be much larger than in the isothermal case at the position of the valleys. How much denser the condensations may become can be answered only by solving the problem formulated in Appendix A of Paper I.

Appealing as the above scenario may be, the difficulty still remains that if a flux tube close to the x-axis is only slightly deformed, then only a small increase in density (if any) will result. Therefore, for a "phase transition" to occur close to the galactic plane, the gas density in the initial state must be close to the critical value. Although this

cannot be excluded from observations, such an assumption would severely restrict the theoretical appeal of the original, general proposition, that the magnetogravitational instability might lead to denser condensations if a non-isothermal equation of state is used.

d. The effect of cosmic rays.

i. Modification of the instability criterion.

In his stability analysis of the stratified initial state Parker (1966) studied the effect of cosmic rays by assuming that

$$\beta \equiv P_{cr}/P = \text{a constant.} \quad (48)$$

The cosmic rays tend to destabilize the system. On the one hand they increase the initial growth rate of an unstable perturbation, and on the other hand they decrease the critical wavelengths for the instability.

The new instability criterion is

$$\lambda_x > \Lambda'_x \equiv 4 \pi H_t \left[ \frac{\alpha \gamma}{2(1+\alpha+\beta-\gamma)(1+\alpha+\beta) - \alpha \gamma} \right]^{1/2} \quad (49a)$$

$$\lambda_y > \Lambda'_y(\lambda_x) \equiv \Lambda'_x (1 - \mu^2)^{-1/2}, \quad (49b)$$

where  $\mu = \Lambda'_x / \lambda_x < 1$ , and the combined ("total") scale height of the gas, field, and cosmic rays in the stratified initial state is given by

$$H_t = (1 + \alpha + \beta) C^2/g. \quad (50)$$

The quantity  $\gamma$  is defined by  $\gamma = d \ln P / d \ln \rho$ . (Note that eqs. [49a] and [49b] reduce to eqs. [31] and [32] of Paper I if  $\gamma = 1$  and  $\beta = 0$ . Parker [1969a] argued on observational grounds that  $\beta$  is close to unity.)

It is straightforward to understand why the cosmic-ray gas has a destabilizing effect. Under small-amplitude deformations of the field lines the volume of a flux tube remains fixed in the special geometry under consideration (Parker 1966; Ames 1973). From the discussion of

§ IVA2, it follows that not only is the cosmic-ray pressure constant on a field line, but it is also a constant of the motion for small-amplitude disturbances. As field lines deform, in order to equalize their pressure along field lines, some cosmic rays "squirt out" of the valleys, where the cross section of flux tubes decreases. Then the already inflated portions of field lines expand further not only because of the magnetic forces there (see § VA1), but also because of the gradient of the cosmic-ray pressure normal to the field lines. With the additional driving force due to cosmic rays the instability proceeds at a faster rate. Also, because cosmic-ray pressure gradients aid the magnetic pressure forces against the tension of the field lines, smaller horizontal wavelengths may become unstable.

ii. Formulation of an equilibrium problem.

In our calculations of final equilibrium states of the gas and field in a galactic gravitational field, we ignored cosmic rays consistently. We did so for several reasons. First, the study of the nonlinear interaction between magnetic, gravitational and pressure forces is involved enough without additional complications. Second, uncertainties in the origin and in the rate of production and "destruction" (or, loss) of cosmic rays render any adopted relation between  $P_{cr}$  and  $n_{cr}$  that is supposed to remain valid for about  $10^7$  years a matter of faith or personal bias as much as a matter of "observational evidence." Finally, the cosmic rays are not necessary for driving the magnetogravitational instability. The physics of the instability and of the final equilibrium states becomes better understood if complications are introduced in some hierarchical order of importance.

Parker (1965a, 1968b) suggested that the presence of cosmic

rays precludes the existence of equilibrium states. If such is the case, the practical importance of our solutions would be reduced considerably. They would represent only the states toward which the system may tend after the "bubbles" of cosmic rays and magnetic fields may break off and leave the galactic disk, as described by Parker.

[Nevertheless, the predictions made on the basis of the equilibrium states (§ VB2) would still be the only ones available for an interstellar medium in which the magnetogravitational instability develops.] Clearly, Parker's arguments warrant a critical evaluation.

The conclusion that cosmic rays may cause an unlimited inflation of the field lines depends crucially on two assumptions. First, some field lines protrude from the surface of a conducting galactic disk into a vacuum region. Second, a copious supply of cosmic rays within the disk keeps their pressure fixed in all protruding flux tubes at all times. The first assumption does not apply to the problem at hand: the gas density decreases exponentially with altitude, and there is no "surface" with protruding field lines. As for Parker's second assumption, it is very difficult to determine with direct arguments whether in a real galaxy the cosmic-ray pressure is a constant of the motion. It is clear, however, that the cosmic-ray pressure within a flux tube, which undergoes considerable expansion in  $10^7$  years (the e-folding time for the magnetogravitational instability), will decrease unless a source supplying cosmic rays copiously in this flux tube is available. Although such sources might be available close to the Galactic plane, it is doubtful that they exist at altitudes larger than a scale height. An examination of figs. 2b and 2c of Paper I shows that these are the altitudes at which the highly deformed flux tubes lie. These flux tubes are the first whose expansion



will be limited by the increasing curvature of the field lines, possibly leading to equilibrium states.

In what follows we shall assume that the total number (rather than the pressure) of cosmic rays in each flux tube remains fixed (or at least quasi-steady) over  $10^7$  years or so, and we shall explore the consequences of this assumption. Since protons whose energies exceed a few Gev contribute most of the cosmic-ray energy, we consider all cosmic rays as highly relativistic and we relate their pressure, mass density, and number density by (see eqs. [16] - [18])

$$P_{cr} = \rho_{cr} C_{cr}^2 = b n_{cr}^{4/3}, \quad (51)$$

where  $b$  is a positive constant.

We may proceed in a manner identical to that of § VB1 to prove the following equilibrium theorem. If the magnetic field lines are held down by the gas in two regions separated by a horizontal distance  $\lambda_x$ , then a quasi-steady number of cosmic rays in each flux tube will not cause an unlimited inflation of the field lines in the space between the two gas condensations. The tension of the field lines eventually exceeds the cosmic-ray pressure gradients.

Equation (41) shows that the tension force varies as  $h^{-2}$ . The cosmic-ray pressure varies as

$$P_{cr} \propto n_{cr}^{4/3} \propto v^{-4/3} \propto h^{-4/3}; \quad (52)$$

so that its gradient normal to the field lines is

$$|\vec{\nabla}_\perp P_{cr}| \propto h^{-7/3}. \quad (53)$$

Therefore, the ratio of the (confining) tension of the field lines to the (expansive) cosmic-ray forces varies as

$$\frac{|B^2(\partial\hat{s}/\partial s)|}{4\pi |\vec{\nabla}_\perp P_{cr}|} \propto h^{+1/3}, \quad (54)$$

revealing that the inflation of field lines will eventually stop (qed).

A "typical" field line in a final equilibrium state is expected to deform in such a manner that its radius of curvature,  $R$ , is comparable to the horizontal wavelength of the magnetogravitational instability corresponding to the maximum growth rate, that is,  $R \sim \lambda_x \sim 1$  kpc. Only then will the tension of the field lines stop the inflation. Thus, the above equilibrium theorem would provide for a fat radio disk of half-thickness  $\sim 1$  kpc in a quasi-steady state.

The compression of the field at the valleys of the field lines might lead one to expect that the synchrotron emission will be larger there than in the wings of a condensation. We recall, however, that the maximum field at the valleys is larger than that at the wings by less than a factor of 2, and that  $B$  decreases with  $y$  faster at the valleys than at the wings (for example, see fig. 3). When this is combined with our suggestion that, at equilibrium, cosmic rays will "squirt out" of the valleys in order to equalize their pressure along field lines, it follows that the expected contrast in synchrotron emission between valleys and wings will be reduced and, perhaps, even be inverted (in galaxies seen nearly face-on, of course). Quantitative estimates may be obtained by solving the equilibrium problem which we now formulate.

We collect the MHS equations describing the system consisting of a highly conducting, isothermal gas, a large-scale magnetic field, and a hot and tenuous ( $\rho_{cr} \rightarrow 0$ ,  $C_{cr} \rightarrow \infty$ ) cosmic-ray gas in a (known) galactic gravitational field (see § IVA):

$$-\vec{\nabla}P - \vec{\nabla}P_{cr} - \rho\vec{\nabla}\psi + \vec{j} \times \vec{B}/c = 0 \quad (55)$$

$$\vec{B} \cdot \vec{\nabla} P_{cr} = 0 \quad (56)$$

$$P = \rho C^2 \quad (57)$$

$$P_{cr} = b n_{cr}^{4/3} \quad (58)$$

$$\vec{\nabla} \times \vec{B} = (4 \pi/c) \vec{j} \quad (59)$$

$$B = \vec{\nabla} \times \vec{A} \quad (60)$$

Note that the quantity  $\vec{j}$  has a contribution from the cosmic rays (see eqs. [21c], [21d], and [65]). We are faced with a system of six equations with seven unknowns! Even worse, of the six equations only five express relations among the seven unknowns; eq. (56) merely states that  $P_{cr}$  is constant on a field line, that is

$$P_{cr} = P_{cr}(A) ; \quad (61)$$

but it does not specify the value of this constant, which is different on different field lines. In going from the MHD to the MHS equations we have lost some equations, which are satisfied identically for static conditions with no bulk motions. These are eq. (5), expressing conservation of mass for the thermal gas, and eqs. (9) and (19), which describe the assumption that the thermal gas and the cosmic ray gas are tied to the magnetic field. To solve the MHS equations one must relate first  $P$  and  $P_{cr}$  on the one hand with  $B$  (or,  $A$ ) on the other. Ad hoc assumptions have been made by other workers at this point (for example, Parker 1968a, 1968b). We shall proceed in a methodical manner, as in § II of Paper I.

We adopt the two-dimensional geometry used by Parker (1966) - see § VA1, and Paper I. We define a scalar function of position,  $q(x,y)$ , by

$$q = P \exp(\psi/C^2), \quad (62)$$

and we write eq. (55) in terms of  $A$ ,  $q$ , and  $P_{cr}$  as

$$j \vec{\nabla} A / c = \exp(-\psi/C^2) \vec{\nabla} q + \vec{\nabla} P_{cr}. \quad (63)$$

By taking the inner product of both sides of eq. (63) with  $\vec{B}$  and by using eqs. (24) and (56) we find that

$$P \exp(\psi/C^2) \equiv q = \text{constant on a field line} = q(A). \quad (64)$$

If we consider the components of both sides of eq. (63) in a direction normal to the field, it follows that

$$\begin{aligned} \frac{j}{c} &= \exp(-\psi/C^2) \frac{dq}{dA} + \frac{dP_{cr}}{dA} \\ &= (j_{gas} + j_{cr})/c. \end{aligned} \quad (65)$$

Now we may write eq. (59) in terms of  $A$ ,  $q$ , and  $P_{cr}$  by using eqs. (60) and (65):

$$\nabla^2 A(x,y) = -4\pi \left[ \frac{dq(A)}{dA} \exp(-\psi/C^2) + \frac{dP_{cr}(A)}{dA} \right]. \quad (66)$$

The solutions of eq. (66) represent equilibrium states of our system. To obtain such solutions one needs to know  $q(A)$  and  $P_{cr}(A)$ . Since neither of these functions is a constant of the motion in the nonlinear flow associated with the magnetogravitational instability, it is not legitimate to calculate (or to specify)  $q(A)$  and  $P_{cr}(A)$  in some initial state and then proceed to determine a final state characterized by the same  $q(A)$  and  $P_{cr}(A)$ . Both functions can and must be calculated from first principles given the manner in which field lines are loaded with thermal and cosmic-ray particles.

A final equilibrium state is accessible to the system evolving away from the stratified initial state only if it has the same mass and the same number of cosmic rays as the initial state in each of its

flux tubes. If we can formulate mathematically these two conservation laws and incorporate them into the MHS equations, it will be possible for a solution of eq. (66) to represent a final state that can be reached from the stratified initial state through continuous deformations of the field lines under flux-freezing; the missing link will have been provided and the system of equations (55) - (60) will have been closed.

We calculated  $q(A)$  in § IIb of Paper I. It is given by

$$q(A) = \frac{C^2}{2} \frac{dm(A)}{dA} / \int_0^X dx \frac{\partial y(x,A)}{\partial A} \exp\left[-\frac{\psi(x,A)}{C^2}\right], \quad (67)$$

where  $X \equiv \lambda_x/2$ , and all other symbols have their usual meaning. The integration is performed over  $x$  along a field line characterized by the value  $A$  of the magnetic potential. Since the mass-to-flux ratio,  $dm/dA$ , is a constant of the motion, we were permitted to calculate it in the initial state (see eq. [16] of Paper I). It is

$$\frac{dm(A)}{dA} = \frac{2 X \rho_i(0)}{B_i(0)} \left[ -\frac{A}{2 H_t B_i(0)} \right], \quad (68)$$

where the ("total") scale height,  $H_t$ , is given by eq. (50). Note that eq. (36), which relates  $P$ ,  $B$ , and  $A$  in the initial state, is slightly modified by the presence of cosmic rays. It becomes

$$\begin{aligned} P(y) &\equiv \frac{B^2(y)}{8 \pi \alpha} \equiv \frac{[-A(y)]^2}{32 \pi \alpha H_t^2} \equiv \frac{P_{cr}(y)}{B} = \frac{b}{B} [n_{cr}(y)]^{4/3} \\ &= \rho(0) C^2 \exp(-y/H_t). \end{aligned} \quad (69)$$

We may now calculate  $P_{cr}(A)$  in a similar manner. The total number of cosmic rays,  $\delta N_{cr}$ , in a length  $\lambda_x$  of a flux tube  $[A, A + \delta A]$  is, by definition,

$$\delta N_{cr} = \int_{-X}^{+X} dx \int_{y(x,A)}^{y(x,A+\delta A)} dy(x,A) n_{cr}[x,y(x,A)]. \quad (70)$$

We consider  $x$  and  $A$  as the independent variables. Since the integration over  $y$  is performed with  $x$  fixed, we may change variables from  $y$  to  $A$  by using the relation

$$dy = dA (\partial y / \partial A). \quad (71)$$

We eliminate  $n_{cr}$  in favor of  $P_{cr}$  by using eq. (58) and we perform the trivial integration over  $A$  to find that

$$\delta N_{cr}(A) = \left[ \frac{P_{cr}(A)}{b} \right]^{3/4} \delta A \int_{-X}^{+X} dx \frac{\partial y(x,A)}{\partial A}. \quad (72)$$

Solving eq. (72) for  $P_{cr}$  and taking the limit  $\delta A \rightarrow dA$  we obtain

$$P_{cr}(A) = b \left[ \frac{dN_{cr}(A)}{dA} / 2 \int_0^X dx \frac{\partial y(x,A)}{\partial A} \right]^{4/3}. \quad (73)$$

The quantity  $dN_{cr}/dA$  is easily calculated from the initial state since it is a constant of the motion (by assumption). We have

$$\begin{aligned} \frac{\delta N_{cr}}{\delta A} &= \frac{n_{cr,i}(y) \lambda_x \delta y}{B_i(y) \delta y} \\ &= \frac{2 X n_{cr,i}(y)}{B_i(0)} \left[ - \frac{A}{2 H_t B_i(0)} \right]^{-1} \\ &= \frac{2 X n_{cr,i}(0)}{B_i(0)} \exp(-3y/4 H_t) \left[ - \frac{A}{2 H_t B_i(0)} \right]^{-1} \\ &= \frac{2 X n_{cr,i}(0)}{B_i(0)} \left[ - \frac{A}{2 H_t B_i(0)} \right]^{3/2} \left[ - \frac{A}{2 H_t B_i(0)} \right]^{-1}. \end{aligned}$$

Thus, we may write

$$\frac{dN_{cr}(A)}{dA} = \frac{2 X n_{cr,i}(0)}{B_i(0)} \left[ - \frac{A}{2 H_t B_i(0)} \right]^{1/2}, \quad (74)$$

where the relations expressed by (69) have been used repeatedly.

Equations (67) and (73) state that the functions  $q(A)$  and  $P_{cr}(A)$ , although constant along a field line, respond to changes in the shape of field lines (and in the volume of a flux tube). They are prescriptions of how to calculate  $q$  and  $P_{cr}$  at equilibrium if the distribution of mass and cosmic rays in the various flux tubes is known now or was known at any time in the past.

The thermal gas and the cosmic-ray gas differ in an important way. Since the cosmic rays are not subject to the gravitational field of the galaxy, the gravitational potential does not appear in eq. (73). Although this expression for  $P_{cr}$  is valid only at equilibrium, the same expression may be used in a time-dependent problem if the speed of sound ( $C_{cr}$ ) in the cosmic-ray gas is considered as infinite (see discussion in § IVA2). Then, as  $A(x,y,t)$  changes in time because of deformation of the field lines, the cosmic-ray pressure equalizes "instantaneously" along a field line and its new value is determined only by the (new) "specific" volume of a flux tube, as shown by eq. (73).

Altogether, to find equilibrium states for our system, eqs. (66), (67), and (73) must be solved simultaneously under appropriate boundary conditions, such as those used in Paper I. We shall not solve this problem here, although the method used for solving the problem in the absence of cosmic rays may be used in this case as well with only a trivial modification.

We remark that the cosmic rays contribute a current density,  $j_{cr}$ , that acts in a direction opposite that of  $j_{gas}$  (at least for a configuration close to the stratified initial state). This is seen as follows. We

may write from eq. (69) that

$$P_{cr,i}(A_i) = \beta \rho_i(0) C^2 \left[ -\frac{A_i}{2 H_t B_i(0)} \right]^2 \quad (75)$$

Also, in the presence of cosmic rays eq. (15) of Paper I is

$$q_i(A_i) = \rho_i(0) C^2 \left[ -2 H_t B_i(0)/A_i \right]^{2(\alpha + \beta)} \quad (76)$$

Equations (75) and (76) show that  $dP_{cr,i}/dA_i$  and  $dq_i/dA_i$  have opposite signs ( $A_i$  is negative everywhere); hence,  $j_{gas}$  and  $j_{cr}$  do so as well (see eq. [65]). This is in conformity with one's intuition that cosmic rays should tend to expand the field lines and weaken the magnetic field.

e. A non-equilibrium initial state

The calculated final equilibrium states have a mass-to-flux ratio in each of their flux tubes characteristic of Parker's (1966) stratified initial state. We alluded in § VB3 that the magnetogravitational instability may develop in a rather different initial state. In fact, if spiral density shock waves (Fujimoto 1966; Roberts 1969; Shu et al. 1973; Woodward 1973) trigger the instability, the initial state is likely to be a non-equilibrium one even if the interstellar medium in the region between spiral arms could be represented by Parker's initial state. The study of spiral structure and galactic shocks is beyond the scope of this work (for an excellent qualitative exposition of our present day knowledge on this subject see Shu [1973]).

For the purposes of this discussion it is sufficient to state that the existence of a small-amplitude spiral density wave in the stellar disk of a galaxy may induce a shock front in the interstellar medium extending several kiloparsecs along the x-axis in the geometry which we have been using. The width of the shock layer along the z-axis is  $\sim 10^2$  pc. The



contrast in gas density between the postshock and preshock regions is usually less than 10 (even in the absence of a magnetic field) and is achieved within  $\sim 10^6$  years (for example, see Shu et al. 1972). Because the e-folding time for the magnetogravitational instability is  $\sim 10^7$  years, if galactic shocks are responsible for triggering the instability one must consider as an initial state a non-equilibrium state representative of conditions in the postshock region before vertical readjustment takes place. Since we have determined final equilibrium states by solving the MHS equations in a dimensionless form with  $\alpha$  of the initial state being the only free parameter in the equations (see Appendix C of Paper I), our results (for which  $\alpha = 1$ ) will change only insofar as in the postshock region  $\alpha$  may become different from unity. What the value of  $\alpha$  is in the interarm region is not known in reality. It seems reasonable to assume, however, that  $\alpha$  is only a fraction of unity there; otherwise the magnetogravitational instability would develop with  $\lambda_x \sim 1$  kpc and would lead to condensations such as the ones which we have calculated - and which have not been observed in the interarm region (at least not yet).

The compression in the galactic shock will increase such a weak  $\alpha$  by the same factor ( $\lesssim 10$ ) as the gas density (see below). So,  $\alpha$  is expected to be somewhat larger than 1 in the postshock region. This will lower the critical wavelength for the instability (see eq. [49]) - and will introduce a perturbation in the z-direction with wavelengths well below the range of the disruptive effects of differential rotation. The instability may be initiated in this manner.

We claimed in § VB2ai that the mechanism which periodically triggers the magnetogravitational instability also replenishes the high altitude gas in the Galaxy. A simple calculation illustrates this point. We ignore

the magnetogravitational instability and the effect of cosmic rays and we take  $\vec{B}$  to be parallel to the x-axis, as before. We consider a plane, isothermal shock in the (x,y)-plane with  $z > 0$  being the unshocked region. The gravitational field is that given by eqs. (31) and (32). In the unshocked region (state 1) the equilibrium quantities are

$$\rho_1(y) = \rho_1(0) \exp(-y/H_1) \quad (77a)$$

$$B_1(y) = B_1(0) \exp(-y/2 H_1) \quad (77b)$$

$$A_1(y) = -2 H_1 B_1(0) \exp(-y/2 H_1) \quad (77c)$$

$$H_1 = (1 + \alpha_1) C^2/g \quad (77d)$$

$$\alpha_1 = B_1^2/8 \pi \rho_1 C^2 = \text{a constant.} \quad (77e)$$

If adjustments in the vertical (y) direction are ignored for the moment, the (non-equilibrium) quantities behind the shock (state 2) will be related to those of state 1 by

$$\rho_2(y) = \kappa \rho_1(y) \quad (78a)$$

$$B_2(y) = \kappa B_1(y) \quad (78b)$$

$$A_2(y) = \kappa A_1(y) \quad (78c)$$

$$H_2 = H_1 \quad (78d)$$

$$\alpha_2 = \kappa \alpha_1 \quad (78e)$$

Equation (78b) follows from  $B_2/\rho_2 = B_1/\rho_1$ , which is valid for one-dimensional compression (for example, see Spitzer 1968a), and eq. (78a). To arrive at eq. (78c) one simply uses the definition  $B = dA/dy$  for this geometry. Equation (78d) states that we have not allowed vertical re-adjustment yet, while eq. (78e) follows from (78a) and (78b) and the definition of  $\alpha$ . The constant  $\kappa$  is in the range [1, 10] and is determined

by the parameters of the gas flow in galactic shocks. With the field lines assumed to remain straight, the increase in  $\alpha$  indicated by eq. (78e) will lead to an expansion in the vertical direction. After such an expansion takes place the equilibrium quantities (state 3) may be written as

$$\rho_3(y) = \rho_3(0) \exp(-y/H_3) \quad (79a)$$

$$B_3(y) = B_3(0) \exp(-y/2 H_3) \quad (79b)$$

$$A_3(y) = -2 H_3 B_3(0) \exp(-y/2 H_3) \quad (79c)$$

$$H_3 = (1 + \alpha_3) C^2/g \quad (79d)$$

$$\alpha_3 = B_3^2/8 \pi \rho_3 C^2. \quad (79e)$$

Because mass (per unit length along  $z$ ) is conserved in going from state 2 to state 3, we must have that

$$\int_0^{\infty} dy \rho_2(y) = \int_0^{\infty} dy \rho_3(y).$$

Using eqs. (78a), (77a), and (79a) we may perform the integrations to find the relation

$$\kappa \rho_1(0) H_1 = \rho_3(0) H_3. \quad (80)$$

Since flux (per unit length along  $z$ ) is also conserved in the transition from state 2 to state 3, we may write that

$$-2 H_1 \kappa B_1(0) = -2 H_3 B_3(0),$$

or that

$$\kappa B_1(0) H_1 = B_3(0) H_3. \quad (81)$$

From eqs. (80) and (81) we obtain

$$\frac{B_3(0)}{\rho_3(0)} = \frac{B_1(0)}{\rho_1(0)}, \quad (82)$$

from which it follows that

$$\frac{\alpha_3}{\alpha_1} = \frac{\rho_3(0)}{\rho_1(0)} \quad (83)$$

We would like to determine  $B_3(0)$  in terms of  $\kappa$  and quantities characteristic of state 1 only. First we substitute the definitions of  $H_1$  and  $H_3$  (eqs. [77d] and [79d], respectively) in eqs. (80) and (81). The result is

$$\kappa [8 \pi P_1(0) + B_1^2(0)] = 8 \pi P_3(0) + B_3^2(0) \quad (84)$$

and

$$\kappa \frac{[8 \pi P_1(0) + B_1^2(0)]}{P_1(0)} B_1(0) = \frac{8 \pi P_3(0) + B_3^2(0)}{P_3(0)} B_3(0), \quad (85)$$

where

$$P_n = \rho_n C^2, \quad n = 1, 2, 3. \quad (86)$$

We solve eq. (85) for  $P_3(0)$  and substitute in (84) to obtain, after some algebra, the quadratic equation for  $B_3(0)$ :

$$B_3^2(0) B_1(0) + B_3(0) 8 \pi P_1(0) - \kappa [8 \pi P_1(0) + B_1^2(0)] B_1(0) = 0. \quad (87)$$

Reinstating  $\alpha_1$ , we find for the roots of (87)

$$\begin{aligned} \frac{B_3(0)}{B_1(0)} &= -\frac{1}{2\alpha_1} \pm \frac{1}{2\alpha_1} [1 + 4\kappa\alpha_1(1 + \alpha_1)]^{1/2} \\ &= +\frac{1}{2\alpha_1} \left\{ [1 + 4\kappa\alpha_1(1 + \alpha_1)]^{1/2} - 1 \right\}, \end{aligned} \quad (88)$$

where only the positive root was kept because the ratio  $B_3(0)/B_1(0)$  must be positive.

Using eqs. (81), (82), and (83) we find the following relations between the quantities of states 1 and 3:

$$\frac{H_3}{H_1} = \kappa \frac{\rho_1(0)}{\rho_3(0)} = \kappa \frac{B_1(0)}{B_3(0)} = \kappa \frac{\alpha_1}{\alpha_3} = \frac{2 \kappa \alpha_1}{[1 + 4 \kappa \alpha_1 (1 + \alpha_1)]^{1/2} - 1} \equiv f(\kappa, \alpha_1). \quad (89)$$

We note that

$$\lim_{\alpha_1 \rightarrow 0} f(\kappa, \alpha_1) = 1, \quad (90)$$

that is,  $H_3 = H_1$ . This is as it should be since in the absence of a magnetic field the scale height is determined only by the temperature of the gas and the gravitational field. On the other hand we have that

$$\lim_{\kappa \rightarrow 1} f(\kappa, \alpha_1) = 1; \quad (91)$$

when there is no compression there is no change.

The limit of very strong fields is of interest. We find that

$$\lim_{\alpha_1 \rightarrow \infty} f(\kappa, \alpha_1) = \kappa^{1/2}, \quad (92)$$

showing that the increase in the scale height that would result, if vertical relaxation without "buckling" of the field lines took place, varies only as the square root of the initial increase in gas density.

For a reasonable range of parameters, that is,

$$3 \leq \kappa \leq 10 \quad \text{and} \quad 0.2 \leq \alpha_1 \leq 1,$$

eq. (89) yields that

$$H_3/H_1 = 1.25 - 2.5. \quad (93)$$

This is the basis of our suggestion that galactic shocks not only may trigger the magnetogravitational instability, but they may also replenish

the high altitude interstellar gas. Of course, if this is the manner in which the instability is initiated, the field lines will deform and gas will drain into the valleys of the field lines at the same time that a general vertical expansion may take place. The instability may proceed at a faster rate because of the external driving force provided by virtue of the fact that the initial state (state 2) is not an equilibrium one. The magnetic stresses, that led to the onset of the instability in the first place, are relieved by the inflation of the field lines with the result that the mean magnetic field along the x-axis behind the shock increases much less than eq. (78b) would predict. This may have some bearing on the predictions of the intensity of synchrotron radiation in spiral arms (see Paper II).

## VI. SELF-GRAVITATING INTERSTELLAR CLOUDS

A. Non-Magnetic Clouds: A Summary

The calculations of Bonnor (1956) and Ebert (1955, 1957) on bounded, isothermal, gaseous spheres led to a criterion for gravitational collapse. The total Mass ( $M$ ) of a cloud must exceed a critical value, which is a function of the cloud temperature ( $T$ ) and the external pressure ( $P_0$ ), namely,

$$M > M_c = 1.2 \frac{c^4}{(G^3 P_0)^{1/2}} \quad (94)$$

where the isothermal speed of sound in the cloud is

$$c = (k T / \mu m_H)^{1/2} \quad (95)$$

The quantity  $k$  is the Boltzmann constant,  $m_H$  is the mass of a hydrogen atom, and  $\mu$  is the mean mass per particle in units of  $m_H$ . To account for the cosmic abundance of helium, one takes

$$\mu = 1.27 \text{ in H I clouds } (n_{\text{He}}/n_{\text{H}} = 0.1); \quad (96a)$$

$$= 2.33 \text{ in molecular clouds } (n_{\text{He}}/2n_{\text{H}_2} = 0.1). \quad (96b)$$

[Often we shall not distinguish among molecular, dark and dust clouds, to which we shall refer collectively as "dense clouds". Their relatively high densities and masses and their low temperatures ensure that they are self-gravitating. Their differences (for example, see Zuckerman and Palmer, 1974) are not relevant in the present discussion.] For conditions typical of H I clouds ( $T \approx 50^\circ\text{K}$ ) and of dark clouds ( $T \approx 10^\circ\text{K}$ ), and for a "standard" intercloud pressure<sup>5</sup> ( $P_0 \approx 1800 \text{ k}$ ), we find that

5. The precise physical parameters of the intercloud medium (see § IIA1) are more important in the context of the present discussion than they

$$M_c \approx 740 M_\odot \text{ for H I clouds;} \quad (97a)$$

$$\approx 8.8 M_\odot \text{ for dark clouds.} \quad (97b)$$

Since individual H I clouds with masses larger than  $10^3 M_\odot$  are rare (Spitzer 1968a), one might conclude that the upper limit on cloud masses is set by the Bonnor-Ebert critical mass. Then, clouds observed to have masses larger than  $M_c$  must, of necessity, be collapsing. Observations relate a different story. Massive H I clouds may not even be self-gravitating because they are not usually dense enough. In those cases in which gravitation is important, turbulence and magnetic fields could aid in supporting a cloud, so that masses larger than  $M_c$  may not be collapsing (Mestel 1965; Spitzer 1968b). But even if the Bonnor-Ebert predictions were in perfect agreement with observations of H I clouds, the conclusions drawn would be very misleading. The scarcity of atomic-hydrogen clouds with masses larger than  $10^3 M_\odot$  has a plausible explanation unrelated to gravitational collapse. Massive clouds may become dense enough to shield their interiors from ultraviolet radiation, thus allowing atomic hydrogen to be converted to molecular hydrogen on the surfaces of grains (for details of this process see Solomon and Wickramasinghe 1969; Hollenback and

---

5.(contd) were in our discussion of non-gravitating condensations. Direct observational evidence sets a lower limit on the intercloud temperature ( $\gtrsim 1000^\circ\text{K}$ ) on the grounds that the intercloud medium is not seen in 21-cm absorption (for example, see Clark 1965), although Colvin et al. (1970) and Hughes et al. (1971) find somewhat smaller lower limits (300 - 800°K). An upper limit ( $\lesssim 4000^\circ\text{K}$ ) is set by the measured widths of 21-cm emission lines (Heiles 1968). However, Field (1973) used the observations of Radhakrishnan et al. (1971), which show no line widths less than 8 km/sec, to conclude that the intercloud temperature is  $\approx 8000^\circ\text{K}$ . He also noted that observations of extinction in the solar neighborhood indicate that the density of dust in the intercloud medium is  $\lesssim 1\%$  of that in clouds. Assuming that the dust-to-gas ratio is fixed, he arrived at a density for the intercloud gas  $\lesssim 0.2 \text{ cm}^{-3}$ . This yields  $P_0 \lesssim 1600 \text{ k}$ , a value not far from the "standard" one, which was derived theoretically (for example, see Spitzer and Scott 1969; Field et al. 1969; Hjellming et al. 1969).



Salpeter 1971; Hollenback, Werner and Salpeter 1971). As a consequence, a large fraction of the total mass of such clouds may be inaccessible to 21-cm observations.

Indeed, observational evidence (direct and indirect) has shown that hydrogen in dense clouds is mainly in molecular form and that  $n_{\text{H}_2}$  is in the range  $10^3 - 10^4 \text{ cm}^{-3}$  in most cases (see reviews by Carruthers 1970; Heiles 1971; Zuckerman and Palmer 1974). Other typical parameters of dark clouds are  $M \gtrsim 100 M_{\odot}$ ,  $D(\text{diameter}) \approx 1 \text{ pc}$ ,  $\sigma_v$  (velocity dispersion) =  $\Delta v$  (full line width at half maximum power/2.3)  $\approx 0.4 \text{ km/sec}$  and, as mentioned above,  $T \approx 10^\circ\text{K}$ . The discrepancy between observations and the Bonnor-Ebert predictions is more serious in this case: observed typical (not maximum) masses are at least a factor of 10 larger than  $M_c$ . If indeed some dark clouds have temperatures as low as  $5^\circ\text{K}$  (Heiles 1971), the discrepancy between observed and predicted masses will be at least as large as a factor of 40.

The possible presence of turbulence in dense clouds cannot by itself eliminate the discrepancy. It may increase by at most a factor of 2 the effectiveness of the thermal energy in balancing the gravitational energy in the virial theorem because supersonic turbulence dissipates rapidly in shocks (for example, see Mestel 1965). In terms of eq. (94),  $M_c$  may increase by at most a factor of 4. If the measured line widths are attributed solely to turbulent velocities, the resulting Mach numbers are usually larger than 2. Even if the scale ( $L$ ) of a turbulent element were as large as the radius of a dark cloud, the dissipation time ( $L/\sigma_v$ ) would be less than or equal to the free-fall time (Mestel and Spitzer 1956; Field 1973). One is left with the disquieting responsibility of specifying how turbulence is regenerated over such a short time scale.

The problem of finding a suitable means of supporting a dense cloud against self-gravitation is alleviated if one postulates that such clouds are not in equilibrium. Bulk radial motions (collapse or expansion) have been invoked to explain the large widths of spectral lines in dense clouds (Shu 1973b; Liszt et al. 1974; Goldreich and Kwan 1974; Scoville and Solomon 1974)<sup>6</sup>. Expansion may take place after a cloud collapses and the newborn stars form H II regions. In general, the pressure of an H II region exceeds that of the surrounding neutral matter, whose density is comparable to that of the H II region but whose temperature is considerably lower. [An excellent review of the dynamics of the expansion of H II regions is given by Spitzer (1968a, 1968b).] Since the expansion of clouds follows star formation in their interiors, expansion is not relevant to the problem at hand, namely, the determination of critical values for the physical parameters of a cloud that may lead to formation of stars in the first place. We shall find below that the Bonnor-Ebert critical mass is indeed an underestimate because of the presence of magnetic fields. Thus, some of the dense clouds which are now thought to be collapsing may not be doing so. But even if all dark clouds are collapsing, the argument that this would imply an unsavory high rate of conversion of interstellar matter into stars may be invalid because star formation may be an inefficient process (see § VIIF3).

In order to include the magnetic field properly in the picture, we must reexamine the assumption of flux-freezing because the length scales which concern us here are two to three orders of magnitude smaller than those relevant in the discussion of § V.

---

6. The subject of providing a theoretical explanation for the observed line widths is very controversial. We shall discuss it in § VII in the light of our equilibrium solutions for self-gravitating, magnetic clouds.

B. Flux-Freezing in Dense Clouds

Although the decay time of the magnetic field due to Ohmic losses in cool, dense clouds ( $T \sim 10^4 K$ ,  $L \sim 1$  pc) is longer than  $10^{17}$  years (see formula in § IIID, footnote 2), the diffusion of the ionized component and the field through the neutral matter may be important (Mestel and Spitzer 1956). The characteristic diffusion time over a scale  $L$  is

$$\tau_D \approx \frac{L}{|\vec{v}_i - \vec{v}_n|}, \quad (98)$$

where  $\vec{v}_i - \vec{v}_n$  is the relative velocity between ions and neutrals. In a quasi-steady state, this is estimated by balancing the magnetic forces, which drive such motion because they act directly only on the ionized matter, with the drag provided through collisions with the neutral matter:

$$\rho_i |\vec{v}_i - \vec{v}_n| / \tau_s = |-\vec{\nabla}_\perp (B^2/8\pi) + B^2 \partial \hat{s} / 4\pi \partial s|. \quad (99)$$

In eq. (99), the magnetic force has been decomposed into a pressure part and a tension part in the usual manner. The quantity  $\tau_s$  is the "slowing-down" time for an ion (usually carbon in H I clouds, and hydrogen in dense clouds) in a field of neutrals (predominantly hydrogen). It is given by (see Spitzer 1968a, p. 92)

$$\begin{aligned} \frac{1}{\tau_s} &= \frac{m_n}{m_i} \frac{1}{\tau_{coll.}} \\ &= \frac{m_n}{m_i} n_n \sigma_{in} \bar{v}_{in}, \end{aligned} \quad (100)$$

where  $\sigma_{in}$  is the ion-neutral collision cross-section and  $\bar{v}_{in}$  ( $\sim C$ ) is the mean random speed of neutrals relative to the ions. Thus, the diffusion time becomes

$$\tau_D = \frac{L n_i n_n m_n \sigma_{in} \bar{v}_{in}}{|-\vec{\nabla}_\perp (B^2/8\pi) + B^2 \partial \hat{s} / 4\pi \partial s|}. \quad (101)$$

Spitzer (1968a, p. 240) calculates  $\tau_D$  for an infinite cylinder of gas threaded by a magnetic field parallel to the axis of symmetry. He assumes that the density is uniform and that magnetic forces balance the gravitational forces in the lateral direction. The result is

$$\tau_D = \frac{\sigma_{iH} \bar{v}_{iH}}{2\pi G m_H} \times \frac{n_i}{n_H} \times (1 + 4 n_{He}/n_H)^{-2}. \quad (102)$$

With  $T = 50^\circ\text{K}$  (that is,  $\bar{v}_{iH} \approx 1 \times 10^5$  cm/sec),  $m_i = 12 m_H$ ,  $\sigma_{iH} \approx 2 \times 10^{-14}$  cm<sup>2</sup>, and accounting for the cosmic abundance of helium, this is

$$\tau_D \approx 5 \times 10^{13} n_i/n_H \text{ years}. \quad (103)$$

Since  $n_i/n_H \gtrsim 5 \times 10^{-4}$  in H I clouds, it follows that  $\tau_D \gtrsim 3 \times 10^{10}$  years. Hence, diffusion may be neglected.

The degree of ionization in dark clouds is probably somewhat smaller than  $10^{-5}$ ; if it were larger, long-range Coulomb collisions between electrons and H<sub>2</sub>CO molecules would excite the 6-cm line of H<sub>2</sub>CO and, thus, would quench the anomalous cooling of this line -- contrary to many observations (see, for example, Zuckerman and Palmer 1974). In typical ( $T \sim 10^\circ\text{K}$ ) dark clouds, therefore, the diffusion time may become as small as  $10^8$  years. This is still much larger than free-fall times at typical dark-cloud densities ( $\tau_{ff} \sim 10^6$  years). We may, therefore, still assume that the magnetic field is frozen in the matter.

Nakano and Tademaru (1972) calculated in detail the degree of ionization in dense clouds of uniform density. At  $n_H > 10^3$  cm<sup>-3</sup>, for the massive, spherical cloud which they considered ( $M = 10^4 M_\odot$ ), ions are contributed by hydrogen due to ionization by cosmic rays and <sup>40</sup>K radioactivity, and by heavy elements due to ionization by X-rays with energy greater than 1 keV. They concluded that, in a collapsing cloud, the diffusion time for

the magnetic field becomes comparable to the free-fall time if  $n_H \gtrsim 2 \times 10^9 \text{ cm}^{-3}$ . This is a significant result, but it is valid only as an order-of-magnitude estimate because (i) spherical contraction is an unlikely possibility in the presence of a magnetic field; (ii) a self-gravitating (let aside a collapsing) cloud cannot possibly maintain a uniform density; and (iii) it is not clear a priori that the tension of the field lines (which was neglected) will be smaller than the magnetic pressure gradients in a highly compressed cloud with a frozen-in field connected smoothly to the field of the surrounding medium. At any rate, the question of how in the first place a cloud can contract to such a high density in the presence of a frozen-in field (and, possibly, rotation) is still one of the outstanding theoretical problems associated with star formation. It is this pre-collapse stage that interests us here.

### C. Magnetic Clouds: Background

#### 1. The Problem of Angular Momentum and "Magnetic Braking"

If an interstellar cloud of typical dimensions rotates as slowly as to have always the same face turned toward the Galactic center (period  $\approx 2 \times 10^8$  years), it is impossible to contract axisymmetrically to stellar sizes while conserving its angular momentum. If that happened, the star that would form would have a period of rotation of about 5 minutes and the centrifugal forces would exceed the gravitational forces by about three orders of magnitude (Spitzer 1968a, p. 231).

It is, however, possible for a cloud to contract indefinitely while conserving its angular momentum if non-axisymmetric configurations are attained (Weber and Shu are investigating this process using the tensor virial theorem). To illustrate this point, we consider a cloud which is initially spherical with density  $\rho_1$ , radius  $R_1$ , and is rotating uniformly

with angular velocity  $\Omega_1$ . Its angular momentum is  $J = \frac{2}{5} MR_1^2 \Omega_1 = \frac{8\pi}{15} \rho_1 R_1^5 \Omega_1$ . If it attains a rod-like shape of uniform density  $\rho_2$ , radius  $r$  and length  $\ell$  ( $r \ll \ell$ ), it may rotate about an axis perpendicular to its axis of symmetry with angular velocity  $\Omega_2$  such that  $J = \frac{1}{12} M\ell^2 \Omega_2 = \frac{\pi r^2}{12} \rho_2 \ell^3 \Omega_2$ . The possibility arises that a cloud may contract without increasing its angular velocity (that is,  $\Omega_1 = \Omega_2$ ). Then,  $\rho_2/\rho_1 = \frac{32}{5} R_1^5/r^2 \ell^3$  and the density can increase arbitrarily as long as  $r$  remains much smaller than  $\ell$ . However, such a sequence of events can take place only if it satisfies the additional local constraints imposed by the force equation. Furthermore, such contraction would involve considerable compression of the interstellar magnetic field no matter what the relative orientation of  $\vec{J}$  and  $\vec{B}$  might be. It is, therefore, an unlikely possibility if the field is frozen in the matter, as the case seems to be.

Since the magnetic field is expected to thread both a cloud and the intercloud medium, the rotation of a cloud twists the field lines and generates Alfvén waves, that transport angular momentum. Mestel and Spitzer (1956) give the characteristic time for this process as roughly equal to the time it takes an Alfvén wave (of speed  $v_A$ ) to travel across the cloud (of radius  $R_{cl}$ ):

$$\tau_J \approx R_{cl}/v_A \quad (104)$$

More recent observations and calculations indicate a gas density in the intercloud medium typically two orders of magnitude smaller than that in clouds. The tenuous intercloud gas will tend to transport angular momentum less efficiently than eq. (104) implies, while, if the Alfvén speed in this medium is larger than in the cloud, it will tend to reduce  $\tau_J$ . Ebert et al. (1960; see Spitzer 1968a, p. 243) consider the simple

case of the uniform rotation of a spherical cloud (of density  $\rho_{cl}$ ) about an axis aligned with a uniform magnetic field, which threads both the cloud and the intercloud medium (of density  $\rho_{ic}$ ), which is initially at rest. The calculated decay time may be expressed as

$$\tau_J = \frac{8}{5} \frac{\rho_{cl}}{\rho_{ic}} \frac{R_{cl}}{v_A}. \quad (105)$$

It must be emphasized that  $v_A$  is the Alfvén speed in the intercloud medium ( $\approx 15$  km/sec at  $B = 3$   $\mu$ gauss and  $n = 0.2$   $\text{cm}^{-3}$ ). If  $R_{cl} \approx 5$  pc and  $\rho_{cl}/\rho_{ic} \approx 10^2$ , then  $\tau_J \approx 5 \times 10^7$  years, which is larger than the cloud free-fall time by a factor of 4.2 (for  $n_{cl} = 20$   $\text{cm}^{-3}$ ). We note, however, that  $\tau_J$  is considerably smaller in the case of dark clouds, which are usually surrounded by envelopes of matter of comparable density. For an order of magnitude estimate, we scale the magnetic field to dark-cloud densities ( $\sim 2 \times 10^3$   $\text{cm}^{-3}$ ) according to the relation  $B \propto \rho^\kappa$ , where  $1/3 \leq \kappa \leq 2/3$  (see § VIIF). Then,  $v_A$  decreases by at most a factor of 4.64 (for  $\kappa = 1/3$ , which is the worst case; if  $\kappa > 1/2$ ,  $v_A$  will increase upon contraction). Since  $\rho_{cl} \sim \rho_{ic}$  in this case and since  $R_{cl} \sim 1$  pc, we find that  $\tau_J \lesssim 5 \times 10^5$  years. It is not surprising that dark clouds do not exhibit appreciable rotation.

Even in the case of normal H I clouds,  $\tau_J$  must be smaller than that given by eq. (105). The region of the intercloud medium which is directly affected by the rotation of the cloud has a radius  $r_A > R_{cl}$  -- eq. (105) contains the implicit assumption that  $r_A = R_{cl}$ . This is so because field lines neighboring the equator of the cloud bend as the cloud rotates and set the intercloud gas into a rotational motion. Equation (105) should be multiplied by a factor  $R_{cl}/r_A$  ( $< 1$ ), where  $r_A$  is the distance from the axis of rotation at which the intercloud medium has received information

about the cloud's rotation in a time  $t$ ; that is,  $r_A \approx v_A t$ . Within a time as small as  $5 \times 10^6$  years, the intercloud medium within a radius of 75 pc from the cloud will be affected. There may exist an "Alfvén cylinder", the surface of which rotates at a speed equal to  $v_A$ . In such a case, and if corotation is established within the Alfvén cylinder, we would have that  $R_{cl}/r_A = v_{cl}/v_A$ , where  $v_{cl}$  is the speed of rotation at the cloud equator. Since observations limit  $v_{cl} < 1$  km/sec,  $\tau_J$  may have been reduced by more than a factor of 15, down to a few times  $10^6$  years. This possibility warrants a more careful investigation in the future.

It must also be emphasized that since observations show that the magnetic field is predominantly parallel to the Galactic plane, it is more likely that the axis of rotation of a cloud will be perpendicular to the field. With the field lines tied to the intercloud medium and the field frozen in the matter, corotation is unlikely in this case, and the magnetic braking of the cloud's rotation may be more effective than in the case in which  $\vec{J}$  was parallel to  $\vec{B}$ . It is possible that the magnetic field completely prevents the period of rotation of a cloud from falling below that of the Galactic rotation, so that there is no relative rotation between the cloud and the field. If that is the case, the equator of a cloud of radius 5 pc would rotate with a speed of only 0.16 km/sec. Observations do not exclude such motion.

In summary: in the absence of a magnetic field, the angular momentum problem may be bypassed by non-axisymmetric contraction. This is an unlikely evolutionary course in the presence of the interstellar field, which, however, may reduce the angular momentum of a cloud significantly in a time comparable to the free-fall time. Since flux-freezing appears to rest on solid foundations at least in the pre-collapse stage (and



possibly for some time after collapse sets in), the equilibrium and stability of magnetic clouds must be studied in greater detail.

## 2. Non-Equilibrium Calculations

### a. Mestel's Spherical Model

Mestel (1966) considered the spherical contraction of an isothermal cloud out of a background medium of uniform density,  $\rho_i$ , permeated by a uniform magnetic field  $B_i$ . He assumed that the density at a radius  $r$  is given by

$$\rho(r) = \rho_i + \rho_c \exp[-(r/r_0)^2] . \quad (106)$$

The quantity  $r_0$  is a radius beyond which  $\rho$  decreases rapidly to its background value, and the central density  $\rho(0) \approx \rho_c$  if  $\rho_c \gg \rho_i$ . Equation (106) is a legitimate assumption because this is not an equilibrium problem. The density having been specified, the magnetic field, which is assumed to be frozen in the matter during the spherical contraction, is uniquely determined. In spherical coordinates  $(r, \theta, \phi)$ , the field is given by

$$B_r = + B_i \cos\theta [\bar{\rho}(r)/\rho_i]^{2/3} , \quad (107a)$$

$$B_\theta = - B_i \sin\theta \frac{\rho(r)}{\bar{\rho}(r)} \left[ \frac{\bar{\rho}(r)}{\rho_i} \right]^{2/3} , \quad (107b)$$

where  $\bar{\rho}(r)$  is the mean density within a sphere of radius  $r$ . Mestel shows that near the center of the cloud ( $r \ll r_0$ ), one has that  $\rho \sim \bar{\rho}$ , so that the field is nearly uniform and equal to  $B_i (\bar{\rho}/\rho_i)^{2/3}$ . In the intermediate region  $1 \ll r/r_0 \ll (\rho_c/\rho_i)^{1/3}$ , the field is almost radial ( $B_\theta \ll B_r$ ) except at  $\theta \approx \pi/2$ . At larger radii,  $r/r_0 \gg (\rho_c/\rho_i)^{1/3}$ ,  $\bar{\rho} \sim \rho_i$  and the field becomes uniform and equal to  $B_i$ .

The nearly radial field, which is solely the result of the imposed spherical contraction, causes large "pinching" forces at the equator -- so much so that magnetic forces much exceed gravitational forces. Mestel

argues that, if this configuration is achieved through rapid, violent contraction of the cloud, flux dissipation, reconnection and detachment of field lines will take place at the equator. He points out, however, that preferential flow of matter along field lines might prevent such configuration from being reached.

Perhaps the most significant result of this study is the derived criterion for lateral collapse. If the initial density, radius, and magnetic field satisfy the inequality

$$\frac{\rho_i r_0}{B_i} > (0.013/G)^{1/2} = 0.114 G^{-1/2}, \quad (108a)$$

the gravitational forces exceed the magnetic forces (at  $\theta = \pi/2$ ) so that further contraction will ensue. Equation (108a) may be written in the alternative form

$$\frac{M}{\Phi_B} > \left( \frac{M}{\Phi_B} \right)_{\text{crit.}} \equiv \left( \frac{M}{B_i \pi r_0^2} \right)_{\text{crit.}} = 0.152 G^{-1/2}. \quad (108b)$$

Evidently, eq. (108b) does not specify a critical mass (unlike eq. [94]); it defines a critical ratio of the total mass and the total flux of the cloud. It may also be considered as defining a critical ("Mestel") surface density for a given background field,  $B_i$ , namely,

$$m_M \equiv \left( \frac{M}{\pi r_0^2} \right)_{\text{crit.}} = 0.152 G^{-1/2} B_i. \quad (108c)$$

With  $B_i$  measured in  $\mu\text{gauss}$ , this is

$$= 1.75 \times 10^{-3} (B_i/3 \mu\text{gauss}).$$

If the background magnetic pressure is equal to the background gas pressure (not an unreasonable assumption for the intercloud medium), that is, if  $\alpha_0 = B_i^2/8\pi P_0 = 1$ , we may compare  $m_M$  with the Bonnor-Ebert critical surface density (see eq. [113] below). We find that

$$(m_M/m_{BE}) = 0.48. \quad (109)$$

This cannot be the case. One expects the critical surface density to be larger in the presence of a magnetic field. The sources of error are: (i) the collapse of the Bonnor-Ebert cloud is partly due to the external pressure, which was neglected in the magnetic case; (ii) the internal pressure of the magnetic cloud was also neglected. On the other hand, Mestel's non-equilibrium configuration actually antagonizes the collapse because of the greater distortion suffered by the field lines compared to the case in which preferential flow along the field takes place.

We note that the collapse criterion (eq. [108b]), in addition to being independent of the cloud temperature (by assumption), is also incomplete in the sense that it is a condition on the ratio of the total mass to the total flux of the cloud. It is clear, however, that the manner in which matter is distributed among the various flux tubes is crucial. For instance, we consider a non-magnetic cloud on the verge of collapse according to the Bonnor-Ebert criterion. We introduce a magnetic field such that a flux  $\phi_B$  threads the cloud. If all field lines are confined to a thin shell at the surface of the cloud (while the interior is field-free), the cloud can still collapse. If, however, the same flux is distributed over a thin cylinder through the center of the cloud, collapse will be impossible. A complete criterion for the collapse of a magnetic cloud should depend on the mass-to-flux ratio in each of the flux tubes threading the cloud as well as on the cloud temperature and the external pressure.

#### b. Strittmatter's Spheroidal Model

Strittmatter (1966) studied the contraction of a magnetic cloud through the scalar and tensor virial theorems (Chandrasekhar and Fermi 1953). The tensor virial theorem shows that the magnetic field is somewhat more effective in preventing the collapse of a cloud than the scalar virial

theorem would indicate. In the case of a highly flattened cloud, however, the two theorems give identical results. The critical mass of such a spheroid is  $(8/3\pi^2)^{1/2}$  (= 0.52) times that of a sphere of the same mass and flux.

Strittmatter assumed that the shape of the cloud remains spheroidal during contraction (the cloud is oblate with its axis of symmetry parallel to the magnetic field) and that the density and the magnetic field remain uniform inside the cloud. The density outside the cloud is assumed negligible and the magnetic field uniform at infinity. He required the continuity of only the normal component of the field across the cloud surface. (In the case of a dipole field, he showed that requiring continuity of the tangential component of the field increases the effectiveness with which the field provides support against gravity; specifically, the magnetic energy increases by about a factor of 2.) With the internal and external pressures neglected, no "equilibrium" is possible for a highly flattened cloud if

$$\frac{M}{\Phi_B} > \left( \frac{M}{\Phi_B} \right)_{\text{crit.}} = \left( \frac{40}{27 \pi^4} \frac{1}{G} \right)^{1/2} = 0.123 \text{ G}^{-1/2}, \quad (110a)$$

or

$$\frac{M}{\pi r_0^2} > m_S = 0.123 \text{ G}^{-1/2} B_i. \quad (110b)$$

If we measure  $B_i$  in  $\mu\text{gauss}$ , eq. (110b) becomes

$$m_S = 1.42 \times 10^{-3} \left( \frac{B_i}{3 \mu\text{gauss}} \right).$$

The critical surface density is somewhat smaller than Mestel's (eq. [108c]). In view of the different methods employed to arrive at the two results, it is reassuring that they differ by only a factor of 1.26. Yet, it is disturbing that the non-magnetic Bonnor-Ebert calculations give a more

stringent criterion for collapse (see eq. [109]). One suspects that exact equilibrium calculations will fair better in this respect.

Strittmatter took great care in applying the virial theorem. However, because many misapplications are frequently made, a comment is in order (see also Mestel 1965, and Strittmatter 1966).

c. A Comment on the Virial Theorem

With the inertial term neglected, the virial theorem expresses a necessary (but not sufficient) integral condition which the various forms of energy present in the system must satisfy at equilibrium. By virtue of the fact that the details of the mechanical balance of forces are washed out, the virial theorem is particularly suited for the study of systems whose details are either not known or too complicated to study through the force equation. Almost by definition then, the time-independent form of the virial theorem, which is strictly correct only for a system at equilibrium, is applied to simple non-equilibrium configurations thought to approximate the real system in an "average" sense. Qualitatively erroneous conclusions may be reached unless one proceeds with care. The calculation of the critical mass for gravitational collapse of a cloud in the presence of a magnetic field is a classic example where the virial theorem is misapplied.

Consider a massive, spherical, isothermal cloud of uniform density threaded by a magnetic field which is uniform in all space. Let the cloud be embedded in a medium of uniform pressure and negligible density. If the mass of the cloud exceeds some critical value depending on the cloud temperature and the external pressure, the virial theorem will suggest that the cloud should collapse. This conclusion is independent of the magnitude of the magnetic field since the volume and surface

magnetic terms in the virial theorem cancel each other exactly -- this is as it should be because the magnetic force  $\vec{j} \times \vec{B}/c$  vanishes everywhere for a uniform field. The field could very well have been of infinite strength! Clearly, a small contraction of the cloud normal to the field will bend the field lines and, for a strong field, will induce currents that will cease further lateral deformation -- contrary to the conclusion reached on the basis of the (misapplied) virial theorem.

### 3. Equilibrium Calculations

It is not an easy task to construct equilibrium configurations of magnetic clouds. Strittmatter (1966, p. 360) described the difficulties very eloquently:

"...The absence of spherical symmetry renders the determination of the gravitational potential a matter of considerable complexity, unless the mass distribution is of a special form (e.g. a uniform spheroid or a set of spherical shells of constant density). A further complication is introduced by the requirement that the magnetic field link smoothly with an external force-free field. Equilibrium models are thus difficult to construct, homologously contracting models about equally so; nonhomologous contraction is almost impossible to study in detail except in special non-magnetic cases..."

These are the difficulties in solving the problem. In actuality, the greatest difficulty arises in formulating a well-posed, self-consistent problem including flux-freezing. Once a problem is posed, to obtain a solution by analytical, quasi-analytical, or numerical techniques (the search degenerating in that order) is usually only a matter of time.

Before we pose and solve the complete problem, we summarize the few

existing equilibrium calculations.

a. A Thin Disk with a Magnetic Field Parallel to its Axis

The equilibrium in a direction parallel to the axis of symmetry of an isothermal, gaseous, self-gravitating disk having an infinite radius and a density independent of radial distance (Spitzer 1942; Ledoux 1951; Spitzer 1968a) remains unaffected by the introduction of a uniform magnetic field parallel to the symmetry (z-) axis. Field (1969) considered the effect of a constant external pressure on the equilibrium in the z-direction. He found that, as the surface density ( $m_s$ ) increases while the external pressure ( $P_o$ ) remains fixed, the thickness of the disk ( $\Delta z$ ) first increases, reaches a maximum

$$\Delta z_{\max} = 1.32 \frac{c^2}{(2 \pi G P_o)^{1/2}} = 0.53 \frac{c^2}{(G P_o)^{1/2}}, \quad (111)$$

and then decreases. The surface density at maximum thickness is

$$m_{s,\max} = 3.04 \left( \frac{P_o}{2 \pi G} \right)^{1/2} = 1.22 \left( \frac{P_o}{G} \right)^{1/2}. \quad (112)$$

This "maximum" surface density that can still be in equilibrium at an external pressure  $P_o$  is somewhat smaller than the corresponding Bonnor-Ebert value, which is

$$\begin{aligned} m_{BE} &\equiv \frac{M_c}{\pi R_c^2} = \frac{5}{\pi} \left( \frac{P_o}{G} \right)^{1/2} = 1.59 \left( \frac{P_o}{G} \right)^{1/2} \\ &= 1.92 \times 10^{-3} \left( \frac{P_o}{1800 \text{ k}} \right)^{1/2} \text{ gm/cm}^2. \end{aligned} \quad (113)$$

The diameter,  $D_c$ , of a Bonnor-Ebert sphere at the verge of collapse is given by

$$D_c = 2R_c = 0.98 \frac{c^2}{(G P_o)^{1/2}}. \quad (114)$$

The fact that  $\Delta z_{\max} < D_c$  and  $m_{s,\max} \lesssim m_{BE}$  reflects the effect of the gravitational field due to the mass of the disk exterior to a radius  $\approx \Delta z_{\max}/2$ . Although the "critical" surface densities  $m_{s,\max}$  and  $m_{BE}$  are nearly equal, qualitatively different effects develop in each case if these values are exceeded. In the Bonnor-Ebert case, a sphere with surface density greater than  $m_{BE}$  collapses, whereas in the one-dimensional geometry the thickness of the disk should merely decrease. It is well known that one-dimensional collapse of an isothermal gas is impossible because the pressure force normal to a thin sheet increases as  $(\Delta z)^{-1}$ , while the gravitational force is independent of  $\Delta z$ .

Strictly one-dimensional calculations parallel to the magnetic field cannot possibly provide any information on magnetic phenomena. So, Field (1969) explored the assumption that a disk of finite radius  $R_0 \approx \Delta z_{\max}$  will actually collapse if  $\Delta z = \Delta z_{\max}$ . This led to a critical mass smaller than the Bonnor-Ebert value, given by eq. (94). That being impossible, the need to account quantitatively for the role of the magnetic field in the equilibrium of interstellar clouds became imperative.

b. An Infinite Cylinder Aligned with the Magnetic Field.

A cold, gaseous, infinite cylinder with a frozen-in field parallel to its axis may exist in mechanical equilibrium, in which the magnetic pressure gradients balance the gravitational forces in the radial direction. We consider an initially uniform density,  $\rho_i$ , and a uniform field,  $B_i$ . After gravitational forces are "switched on", the equilibrium density is given by (see Field 1973)

$$\rho(r) = \rho(0) J_0(kr), \quad (115)$$

where

$$k = \frac{4\pi\rho_i}{B_i} G^{1/2}. \quad (116)$$



Since the radius of the cylinder is defined by  $J_0(kR) = 0$ , it follows that

$$\begin{aligned} R &= 2.4/k \\ &= 2.4 \frac{B_i}{4\pi\rho_i} G^{-1/2} \end{aligned} \quad (117)$$

If we take  $B_i = 3 \mu\text{gauss}$  and  $\rho_i = 2 \times 10^{-24} \text{ gm/cm}^3$  ( $\approx$  the mean interstellar density), we find that

$$R \approx 370 \text{ pc}, \quad (118)$$

a value too large to be of practical significance. Although larger values of  $\rho_i$  will yield proportionally lower values of  $R$ , it is not legitimate to proceed in that manner because the frozen-in field ( $B_i$ ) must increase by the same factor as the density in eq. (117). On the other hand, smaller radii cannot be achieved by considering a finite cylinder and allowing compression along its axis followed by lateral contraction due to the increased gravitational forces. Field pointed out that a cylinder of finite length will transform into a disk under the effect of self-gravitation. What, then, accounts for the apparent elongation of dark clouds along the field (Shajn 1955)?

Of 31 clouds studied, Verschuur (1970a) finds that the relative angle between the field and the largest dimension of a cloud is less than  $10^\circ$  in 16 cases, less than  $40^\circ$  in 21 cases, and larger than  $40^\circ$  only in 10 cases. It must be noted, however, that the field direction, with which the cloud elongation was compared, is that given by the theoretical model of Mathewson (1968) which is in conflict with the recent Faraday rotation observations of Wright (1973) and Manchester (1974) -- see discussion in § IIIC.

If a cloud is not self-gravitating, we can understand its possible

elongation along the field, especially if it is in a region in which the magnetogravitational instability develops. Under the action of the galactic gravitational field the cloud will be stretched along the magnetic field lines. Also, if conducting matter is deposited in a particular flux tube at a pressure higher than that of the ambient medium, it can expand more easily along the field than across it. If, however, a cloud is known to be self-gravitating and to be aligned with the magnetic field, and if no rotation about an axis normal to the field and no internal source of energy (for example, H II regions) are observed, rather than abandoning our faith in Newton's second law, we may have to re-evaluate our ideas and confidence in the methods used for inferring the direction of the interstellar magnetic field.

c. An Axisymmetric Model without Flux-Freezing.

D. A. Parker (1973) constructed equilibrium solutions for a self-gravitating, isothermal cloud ( $M = 10^3 M_{\odot}$ ,  $T = 75^{\circ}\text{K}$ ) surrounded by a hot and tenuous H II region of pressure  $2.37 \times 1800 \text{ k}$ . An axisymmetric magnetic field permeates both media and is both force-free and curl-free in the H II region and uniform at infinity. Solutions with  $B_{\infty} = 0.25, 1.0, \text{ and } 2.0 \text{ } \mu\text{gauss}$  are obtained. The normal and tangential components of the field are continuous across the cloud boundary, but the field is not frozen in the matter. Consequently, although a solution satisfies the MHS equations and the boundary conditions (and an ad hoc assumption<sup>7</sup> made in order to close the MHS equations), neither the magnetic flux threading the cloud nor the manner in which it is distributed can be

7. D. A. Parker's assumption that  $\lambda \equiv f = \text{const.}$  in his eq. [13] can easily be shown to imply the requirement that the current density at equilibrium be given by  $j_{\phi}/c = -\lambda r \rho$ , where  $\rho$  is the gas density; we use cylindrical coordinates ( $r, \phi, z$ ). This is too stringent a condition on the admissible solutions.

known before a solution is actually at hand. Even then, knowledge of the magnetic flux provides little useful information because the field can slip through the cloud, or the field lines may reconnect just to allow force balance if the cloud is thrown out of equilibrium. In fact, in some of D. A. Parker's equilibrium configurations, field lines close to the equator form closed loops already. Thus, the effectiveness of the magnetic field in preventing gravitational collapse cannot be quantified from such equilibrium calculations.

The problem was formulated in spherical coordinates  $(r, \theta, \phi)$  in terms of the gravitational potential,  $\psi$ , and the magnetic stream-function,  $\Psi$ . [The magnetic field is given by  $B_r = -(r^2 \sin\theta)^{-1} \partial\Psi/\partial\theta$ ,  $B_\theta = (r\sin\theta)^{-1} \partial\Psi/\partial r$ .] The method of solution was a variation of the "self-consistent field" iterative method of Ostriker and Mark (1968). A mathematical sphere is chosen so as to surround the cloud. The Poisson equation for  $\psi$  and the Poisson-like equation for  $\Psi$  are solved within the sphere once an initial guess of the density and the cloud boundary is made. The force equation (actually, the Bernoulli constant) is then used to obtain a new density, thus permitting continuation of the iteration process. Solutions of the homogeneous equations outside the sphere are matched to the interior solutions so that the magnetic field is continuous across the boundary. Since the potentials are valid only within the sphere circumscribing the original cloud configuration, significant errors are introduced if the cloud becomes very flattened. Another source of inaccuracy is the choice of spherical coordinates, which are not particularly suited for flattened objects. Nevertheless, the results do exhibit some of the qualitative features which are expected of magnetic clouds.

The cloud flattens along the magnetic field, the more so the stronger

the background field ( $B_\infty$ ) is. The isodensity contours behave likewise. The choice of the initial parameters, however, is such that the magnetic pressure is negligible or small compared to the gas pressure in the surrounding medium. (In our notation,  $\alpha_0 \equiv B_\infty^2/8\pi P_\infty = 0.004, 0.064, 0.256$  in Parker's three cases.) Therefore, it is not surprising that in the computed equilibrium states the magnetic field at the center of the cloud is amplified by as much as a factor of 9.48 in one case without the magnetic forces becoming dominant. As it can be deduced from the maximum ratio of central to surface densities (= 4.34) achieved in any one of Parker's solutions, the external pressure is playing a significant (but not dominating) role compared to self-gravitation -- see discussion in § VII below. On the other hand, the internal pressure forces are comparable to gravitational forces but larger than the magnetic forces in the weak field ( $B_\infty = 0.25 \mu\text{gauss}$ ) case; pressure forces become more important in the case  $B_\infty = 2 \mu\text{gauss}$  because of flattening.

Parker found it necessary to exclude solutions with positive values of the arbitrary parameter  $\lambda$  (see his eq. [13]) because the central magnetic field pointed in an opposite direction from that of  $\vec{B}_\infty = \hat{e}_z B_\infty$ . In view of our remark above, that  $j_\phi/c = -\lambda r\rho$  (see footnote 7), we can understand this phenomenon. It is clear that once  $\vec{B}_\infty$  has been chosen to point along the +z-axis,  $j_\phi$  must be positive (that is,  $\vec{j}$  must point in the + $\phi$ -direction); if  $j_\phi$  is negative, Ampere's law implies that the field must be in the -z-direction at least on the axis of symmetry. Therefore, to preserve the direction of  $\vec{B}$ , the parameter  $\lambda$  must be negative.

D. A. Parker also considered uniform rotation (with angular velocity  $\Omega$ ) of the cloud about its axis of symmetry, which is aligned with the magnetic field. This is permissible because the density of the surrounding

H II region was assumed negligible. Although corotation of the field at infinity is not expected in practice, the results are instructive. As one could anticipate, rotation simply dilutes the gravitational potential only in the lateral direction by an amount  $r^2 \Omega^2/2$ , giving rise to flatter clouds and to field lines which are less distorted than in the case without rotation.

We do not think that Parker's results support his conclusion that "the magnetic field exerts strong pinching forces in a narrow equatorial region" (D. A. Parker 1973, p. 64). His Tables V, VI, and VIII show that, at the equator, the magnetic force is always smaller than the pressure force. The field lines formed neutral O-rings at the equator in some cases merely because flux-freezing, which would imply that the stream-function  $\Psi(r, z)$  is a single-valued function of  $r$  at a fixed  $z$ , was not imposed.

VII. NONHOMOLOGOUS CONTRACTION AND EQUILIBRIA OF  
SELF-GRAVITATING INTERSTELLAR CLOUDS EMBEDDED IN  
AN INTERCLOUD MEDIUM: FLUX-FREEZING

A. Formulation of the Problem

1. The Equilibrium Equations

The equilibrium of a self-gravitating, conducting, isothermal, gaseous cloud surrounded by an intercloud medium of qualitatively similar properties is described by the MHS equations:

$$-\vec{\nabla} P_k - \rho_k \vec{\nabla} \psi + \vec{j}_k \times \vec{B}/c = 0, \quad k = 1, 2; \quad (119)$$

$$\vec{\nabla} \times \vec{B} = (4\pi/c) \sum_{k=1}^2 \vec{j}_k \quad (120)$$

$$P_k = \rho_k C_k^2, \quad k = 1, 2; \quad (121)$$

$$\nabla^2 \psi = 4\pi G \sum_{k=1}^2 \rho_k. \quad (122)$$

All quantities have their usual meaning. The subscripts 1 and 2 refer to the cloud and intercloud media, respectively. Unlike we did in § V, in this section we consider the gravitational forces due to the gas only ( $\rho_* = 0$  in eq. [10]). Cloud and intercloud matter does not coexist in the same region of space (formally,  $f_1 \cap f_2 = 0$ , where  $f$  is the magnitude of any one of the subscripted quantities in eqs. [119] - [122]). The two media interact through their gravitational and magnetic fields as shown in the above equations and, in general, through pressure forces on their common boundary (see below). We note that eqs. (119)-(122) constitute a system of six equations with eight unknowns. Flux-freezing and conservation of mass that would close the system have not been imposed yet. We shall incorporate these conservation laws in our equations properly in § VIIA2.

It is convenient to introduce the magnetic vector potential, defined by eq. (13), that is,

$$\vec{B} = \vec{\nabla} \times \vec{A}, \quad (123)$$

because Maxwell's equation

$$\vec{\nabla} \cdot \vec{B} = 0 \quad (124)$$

is then satisfied identically.

We consider a three-dimensional geometry with axial symmetry about the z-axis. The z-axis may be thought of as running locally along a spiral arm and lying in the Galactic plane, although this is not essential. We use cylindrical coordinates  $(r, \phi, z)$  throughout this section. (To avoid confusion, we denote the position vector in spherical coordinates by  $\vec{x}$  and its magnitude by  $|\vec{x}|$ , which is distinguishable from the Cartesian coordinate  $x$ .) We choose the origin of coordinates at the center of the cloud so that there is reflection symmetry about the plane  $z = 0$ . Then we may consider only the right-half plane  $z \geq 0$ .

With  $\vec{B}$  being a poloidal and  $\vec{A}$  a toroidal vector, the scalar function  $\phi(r, z)$ , defined by

$$\phi(r, z) \equiv r A_{\phi}(r, z) \equiv r A(r, z), \quad (125)$$

is both constant on a magnetic surface as well as a constant of the motion (see § IVB2, eqs. [29] and [30]). We may, therefore, use  $\phi$  to label the magnetic surfaces once and for all. The intersection of a magnetic surface with the  $(r, z)$ -plane is referred to as a field line. Note that the magnetic field may be written in terms of  $\phi$  as

$$\vec{B} = -r^{-1} \hat{e}_{\phi} \times \vec{\nabla} \phi, \quad (126)$$

and that the magnetic flux ( $\phi_B$ ) through a contour of radius  $r$  is given by (see § IVB2)

$$\phi_B = 2 \pi \phi. \quad (127)$$

In each of the two media we define a scalar function of position,  $q_k(r, z)$ , by

$$q_k = P_k \exp(\psi/C_k^2), \quad k = 1, 2; \quad (128)$$

and we write eq. (119) in terms of  $\phi$  and  $q_k$  as

$$j_k \nabla\phi/cr = \exp(-\psi/C_k^2) \nabla q_k, \quad k = 1, 2. \quad (129)$$

By what is now a familiar procedure, we may show that

$$P_k \exp(\psi/C_k^2) \equiv q_k = \text{constant on a field line} = q_k(\phi), \quad k = 1, 2; \quad (130)$$

and that

$$\frac{j_k}{cr} \exp(\psi/C_k^2) = \frac{dq_k(\phi)}{d\phi}, \quad k = 1, 2; \quad (131)$$

where we have used the fact that  $\nabla q_k$  is toroidal, and we have defined  $j_k \equiv (j_\phi)_k$ . The meaning of eqs. (130) and (131) is analogous to that of equations (8) and (9) of Paper I (see discussion following eq. [9] therein).

Using eqs. (123) and (131), eq. (120) becomes

$$\nabla \times \nabla \times \vec{A} = \hat{e}_\phi 4\pi r \sum_{k=1}^2 \exp(-\psi/C_k^2) \frac{dq_k}{d\phi}. \quad (132)$$

By expanding the left-hand side, we may write eq. (132) as

$$\frac{\partial}{\partial r} \left[ \frac{1}{r} \frac{\partial}{\partial r} (rA) \right] + \frac{\partial^2 A}{\partial z^2} = -4\pi r \sum_{k=1}^2 \exp(-\psi/C_k^2) \frac{dq_k(\phi)}{d\phi}. \quad (133)$$

This is to be solved simultaneously with eq. (122), which may be written in an expanded form as

$$\begin{aligned} \frac{1}{r} \frac{\partial}{\partial r} \left( r \frac{\partial \psi}{\partial r} \right) + \frac{\partial^2 \psi}{\partial z^2} &= 4\pi G \sum_{k=1}^2 C_k^{-2} q_k(\phi) \exp(-\psi/C_k^2) \\ &\equiv 4\pi G \rho. \end{aligned} \quad (134)$$

We have made use of eqs. (121) and (130) in eliminating  $\rho_k$  from the right-hand side of eq. (122). Equations (133) and (134) are coupled, nonlinear differential equations for  $\psi$  and  $\phi$ ; the quantity  $q_k$  ( $k = 1, 2$ ) has yet to be determined as a function of  $\phi$ . We shall retain  $A$ , instead of  $\phi$ , as



the dependent function in eq. (133) because it is convenient to work with a self-adjoint form of this equation -- transforming from  $A$  to  $\phi$  and vice versa through eq. (125) is a trivial matter. To complete the description of the cloud and intercloud media, we must calculate the functions  $q_k(\phi)$  in a manner consistent with conservation of mass and flux.

2. Calculation of the Functions  $q_k(\phi)$ ,  $k = 1, 2$ .

The cloud boundary may be specified uniquely by the function  $Z_{cl}(\phi)$ , which represents the projections onto the  $z$ -axis of the intersections of field lines and the cloud boundary (see fig. 7). This amounts to choosing a coordinate system  $(z, \phi)$ , whose advantage will become evident shortly. Then, half of the mass ( $\delta m_k$ ) of each medium in a flux tube between field lines characterized by  $\phi$  and  $\phi + \delta\phi$  is, by definition,

$$\delta m_k(\phi) = \int_{L_k(\phi)}^{U_k(\phi)} dz \int_{r(z,\phi)}^{r(z,\phi+\delta\phi)} dr 2\pi r \rho_k(r, z), \quad k = 1, 2. \quad (135)$$

Note that the integration over  $z$  is performed along the field line  $\phi$ , between the limits

$$\begin{aligned} L_k(\phi) &= 0, & \text{if } k &= 1; \\ &= Z_{cl}(\phi), & \text{if } k &= 2 \end{aligned} \quad (136a)$$

and

$$\begin{aligned} U_k(\phi) &= Z_{cl}(\phi), & \text{if } k &= 1; \\ &= Z_{max}(\phi), & \text{if } k &= 2. \end{aligned} \quad (136b)$$

If the system is assumed periodic in  $z$  with wavelength  $\lambda_z$ , then

$Z_{max} = \lambda_z/2$ . This would be the case if the contribution of the galactic gravitational potential were included in eq. (122). If the system extends to infinity, then  $Z_{max} = \infty$ .

Since the integration over  $r$  is performed keeping  $z$  fixed (see fig. 7), we may write

$$dr = d\phi \left( \frac{\partial r}{\partial \phi} \right) \quad (137)$$

and change variables from  $r$  to  $\phi$ . Using eqs. (121) and (130), we eliminate  $\rho_k$  in favor of  $\phi$  and we perform the trivial integration over  $\phi$  in eq. (135). We then solve for  $q_k(\phi)$  to find that

$$q_k(\phi) = \frac{C_k^2}{2\pi} \frac{dm_k(\phi)}{d\phi} \left/ \int_{L_k(\phi)}^{U_k(\phi)} dz r(z, \phi) \frac{\partial r(z, \phi)}{\partial \phi} \exp \left[ - \frac{\psi(z, \phi)}{C_k^2} \right] \right. \quad (138)$$

$k = 1, 2.$

The quantity  $r(z, \phi)$  refers to the  $r$ -coordinate of the field line  $\phi$  at  $z$ .

If we ignore conversion of one phase of matter into the other, the functions  $q_k$  ( $k = 1, 2$ ) are always given by eq. (138) in any equilibrium state of the system, since the mass-to-flux ratio,  $dm_k/d\phi$ , in each flux tube is a constant of the motion for each phase. If this quantity were known either through observations, or through a complete theoretical understanding of the mechanism which creates the interstellar flux, a unique equilibrium configuration for a dense cloud could be calculated by solving eqs. (133), (134), and (138) simultaneously, subject to appropriate boundary conditions (see below).

### 3. Approximate Description of the Intercloud Medium

The preceding formalism gives a general description of the intercloud medium. It takes account of the self-gravitation of the intercloud gas and it does not assume that the magnetic field is either force-free or curl-free. We shall not solve this general problem in this paper, although its solution is straightforward. As we shall see in § VIIF, there may be a need for the solution of this problem. Nevertheless, it seems

senseless to proceed in that direction without understanding first the effect of the following, somewhat simplified description of the intercloud medium on the equilibrium of a dense cloud.

Observations indicate that the intercloud medium is rather hot and tenuous compared to interstellar clouds (see § IIA1 and footnote 5 in § VIA). We shall, therefore, assume that

$$\rho_0 \equiv \rho_2 \rightarrow 0 \quad (139a)$$

and

$$C_0 \equiv C_2 \rightarrow \infty. \quad (139b)$$

Consequently, the intercloud medium is unaffected by the gravitational field of the cloud and the intercloud pressure is constant along field lines.

If we assume uniformity at infinity, it follows that

$$P_0 \equiv P_2 = \text{constant} \quad (140)$$

everywhere, and eq. (128) yields

$$q_0 \equiv q_2 = P_0, \quad (141)$$

so that

$$\frac{dq_0}{d\phi} = 0. \quad (142)$$

Thus, the contribution of the intercloud medium to the right-hand sides of eqs. (133) and (134) vanishes. The assumed poloidal field and uniformity at infinity render the rarefied (eq. [139a]) intercloud medium not only force-free, but current-free as well. In this approximation, the intercloud medium simply confines a dense cloud through pressure forces and exerts magnetic stresses at the cloud surface. Care must now be taken so that no infinite forces appear across the cloud surface.

#### 4. Continuity Conditions Across the Cloud Boundary

##### a. Gravitational Field

We write the Poisson equation in terms of  $\vec{g}$  as (see eq. [12])

$$\vec{\nabla} \cdot \vec{g} = -4\pi G \rho. \quad (143)$$

To show continuity of the component of  $\vec{g}$  normal to the cloud surface, we integrate over the volume of a "pill-box" of height  $h$  and surface  $\Delta S$ , parallel to the cloud surface, and we use Gauss' theorem to find

$$[g_n] \Delta S = -4\pi G \rho \Delta S h/2.$$

We take the limit  $h \rightarrow 0$  to obtain that

$$[g_n] = 0. \quad (144)$$

One proves the continuity of the component of  $\vec{g}$  tangent to the cloud surface by first noticing that eq. (12) implies that

$$\vec{\nabla} \times \vec{g} = 0. \quad (145)$$

An integration over an elemental surface having two sides parallel and two normal to the cloud surface and conversion into a line integral followed by the usual limiting process yields

$$[g_{tan}] = 0. \quad (146)$$

That the gravitational potential is also continuous across the cloud surface follows from

$$d\psi = \vec{\nabla}\psi \cdot d\vec{x} = -\vec{g} \cdot d\vec{x} \quad (147)$$

and an integration over a path with one end-point just inside and the second end-point just outside the cloud surface. Use is then made of eqs. (144) and (146) to obtain

$$[\psi] = 0. \quad (148)$$

b. Gas Pressure

The pressure of the intercloud medium is constant everywhere (see eq. [140]). If we let  $s$  denote distance along field lines, we may write the component of the force equation parallel to  $\vec{B}$  as

$$\frac{\partial P}{\partial s} = + \rho g_{\parallel} , \quad (149)$$

where  $g_{\parallel} = -\partial\psi/\partial s$ . There exists a jump in the right-hand side of eq. (149) across the cloud boundary, but it is finite because  $\vec{g}$  is continuous (see eqs. [144] and [146]) and  $[\rho]$  is bounded and equal to the cloud density at the surface,  $\rho_S$ . Therefore,

$$[P] = 0 \quad (150)$$

and we have as a consequence that

$$\rho_S = \frac{P_0}{C_1^2} . \quad (151)$$

Note that in deriving the condition (150) we made no assumption whatsoever about the angle at which field lines intersect the cloud boundary.

c. Magnetic Field

Our formulation of the problem in terms of the magnetic vector potential, rather than the magnetic field itself, guarantees the continuity of the component  $(B_n)$  of  $\vec{B}$  normal to the cloud surface (see eqs. [123] and [124]).

To show that the tangential component of  $B$  is also continuous, we first write the force equation as

$$-\vec{\nabla} \left( P + \frac{B^2}{8\pi} \right) + \rho \vec{g} + \frac{1}{4\pi} (\vec{B} \cdot \vec{\nabla}) \vec{B} = 0 .$$

We now take the dot product of the left-hand side with  $\delta\vec{x}$ , an infinitesimal

displacement from one side of the boundary to the other. In the limit  $\delta \vec{x} \rightarrow 0$ , we find [recall that  $\delta(\ ) = \delta \vec{x} \cdot \vec{\nabla}(\ )$ ]

$$\delta \left( P + \frac{B^2}{8\pi} \right) = \left[ P + \frac{B^2}{8\pi} \right] = 0, \quad (152)$$

where we have used the continuity of  $\vec{g}$  across the boundary and the fact that the jump in the gas density is finite. Because of eq. (150), it follows that

$$[B^2] = 0. \quad (153)$$

Since  $B^2 = B_n^2 + B_{\text{tan}}^2$  (where  $B_{\text{tan}}$  is the component of the field tangent to the cloud surface) and  $[B_n] = 0$ , eq. (153) implies that

$$[B_{\text{tan}}] = 0. \quad (154)$$

d. The Function  $q(\phi)$ .

It follows from the definition of  $q_k$  (eq. [128]) and eq. (141) that the discontinuity of  $q$  ( $\equiv q_1$  within and  $q_2$  outside the cloud) across the cloud surface is given by

$$[q] = P_0 \{ \exp(\psi_S/C_1^2) - 1 \}, \quad (155)$$

which is finite.

An important point must be evident by now. The formulation of the problem in terms of potentials, rather than the fields themselves, led to differential equations which have built-in all the necessary continuity conditions across the properly defined (by eq. [151]) cloud boundary. Hence, we do not need to solve the full equations within the cloud, the homogeneous equations outside, and then match the two solutions. It is now possible to solve the equations over a large region (which could be

infinite) surrounding the cloud and the relevant part of the intercloud medium. First we must specify the boundary conditions.

### 5. Boundary Conditions

Since  $\vec{A}$  is a vector with only a  $\phi$ -component and since we assumed axial symmetry, we must have that

$$A(r = 0, z) = 0; \quad (156)$$

otherwise its direction at  $r = 0$  would not be uniquely defined. Reflection symmetry about the plane  $z = 0$  implies that

$$\left. \frac{\partial A(r, z)}{\partial z} \right|_{z=0} = 0. \quad (157)$$

We require that  $\vec{B}$  be uniform at infinity and equal to  $\hat{e}_z B_\infty$ . In practice, "infinity" can be the surface of a large cylinder of radius  $R$  and half-height  $Z$ , such that  $R$  and  $Z$  are much larger than the size of the cloud.

Then we may write

$$A(R, z) = B_\infty R/2 \quad (158)$$

and

$$A(r, Z) = B_\infty r/2. \quad (159)$$

Once we have a solution at hand, we may easily investigate the effect of varying  $R$  and  $Z$ . (Instead of eq. [159] we could use periodic boundary conditions equally well, in which case  $\partial A / \partial z \big|_{z=Z} = 0$ . This would be the case if we considered the effect of the galactic gravitational field.)

Without the following being an independent boundary condition, we note that the total flux (divided by  $2\pi$ ) through the large cylinder of radius  $R$  is given by

$$\Phi_{\text{total}} = B_\infty R^2/2.$$

We also assume that on the surface of the large cylinder, centered about the cloud, the gravitational potential is that due to a point mass equal to the mass of the cloud ( $M$ ) and located at the origin of coordinates, that is,

$$\psi(R, z) = - \frac{GM}{(R^2 + z^2)^{1/2}} \quad (160)$$

and

$$\psi(r, Z) = - \frac{GM}{(r^2 + Z^2)^{1/2}} \quad (161)$$

Since the next term in a multipole expansion of the gravitational potential is the quadrupole one, the error due to this approximation is of order  $(R_i/R)^2$  in the case  $R = Z$ , where  $R_i$  is a representative dimension of the cloud. We simply have to choose a large enough  $R$  for sufficient accuracy.

The assumed reflection symmetry about the plane  $z = 0$  implies that

$$\left. \frac{\partial \psi(r, z)}{\partial z} \right|_{z=0} = 0 \quad (162)$$

Since the  $r$ -component of the gravitational field must vanish on the  $z$ -axis (this follows directly from eq. [143] by application of Gauss' theorem), we must also have that

$$\left. \frac{\partial \psi(r, z)}{\partial r} \right|_{r=0} = 0 \quad (163)$$

Having specified the boundary conditions, our problem is well-posed. We may solve it provided that we know the mass-to-flux ratio in each flux tube threading the cloud. To estimate this quantity, we shall make use of a reference state of the system.



### B. A Reference (Non-Equilibrium) State

The mass-to-flux ratio ( $dm/d\phi$ ) in a dense cloud may be obtained from high-resolution (albeit nonexistent) observations of the distribution of mass and flux within such a cloud. We hope that in the time elapsed since the publication of Paper I, where we pointed out how crucial the quantity  $dm/d\phi$  is in determining the accessible states (and, in part, the dynamics) of the interstellar gas, observers are putting some effort in this direction. In the meantime, we are forced to estimate  $dm/d\phi$  for a dense cloud relying mainly on a "principle of avoidance." Our estimate must be such that it avoids contradicting either any physical law, or whatever meager observational evidence might exist.

There is such a state readily available and, in fact, overused. Virtually all estimates of cloud parameters have relied on the assumptions that a cloud is spherical, of uniform density and, wherever a magnetic field is involved, it is also taken as uniform throughout. Clearly, this is not an equilibrium state for a self-gravitating, magnetic cloud. We shall use this state to calculate the mass-to-flux ratio both because it is a simple one and also because we would like to illustrate how different from this an equilibrium state actually is, even though the two have the same mass and the same flux. We assume that the mass-to-flux ratio of our system is the same as that of a spherical cloud of mass  $M$ , radius  $R_i$ , uniform density  $\rho_i$  and permeated by a uniform magnetic field  $B_i$ . The quantities  $\rho_i$  and  $B_i$  are not fundamental and we shall assume no particular values for them. However,  $R_i$  determines  $dm/d\phi$  in this geometry (see below). We easily obtain the various quantities in this state.

$$\text{Half the cloud mass} = M/2 = (2 \pi/3) \rho_i R_i^3 \quad (164)$$

$$\text{Total flux through the cloud} = \pi R_i^2 B_i = 2 \pi \phi_{cl} \quad (165)$$

We also have that

$$A_i(r) = B_i r/2, \quad (166)$$

so that

$$\Phi(r) = B_i r^2/2 = \Phi_B(r)/2 \pi. \quad (167)$$

The gravitational potential and field are continuous across the surface and are given by

$$\psi_i = -\frac{4\pi}{3} G \rho_i \left( \frac{3R_i^2 - |\vec{x}|^2}{2} \right), \quad |\vec{x}| \leq R_i; \quad (168a)$$

$$= -\frac{4\pi}{3} G \rho_i \frac{R_i^3}{|\vec{x}|}, \quad |\vec{x}| \geq R_i; \quad (168b)$$

and

$$g = -\frac{4\pi}{3} G \rho_i |\vec{x}|, \quad |\vec{x}| \leq R_i; \quad (169a)$$

$$= -\frac{4\pi}{3} G \rho_i \frac{R_i^3}{|\vec{x}|^2}, \quad |\vec{x}| \geq R_i, \quad (169b)$$

where  $|\vec{x}|$  is the radial distance in spherical coordinates ( $|\vec{x}|, \theta, \phi$ ).

The function  $q$  is

$$q_i = P_i \exp(\psi_i/C^2), \quad |\vec{x}| < R_i; \quad (170a)$$

$$= P_0, \quad |\vec{x}| > R_i; \quad (170b)$$

where  $\psi_i$  is given by eqs. (168a, 168b),  $C$  is the isothermal speed of sound in the cloud (we dropped the subscript since this is the only  $C$  present), and  $P_0$  is the intercloud pressure. As usually, we consider an isothermal equation of state

$$P_i = \rho_i C^2. \quad (171)$$

We note that  $q_i$  cannot be expressed as a function of  $\phi_i$  alone. This is

as expected because the reference state is not an equilibrium one.

We now calculate the mass-to-flux ratio in each flux tube. It is zero outside the cloud by assumption (see eq. [139a]). We have that

$$\begin{aligned} \frac{1}{2} \text{ mass in } (r, r+\delta r) &\equiv \delta m = 2\pi \rho_i \int_0^{z_{cl}} dz \int_r^{r+\delta r} dr r \\ &= 2\pi \rho_i r \delta r (R_i^2 - r^2)^{1/2}, \quad r \leq R_i; \end{aligned} \quad (172)$$

and that

$$\text{flux in } (r, r + \delta r) \equiv \delta \phi_B = 2\pi r \delta r B_i. \quad (173)$$

So, we recall eq. (127) to find

$$\delta \phi = B_i r \delta r. \quad (174)$$

Neither  $\delta m$  nor  $\delta \phi$  bear the subscript "i" (standing for "initial" state) because both quantities are constants of the motion by mass and flux conservation. Since the field lines are straight and parallel to the z-axis,  $\phi$  is a function of r alone and we may combine eqs. (172) and (174) to obtain the desired quantity  $dm/d\phi$ :

$$\begin{aligned} \frac{dm(\phi)}{d\phi} &= 2\pi \frac{\rho_i R_i}{B_i} \left(1 - \frac{\phi}{\phi_{cl}}\right)^{1/2}, \quad \phi \leq \phi_{cl} \\ &= 0, \quad \phi \geq \phi_{cl}; \end{aligned} \quad (175)$$

where  $\phi_{cl}$  is given by eq. (165).

Before solving our equations, we write them in a dimensionless form.

### C. The Dimensionless Problem

We measure the magnetic field in units of its value at infinity,  $B_i$ , and the gas density in units of its value in the spherical reference state,  $\rho_i$ . The unit of length is chosen as  $C/(4\pi G \rho_i)^{1/2}$ , which is related to the Jeans length in the reference state. Then the unit of time is fixed

by specifying the unit of speed as  $C$ , the isothermal speed of sound in the cloud. It follows that the units of various quantities of interest are:

$$\begin{aligned} \{P\} &= \rho_i C^2, & \{A\} &= CB_i / (4\pi G \rho_i)^{1/2}, & \{\Phi\} &= C^2 B_i / 4\pi G \rho_i, \\ \{M\} &= \rho_i C^3 / (4\pi G \rho_i)^{3/2}, & \{dm/d\Phi\} &= \rho_i C / B_i (4\pi G \rho_i)^{1/2}. \end{aligned} \quad (176)$$

### 1. The Basic Equations

In dimensionless form, our fundamental eqs. (133), (134), and (138) become

$$\begin{aligned} \frac{\partial}{\partial r} \left[ \frac{1}{r} \frac{\partial}{\partial r} (rA) \right] + \frac{\partial^2 A}{\partial z^2} &= - \frac{1}{2\alpha_i} r \frac{dq(\Phi)}{d\Phi} \exp(-\psi), \text{ inside;} \\ &= 0, \text{ outside;} \end{aligned} \quad (177)$$

$$\begin{aligned} \frac{1}{r} \frac{\partial}{\partial r} \left( r \frac{\partial \psi}{\partial r} \right) + \frac{\partial^2 \psi}{\partial z^2} &= q(\Phi) \exp(-\psi), \text{ inside;} \\ &= 0, \text{ outside;} \end{aligned} \quad (178)$$

$$\begin{aligned} q(\Phi) &= \frac{1}{2\pi} \frac{dm(\Phi)}{d\Phi} / \int_0^{z_{cl}(\Phi)} dz r(z, \Phi) \frac{\partial r(z, \Phi)}{\partial \Phi} \exp[-\psi(z, \Phi)], \text{ inside;} \\ &= P_o, \text{ outside,} \end{aligned} \quad (179)$$

where (see eq. [175])

$$\begin{aligned} \frac{dm(\Phi)}{d\Phi} &= 2\pi R_i \left( 1 - \frac{\Phi}{\Phi_{cl}} \right)^{1/2}, & \Phi &\leq \Phi_{cl}; \\ &= 0, & \Phi &\geq \Phi_{cl}, \end{aligned} \quad (180)$$

and  $\alpha_i$  is the (constant) ratio of the magnetic-to-gas pressures inside the cloud in the reference state, that is,

$$\alpha_i \equiv B_i^2 / 8\pi P_i. \quad (181)$$

The terms "inside" and "outside" stand for "inside the cloud" and "outside the cloud", respectively.

2. Boundary Conditions

It is straightforward to put the boundary conditions, expressed by eqs. (156)-(163), in dimensionless form. The result is

$$A(r = 0, z) = 0 \quad (182a)$$

$$A(R, z) = R/2 \quad (182b)$$

$$A(r, Z) = r/2 \quad (182c)$$

$$\left. \frac{\partial A(r, z)}{\partial z} \right|_{z=0} = 0 \quad (182d)$$

$$\left. \frac{\partial \psi(r, z)}{\partial r} \right|_{r=0} = 0 \quad (182e)$$

$$\left. \frac{\partial \psi(r, z)}{\partial z} \right|_{z=0} = 0 \quad (182f)$$

$$\psi(R, z) = - R_i^3 / 3(R^2 + z^2)^{1/2} \quad (182g)$$

$$\psi(r, Z) = - R_i^3 / 3(r^2 + Z^2)^{1/2} \quad (182h)$$

The dimensionless form of eq. (151), which specifies the location of the cloud boundary, is

$$\rho_S = P_0 \quad (183)$$

3. The Reference State

We write in dimensionless form some of the parameters calculated from the reference state for later convenience (see eqs. [164] - [170]):

$$M/2 = 2\pi R_i^3/3, \quad \phi_{cl} = R_i^2/2, \quad \phi_{total} = R^2/2 \quad (184)$$

$$A_i = r/2, \quad \phi_i = r^2/2 \quad (185)$$

$$\begin{aligned}\psi_i &= - (3 R_i^2 - |\vec{x}|^2)/6, & r \leq R_i; \\ &= - R_i^3/3|\vec{x}|, & r \geq R_i\end{aligned}\tag{186}$$

$$\begin{aligned}q_i &= \exp(\psi_i), & |\vec{x}| \leq R_i; \\ &= P_0, & |\vec{x}| > R_i.\end{aligned}\tag{187}$$

We express, for later reference, the initial gravitational energy ( $W_g$ ) of the cloud and the magnetic energy ( $W_m$ ) inside the cloud in units of the cloud thermal energy ( $U$ ). In terms of our dimensionless parameters, we find the following ratios:

$$|W_g| / U = (2/15) R_i^2 \tag{187-A}$$

and

$$W_m / U = (2/3) \alpha_i, \tag{187-B}$$

which provide a rough measure of the relative strength of gravitational, magnetic and pressure forces (cf. § VIC2c).

#### 4. Free Parameters

It is clear that there are three free parameters in the equations, namely,  $\alpha_i$ ,  $P_0$ , and  $R_i$ . We may understand this on physical grounds. The Bonnor-Ebert (non-magnetic) problem had only one free parameter related to the characteristic Jeans length. Such a dimensionless length is expected to appear in our case as well. A second free parameter expressing the relative strength of the magnetic and gas pressures in the intercloud medium at infinity must also exist. Let it be

$$\alpha_0 = B_i^2/8\pi P_0. \tag{188}$$

If the distribution of mass in the flux tubes threading the cloud (that is, if the function  $dm/d\phi$ ) were known through a detailed understanding

of the mechanism responsible for the generation of the interstellar field, the above two free parameters would be sufficient to categorize an equilibrium state of the system. Neither observations nor theoretical considerations can determine  $dm/d\phi$  at present. Hence, in reality, our problem contains two free parameters and a free function. It is only because of the simplifying assumption, that the system developed from an "initial" uniform state through continuous deformations of the field lines (under flux-freezing), that the free function may be specified by only one additional parameter.

For completeness, we note that if we had chosen as units of length and density the quantities  $C^2/(4\pi G P_0)^{1/2}$  and  $P_0/C^2$ , respectively,  $\alpha_0$  would have replaced  $\alpha_i$  in eq. (177) and  $P_0$  would have been replaced by unity in eq. (179). However,  $R_i$  would not have been sufficient by itself to specify  $dm/d\phi$ ; specification of the density of the reference state,  $\rho_i$ , would have been necessary (see eq. [175]). We choose to work with the set  $(\alpha_i, P_0, R_i)$  rather than  $(\alpha_0, \rho_i, R_i)$ . The external pressure  $P_0$  is directly related to forces at the cloud boundary; we may obtain equilibrium solutions in which the cloud has expanded or contracted relative to the reference, spherical state by simply choosing  $P_0 < 1$ , or  $P_0 > 1$ , respectively, if gravity is weak.

By definition, the parameters  $\alpha_0$ ,  $\alpha_i$ , and  $P_0$  are related:

$$\alpha_i = \alpha_0 P_0 . \quad (189)$$

Altogether then, the free parameters are  $R_i$  and any two of the three quantities in eq. (189).

#### D. Method of Solution

There were no analytical or numerical methods available to solve the simpler problem of Paper I. We could not expect that there would be any

for the present problem. Equations (177) and (178) are formally similar (but not identical) to eq. (C1) solved in Paper I. A similar approach suggests itself. However, we now face the complication that eqs. (177) and (178) must be solved simultaneously. To complicate matters further, the cloud boundary is not known in advance; it must, therefore, be treated as a free boundary. We found that no amount of advanced knowledge of mathematical and numerical techniques could help us. A method based on simple physical thinking worked. Its underlying ideas are as follows -- for further details, see Appendix A.

Guess a gravitational and a magnetic potential  $\psi$  and  $A$ , respectively, (and, therefore, a gravitational and a magnetic field). Distribute the matter in the various flux tubes within a (guessed) cloud boundary in such a manner (consistent with the conservation of the mass-to-flux ratio) that gravitational and pressure forces are in exact balance along field lines. In general, this distribution of matter will not be consistent with the guessed  $\psi$  or with the guessed cloud boundary. Calculate, therefore, the new  $\psi$  and the new cloud boundary implied by the new distribution of matter. Use the latest  $\psi$  and the latest distribution of matter to calculate the current density necessary to balance all forces in a direction perpendicular to field lines. This current density will not, in general, be consistent with the guessed set of field lines [ $\phi(r, z) = rA(r, z)$ ]. It (and the latest  $\psi$ ) must, therefore, be used to determine a new set of field lines. The entire process is repeated until the distribution of matter, the gravitational field, the current density, and the magnetic field are all mutually consistent and pressure equilibrium across the cloud boundary is satisfied.

In practice, the above iterative method of solution is unlikely to converge. It is necessary to introduce two independent relaxation para-



meters (see Appendix A), which provide a quantitative measure of how much better or worse the potentials of one iteration are compared with those of the previous iteration. In addition, to avoid violent oscillations of the cloud boundary, we introduced a third relaxation parameter. We shall refer to our method of solution as a "relaxation iterative procedure" (RIP) or, more specifically, as a "triple-relaxation iterative procedure" (TRIP) -- indicating the number of relaxation parameters involved.

### E. Equilibrium States

#### 1. A Preview of the Results

To span the entire three-parameter space of solutions is not only impossible, but also senseless. Physical considerations can limit the parameter space from the outset. Moreover, the behavior of solutions beyond a certain range of values of each of the three free parameters seems to introduce no new features.

The first physical consideration stems from our stated interest in star formation. Irrespective of the mechanism that may bring a cloud to a critical state, self-gravitation must become important if a cloud is to collapse. We, therefore, exclude from our present study the cases in which the mass-to-flux ratio is so small that gravitational forces play only a minor role in the equilibrium of a cloud. Nevertheless, we used these cases to test the accuracy of TRIP. A small enough  $R_i$  represents this class of cases. (Recall that the mass of the cloud is proportional to  $R_i^3$  while its flux varies as  $R_i^2$ ; so,  $M/\phi_{cl} \propto R_i$ ). Given an  $\alpha_i$  and a  $P_0$  (see eqs. [181], [171] and the unit of pressure in eq. [176]), we choose  $R_i$  small enough so that the equilibrium state is one of pure pressure balance between the cloud and the intercloud medium. The initial cloud boundary expands or contracts along field lines according to whether

$P_0 < 1$  or  $P_0 > 1$ , respectively; the magnetic field remains uniform everywhere. The location of the boundary may easily be calculated analytically. We found that the computed and calculated states differed by at most 1%. (For a more detailed discussion of numerical matters, see Appendix A.) Although some of these states represent a prolate (or, filamentary) distribution of matter about the magnetic field (which simply provides a rigidity to a filament with respect to changes in its shape) and may have some relevance to the interstellar medium (see discussion in § VIC3b), we shall discuss them no further in this work.

To study the effect of gravitational forces on the equilibrium states, we fixed  $\alpha_i$  and we chose  $P_0 \leq 1$ . Thus, with the intercloud pressure initially smaller than the cloud pressure, a cloud may contract with respect to the spherical reference state only as a result of self-gravitation. The larger  $R_i$  is, the more the cloud contracts, until an increase of  $R_i$  by as little as  $\approx 1\%$  yields no more solutions. For a given  $\alpha_i$  and  $P_0$ , we shall refer to such a state as a "critical" state for gravitational collapse, realizing that the true critical mass for the given flux and the given external pressure may actually be a few percent larger than the values determined in this manner -- if an equilibrium state is too close to the critical one, numerical noise may set it into collapse.

We studied the effect of the external pressure by fixing  $\alpha_i$  and  $R_i$  to such values that the cloud was hardly self-gravitating, and then we kept increasing  $P_0$  above unity. Gravitational forces came into play before long. There is, however, an important difference between equilibrium states with small and those with large external pressure that allows us to determine whether a dense cloud formed by slow accretion of matter or by an increase in the intercloud pressure (see § VIIF). If high resolution observations determine the detailed distribution of matter within a dense

cloud, our solutions suggest that we may discriminate between these two mechanisms of dense cloud formation on the basis of that observational evidence alone.

The useful range of free parameters with which we shall concern ourselves here is

$$0.2 \leq \alpha_i \leq 1.0, \quad 0.5 \leq P_0 \leq 4.9. \quad (190)$$

For most pairs of parameters  $(\alpha_i, P_0)$  studied, we kept increasing  $R_i$  until a critical state was determined. The value  $\alpha_i = 1.0$  is already large enough to reveal the behavior of solutions with  $\alpha_i \gg 1$ . Although eq. (189) and the range of values shown in eq. (190) imply that  $0.04 \leq \alpha_0 \leq 2.0$ , we only studied in detail those cases for which  $0.1 \leq \alpha_0 \leq 2.0$ . These values of  $\alpha_0$  are certainly representative of conditions in the intercloud medium as observations and theoretical considerations indicate at present.

The following are a few of our general conclusions to be discussed below. In all critical states determined, the cloud mass exceeds the Bonnor-Ebert value for a cloud of identical temperature and external pressure. A cloud flattens along the field before reaching a critical state; it is flatter the stronger the field. It is also flatter the larger the intercloud pressure. Compared to its value in the reference state,  $\alpha$  often decreases in the equatorial plane because of flattening. This suggests that the effect of the cloud pressure on the nonhomologous contraction and collapse of a cloud cannot be neglected, unlike the case of homologous contraction. Spherical contraction of a cloud as a whole in the presence of an interstellar field of reasonable magnitude has but an academic significance. So does homologous contraction.

The Bonnor-Ebert calculations have shown that a critical state is characterized by a ratio of the central-to-surface density always equal

to 14.3 regardless of the cloud temperature and the intercloud pressure. Our solutions show that the critical ratio  $\rho_c/\rho_s$  increases as  $P_0$  decreases; it also increases as  $\alpha_i$  increases. There are good physical reasons for this behavior and we shall discuss them below.

We now examine some of the equilibrium states in more detail. We use the dimensionless variables of § VIIC throughout, unless we note otherwise. We shall give a few examples in dimensional form at the end, where we shall also provide general conversion formulae and scaling laws.

## 2. Dependence on $R_i$

For a fixed pair of parameters  $(\alpha_i, P_0)$ , we determined equilibrium states for different values of  $R_i$ . This situation corresponds to a study of a collection of spherical clouds of constant (but unspecified) temperature, of uniform (but unspecified) density embedded in an intercloud medium, whose pressure is some fixed multiple ( $\approx 1$ ) of the initial cloud pressure, and threaded by a uniform (but unspecified) magnetic field. Each cloud has a different radius. We then release the clouds to reach mechanical equilibrium. We discard the ones with small enough radii for self-gravitation to be unimportant and we discuss representative ones among those which did not collapse.

We take the magnetic pressure to be initially half of the cloud pressure ( $\alpha_i = 0.5$ ) and the intercloud pressure to be somewhat smaller than the cloud pressure ( $P_0 = 0.9$ ). If it were not for self-gravity, a cloud with these parameters would expand along field lines. Figures 8a, 8b, and 8c exhibit three equilibrium states characterized by three different values of  $R_i$ , namely, 2.5, 2.7, and 2.8, respectively. Increasing  $R_i$  further by 2% gave no solution; the cloud collapsed for a large number of choices of relaxation parameters. The state  $R_i = 2.8$  will be referred

to as a critical state. Each ordinate represents radial distance from the axis of symmetry (z-axis), while each abscissa represents distance from the center of the cloud along the axis of symmetry. For ease in comparing an equilibrium state with the uniform reference state, we labeled both axes in units of  $R_1$ , the initial radius of the cloud in each of the three cases. The curves bearing arrows represent field lines; each is labeled by its r-coordinate in the corresponding reference state, in which field lines were straight and equidistant. The solid, oblate curves are isodensity contours and are labeled by the value of the density at equilibrium (in units of the uniform density,  $\rho_1$ , of the spherical reference state). The spacing ( $\Delta\rho$ ) between successive isodensity contours is fixed so that the distance between them is inversely proportional to the mean pressure gradient in the interval. The outermost curve represents the cloud boundary ( $\rho = P_0$  there). The dashed curves represent contours of equal magnetic-field strength. To avoid repeating the awkward term "equal-magnetic-field-strength contours", we shall refer to these curves as "isopedion" contours.<sup>8</sup> Figures 8a, 8b, and 8c (and all similar figures below) show only the immediate neighborhood of the cloud in each case because at distances larger than about  $2R_1$  from the cloud center the field is virtually uniform and within a few percent of its value at infinity.

One may take as a measure of the degree of flattening of a cloud the quantity

$$f \equiv z_{\max}/r_{\max}, \quad (191)$$

where  $z_{\max}$  is the maximum extent of the cloud along the z-axis and  $r_{\max}$  is the equatorial radius of the cloud at equilibrium. The flatter the

8. The term "isopedion" (pronounced isap'edion) derives from the Greek isos + pedion and translates literally into "of equal field [strength]."

cloud, the smaller  $f$  is. . . Several qualitative features of the solutions become evident by examination of figures 8a, 8b, and 8c.

As  $R_i$  increases, the cloud contracts further and further (compared with its corresponding spherical initial state). The magnetic field impedes contraction in the lateral direction. The flattening increases with increasing  $R_i$  and so does the central density and the central magnetic field. The isodensity contours are oblate, indicating the relative ease with which mass can slide along field lines than across them under flux-freezing. In fact, the isodensity contours are more oblate near the cloud center than they are at the boundary -- the more so the larger  $R_i$  is. The magnetic field strength has a maximum at the cloud center and a minimum at exactly the position of the equator ( $B_{\min} = 0.912, 0.793, \text{ and } 0.753$ , respectively, for each of the states of fig. 8). This is a general property of the solutions.

From the isodensity and the isopedion contours of each equilibrium state, one may estimate the ratio of the magnetic and gas pressures by using the expression

$$\alpha_f(r, z) = \alpha_i B_f^2(r, z) / \rho_f(r, z). \quad (192)$$

In the equatorial plane ( $z = 0$ ),  $\alpha_f$  has a maximum at  $r = 0$ . On the contrary,  $\alpha_f$  increases as  $z$  increases while  $r$  is kept fixed. The former behavior of  $\alpha_f$  reflects the relative ease with which matter slides along field lines, the most deformed of which occur at (very roughly)  $r \approx 0.6 R_i$ . The increase of  $\alpha_f$  with  $z$  is mainly due to the "unloading" of matter from the outlying portions of field lines under the action of the gravitational field of the cloud.

As  $R_i$  increases (and the gravitational forces become stronger),  $\alpha_f$  at the cloud center increases. In all cases, the general behavior of  $\alpha_f$

within the cloud is as described in the preceding paragraph. We note that  $\alpha_f$  at the cloud center has decreased below  $\alpha_i$  in each of the three states of fig. 8 (by 20.9%, 13.4%, and 0.1%, respectively). However, this is by no means a general phenomenon. If  $\alpha_i$  is chosen small enough,  $\alpha_f(0,0)$  is expected to increase because then  $B_f(0,0) \propto \rho_f(0,0)^\kappa$ , where  $\kappa \approx 2/3$ , so that  $\alpha_f(0,0) \propto \rho_c^{1/3}$ . (We shall discuss the exponent  $\kappa$  below. We have verified that  $\alpha_f(0,0)$  increases somewhat above  $\alpha_i$  in the case  $\alpha_i = 0.2$ .)

In figures 9a, 9b, and 9c, we plotted the dimensionless column (or surface) density of each of the above three states as a function of position. Column densities for two orientations of the line of sight are shown in each figure. (i) With a line of sight parallel to the axis of symmetry, an observer would see the column density  $\sigma_f(r)$  as he moves a telescope beam away from the cloud center. (ii) If the line of sight lies in the equatorial plane, one would observe the column density  $\sigma_f(z)$  for a similar motion of the beam. [The subscript f signifies a "final" (that is, equilibrium) state.] The column density  $\sigma_i$  of the corresponding spherical reference state is shown in each figure for comparison. [The subscript i signifies the reference ("initial") state.] We now compare figs. 9a, 9b, and 9c.

As  $R_i$  increases, the peak column density  $\sigma_f(r=0)$  increases, reflecting the larger lateral compression of the field by the stronger gravitational forces. Yet, the maxima of the curves  $\sigma_f(r)$  are relatively flat because the magnetic field resists compression in a direction normal to the field lines. At equilibrium, the fraction of the cloud mass found at large radii is relatively small; in particular, it is smaller than that predicted by the uniform initial state. The departure of the column density  $\sigma_f(r)$  of an equilibrium state from that of the corresponding uniform state is

solely due to compression normal to the field lines; one-dimensional contraction parallel to the field does not increase  $\sigma(r)$ .

The surface density as a function of  $z$ ,  $\sigma_f(z)$ , shows a higher as well as sharper maximum than  $\sigma_f(r)$ , indicating a larger compression parallel to field lines. The maximum value  $\sigma_f(z = 0)$  increases as  $R_i$  does; so does the ratio  $\sigma_f(z = 0)/\sigma_f(r = 0)$ , which provides another measure of the flattening of the cloud. At equilibrium, a considerably smaller fraction of the cloud mass exists away from the cloud center along the axis of symmetry than it did in the corresponding uniform state.

Figure 10 exhibits the functions  $q(\Phi)$  in each of the three states under consideration; they are plotted against the normalized flux  $\Phi/\Phi_{c\ell}$ . Since all three states have the same  $\alpha_i$  and  $P_0$ , each curve is labeled only by the value of  $R_i$  of the corresponding initial state. Note that  $\Phi_{c\ell}$  is different in each state because it depends on  $R_i$  (see eq. [184]). As  $R_i$  increases, the curve  $q(\Phi)$  suffers a downward shift. This is so because  $q$  depends exponentially on the gravitational potential (which becomes more negative as  $R_i$  increases) and only linearly on the pressure (see eq. [128]).

Before discussing the dependence of solutions on the external pressure, we point out that the critical state of fig. 8c has  $\rho_c/\rho_S = 15.9$ , a value larger than the Bonnor-Ebert critical ratio. We shall return to this point in discussing some general conclusions.

### 3. Dependence on $P_0$

How do the properties of equilibrium states vary as we increase  $P_0$  while keeping  $\alpha_i$  and  $R_i$  fixed? A series of solutions which differ only in  $P_0$  corresponds to equilibrium states of an initially spherical cloud of uniform (but unspecified) density, of constant (but unspecified)



temperature and of a fixed initial radius, threaded by a uniform (but unspecified) magnetic field which differ only by the value of the external pressure. We shall not discuss the case in which the intercloud pressure is smaller than the internal (cloud) pressure so that the cloud acquires a prolate shape by expanding along field lines. We choose  $R_1$  small enough ( $= 2.4$ ) so that gravitational forces are initially weaker than (internal) pressure forces (see eq. [187-A]), and we take as before  $\alpha_1 = 0.5$ .

Figures 11a, 11b, and 11c represent equilibrium states with  $P_0 = 1.9$ , 2.9, and 3.9, respectively. We could not obtain a solution with  $P_0 = 4.9$ . The isodensity and isopedion contours and the field lines are labeled as in figs. 8a, 8b, and 8c. Figures 11a, 11b, and 11c reveal the following variation of physical parameters as  $P_0$  increases. (i) The cloud contracts in such a manner that its oblateness increases. The degree of flattening (see eq. [191]) is  $f = 0.47$ , 0.40, and 0.34, respectively. (ii) The central density as well as the ratio of central density and surface density also increase ( $\rho_c = 7.32$ , 13.2, 31.1, and  $\rho_c/\rho_S = 3.85$ , 4.55, 7.97). (iii) The central magnetic field is enhanced further, while, on the contrary, the minimum value of the field at the cloud equator decreases ( $B_{\min} = 0.791$ , 0.557, 0.370). (iv) The ratio of the magnetic and gas pressures at the center increases [ $\alpha_f(0, 0) = 0.39$ , 0.45, 0.53], whereas at the equator it decreases [ $\alpha_f(r_{\max}, 0) = 0.165$ , 0.053, 0.017]. It is still the case that at a distance of about  $2R_1$  from the cloud center the magnetic field is nearly uniform and within a few percent of its value at infinity. The above dependence of the physical parameters of the cloud on  $P_0$  can be understood on physical grounds.

That the cloud should become flatter as the external pressure increases follows from the fact that along field lines the only opposing force is due to (internal) pressure gradients, while in the lateral direction

magnetic forces come into play. The increase in the central magnetic field and gas density with increasing  $P_0$  has as a primary cause the inevitable compression associated with the larger external pressure and as a secondary cause the stronger gravitational field, which the primary compression gives rise to. However, the increase in the ratio of the central-to-surface gas densities is a secondary effect entirely due to the presence of gravitational forces; such an increase in  $\rho_c/\rho_s$  does not appear if self-gravity is unimportant, in which case the (dimensionless) density is uniform inside the cloud and equal to  $P_0$ . Finally, the increase of  $\alpha_f$  with  $P_0$  at the cloud center is partly due to gravity.

If  $R_1$  is very small (so that gravitational forces are negligible), an increase in  $P_0$  results in a compression of the cloud along field lines. As a consequence,  $\alpha_f$  decreases everywhere inside the cloud (unless  $\alpha_i \ll 1$ ).

It is also reasonable that  $\alpha_f$  at the equator should decrease as the external pressure increases. This is a consequence of (i) the equality of (the dimensionless)  $\rho_s$  and  $P_0$  at equilibrium, and (ii) the decrease in  $B_{\min}$  (at the equator) which accompanies the larger distance between the field line just attached to the cloud equator and those outside the cloud (which have no mass loaded on them, so that they cannot but be "left behind" as the cloud contracts).

Figures 12a, 12b, and 12c exhibit the surface densities corresponding to the states of figs. 11a, 11b, and 11c, respectively. The curves are labeled as in figs. 9a, 9b, and 9c. It will suffice to remark that the variation of the surface densities  $\sigma_f(r)$  and  $\sigma_f(z)$  with  $P_0$  is qualitatively similar to their variation with  $R_1$  (discussed in § VIIE2 above), except that the maxima are now higher and sharper -- a consequence of the larger compression caused by a larger  $P_0$ .

The variation of  $q$  with  $\phi$  for each state of fig. 11 is of interest and is shown in fig. 13. Since  $\alpha_i$  and  $R_i$  are the same for all three states, each curve is labeled with the value of  $P_0$  in that state. Note that  $\phi_{cl}$  is the same for all three states now (contrast fig. 10). As  $P_0$  increases, a downward shift takes place as discussed in connection with fig. 10. The shift is larger at the center of the cloud than at the equator. This is so because of the exponential dependence of  $q$  on the gravitational potential, which, upon compression, becomes considerably altered (more negative) at the cloud center but not so much at the equator. The increase of the slope of  $q(\phi)$ , as  $P_0$  increases, implies larger current densities and stronger magnetic forces (see eq. [131]) and is a result of the relatively large deformation suffered by field lines.

#### 4. Dependence on $\alpha_i$

With  $P_0 = 0.9$  and  $R_i = 2.5$ , we obtain equilibrium states for  $\alpha_i = 0.2$ , 0.5, and 1.0. This situation corresponds to a study of the equilibrium states of an initially spherical cloud of uniform (but unspecified) density, of constant (but unspecified) temperature, threaded by a uniform (but unspecified) magnetic field and of a fixed initial radius as the ratio of the magnetic-to-gas pressure at infinity increases (see eq. [189]) from 0.222 to 0.556 to 1.111. We chose  $R_i$  such that the initial gravitational energy of the cloud was smaller than the thermal energy but not negligible; specifically,  $|W_g|/U = 0.83$  (see eq. [187-A]). The value of  $P_0$  was taken somewhat smaller than unity to eliminate compression due to the external pressure.

We have already discussed the state with  $\alpha_i = 0.5$  (see figs. 8a and 9a). Figures 14a and 14b exhibit the isodensity and isopedion contours and the field lines of the equilibrium states characterized, respectively,

by  $\alpha_i = 0.2$  and  $1.0$ . By comparing figs. 14a, 8a, and 14b, we conclude the following as  $\alpha_i$  increases. (i) The cloud becomes flatter -- especially the interior isodensity contours. (ii) The central density decreases ( $\rho_c/\rho_s = 6.31, 3.82, 3.14$ ). (iii) The central magnetic field also decreases, while its minimum value at the equator increases ( $B_{\min} = 0.834, 0.912, 0.943$ ). (iv) Compared to its value in the initial state, the ratio of the magnetic-to-gas pressure decreases as  $\alpha_i$  increases [ $\alpha_f(0,0)/\alpha_i = 1.20, 0.79, 0.64$ ], whereas its minimum value at the equator increases [ $\alpha_f(r_{\max},0)/\alpha_i = 0.77, 0.92, 0.99$ ]. (v) The larger  $\alpha_i$ , the closer the distance from the cloud center at which the magnetic field reaches its value at infinity within a few percent.

We note that the cloud boundary changed by somewhat less than 10% as  $\alpha_i$  increased by a factor of 5, and that readjustment took place mainly in the lateral direction. This is so because we had chosen  $R_i$  such that gravitational forces did not dominate the pressure forces. Thus, the field lines of the equilibrium state with  $\alpha_i = 0.2$  were not very deformed in the first place. By increasing  $\alpha_i$  (and, therefore, the relative strength of the magnetic field), the field lines straightened out. But the resulting redistribution of matter was not large enough to alter significantly the gravitational field at the boundary which is (almost) determined by the total mass only. Yet, the redistribution of matter that accompanies the straightening of field lines affects significantly the gravitational forces near the center (recall eq. [143] and Gauss' law). This is evidenced by the decrease of  $\rho_c$  (and  $B_c$ ) by a factor of two as we go from the state of fig. 14a to that of fig. 14b.

It is significant that the ratio  $\alpha_f(0,0)/\alpha_i$  was larger than unity in the case  $\alpha_i = 0.2$  and smaller than unity in the other two cases. This

implies that in the proportionality  $B_c \propto \rho_c^\kappa$  the exponent is greater than 1/2 if  $\alpha_i$  is small and smaller than 1/2 otherwise. We are beginning to get a handle on the exponent  $\kappa$ , which other workers have routinely been taking as 2/3.

The changes in the surface densities  $\sigma_f(r)$  and  $\sigma_f(z)$  as  $\alpha_i$  increases are obtained by comparing figs. 15a, 9a, and 15b (corresponding, respectively, to the equilibrium states of figs. 14a, 8a, and 14b). It is clear that, as  $\alpha_i$  increases, the surface density through the cloud center decreases due to the smaller compression. Further comments on these figures would be redundant in view of our detailed discussion above.

In fig. 16, we plotted  $q(\phi)$  for the three states of figs. 14a, 8a, and 14b. The curves are labeled with the values of  $\alpha_i$ . As  $\alpha_i$  increases, the curve  $q(\phi)$  shifts upward and becomes steeper. The shift is larger at the equator ( $\phi/\phi_{cl} = 1.0$ ) because  $P_o$  is fixed and  $\psi$ , which is negative everywhere, increases (see eq. [128]); at the center, the increase in  $\psi$  is partly compensated by the reduced gas pressure.

#### F. Discussion of Results and Comparison with Observations

Under the assumption that the magnetic field is frozen in the matter, we have determined equilibrium states which can be reached by isothermal, self-gravitating, magnetic interstellar clouds contracting nonhomologously from an initially uniform, spherical state and surrounded by a hot and tenuous intercloud medium. Even though we solved a time independent problem, we were able to make a connection between an initial and a final state by conserving the mass-to-flux ratio ( $dm/d\phi$ ) in each flux tube of the system. We emphasized, however, that, if the function  $dm/d\phi$  were known either from theoretical considerations or from observations, our method would determine a unique equilibrium state for each cloud if the pressure and the magnetic

field of the intercloud medium are known.

### 1. Some General Conclusions

The physical parameters of an equilibrium state show large departures from those of a corresponding uniform, spherical state. Equilibrium states are characterized by oblate isodensity contours, the more so the stronger the initial magnetic pressure relative to the gas pressure and the larger the thermal pressure of the external medium. It is not difficult to obtain an enhancement of the column density through the center of a cloud by an order of magnitude even for the moderate range of parameters for which we presented solutions (see, for example, fig. 12c). The mass density,  $\rho$ , may easily vary by more than an order of magnitude between the center and the surface of a cloud (for example, see fig. 8c and, even better, fig. 19a below). The ratio  $\rho_c/\rho_S$  in a critical state is larger, the larger  $\alpha_i$  and the smaller  $P_0$  are -- in fig. 19a, this ratio is equal to 23. Since cloud masses are usually estimated by assuming a spherical shape and a uniform density, they may be overestimates. If a cloud is observed to have a more or less circular cross section, it does not follow that its dimension parallel to the line of sight is nearly equal to the observed one.

#### a. The Slope of $\log B_c$ versus $\log \rho_c$

An invaluable contribution to our understanding of the formation of interstellar clouds by contraction from a more diffuse state of matter with a frozen-in field may soon be made by more accurate observations of the Zeeman effect in molecular clouds. We mentioned in § IIID that the somewhat uncertain data for H I clouds shows a correlation between  $\log B$  and  $\log n_H$ . We also pointed out that, although Verschuur (1970a) drew a straight line of slope 2/3 through the data points, a line with a slope of 1/3 would fit the uncertain data at least as well. We used our

equilibrium solutions to predict what such a slope should be.

Figure 17 is a master plot on a log-log scale of the ratio,  $B_c/B_i$ , of the central magnetic field and its initial (uniform) value against the ratio,  $\rho_c/\rho_i$ , of the corresponding values of the gas density. Each value of  $\alpha_i$  gives rise to a different curve. Three curves are shown (for  $\alpha_i = 0.2, 0.5, \text{ and } 1.0$ ). To obtain the curve labeled ( $\alpha_i =$ ) 0.2 we used thirteen (13) equilibrium states. The curve  $\alpha_i = 0.5$  represents thirty (30) equilibrium states, and that with  $\alpha_i = 1.0$  fourteen (14) states. The scatter of points about each curve was scarcely larger than its thickness. For each value of  $\alpha_i$ , two states differing only in  $R_i$  are located in such a manner that the state with the larger  $R_i$  is higher up along the curve (representing a larger central field and a larger density). Similarly, two states differing only in  $P_o$  fall on a curve of constant  $\alpha_i$  in a way that the state with the larger  $P_o$  is located higher up along the curve. States which have the same  $R_i$  and  $P_o$  but different  $\alpha_i$  fall on a nearly straight line with slope roughly equal to 1 -- one may check this for the three states of figs. 14a, 8a, and 14b. The dashed curve is a line with slope 2/3, representing isotropic contraction.

It is clear that, as  $\alpha_i$  increases, to produce a particular enhancement of the magnetic field a considerably larger central density is required. It is important to note that the slope of each curve varies along its length; it is smaller the smaller the density enhancement. As we have seen in subsection E above, smaller density contrasts result from small  $R_i$  -- corresponding to weak gravitational forces. Therefore, the above variation of the slope of each curve conforms with the reasonable expectation that, until gravitational forces become strong enough, contraction due to an increase in the external pressure proceeds mainly along field lines. Since

most H I interstellar clouds are not self-gravitating, as evidenced by their low densities, whatever their formation mechanism, it must be effective over very large distances along field lines. [For a cylinder of intercloud matter ( $n_{ic} \approx 0.2 \text{ cm}^{-3}$ ) of radius 5 pc to contain a mass of  $300 M_{\odot}$ , it must have a length of about 710 pc.]

Beichman and Chaisson (1974) measured an apparent Zeeman splitting in the 1665-MHz line of the  $^2\Pi_{3/2}$ ,  $J = 3/2$  ground state of OH, which produces a splitting of 3.27 Hz per milligauss (Radford 1961). They reported a field of about 3 mgauss. The authors themselves caution, however, that the interpretation of their observation is inconclusive because the observed circular polarization may originate in two different regions of maser action moving with different radial velocities within their beam width. [As it was earlier pointed out by Heer (1966), circular polarization may result from saturation effects in a maser amplifier with energy levels similar to those of OH.] Clearly, further observations are necessary to settle this issue. Whatever the observations may show, the theoretical justification provided by Beichman and Chaisson for their result is in error. They took  $10^{4.5} \text{ cm}^{-3}$  as a known density of the Orion molecular cloud and argued that, since the interstellar magnetic field is 3  $\mu$ gauss at a density of about  $1 \text{ cm}^{-3}$ , a density of  $10^{4.5} \text{ cm}^{-3}$  implies a field of about 1 mgauss according to the "law"  $B \propto \rho^{2/3}$ . As we have just seen, the exponent ( $\kappa$ ) is more likely to be less (perhaps even much less) than 1/2. Even a magnetic field weaker by one or two orders of magnitude than the one which these authors claimed to have measured would certainly have been able to make further contraction proceed nonhomologously and non-isotropically -- thus decreasing  $\kappa$  from their assumed value of 2/3. We are not suggesting that large magnetic fields are impossible to achieve. We



are proposing, however, that such fields will be found in highly flattened clouds<sup>9</sup> of very high density ( $10^6 - 10^9 \text{ cm}^{-3}$  for  $1/3 \leq \kappa \leq 1/2$ ).

Unless the magnetic field is initially very weak ( $\alpha_i \ll 1$ ), the formation of a cloud will enhance the field according to a relation  $B_c \propto \rho_c^\kappa$ , where  $\kappa$  is a positive function less than  $2/3$  that varies slowly as the contraction proceeds. Since fig. 17 shows that  $\kappa$  is likely to be  $1/2$  or less, it follows that  $\alpha$  at the cloud center may remain constant or even decrease upon contraction. We have also seen that, in the equatorial plane,  $\alpha$  decreases with distance from the cloud center. This likely constancy or decrease of  $\alpha$  upon contraction would have profound effects on the further evolution of a cloud as it relates to star formation. In particular, it follows from the work of Chandrasekhar and Fermi (1953) on the Jeans instability in a uniform medium that the minimum scale  $L_J$  that can collapse in a direction normal to the field is

$$\begin{aligned} L_J^2 &= \frac{\pi}{4G\rho} (C^2 + v_A^2) \\ &= \frac{\pi C^2}{4G\rho} (1 + 2\alpha). \end{aligned} \tag{193}$$

With  $\alpha$  decreasing upon contraction and flattening, the possibility of fragmentation, which cannot occur during spherical isotropic contraction, arises (see also subsection F4 below). The effect will be more pronounced the larger  $\alpha$  is initially. Since stars form predominantly in groups, fragmentation must be predicted by any theory of star formation. Fig. 17 reveals only the rudiments of such a process; it would be very useful to extend it to include larger enhancements of the central field and gas

9. Recall that, in all cases which we studied, the stronger gravity was, the flatter the isodensity contours became -- especially near the cloud center.

density by considering larger values of  $P_0$ .

One might think that, because the above discussion is based on the assumption that the cloud remains isothermal during contraction, the conclusions reached would be qualitatively different if the cloud is allowed to cool and thereby increase  $\alpha$ . This is not so. If indeed the cloud cools, the effectiveness of the internal pressure in balancing self-gravity along field lines is reduced. Further flattening of the cloud is inevitable which will tend to decrease the value of  $\alpha$ . In fact, from our present and previous considerations, it seems that a self-adjusting mechanism is operative that maintains  $\alpha$  close (if not smaller than) its initial value.

b. Correlation between the External Pressure and the Central Density.

The deduced correlation between the external pressure and the density at the cloud center (see figs. 11a, 11b, and 11c) while  $\alpha_i$  and  $R_i$  are kept fixed is shown in fig. 18 as a critical state is approached. The states plotted have  $\alpha_i = 0.5$  and  $R_i = 2.4$ . The plotted values of  $P_0$  range from 1.1 to 3.9. This yielded densities in the range [4.1, 31.1]. As in the case of fig. 17, the scatter of points about the solid line was negligible. We reported in § VII E3 that the state with  $P_0 = 4.9$  collapsed. A state with  $P_0 = 4.0$  yielded a central density of about 50, but we have not included it in fig. 18 because it collapsed for a slightly different choice of relaxation parameters. Apparently, not only are we close to the critical state, but the parameters of the equilibrium states close to the "plateau" of fig. 18 are very sensitive to  $P_0$ . This is reassuring for the following reasons.

The non-magnetic Bonnor-Ebert calculations showed a similar dependence of the central density on the external pressure. In fact, for each value of  $P_0$  two equilibrium states were possible: an extended one and a compact one.

That is, a plot analogous to that of fig. 18 reached a maximum for some  $\rho_c$  and then decreased for larger values of  $\rho_c$ . The branch of the curve with a negative slope represented unstable states: to maintain a larger central density, a smaller external pressure was required. The region of increasing  $P_0$  with increasing  $\rho_c$  represented stable configurations.

We tried to determine one of the possible unstable equilibrium states, but our iterative procedure repeatedly led to collapse. This, together with the fact that fig. 18 is the analogue of the stable branch of the non-magnetic equilibrium states, are taken as strong indications (although not a proof) that our iterative scheme can pick out only physically stable equilibrium states. Unlike the case treated in Paper I, no unstable equilibrium state can be determined by analytical means which we could then use to test our above assertion.

The Bonnor-Ebert calculations showed that the maximum of the curve  $\log P_0$  versus  $\log \rho_c$  occurs at lower values of  $P_0$  as the mass of a cloud increases. This reflects the effect of the stronger gravitational forces due to the larger mass. The analogous phenomenon occurs in our case. For example, the critical state of fig. 8c, which is characterized by the same  $\alpha_1$  as the states of fig. 18, has  $P_0 = 0.9$  and  $R_1 = 2.8$  and, therefore, a mass larger by a factor  $(2.8/2.4)^3 \approx 1.6$ . Since its central density is 14.3, if we attempt to plot it on fig. 18 it would fall slightly below the horizontal axis and certainly leftward of the peak of the solid curve.

The qualitative effect of varying  $\alpha_1$  is to shift the curve of fig. 18 -- to the left for a larger  $\alpha_1$  and to the right for a smaller one. This is so because the same external pressure causes a smaller compression and, therefore, a smaller central density the larger  $\alpha_1$  is.

c. The Ratio  $\rho_c/\rho_S$ .

We have seen that the ratio  $\rho_c/\rho_S$  increases as  $R_i$  or  $P_0$  increases, while it decreases if  $\alpha_i$  increases. At a critical state, however,  $\rho_c/\rho_S$  increases as  $\alpha_i$  increases or as  $P_0$  decreases. This is intuitively clear. A larger  $\alpha_i$  implies stronger magnetic forces, which can be overcome only by stronger gravitational forces arising from a denser central core. Similarly, a weak external pressure does not aid the gravitational forces against the magnetic forces; to overpower the latter, a larger central condensation is required. Yet, this dependence of  $\rho_c/\rho_S$  on  $P_0$  is, in part, artificial.

If  $P_0 < 1$  the cloud boundary would expand, provided that gravitational forces were not present, so that pressure balance across the surface would be achieved. Even if gravitational forces are present, it is a well-known result that the radius of an isothermal (non-magnetic) cloud would tend to infinity as  $P_0 \rightarrow 0$ . In the magnetic case, the polar radius of the cloud will do so because the magnetic forces vanish along the axis of symmetry. The extent of the cloud normal to field lines will be limited because of flux-freezing. Since gravitational forces will maintain some degree of central concentration, the ratio  $\rho_c/\rho_S$  will increase as  $P_0$  ( $= \rho_S$  in our dimensionless variables) decreases. In this sense, this result is artificial. One can see this formally by integrating the force equation (149) from the center of the cloud to its surface along the axis of symmetry to obtain the dimensionless result:

$$\rho_c = \rho_S + \int_0^{z_{\max}(\rho_S)} ds \rho g_s. \quad (194)$$

Although  $\rho_c$  may decrease as  $P_0$  decreases, if we divide through by  $\rho_S$  as the latter tends to zero,  $\rho_c/\rho_S$  will keep increasing.

In spite of its "artificiality", the ratio  $\rho_c/\rho_S$  is useful. If

it is measured to be large, one can deduce that the pressure of the external medium is small. Since, as we have seen in § VIA (footnote 5), only an upper limit on the intercloud pressure is known, a by-product of obtaining an accurate density distribution within a dense cloud will be an implied range of values for the intercloud pressure. To illustrate this point further, we present a critical state with  $P_o = 0.5$  and  $\alpha_i = 1.0$  in fig. 19a and its usual column densities in fig. 19b.

The radius  $R_i$  is equal to 3.20. A state with  $R_i = 3.21$  collapsed for different sets of relaxation parameters; hence, we refer to the state with  $R_i = 3.20$  as a critical state. The isodensity contours reveal that there is a very oblate central core of relatively high density and a fairly extended envelop of relatively low density; the ratio  $\rho_c/\rho_S$  is equal to 23.0. (One may contrast the state of fig. 11c characterized by  $P_o = 3.9$ .) The same effect is noted in the column densities of fig. 19b, where the curves  $\sigma_f(z)$  and  $\sigma_f(r)$  fall fairly rapidly at first and then a "knee" appears before they fall to zero at the boundary -- contrast fig. 12c. Clearly, there is a qualitative, as well as a quantitative, difference between states with large and states with small external pressure. One can utilize this difference to make a statement on the mechanism responsible for the formation of dense interstellar clouds.

There are two alternative possibilities. (i) A cloud grows by slow accretion of matter (mainly along field lines) until self-gravitation becomes dominant. (ii) A rise in the external pressure increases the central density and thereby enhances the strength of the gravitational forces. Our solutions suggest that, at least in principle, one may distinguish between the two mechanisms from high-resolution observations of the distribution of matter within a dense cloud. The first mechanism will

produce an extended envelop of relatively (compared to the core) low density with a more or less cylindrical boundary, whereas the second mechanism will give rise to no such envelop and, in addition, will produce a cloud boundary more closely resembling in shape the interior isodensity contours. We remark that extended envelops appeared in equilibrium states even when  $\alpha_i$  was small, as long as  $P_0$  was small, although in these cases the cloud boundary was nearly spherical.

One might think that the ratio  $\rho_c/\rho_S = 23.0$  in the critical state of fig. 19a exceeds the Bonnor-Ebert critical value mainly because of the "artificial" reason cited above. It is useful, therefore, to calculate  $\rho_c/\bar{\rho}$ , where  $\bar{\rho}$  is the mean density of the cloud. This ratio is expected to undergo a slower increase as  $P_0$  decreases. We recall that in the Bonnor-Ebert critical state this is

$$(\rho_c/\bar{\rho})_{BE} = 5.78. \quad (195)$$

In the (magnetic) state of fig. 19a, we find that

$$(\rho_c/\bar{\rho})_M = 6.9. \quad (196)$$

The effect of the magnetic field is still to increase this critical ratio.

#### d. Critical States

Critical states are equilibrium states on the verge of gravitational instability. They are useful because they set theoretical upper limits on several observable cloud parameters (see § VI). We have presented only two such states, those of figs. 8c and 19a, characterized by  $(\alpha_i = 0.5, P_0 = 0.9, R_i = 2.8)$  and  $(\alpha_i = 1.0, P_0 = 0.5, R_i = 3.20)$ , respectively. We also alluded, in discussing fig. 18, that there is a critical state somewhat more compact than that of fig. 11c. The physical quantities of a critical state depend on two of our three free parameters --

the constraint of being on the verge of collapse removes one parameter.

We determined most critical states by fixing  $\alpha_i$  and  $P_o$  and increasing  $R_i$  until no further solutions could be found. Physically, this corresponds to the situation in which the ratio of the magnetic and gas pressures at infinity as well as the cloud density are kept fixed while the cloud radius increases (thus, including proportionally more mass than it does flux).

Quite generally, for a fixed  $\alpha_i$ , smaller values of  $R_i$  may collapse as  $P_o$  increases. For a fixed  $P_o$ , larger values of  $R_i$  are required for collapse as  $\alpha_i$  increases. The former behavior simply states that as the external pressure contributes more to the contraction of the cloud, smaller masses become able to collapse. The latter behavior states that larger masses are required for collapse if magnetic forces become stronger. Since the values of  $\alpha_i$  and  $P_o$  are not known in reality, we shall confine ourselves to a discussion of the physical parameters of a single critical state, that of fig. 19a, in a dimensional form. The conversion formulae that follow may be used to find the dimensional parameters of any other state presented. When observations provide us with the necessary information on  $dm/d\phi$  and  $P_o$ , it will be worth returning and extending this discussion.

## 2. Returning to the World of Dimensional Quantities

Dimensionless quantities are indispensable in solving a problem, but often their numerical values have a meaning only for the particular author and a few devoted readers. It is imperative that at least one example be provided in dimensional form. We choose the critical state of figs. 19a and 19b because  $\alpha_i = 1.0$  and  $P_o = 0.5$ , yielding  $\alpha_o = 2.0$ , a value close to what we currently believe as representative of conditions in a spiral arm behind a galactic shock (see Paper II, § II). It is, however, impossible

at present to decide whether the value  $\alpha_i = 1.0$  is representative of conditions which would prevail if we (mentally) took a dense cloud and expanded it in such a way that the field lines straightened out while its density became uniform (see also discussion below). To know the value of  $\alpha_i$  requires a detailed knowledge of how dense clouds form -- an open question in theoretical astrophysics. Under the additional limitation that the true mass-to-flux ratio of a dense cloud may be very different from the assumed simple function (see § VIIB), we proceed with our example.

We let  $T_{50}$  denote the cloud temperature (T) in units of  $50^\circ\text{K}$  and  $P_{18}$  denote the intercloud pressure ( $P_{\text{ext}}$ ) in units of  $1800 \text{ k deg/cm}^3$ . Then the isothermal speed of sound in the cloud is (see eqs. [95] and [96])

$$C = 0.64 (T_{50} / \mu)^{1/2} \text{ km/sec.} \quad (197)$$

Let  $P_o$  be defined by

$$P_o = P_{\text{ext}} / \rho_i C^2, \quad (198)$$

where  $\rho_i$  is the uniform cloud density in the spherical initial state and is related to the initial number density ( $n_i$ ), including helium, by

$$\rho_i = n_i \mu m_H. \quad (199)$$

By solving eq. (199) for  $n_i$  and using eqs. (197) -- careful with the units! -- and (198), we find that

$$n_i = 36 P_{18} / P_o T_{50} \text{ cm}^{-3}. \quad (200)$$

The number density of hydrogen is obtained from the total number density through division by

$$\eta = 1.1 \quad \text{for H I clouds;} \quad (201a)$$

$$= 1.2 \quad \text{for H}_2 \text{ clouds.} \quad (201b)$$



If the dimensional initial cloud radius is  $R_{cl}$ , then

$$\begin{aligned} R_{cl} &= R_i C / (4 \pi G \rho_i)^{1/2} \\ &= 2.92 R_i P_o^{1/2} T_{50} / \mu P_{18}^{1/2} \text{ pc,} \end{aligned} \quad (202)$$

where we have used eqs. (198) and (197) to eliminate  $\rho_i$  and  $C$ , respectively.

To convert the column (or, surface) densities  $\sigma_f$  and  $\sigma_i$  of figs. 9, 12, 15, and 19b to dimensional form, we need to multiply by the unit of density,  $\rho_i$ , and the unit of length,  $C / (4\pi G \rho_i)^{1/2}$ . We denote the dimensional surface density by  $m_s$  and we easily find that

$$m_s = 0.54 \times 10^3 (P_{18}/P_o)^{1/2} \times \left\{ \begin{array}{l} \sigma_f \\ \sigma_i \end{array} \right\} \text{ gm/cm}^2, \quad (203)$$

where  $\sigma_f$  and  $\sigma_i$  are shown in the aforementioned figures. The (number) column density of hydrogen (not the total) is, of course, obtained from  $m_s$  through multiplication by  $(n \mu m_H)^{-1}$ , that is,

$$N_H = 2.3 \times 10^{20} (P_{18}/P_o)^{1/2} \times \left\{ \begin{array}{l} \sigma_f \\ \sigma_i \end{array} \right\} \text{ cm}^{-2}, \text{ for H I clouds; } \quad (204a)$$

and

$$N_{H_2} = N_H / 2, \quad \text{for molecular clouds.} \quad (204b)$$

The mass of the cloud is given by

$$\begin{aligned} M &= (4 \pi / 3) \rho_i R_{cl}^3 \\ &= 91.8 R_i^3 P_o^{1/2} T_{50}^2 / \mu^2 P_{18}^{1/2} M_\odot. \end{aligned} \quad (205)$$

Finally, from the definition of  $\alpha_i$  we obtain

$$\begin{aligned} B_i &= (8 \pi \rho_i C^2 \alpha_i)^{1/2} \\ &= 2.5 (\alpha_i P_{18}/P_o)^{1/2} \text{ } \mu\text{gauss.} \end{aligned} \quad (206)$$

In solving our problem we expressed the density and the magnetic field in units of their initial values. So, to find their dimensional values in an equilibrium state, say at the cloud center, one simply takes the dimensionless values in that state and multiplies by the results obtained from eqs. (200) and (206), respectively.

For the critical state of fig. 19a ( $\alpha_i = 1.0$ ,  $P_0 = 0.5$ ,  $R_i = 3.20$ ) and its corresponding initial state, we calculate the following values in the case of an H I cloud with  $T = 50^\circ\text{K}$  and an intercloud medium with  $P_{\text{ext}} = 1800 \text{ k deg/cm}^3$ .

Initial State:

$$\begin{aligned} \dot{C} &= 0.57 \text{ km/sec} \\ M &= 1320 M_\odot \text{ (compare eq. [97a])} \\ n_i &= 72 \text{ cm}^{-3}, \quad n_i(\text{H}) = 65.4 \text{ cm}^{-3} \quad (207) \\ R_{\text{cl}} &= 5.2 \text{ pc} \\ B_i &= 3.54 \text{ } \mu\text{gauss} \end{aligned}$$

Final State:

$$\begin{aligned} n_c &= 828 \text{ cm}^{-3}, & n_c(\text{H}) &= 753 \text{ cm}^{-3} \\ n_S &= 36 \text{ cm}^{-3}, & n_S(\text{H}) &= 32.7 \text{ cm}^{-3} \\ \bar{n} &= 122 \text{ cm}^{-3}, & \bar{n}(\text{H}) &= 111 \text{ cm}^{-3} \\ r_{\text{max}} &= 4.76 \text{ pc} \\ z_{\text{max}} &= 2.60 \text{ pc} \\ B_c &= 9.42 \text{ } \mu\text{gauss} \\ \alpha_c/\alpha_i &= 0.62 \\ N_H(r=0) &= 4.52 \times 10^{21} \text{ cm}^{-2} \\ N_H(z=0) &= 1.0 \times 10^{22} \text{ cm}^{-2} \\ m_s(r=0) &= 10.6 \times 10^{-3} \text{ gm/cm}^2 \\ m_s(z=0) &= 23.5 \times 10^{-3} \text{ gm/cm}^2 \end{aligned} \quad (208)$$

The quantity  $N_H(r = 0)$  denotes the column density of hydrogen when the line of sight is along the axis of symmetry, and  $N_H(z = 0)$  when the line of sight lies in the equatorial plane and passes through the center of the cloud. The quantities  $m_s(r = 0)$  and  $m_s(z = 0)$  have a similar meaning. Since a telescope beam has a finite angular width, however, the observed column densities will be smaller than the maximum values. We therefore calculated the ratio  $m_{TM} = (\text{total mass/area normal to the line of sight})$  for the above two orientations of the line of sight -- this is the quantity observed if the cloud lies entirely within the telescope beam. Values for other viewing angles will lie between these two. We find that

$$3.9 \times 10^{-3} \leq m_{TM} \leq 5.7 \times 10^{-3} \text{ gm/cm}^2. \quad (209)$$

The ratio of  $m_{TM}$  and Mestel's critical value is (see eq. [108c])

$$1.9 \leq m_{TM}/m_M \leq 2.8. \quad (210)$$

Indeed, equilibrium calculations, in addition to giving us the detailed structure of a cloud, have fared better than non-equilibrium calculations in predicting the parameters of a critical state.

The maximum observed column density of atomic hydrogen is  $3 \times 10^{21} \text{ cm}^{-2}$  (van Woerden 1967). Our calculations indicate that such a cloud is not collapsing. The rest of the calculated physical quantities are either reasonable, or exceed the observed values -- a desirable result. We mentioned in § VIA, however, that the scarcity of H I clouds with masses larger than  $1000 M_\odot$  may be due to their conversion into molecular clouds. How, then, do our results compare with observed quantities in dense (dark or molecular) clouds? (Before leaving H I clouds, we note that the state of fig. 11c corresponds to a mass of  $1554 M_\odot$  for the same "standard" parameters as assumed above.)

We take  $T = 10^\circ\text{K}$ , appropriate to a dark cloud, and  $P_{\text{ext}} = 1800 \text{ k deg/cm}^3$ . The mass now becomes (see eq. [205]) only  $15.7 M_\odot$ , while the final central and mean densities have increased to  $n_c(\text{H}_2) = 3.45 \times 10^3 \text{ cm}^{-3}$  and  $\bar{n}(\text{H}_2) = 508 \text{ cm}^{-3}$ . The calculated equatorial and polar radii of such a cloud are (see eq. [202])  $r_{\text{max}} = 0.75 \text{ pc}$  and  $z_{\text{max}} = 0.41 \text{ pc}$ . Although the maximum density is well within the range of observed values ( $10^3 - 10^4 \text{ cm}^{-3}$ ; see § VIA) and the predicted dimensions are in good agreement with observations, the total mass (of this particular equilibrium state) is a factor of about 6 smaller than the observed values. In spite of the possibility that the observed values may be overestimates, as we remarked above, we do not think that that is the major source of discrepancy, whose sources are very likely to be the following.

(i) The simplifying assumption that a dark cloud has the same mass-to-flux ratio as some uniform reference state. We have already discussed the uncertainties accompanying the assumed  $dm/d\phi$  as well as the values of  $\alpha_i$ .

(ii) Matter in the immediate neighborhood of a dense cloud is unlikely to have a negligible density. This would invalidate our assumption that the external medium is force-free. Although we had formulated the problem in subsections A1 and A2 above without imposing this condition, we solved it only with the force-free approximation of the intercloud medium. When the parameters of this medium are better known, especially in the neighborhood of dense clouds, it will be worth solving the more general problem. An external medium which is not force-free is also likely to permit a larger lateral contraction of a cloud and, therefore, a larger enhancement of the magnetic field. As long as the external medium is force-free, even with an external magnetic pressure small

compared to the intercloud thermal pressure, enhancements of the field by more than an order of magnitude are difficult to obtain.

(iii) If the galactic gravitational field is introduced, in which case the boundary condition of uniform field at infinity must be substituted by a more realistic, periodic boundary condition, the field lines in the intercloud medium will inflate in the manner described in § V. This will weaken the general intercloud field -- and it is the mean value of this field (not of a uniform one) along the line of sight which we measure as 3  $\mu$ gauss. Thus, the ratio  $B_c/B_\infty$  will also increase.

(iv) We have sought solutions with  $0.5 \leq P_0 \leq 4.9$ . Since the dimensionless quantity  $P_0$  is the ratio of the intercloud and the cloud pressures in the uniform initial state and since we assumed an isothermal transition from an initial to a final state, it might have been more appropriate to have chosen  $P_0 \gg 1$ . Dense clouds have relatively low temperatures. Moreover, when (mentally) expanded to a uniform state (say,  $R_{cl}$  increases by a factor of 2 or 3), their densities will drop by a factor 10 - 30. If they are in pressure equilibrium in their final states, then a  $P_0 \approx 10 - 30$  would describe conditions existing in the initial states. Because of eq. (189) and since we have argued that  $\alpha_0$  is roughly equal to unity, it follows that  $\alpha_i \approx 20$  would then be more appropriate for dense clouds. As our results can show by a reasonable extrapolation, an equilibrium state with such parameters will be highly flattened. Such configurations are, in fact, observed at least within the Orion cloud complex (see Morris et al. 1974).

### 3. Line Widths in Dense Clouds

Supersonic turbulence as a source of the observed line widths in dense clouds has already been ruled out on the basis of its short life time (see

§ VIA). Motions associated with gravitational collapse could explain in a natural way the observed large line widths (see § VIA for references) if only some decrease in the line widths takes place as one observes regions further from the cloud center. One can see why this is so as follows. A cold, spherical, non-magnetic, massive cloud would collapse under self-gravitation with a free-fall velocity

$$v(|\vec{x}|) = -[2 G M(|\vec{x}|) / |\vec{x}|]^{1/2}, \quad (211)$$

where  $M(|\vec{x}|)$  is the mass inside the radius  $|\vec{x}|$ . If one assumes that the density is uniform, it follows from eq. (211) that

$$v(|\vec{x}|) \propto |\vec{x}|. \quad (212)$$

In this picture, the line of sight going through the center of the cloud will detect the largest radial velocities, which, in turn, will produce the largest line widths.

It is well known, however, that, if gravitational forces are present, a central condensation is inevitable. A density which decreases as  $|\vec{x}|$  increases could give rise to a free-fall velocity that increases toward the cloud center. Equation (211) shows that this will be the case if  $\rho$  falls off more rapidly than  $|\vec{x}|^{-2}$ . The observable implications of such a case would be that the center of a spectral line would be formed at the outermost layers of the cloud while the wings of the line would be produced at the cloud center. Observations show that the most intense radiation comes from the center of a cloud and that the center of a spectral line is more intense than its wings. This seems to suggest that the density must fall off less rapidly than  $|\vec{x}|^{-2}$ .

Equation (212) is usually used in referring to collapsing clouds.

Then the argument is made (for example, see Morris et al. 1974) that because line widths do not vary much between the center and the boundary of a cloud, collapse cannot be taking place. This is erroneous because collapse may in fact be taking place in such a manner that

$$v(|\vec{x}|) \propto |\vec{x}|^k, \quad (213)$$

where  $k$  is a positive constant less than one.

Zuckerman and Palmer (1974) also claim that the collapse hypothesis is ruled out by the high rate of star formation that would be implied if all dense clouds were collapsing. We remarked in § VI that this is not so if star formation is not an efficient process. Observational evidence indicates that indeed star formation does not proceed with a 100 percent efficiency (see review by Shu 1973b). Massive clouds often contain  $10^5 - 10^6 M_{\odot}$ , while the mass of stellar clusters in the Galaxy is smaller than  $10^3 M_{\odot}$ .

The traditional theoretical argument that has been advanced to support an inefficient star formation process is that, following star formation, the bulk of a massive cloud will be dispersed. A typical O5 star, the argument continues, would emit about  $10^{51}$  ergs during its lifetime mostly in the ultraviolet. A type II supernova liberates a comparable amount of energy. This energy would seem sufficient to disperse a  $10^5 M_{\odot}$  cloud, whose (negative) gravitational energy is typically  $10^{50}$  ergs. This argument is fallacious because kinetic energy is not conserved. One must consider the conservation of linear momentum in each element of solid angle during spherical expansion of the gas. In the case of a supernova (ejected mass  $m < 1 M_{\odot}$ ) and an O5 star, the velocities imparted to the gas of mass  $M_c$  ( $10^4 - 10^6 M_{\odot}$ ) are, respectively,

$$v_{g,s} = (2 m E)^{1/2} / M_c \quad (214a)$$

$$\approx 10^{-1} m^{1/2} \left( \frac{10^5}{M_c} \right) \text{ km/sec}$$

and

$$v_{g,*} = E / c M_c \quad (214b)$$

$$\approx 10^{-3} \left( \frac{10^5}{M_c} \right) \text{ km/sec,}$$

where  $m$  and  $M_c$  are measured in solar masses and  $E = 10^{51}$  ergs. Even for  $M_c$  as small as  $10^4 M_\odot$ ,  $v_g$  is less or much less than the speed of sound in the gas. If star formation is an inefficient process, the cause must lie elsewhere. We shall offer a likely explanation below. Now we continue our discussion of line widths.

Zuckerman and Evans (1974) have advanced an interesting argument against the collapse of dense clouds. In the presence of a large-scale contraction, in which velocity increases with distance from the cloud center, photons emitted from the far side of the cloud (for example, by CO molecules) are somewhat blue-shifted so that they are not absorbed by intervening matter. Thus, one "sees" through the entire cloud. A molecular species (such as  $H_2CO$ ), however, that absorbs radiation emitted by H II regions found near the cloud center, must be located between the center and the nearest edge of the cloud. Since the cloud is collapsing, by assumption, the absorbing species must be moving away from the observer. Consequently, absorption and emission lines within a single dense cloud must exhibit a relative shift in radial velocity. Since such a shift is usually smaller than one-fourth of the CO line width, Zuckerman and Evans interpret this as evidence against collapse.



The alternative proposed by Zuckerman and Evans to explain the large line widths in molecular clouds is extremely unattractive. They suggest that 50% of the mass of a dense cloud exists in the outer 20% of the radius without explaining how that much matter can be supported against gravity at that distance -- whatever happened to Newton's second law? In addition, they assume that the cloud ( $M \sim 10^5 M_{\odot}$ ) is broken up into chunks of about  $10^3 M_{\odot}$  and that it is the more or less random motion of these objects that is responsible for the observed line widths. How these objects avoid one another remains a mystery. Why they themselves do not collapse, since they more than satisfy the Bonnor-Ebert critical condition (see eq. [97b]), is left unanswered by the authors.

An as yet unproposed mechanism may be able to account for the observed line widths in dense clouds: oscillations of a dense cloud as a whole about a stable equilibrium state such as any one of the states which we have calculated. We have argued above that a self-adjusting mechanism is operating in self-gravitating, magnetic clouds that tends to keep  $\alpha_c$  close to its initial value,  $\alpha_i$ . We have also argued that it is reasonable that  $\alpha_i$  should be in the range 10 - 30, which implies a very flattened configuration. Such a cloud can undergo oscillations that do not necessarily push it over the threshold of gravitational instability. Two normal modes are obvious.

(i) The cloud contracts both along its major and minor axes simultaneously; this mode could conceivably lead to collapse.

(ii) The cloud expands along its minor axis (axis of symmetry) while it contracts in a direction normal to the field, and vice versa. Such oscillations cannot cause collapse -- recall that one dimensional compression along field lines due to self-gravity cannot proceed indefinitely.

The question is whether such oscillations can be maintained for times exceeding the free-fall time. A plausibility argument indicates that they can. The only significant damping mechanism is the dissipation of energy in hydromagnetic shocks. However, since the Mach numbers implied by observations are in the range 2 - 4, an  $\alpha_i$  as small as 8 will suffice to prevent the formation of such shocks. This possible mechanism for interpreting large line widths in molecular clouds certainly warrants a more careful future investigation. One could solve an initial value problem, in which some displacement or velocity is given to the cloud elements of an equilibrium state. We only remark here that an increase (temporary or permanent) of the intercloud pressure (say, due to passage through a spiral density wave) may set a dense cloud into such an oscillation.

#### 4. Why is Star Formation Inefficient?

Mestel (1965) pointed out that a collapsing cloud may fragment because of flattening -- recall that Strittmatter (1966) demonstrated that a highly flattened, uniform ellipsoid can collapse normal to the field if its mass is only about 1/2 that required for the collapse of a spherical, uniform cloud of the same mass and flux (see § VIC2b). This permits a cloud and all fragments to remain "strongly magnetic" (in Mestel's words) throughout the collapse stage. However, stars either have no magnetic fields at all or very weak fields compared to those which would be implied if the interstellar field remained frozen in the matter. Therefore, at some stage of the star formation process, the field must either dissipate or diffuse through the matter -- the latter being a more likely process (see § VIB). Mestel (1966) argued that, as a cloud contracts, the nearly oppositely directed field lines at the equatorial plane give rise to strong

"pinching" forces that dissipate flux, reconnect field lines, and the magnetic field of a cloud is effectively detached from that of the background medium. We think that pinching forces are peculiar to Mestel's spherical, non-equilibrium model discussed in § VIC2a. Moreover, this sequence of events would lead to a rather efficient star formation -- contrary to observations.

There is an alternative possibility. Our equilibrium calculations support the idea that the cloud flattens. But, for this very reason, no pinching forces appeared in the equatorial plane. We think that, after collapse sets in and flattening proceeds further, the increasing curvature of the field lines will stop further lateral contraction of the outlying (but not the central) layers of a cloud near the equator. Thus, the field may not detach from the background. The criterion for this to take place is that the tension of the field lines overwhelm gravity near the equator. Roughly, the tension is inversely proportional to the thickness of the cloud, and the gravitational force is inversely proportional to the second power of the equatorial radius.<sup>10</sup> Hence, contraction will stop in this region if only the ratio  $r_{\max}^2/z_{\max}$  increases upon contraction. This is not too stringent a condition. It is conceivable that a substantial fraction of the cloud mass is "left behind" while the cloud core engages in the exciting process of star formation.

---

10. We are assuming here that the cloud is approximated by a thin disk of high central density and that it contracts through a sequence of quasi-equilibrium configurations (see § VIII below). Since the intercloud pressure is fixed and the cloud isothermal and since pressure is continuous across the cloud surface (see eq. [150]), the gas density just inside the equator will remain fixed (see eq. [151]). This situation is substantially different from a contracting thin disk of uniform density throughout, in which case the gravitational force,  $\rho g$ , varies as  $(1/r_{\max}^4 z_{\max})$ . In the latter, less realistic case, one would conclude that once gravitational forces exceed magnetic forces, contraction would continue indefinitely. This erroneous conclusion is the norm in current thinking.

## VIII. EQUILIBRIUM CALCULATIONS AND STAR FORMATION

Star formation is a process for which, at least most directly, a gravitational instability is responsible. It is impossible to understand (not merely to simulate) the initiation of this process theoretically without having some equilibrium state at hand on which one can perform a stability analysis. One may undertake a multitude of time-dependent numerical calculations with an infinite variety of initial and boundary conditions, such as a very large mass within a very small, fixed radius, that leave no alternative to a cloud (invariably assumed to contain no magnetic fields) but to collapse (see, for example, review by Larson 1973). What are often presented as very significant results of such calculations, for example, a high-density central core and an extended envelop in which  $\rho \propto r^{-2}$ , can in fact be deduced without resorting to lengthy, time-dependent numerical procedures. A central condensation is an inevitable consequence of the presence of gravitational forces. Furthermore, the variation of density as  $r^{-2}$  stems from the existence of a simple similarity solution for the equations of motion (see Larson 1969). As for the remaining conclusions of such calculations, they have to be revised substantially when a magnetic field is present.

The accessible equilibrium states of (a model of) the magnetic cloud-intercloud system, on both a large and a small scale, are not useful merely for performing stability analyses on them. Since their physical properties are usually determined by a small number of parameters (one in the large-scale problem of § V, and three in the small-scale problem of § VII), it is possible to predict in advance of any numerical time-dependent calculation whether the initial conditions are such that any equilibrium states are accessible to the system. In the case of self-

gravitating clouds, it is certainly true that, if the initial parameters are specified such that an accessible state is close to a critical one, transient (such as inertial) effects may lead to collapse. This, nevertheless, enhances the usefulness of a knowledge of equilibrium states, rather than reducing it. Yet, equilibrium states are useful in a much more practical sense.

First, they seem to exist on both the large and the small scales with which we concerned ourselves in this work. Second, as Mestel (1965) suggested, such a process as the free-fall of an interstellar cloud may be a rare phenomenon and that the rate of contraction may be limited first by the presence of magnetic fields, and, at a later stage, perhaps by the rate of diffusion of ions and the field through the neutral matter. In fact, Mestel (1965) suggests that star formation may proceed in a sequence of quasi-equilibrium configurations of strongly magnetic clouds, which flatten and fragment, but never actually free-fall.

Observations, of course, will ultimately decide whether our equilibrium calculations and their predictions have advanced our understanding of some of the processes (such as cloud formation, equilibrium, and stability) that are intimately related to the birth of stars. This is the way of science.

## ACKNOWLEDGEMENTS

This work would be incomplete without an expression of gratitude for Professor George B. Field for three years of personal tutelage and tolerance. The confidence with which I presented the numerical results on the magnetic Rayleigh-Taylor instability is partly drawn from tests suggested by Dr. Paul Concus, whose interest in the numerical aspects of the problem made an otherwise tedious task a rewarding experience. The educational importance of the many "free-wheeling" discussions which I have shared with Professor Frank H. Shu can hardly be overemphasized. For her expert typing and her invaluable assistance on technical matters, my sincere thanks go to Mrs. Ardie Rutan.

The main source of support for this work was the National Science Foundation, under Grant GP-36194X. Support from the Theoretical Physics Group and the Mathematics and Computing Group of the Lawrence Berkeley Laboratory is also gratefully acknowledged.

TABLE 1

MAGNETIC FIELD OBTAINED FROM ZEEMAN SPLITTING OF THE 21-cm LINE

Direction	$l$ (degrees)	$b$ (degrees)	$v_{\text{cloud}}(\text{LSR})$ (km/sec)	Field* ( $\mu\text{gauss}$ )
Taurus A	185	- 6	+ 10	- 3.5 $\pm$ 0.7
			+ 4	- 1.5 $\pm$ 0.9
Cassiopeia A	112	- 2	- 38	+18.0 $\pm$ 1.9
			- 48	+10.8 $\pm$ 1.7
Orion A	209	-19	+ 7	-50 $\pm$ 15
			+ 2	-70 $\pm$ 20 (?)
M17	15	- 1	+ 14	+25 $\pm$ 10

\*A negative value indicates a direction toward the observer.

## REFERENCES

1. Aannestad, P. A., and Purcell, E.M. 1973, *Ann. Rev. Astron. & Astrophys.*, 11, 309.
2. Ames, S., 1973, *Ap. J.*, 182, 387.
3. Appenzeller, I. 1968, *Ap. J.*, 151, 907.
4. Baade, W. 1944, *Ap. J.*, 100, 137.
5. Beichman, C. A., and Chaisson, E. J. 1974, *Ap. J. (Letters)*, 190, L21.
6. Bergeron, I., and Souffrin, S. 1971, *Astron. & Astrophys.*, 11, 40.
7. Biermann, L., and Davis, L., Jr. 1960, *Zs. f. Ap.*, 51, 19.
8. Biermann, L., and Schlüter, A. 1951, *Phys. Rev.*, 82, 863.
9. Bless, R.C. 1968, in Stars and Stellar Systems, Vol. 7, Nebulae and Interstellar Matter, ed. B. Middlehurst and L. H. Aller (Chicago: University of Chicago Press), pp. 667-684.
10. Bonnor, W.B. 1956, *Monthly Notices*, 116, 351.
11. Carruthers, G. R. 1970, *Space Sci. Rev.*, 10, 459.
12. Chandrasekhar, S., and Fermi, E. 1953, *Ap. J.*, 118, 116.
13. Clark, B. G. 1965, *Ap. J.*, 142, 1398.
14. Colvin, R. S., Hughes, M. P., Thompson, A. R., and Verschuur, G. L. 1970, *Ap. Letters*, 6, 211.
15. Daniel, R. R., and Stephens, S. A. 1970, *Space Sci. Rev.*, 10, 599.
16. Davis, L., Jr. 1958, *Ap. J.*, 128, 508.
17. Davis, L., Jr., and Berge, G. L. 1968, in Stars and Stellar Systems, Vol. 7, Nebulae and Interstellar Matter, ed. B. Middlehurst and L. H. Aller (Chicago: Univ. of Chiago Press), pp. 755-770.
18. Davis, L., Jr., and Greenstein, J. L. 1951, *Ap. J.*, 114, 206.
19. Defouw, R. J. 1970, *Ap. J.*, 161, 55.



## REFERENCES - contd.

20. Earl, J. A. 1961, Phys. Rev. Letters, 6, 125.
21. Ebert, R. 1955, Zs. f. Ap., 37, 217.
22. \_\_\_\_\_. 1957, *ibid.*, 42, 263.
23. Ebert, R., Hoerner, S. von, and Temesváry, S. 1960, Die Entstehung von Sternen durch Kondensation diffuser Materie (Heidelberg: J. Springer).
24. Field, G. B. 1962, in Interstellar Matter in Galaxies, ed. L. Woltjer (New York: W. A. Benjamin, Inc.), 183.
25. \_\_\_\_\_. 1965, Ap. J., 142, 531.
26. \_\_\_\_\_. 1969, 16th Annual International Astrophys. Symp., Institut d' Astrophysique, Liege, 29.
27. \_\_\_\_\_. 1970, Lecture Notes (Unpublished).
28. \_\_\_\_\_. 1973, in Molecules in the Galactic Environment, ed. M. A. Gordon and L. E. Snyder (New York: Wiley-Interscience), p. 21.
29. Field, G. B., Goldsmith, D. W., and Habing, H. J. 1969, Ap. J. (Letters), 155, L149.
30. Field, G. B., and Saslaw, W. C. 1965, Ap. J., 142, 568.
31. Fricke, W. 1954, Ap. J., 120, 356.
32. Fujimoto, M. 1966, in IAU Symp. No. 29, p. 453.
33. Gardner, F. F., and Davies, R. D. 1966, Australian J. Phys., 19, 441.
34. Gardner, F. F., Morris, D., and Whiteoak, J. B. 1969, Australia J. Phys., 22, 813.
35. Gardner, F. F., Whiteoak, J. B., and Morris, D. 1967, Nature, 214, 371.
36. Ginzburg, V. L., and Syrovatskii, S. I. 1965, Ann. Rev. Astron. & Astrophys., 3, 297.

## REFERENCES - continued

37. Goldreich, P., and Kwan, J. 1974, Ap. J., 189, 441.
38. Goldreich, P., and Lynden-Bell, D. 1965, Mon. Notices, Roy. Astron. Soc., 130, 125.
39. Goldsmith, D. W. 1970, Ap. J., 161, 41.
40. Habing, H. J., and Goldsmith, D. W. 1971, Ap. J., 166, 525.
41. Hall, J. S. 1949, Science, 109, 166.
42. Hayakawa, S., Nishimura, S., and Takayanaki, K. 1961, Pub. Astr. Soc. Japan, 13, 184.
43. Heer, C. V. 1966, Phys. Rev. Letters, 17, 774.
44. Heiles, C. 1968, Ap. J. Suppl., 15, No. 136.
45. \_\_\_\_\_. 1971, Ann. Rev. Astron. & Astrophys., 9, 293.
46. \_\_\_\_\_. 1973, paper presented at IAU Symp. No. 60.
47. Heiles, C., and Jenkins, E. 1973, papers presented at 139th and 140th meeting of the AAS.
48. Hiltner, W. A. 1949, Science, 109, 165.
49. Hjellming, R. M., Gordon, C. P., and Gordon, K. J. 1969, Astron. & Astrophys., 2, 202.
50. Hollenback, D. J., and Salpeter, E. E. 1971, Ap. J., 163, 155.
51. Hollenback, D. J., Werner, M. W., and Salpeter, E. E. 1971, Ap. J., 163, 165.
52. Hornby, J. M. 1966, Mon. Notices Roy. Astr. Soc., 133, 213.
53. Hughes, M. P., Thompson, A. R., and Colvin, R. S. 1971, Ap. J. Suppl., 23, No. 200.
54. Hulst, H. C. van de 1967, Ann. Rev. Astron. & Astrophys., 5, 167.
55. Jeans, J. H. 1928, Astronomy and Cosmogony (Cambridge: Cambridge Univ. Press).

## REFERENCES - contd.

56. Jones, R. V., and Spitzer, L., Jr. 1967, Ap. J., 147, 943.
57. Jura, M., and Dalgarno, A. 1972, Ap. J., 174, 365.
58. Kerr, F. J. 1968, in Stars and Stellar Systems, Vol. 7, Nebulae and Interstellar Matter, ed. B. Middlehurst and L. H. Aller (Chicago: Univ. of Chicago Press), pp. 575-622.
59. Kulsrud, R. M., and Pearce, W. 1969, Ap. J., 156, 445.
60. Larson, R. B. 1969, Mon. Notices Roy. Astr. Soc., 145, 271.
61. \_\_\_\_\_ . 1973, Ann. Rev. Astr. & Astrophys., 11, 219.
62. Ledoux, P. 1951, Ann. d'Ap., 14, 438.
63. Lerche, I. 1967, Ap. J., 149, 395.
64. \_\_\_\_\_ . 1969, in Advances in Plasma Physics, Vol. 2, ed. A. Simon and W. B. Thompson, (New York: Interscience), pp. 47 - 138.
65. Liszt, H. S., Wilson, W. W., Penzias, A. A., Jefferts, K. B., Wannier, P. G., and Solomon, P. M. 1974, Ap. J., 190, 557.
66. Manchester, R. N. 1974, Ap. J., 188, 637.
67. Mansfield, V. N. 1973, Ap. J., 179, 815.
68. Mathewson, D. S. 1968, Ap. J. (Letters), 153, L47.
69. \_\_\_\_\_ . 1969, Proc. Astr. Soc. Australia, 1, 209.
70. Mathewson, D. S., and Ford, V. L. 1970, Mem. Roy. Astr. Soc., 74, 143.
71. Mathewson, D. S., and Nicholls, D. C. 1968, Ap. J. (Letters), 154, L11.
72. Mathewson, D. S., van der Kruit, P. C., and Brouw, W. N. 1972, Astron. & Astrophys., 17, 468.
73. McCray, R., and Schwarz, J. 1971, in The Gum Nebula and Related Problems, ed. S. P. Maran, J. C. Brandt, and T. P. Stecher (Goddard Space Flight Center Report No. X-683-71-375), p. 60.
74. McCrea, W. H. 1957, Mon. Notices, 117, 562.

## REFERENCES - continued

75. Mestel, L. 1965, Quarterly J. Roy. Astr. Soc., 6, 161, 265.
76. \_\_\_\_\_. 1966, Mon. Notices Roy. Astr. Soc., 133, 265.
77. Mestel, L., and Spitzer, L., Jr. 1956, Mon. Notices, Roy Astr. Soc.,  
116, 503.
78. Meyer, P. 1969, Ann. Rev. Astr. & Astrophys., 7, 1.
79. Meyer, P., and Vogt, R. 1961, Phys. Rev. Letters, 6, 193.
80. Miller, C. R. 1962, On the Orientation of Dust Grains in Interstellar  
Space, Ph.D. thesis, California Institute of Technology.
81. Morris, D., and Berge, G. L. 1964, Astron. J., 69, 641.
82. Morris, M., Zuckerman, B., Turner, B. E., and Palmer, P. 1974,  
Ap. J. (Letters), 192, L23.
83. Mouschovias, T. Ch. 1973, paper presented at the 141st Meeting of  
the AAS.
84. \_\_\_\_\_. 1974, Ap. J., 192, 37. (Paper I; reprint  
attached).
85. Mouschovias, T. Ch., Shu, F. H., and Woodward, P. R. 1974, Astron. &  
Astrophys., 33, 73 (Paper II).
86. Nakano, T., and Tadamaru, E. 1972, Ap. J., 173, 87.
87. Oort, J. H. 1954, B.A.N., 12, 177, No. 455.
88. \_\_\_\_\_. 1965, in Stars and Stellar Systems, Vol. 5, Galactic  
Structure, ed. A. Blaauw and M. Schmidt (Chicago: Univ. of  
Chicago Press), pp. 455-511.
89. Ostriker, J. P., and Mark, J. W-K. 1968, Ap. J., 151, 1075.
90. Parker, D. A. 1973, Mon. Notices Roy. Astr. Soc., 163, 41.
91. Parker, E. N. 1965a, Ap. J., 142, 584.
92. \_\_\_\_\_. 1965b, *ibid.*, 142, 1086.

REFERENCES - continued

93. Parker, E. N. 1966, *ibid.*, 145, 811.
94. \_\_\_\_\_ . 1967a, *ibid.*, 149, 517.
95. \_\_\_\_\_ . 1967b, *ibid.*, 149, 535.
96. \_\_\_\_\_ . 1968a, *ibid.*, 154, 57.
97. \_\_\_\_\_ . 1968b, in Stars and Stellar Systems, Vol. 7,  
Nebulae and Interstellar Matter, ed. B. Middlehurst and  
L. H. Aller (Chicago: Univ. of Chicago Press), pp. 707-754.
98. \_\_\_\_\_ . 1969a, *Space Sci. Rev.*, 9, 651.
99. \_\_\_\_\_ . 1969b, *Ap. J.*, 157, 1129.
100. Penston, M. V., Munday, V. A., Stickland, D. J., and Penston, M. J.  
1969, *Mon. Notices Roy. Astr. Soc.*, 142, 355.
101. Pikel'ner, S. 1967, *Astr. Zh.*, 44, 1915.
102. Price, R. M. 1974, *Astron. & Astrophys.*, 33, 33.
103. Radford, H. E. 1961, *Phys. Rev.*, 122, 114.
104. Radhakrishnan, V., Murray, J. D., Lockhart, P., and Whittle, R. P. J.  
1971, *Ap. J. Suppl.*, 24, No. 203.
105. Raimond, E. 1966, *B.A.N.*, 18, 191.
106. Rank, D. M., Townes, C. H., and Welch, W. J. 1971, *Science*, 174, 1083.
107. Roberts, W. W. 1969, *Ap. J.*, 158, 123.
108. Rots, A. H. 1974, Ph.D. Thesis (Groningen University).
109. Safranov, V. F. 1960a, *Dokl. Akad. Nauk (USSR)*, 130, 53.
110. \_\_\_\_\_ . 1960b, *Ann. d'Ap.*, 23, 979.
111. Schatzman, E. 1958, *Rev. Mod. Phys.*, 30, 1012 (Proc. IAU Symp. No. 8).
112. Schmidt, M. 1959, *Ap. J.*, 129, 243.
113. Schwarz, J., McCray, R., and Stein, R. F. 1972, *Ap. J.*, 175, 673.
114. Scoville, N. Z., and Solomon, P. M. 1974, *Ap. J. (Letters)*, 187, L67.

## REFERENCES - continued

115. Serkowski, K. 1973, IAU Symp. No. 52, p. 145.
116. Shajn, G. A. 1955, *Astron. Zh.*, 32, 381.
117. Shu, F. H. 1973, *American Scientist*, 61, 524.
118. \_\_\_\_\_. 1973b, IAU Symp. on Interstellar Dust and Related Topics, eds. M. Greenberg and H. C. van de Hulst, pp. 257-262.
119. \_\_\_\_\_. 1974, *Astron. & Astrophys.*, 33, 55.
120. Shu, F. H., Milione, V., and Roberts, W. W. 1973, *Ap. J.*, 183, 819.
121. Shu, F. H., Milione, V., Gebel, W., Yuan, C., Goldsmith, D. W., and Roberts, W. W. 1972, *Ap. J.*, 173, 557.
122. Solomon, P. M. 1973, *Physics Today*, 26, No. 3, 32.
123. Solomon, P. M., and Wickramasinghe, N. C. 1969, *Ap. J.*, 158, 449.
124. Spitzer, L., Jr. 1942, *Ap. J.*, 95, 329.
125. \_\_\_\_\_. 1951, *Problems of Cosmical Aerodynamics*, (Central Air Documents Office, Dayton, Ohio), p. 31.
126. \_\_\_\_\_. 1962, Physics of Fully Ionized Gases, 2nd edition, (New York: Interscience).
127. \_\_\_\_\_. 1968a, Diffuse Matter in Space (New York: Interscience).
128. \_\_\_\_\_. 1968b, in Stars and Stellar Systems, Vol. 7, Nebulae and interstellar Matter, ed, B. Middlehurst and L. H. Aller (Chicago: Univ. of Chicago Press), pp. 1 - 63.
129. Spitzer, L., Jr., and Scott, E. H. 1969, *Ap. J.*, 157, 161.
130. Strittmatter, P. A. 1966, *Mon. Notices Roy. Astr. Soc.*, 132, 359.
131. Swarztrauber, P. N. 1972, A Direct Method for the Discrete Solution of Separable Elliptic Equations, NCAR internal report.
132. Turner, B. E., and Vershuur, G. L. 1970, *Ap. J.*, 162, 341.

REFERENCES - continued

133. Verschuur, G. L. 1970a, Interstellar Gas Dynamics, ed. H. J. Habing (Dordrecht: D. Reidel Publishing Co.), pp. 150-167.
134. \_\_\_\_\_ . 1970b, Ap. J., 161, 867.
135. \_\_\_\_\_ . 1971, *ibid.*, 165, 651.
136. \_\_\_\_\_ . 1974, in Galactic and Extra-Galactic Radio Astronomy, ed. G. L. Verschuur and K. I. Kellermann (New York: Springer-Verlag), p. 179.
137. Watson, W. 1972, Ap. J., 176, 103, 271.
138. Woerden, H. van 1967, IAU Symp. No. 31, p. 3.
139. Woltjer, L. 1965, in Stars and Stellar Systems, Vol. 5, Galactic Structure, ed. A. Blaauw and M. Schmidt (Chicago: Univ. of Chicago Press), pp. 531-587.
140. Woodward, P. R. 1973, Ph.D. Thesis, (University of California, Berkeley).
141. Wright, W. E. 1973, Ph.D. Thesis (California Institute of Technology).
142. Zuckerman, B., and Evans, N. J. 1974, Ap. J. (Letters), 192, L152.
143. Zuckerman, B., and Palmer, P. 1974, Ann. Rev. Astr. and Astrophys., 12, 279.

## LEGENDS FOR FIGURES

1. A typical perturbation of the field lines of Parker's (1966) stratified initial state (schematic). The system is periodic in  $x$  and extends to infinity in  $y$ . There is reflection symmetry about the  $x$ -axis. Some field lines are left undeformed by the perturbation. Note that the deformed field lines curve in an opposite sense above and below each undeformed field line.
2. Two field lines,  $A$  and  $A+\Delta A$ , started out being close together in the stratified initial state. As expansion occurs at the "wings" (that is, at  $x = X$ ) of a condensation, their peak-to-peak vertical separation,  $h$ , increases. The mean value of the magnetic field,  $\bar{B}$ , between points  $a$  and  $b$  varies as  $h^{-1}$ . So, the magnetic-pressure force  $|\nabla_{\perp}^2 B^2 / 8\pi|$ , which tends to inflate the field lines further, varies as  $h^{-3}$ . However, the tension of the field lines,  $|B^2 (\partial \hat{s} / \partial s)| / 4\pi$ , in the space between  $a$  and  $b$  varies as  $h^{-2} \lambda_x^{-1}$ , where the horizontal wavelength  $\lambda_x$  is fixed and  $\hat{s}$  is a unit vector tangent to a field line. Thus, the field lines will not expand indefinitely. [Note that  $|\partial \hat{s} / \partial s| = (\text{radius of curvature})^{-1} \approx \lambda_x^{-1}$ .]
3. Variation of the magnetic field with  $y$  at the valley ( $x = 0$ ) and the wings ( $x = X$ ) of the condensation of Fig. 2c of Paper I. The field of the stratified initial state (in which  $\alpha = 1$ ) is also shown for comparison. The field is normalized to its value on the  $x$ -axis in the initial state. The unit of length is  $C^2/g$ .
4. Variation of the gas density with  $y$  at the valley ( $x = 0$ ) and at the wings ( $x = X$ ) of the condensation of Fig. 2c of Paper I. The density of the stratified initial state (in which  $\alpha = 1$ ) is also shown for comparison. The density is normalized to its value on the  $x$ -axis in the initial state. The unit of length is  $C^2/g$ .

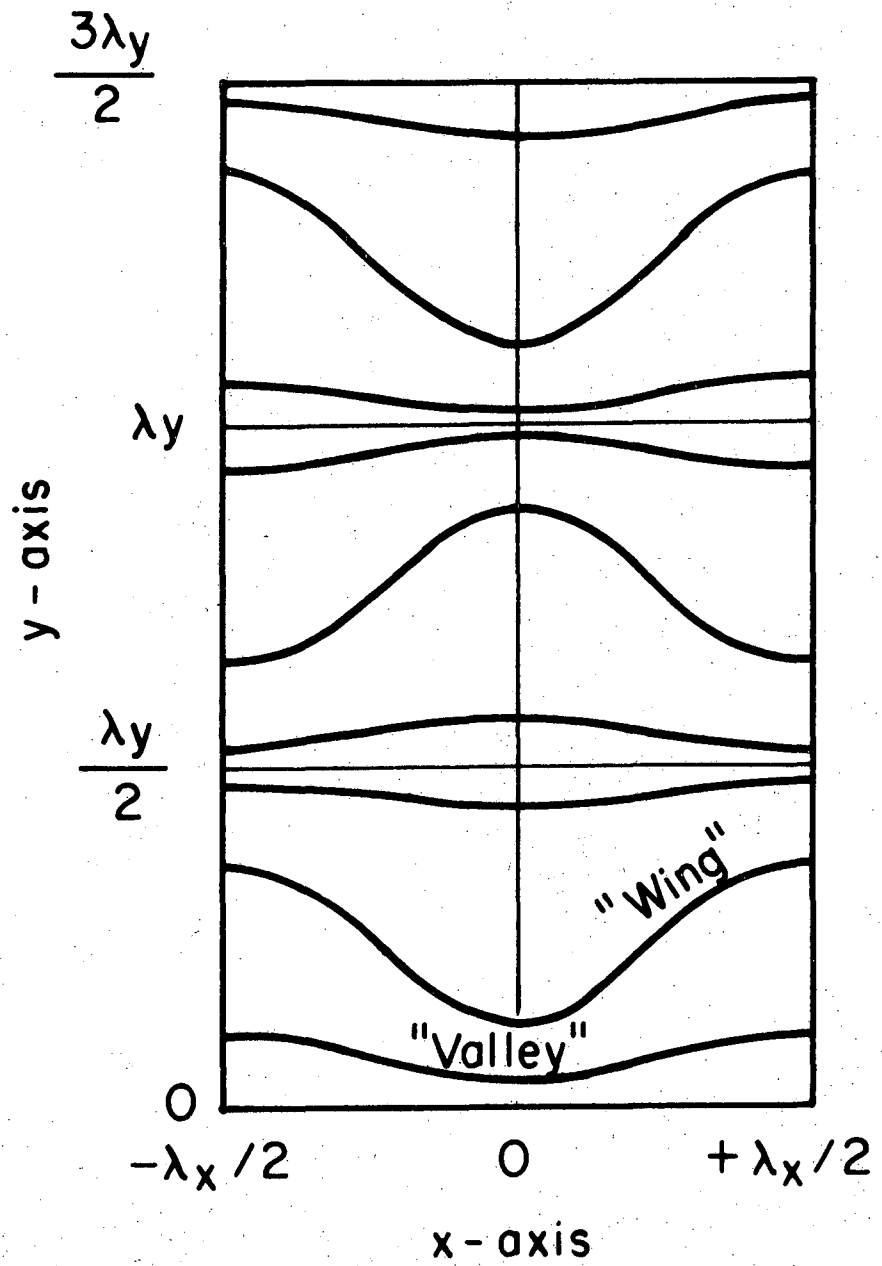


5. The dependence of the ratio of the magnetic-to-gas pressure on  $y$  at  $x = 0$  and  $x = X$  in the equilibrium state of Fig. 2c of Paper I. Note that  $\alpha$  varies considerably with position even though it was equal to unity everywhere in the initial state.
6. Vertical gravitational field of the Galaxy (taken from Oort, 1965).
7. The geometry used in § VII. There is axial symmetry about the  $z$ -axis and reflection symmetry about the plane  $z = 0$ . Instead of the cylindrical coordinates  $(r, z)$ , it is often convenient to use the non-orthogonal coordinates  $(\phi, z)$ , where  $\phi(r, z)$  is constant on a magnetic surface (see Eq. [125]). For a fixed  $z$ , we effect the change of variables from  $r$  to  $\phi$  by  $dr = d\phi(\partial r/\partial\phi)$ . The cloud boundary may be specified by the function  $Z_{cl} = Z_{cl}(\phi)$ .
- 8a, 8b, 8c. Equilibrium states characterized by the same  $\alpha_i (= 0.5)$  and  $P_0 (= 0.9)$  but different  $R_i (= 2.5, 2.7$  and  $2.8, \text{ respectively})$  -- see § VIIC for units. In each figure, we label both axes in units of the initial radius of the cloud,  $R_i$ ; the scale is the same for both axes. The curves bearing arrows represent field lines; each is labeled by its  $r$ -coordinate in the initial state (see § VIIB), in which field lines are equidistant and parallel to the  $z$ -axis. The solid, oblate curves are isodensity contours and they are labeled by the value of the density in units of the (uniform) density of the initial state. The dashed curves are contours of equal magnetic-field strength ("isopedion" contours). They are labeled by the magnitude of the field in units of the (uniform) field of the initial state.

From the isodensity and isopedion contours of each figure, one may estimate  $\alpha$  at equilibrium by using the formula  $\alpha_f = \alpha_i B_f^2/\rho_f$ .

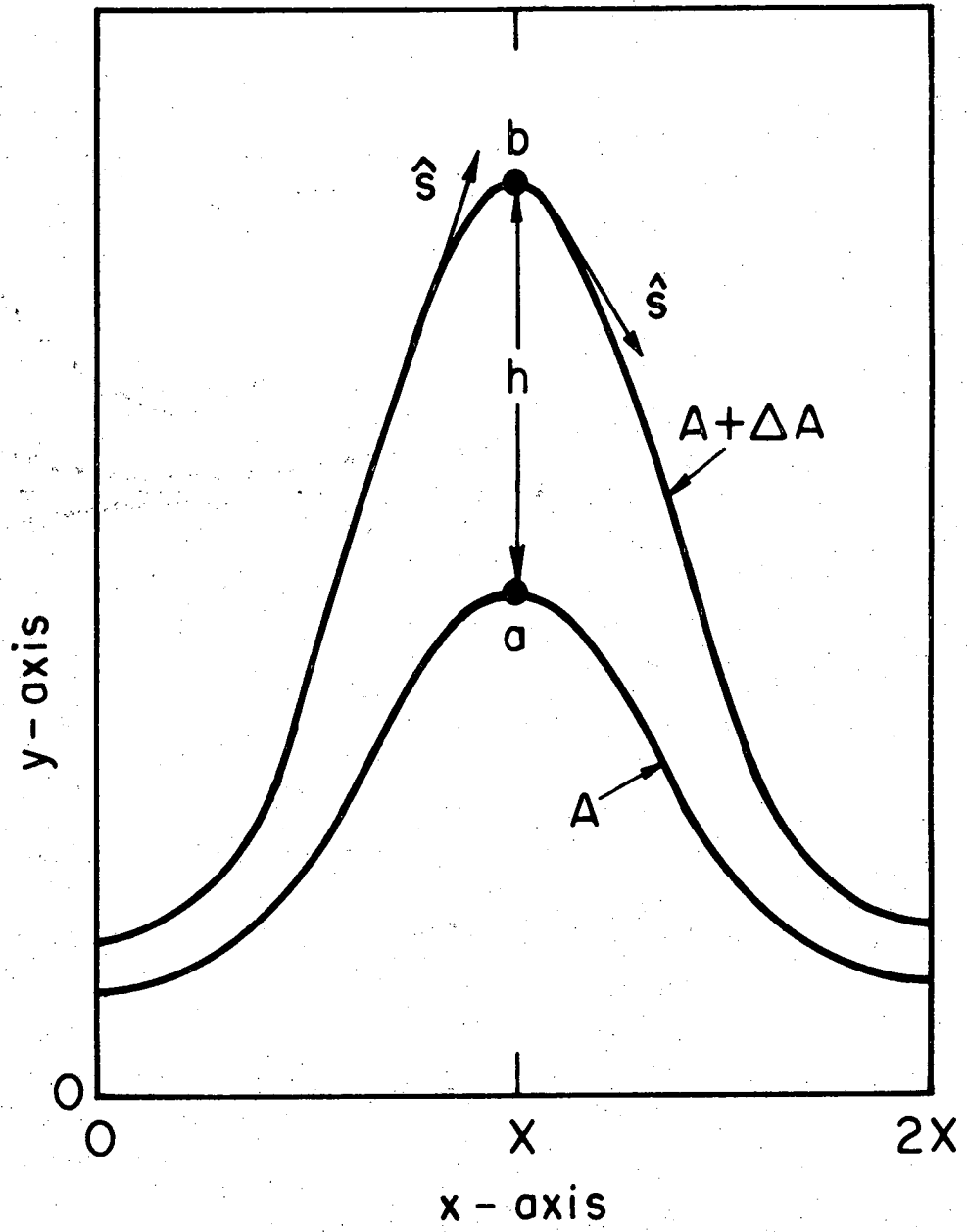
- 9a, 9b, 9c. Column (or, surface) densities for the equilibrium states of figs. 8a, 8b, and 8c, respectively, for two orientations of the line of sight. In each figure,  $\sigma_f(r)$  denotes the column density as a function of distance from the (z-) axis of symmetry (the line of sight is parallel to the symmetry axis);  $\sigma_f(z)$  is the column density as a function of z (the line of sight is parallel to the equatorial plane,  $z = 0$ ); the column density of the corresponding uniform initial state is labeled by  $\sigma_i$ . For ease in comparing an equilibrium state with the uniform initial state, the horizontal axes in each figure are labeled in units of the initial radius of the cloud,  $R_i$  ( $=2.5, 2.7, 2.8$ , respectively, in figs. 9a, 9b, and 9c). The unit of surface density is  $\rho_i C / (4 \pi G \rho_i)^{1/2}$  -- see § VIIC. Note that, since the magnetic field resists lateral compression,  $\sigma_f(r)$  has a smaller and shallower maximum than  $\sigma_f(z)$ . The ratio  $\sigma_f(z = 0) / \sigma_f(r = 0)$  may be taken as a measure of the degree of flattening of the cloud.
10. The function  $q(\Phi)$  for each of the equilibrium states of figs. 8a, 8b, and 8c. The abscissa is labeled in units of the total magnetic flux ( $2 \pi \Phi_{cl}$ ) threading each cloud. Each curve is identified by the value of the cloud radius in the uniform initial state -- see § VIIC for units.
- 11a, 11b, 11c. Equilibrium states characterized by the same  $\alpha_i$  ( $=0.5$ ) and  $R_i$  ( $=2.4$ ) but different  $P_0$  ( $=1.9, 2.9, \text{ and } 3.9$ , respectively). Iso-density and isopedion contours and field lines are denoted and labeled as in fig. 8.
- 12a, 12b, 12c. Column densities for the equilibrium states of figs. 11a, 11b, and 11c, respectively, for the same two orientations of the line of sight as in fig. 9. Notation and labeling of curves is as in fig. 9.

13. The function  $q(\phi)$  for each of the equilibrium states of figs. 11a, 11b, and 11c. Each curve is labeled by the value of  $P_0$  in the corresponding state.
- 14a, 14b. Equilibrium states characterized by the same  $P_0 (=0.9)$  and  $R_i (= 2.5)$  but different  $\alpha_i$  ( $=0.2$  and  $1.0$ , respectively). Fig. 8a shows the equilibrium state with  $\alpha_i = 0.5$  and the same  $P_0$  and  $R_i$  as the above two states. Notation and labeling of curves is as in fig. 8.
- 15a, 15b. Column densities for the equilibrium states of figs. 14a and 14b, respectively. For further details, see legend of fig. 9.
16. The function  $q(\phi)$  for each of the equilibrium states of figs. 14a, 8a, and 14b. Each curve is labeled by the value of  $\alpha_i$  in the corresponding uniform initial state. Notation is as in fig. 10.
17. Relation between the enhancement of the central magnetic field and that of the central density. Each curve is labeled by the value of  $\alpha_i$  and represents many different equilibrium states (see § VIIF1a for details).
18. The external pressure (in units of the initial cloud pressure) plotted against the enhancement of the central density for a fixed value of  $\alpha_i$  and  $R_i$  (see § VIIF1b).
- 19a, 19b. A critical state and its column densities. The three parameters  $\alpha_i$ ,  $P_0$ , and  $R_i$  have the values  $1.0$ ,  $0.5$ , and  $3.20$ , respectively. The properties of this state are discussed in detail in § VIIF2.



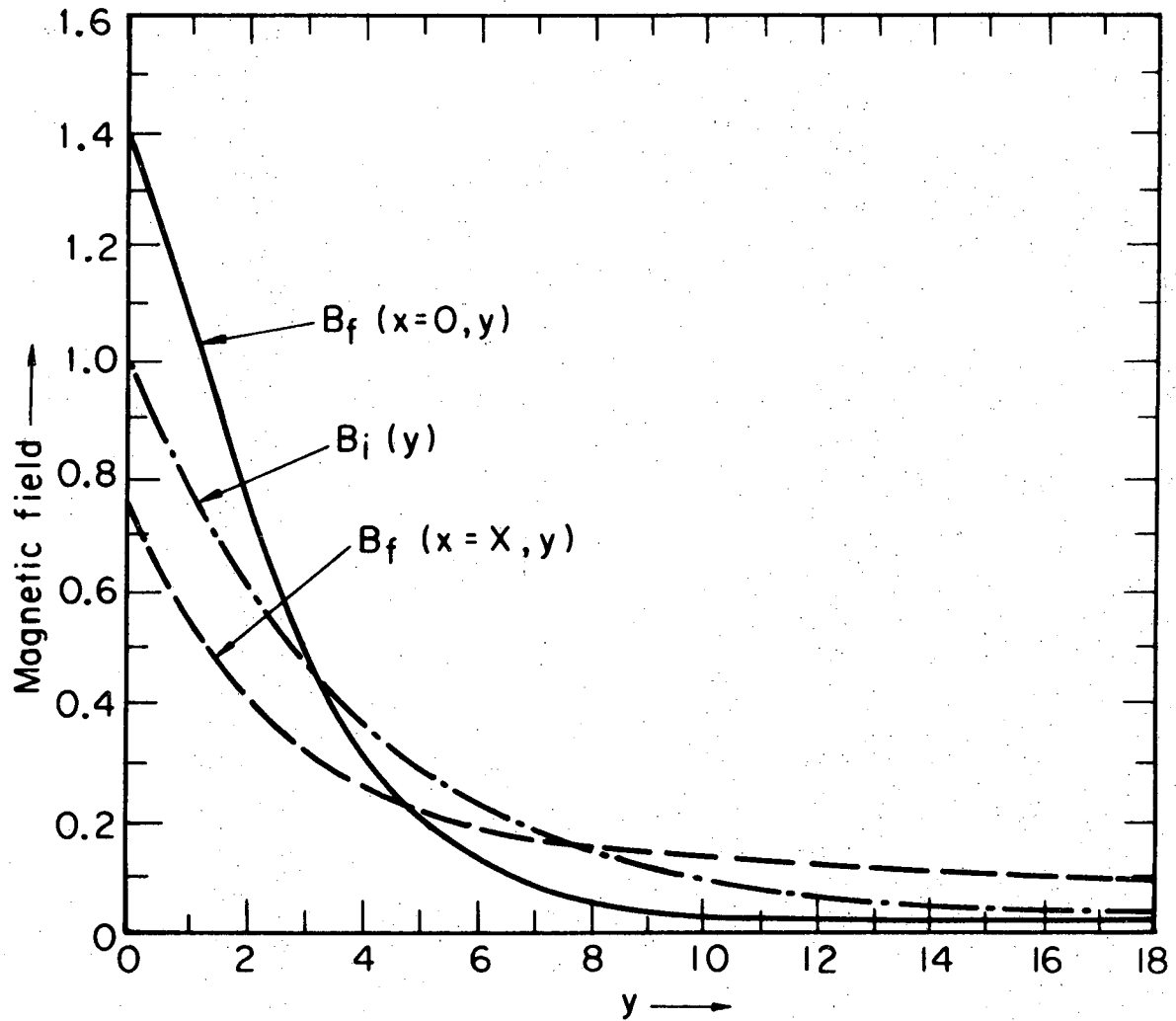
XBL752-2248

Fig. 1



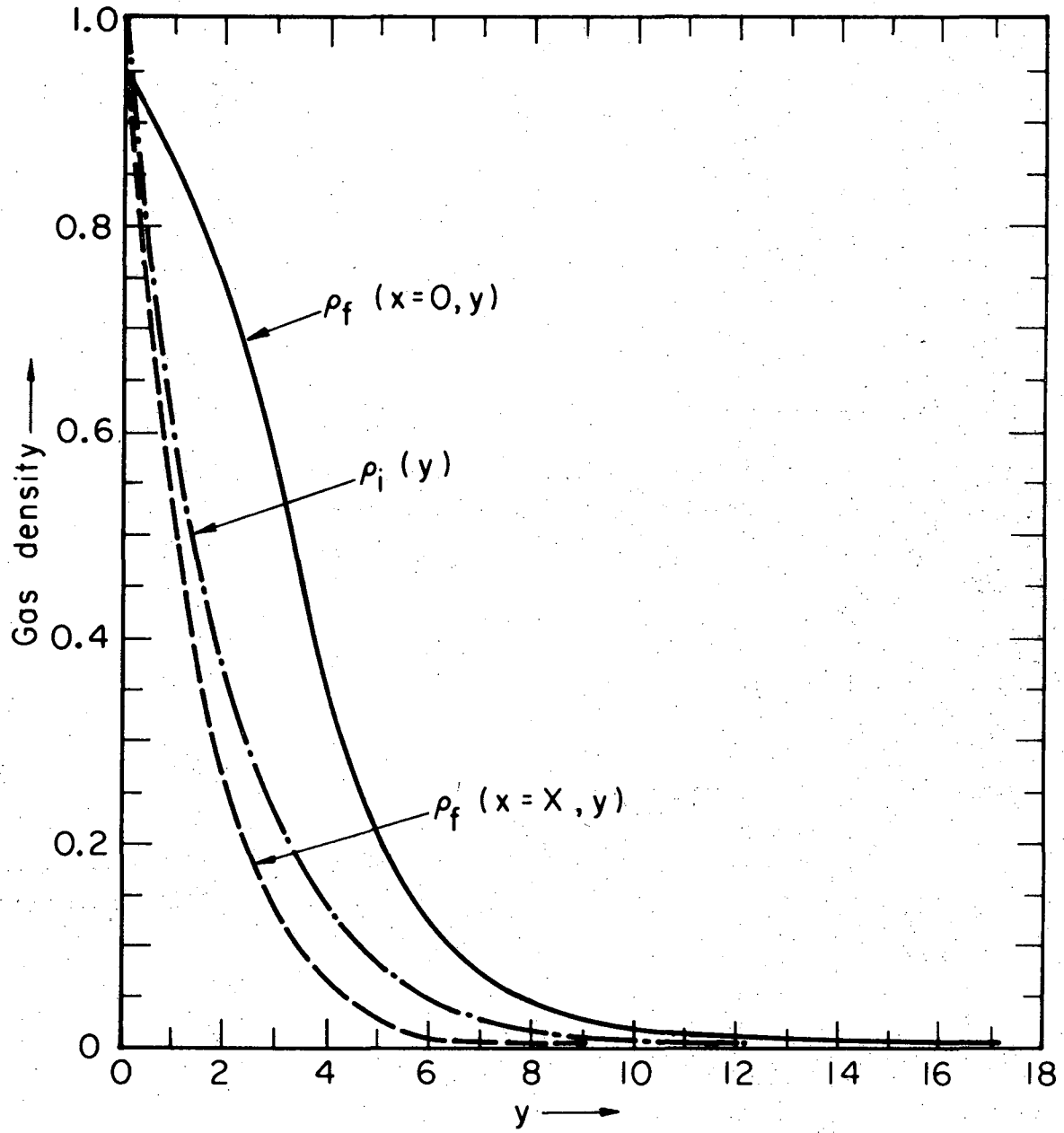
XBL 752-2251

Fig. 2



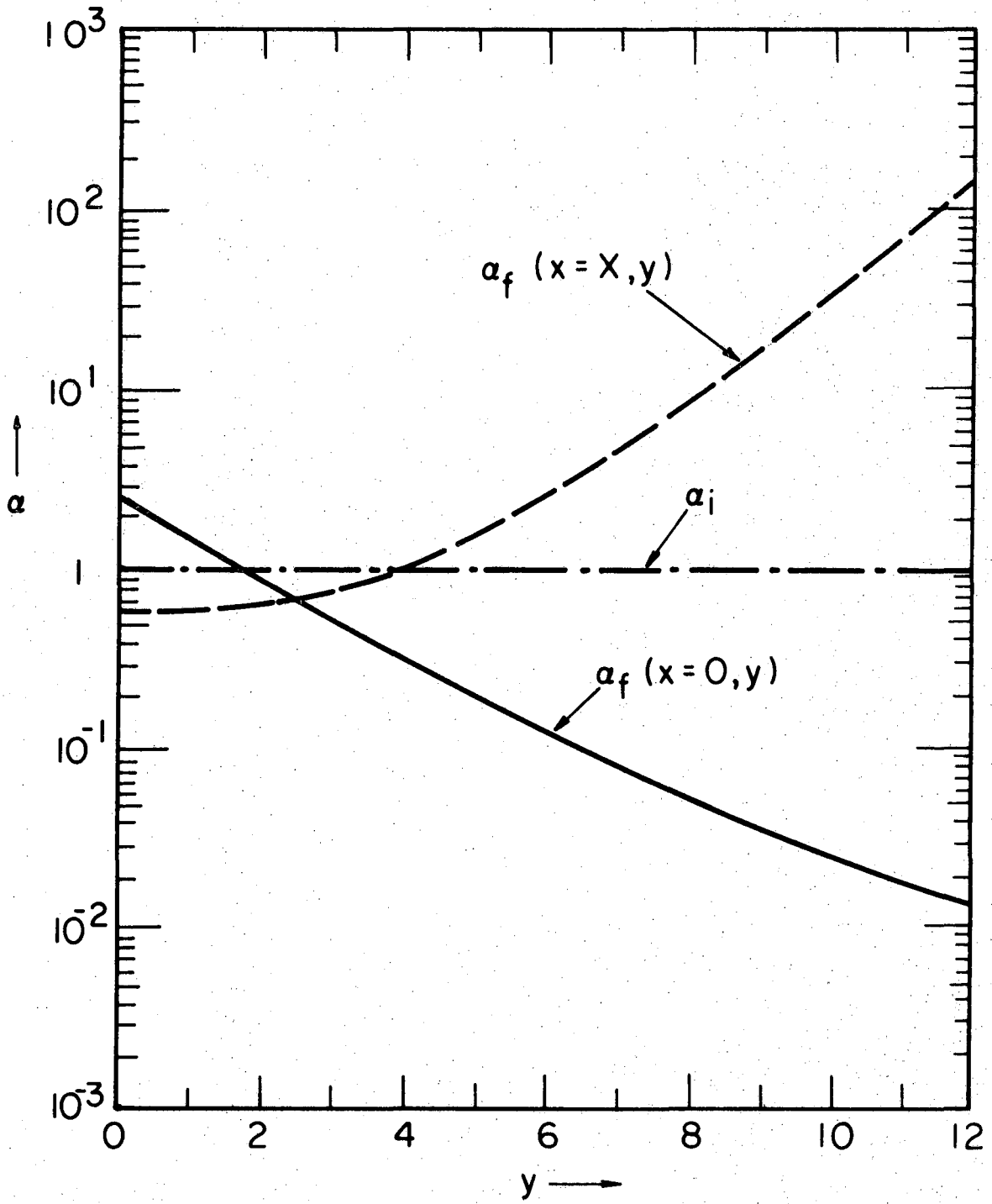
XBL752-2250

Fig. 3



XBL 754-2754

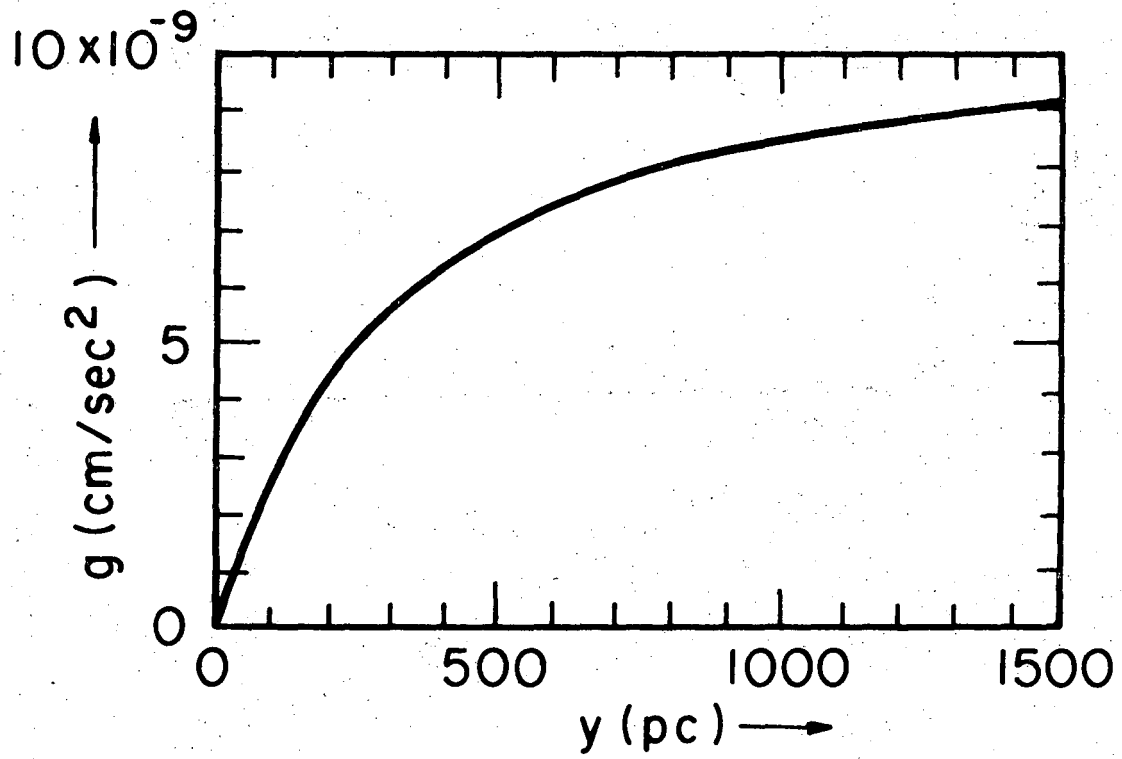
Fig. 4



XBL752-2249

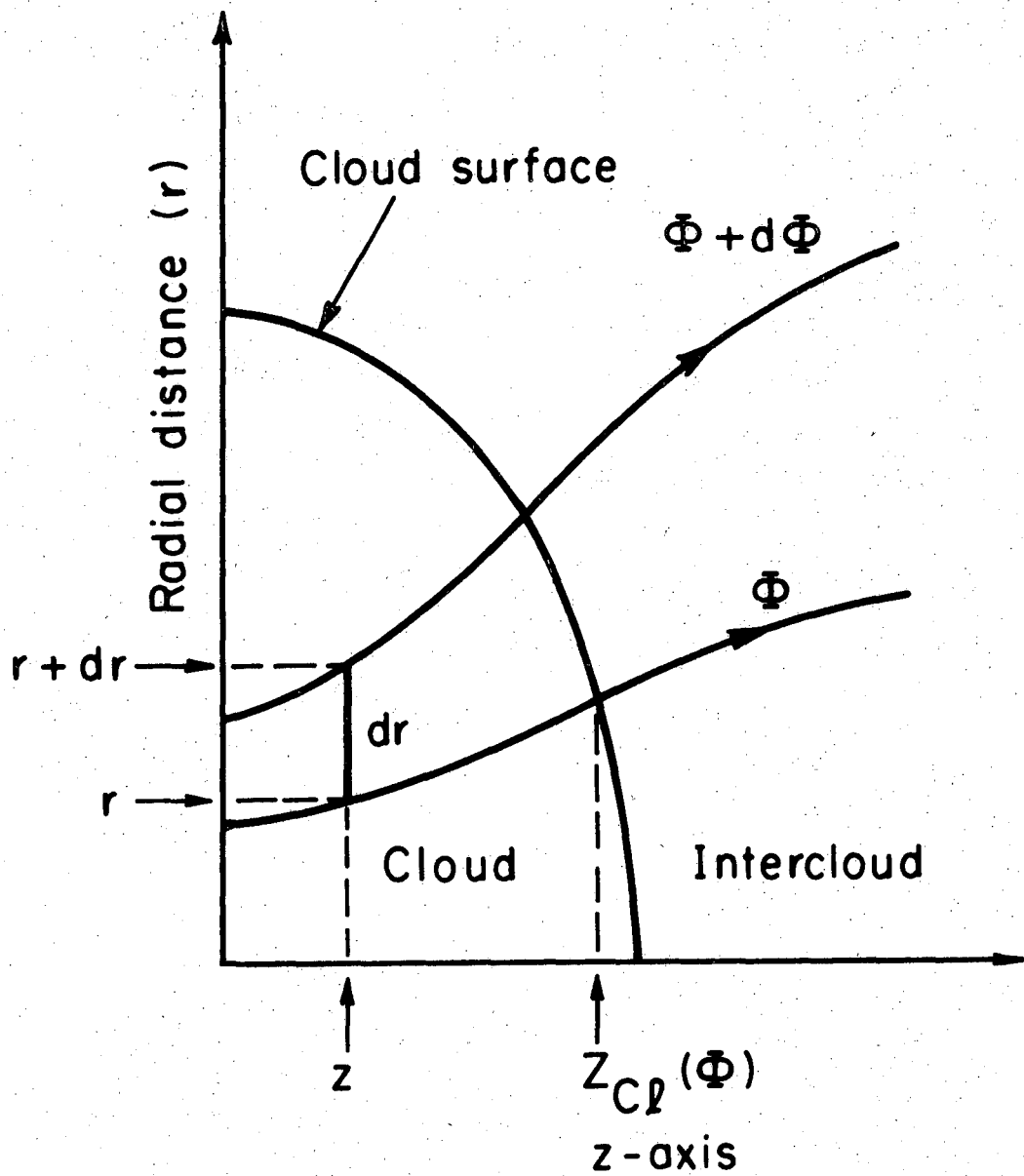
Fig. 5





XBL752-2253

Fig. 6.



XBL752-2252

Fig. 7

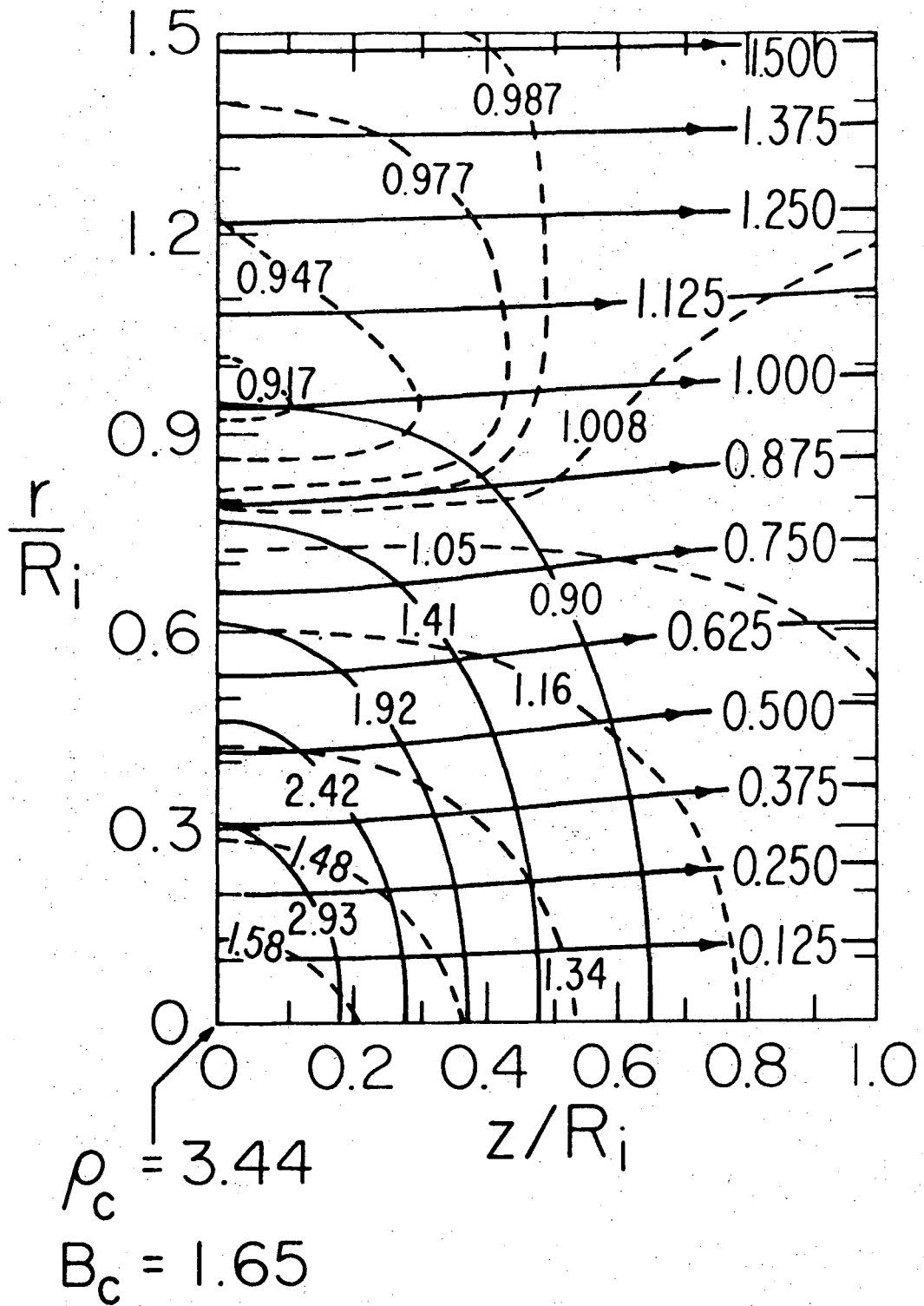


Fig. 8a

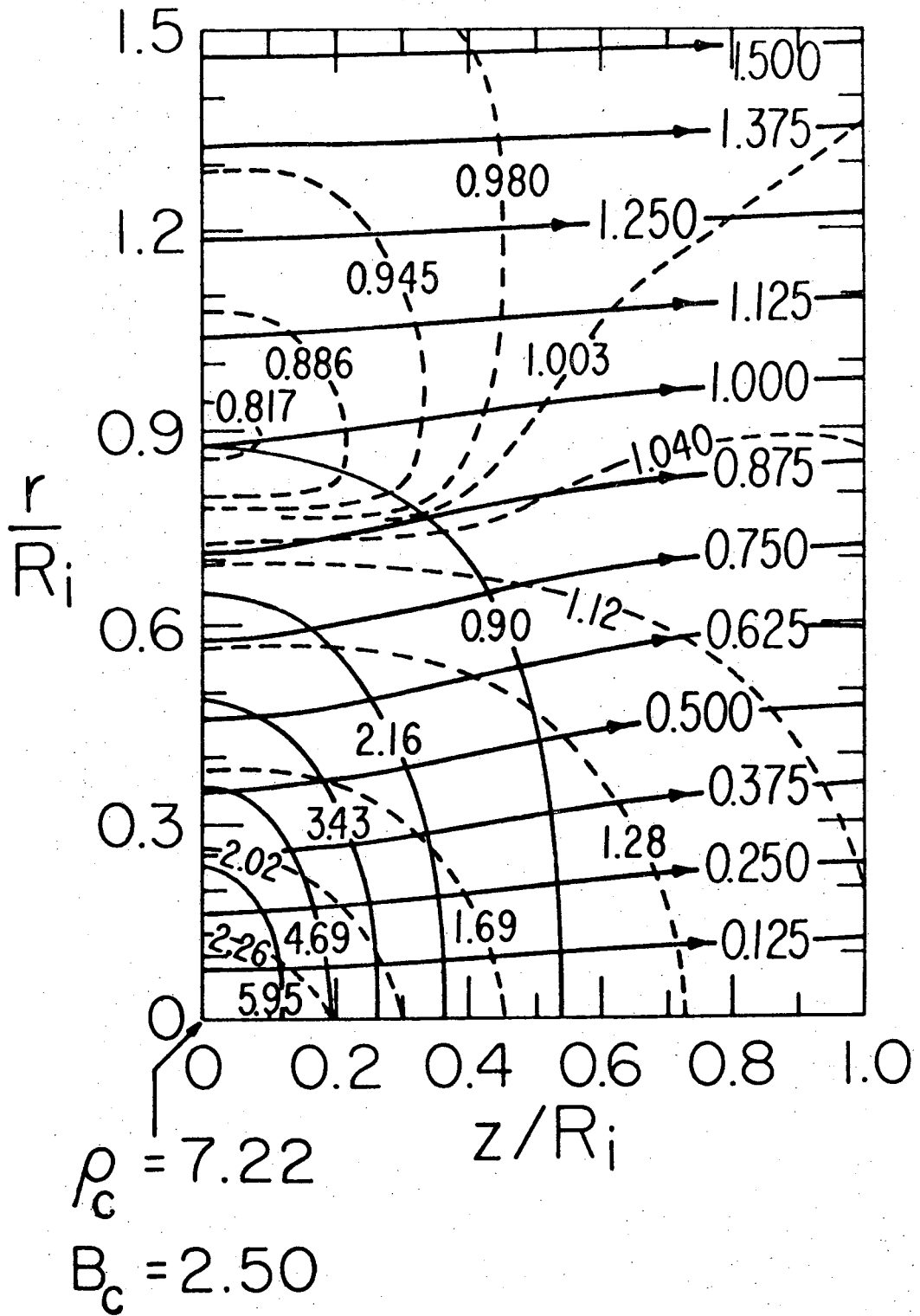


Fig. 8b

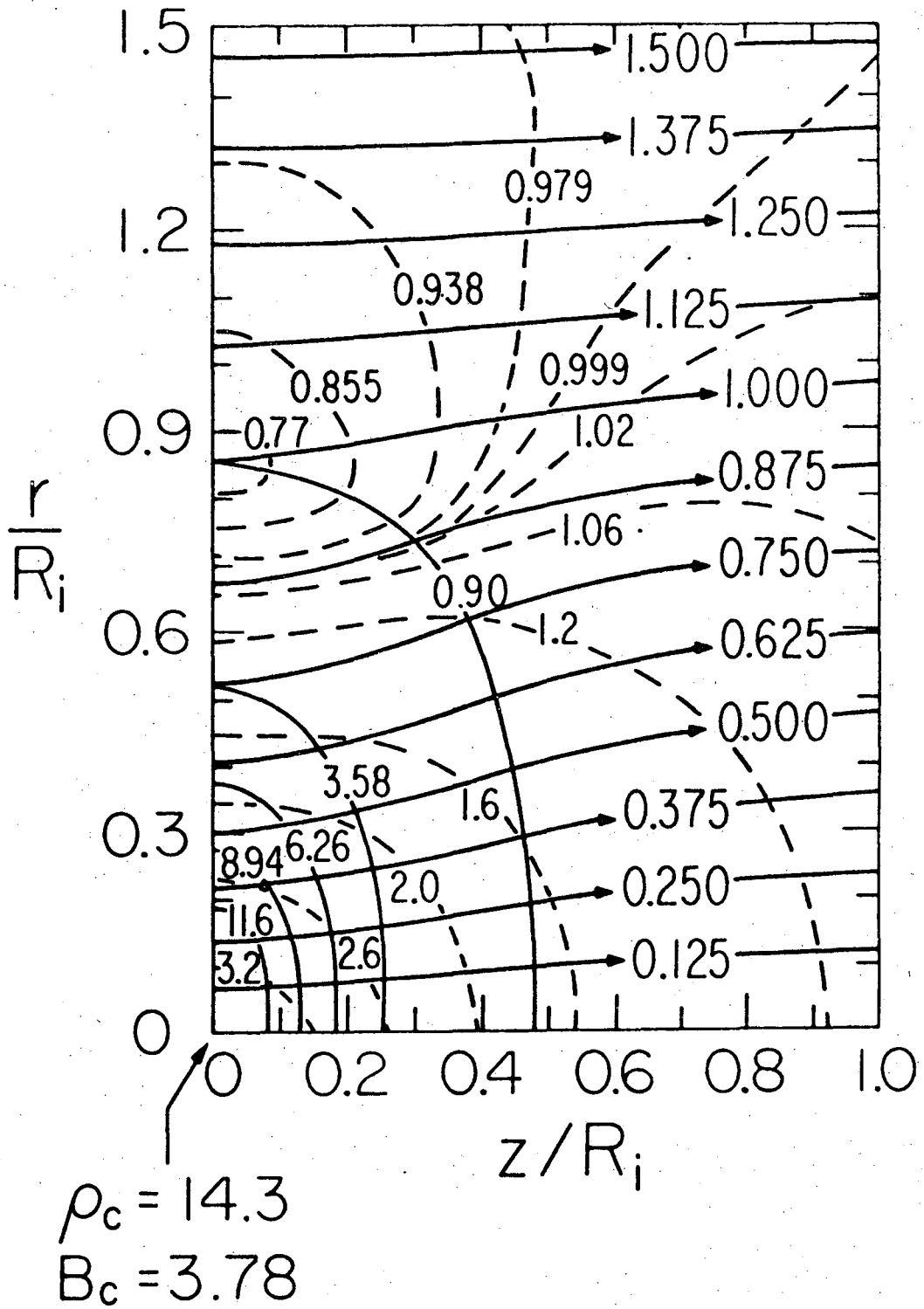


Fig. 8c

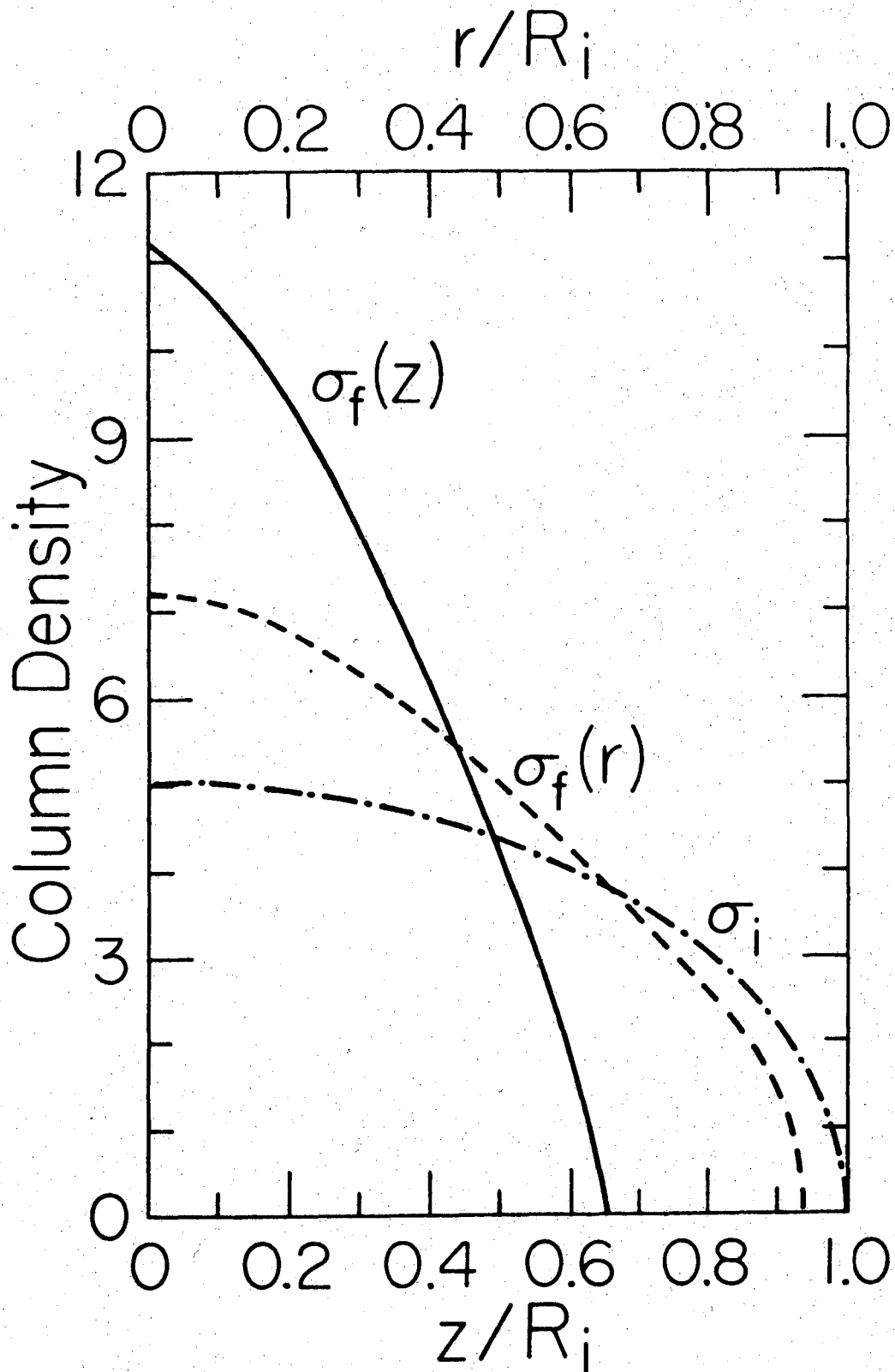


Fig. 9a

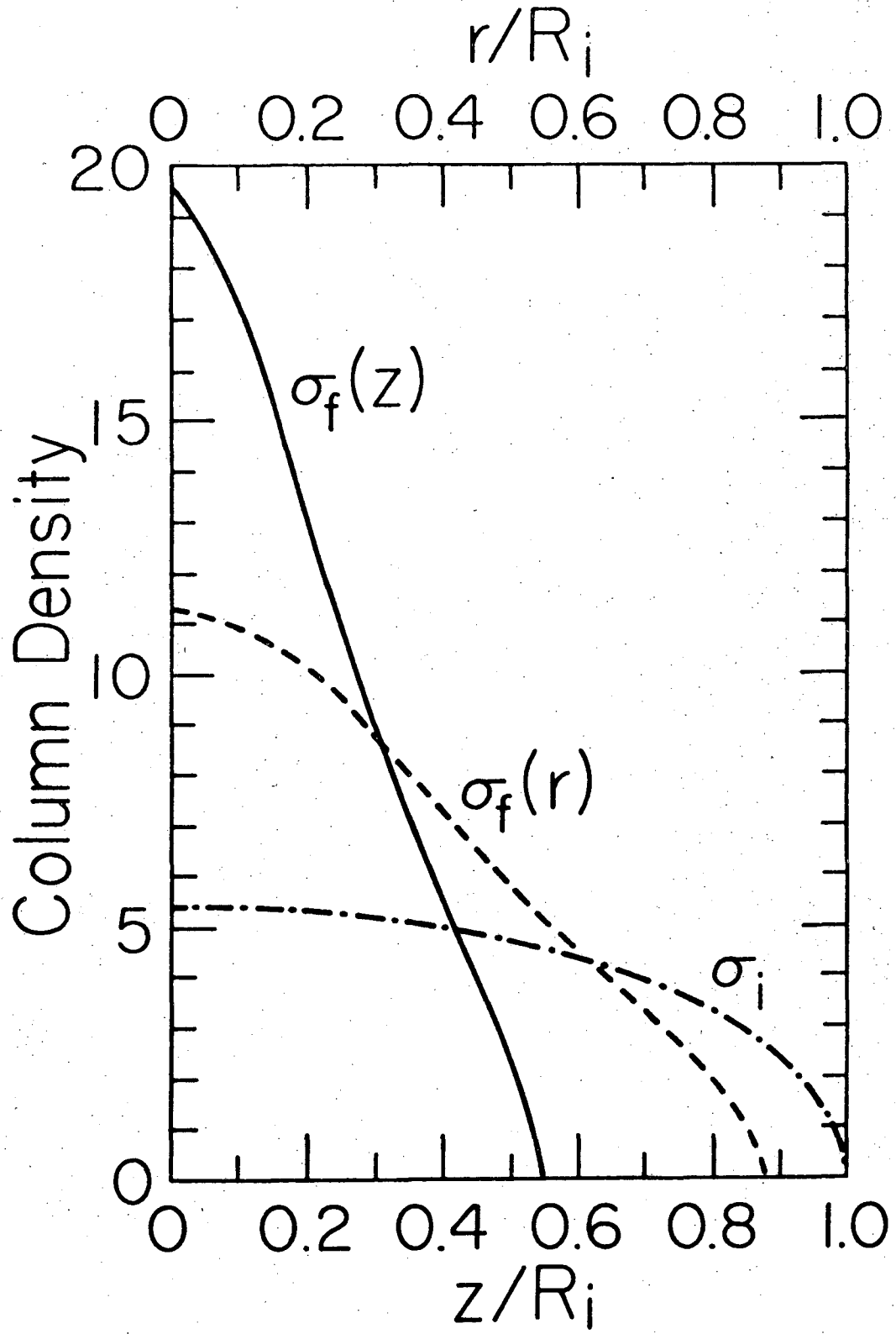


Fig. 9b

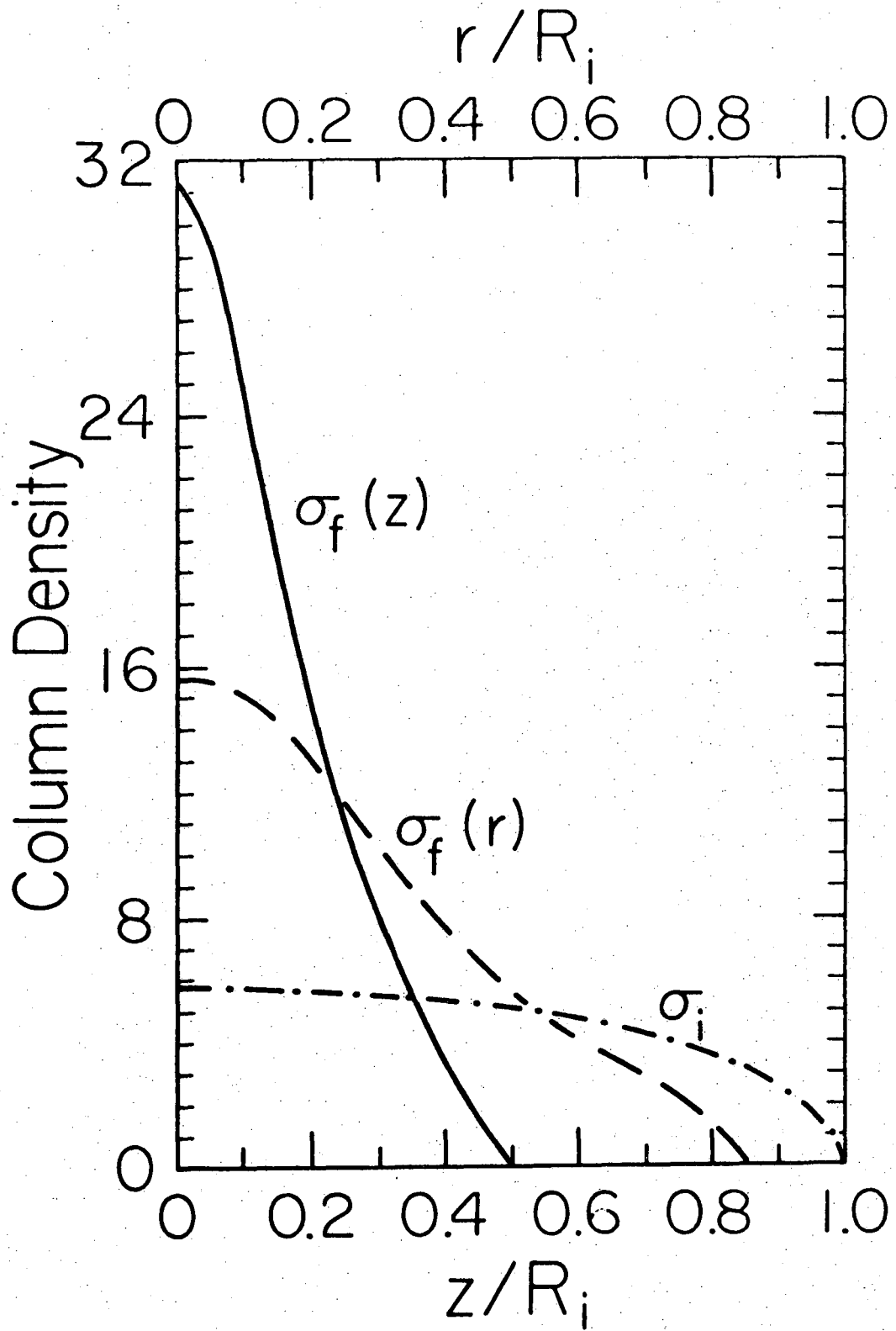


Fig. 9c



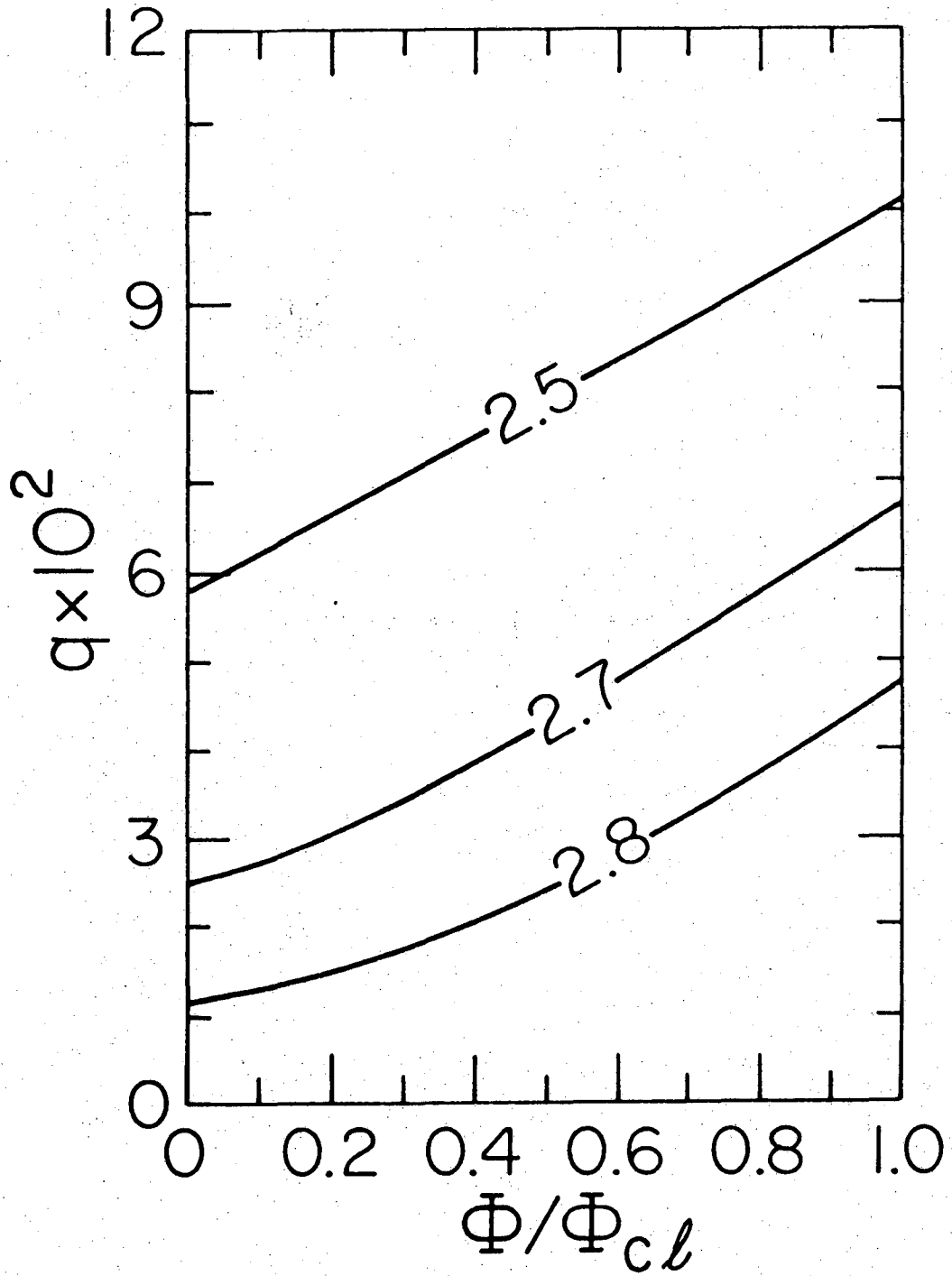


Fig. 10

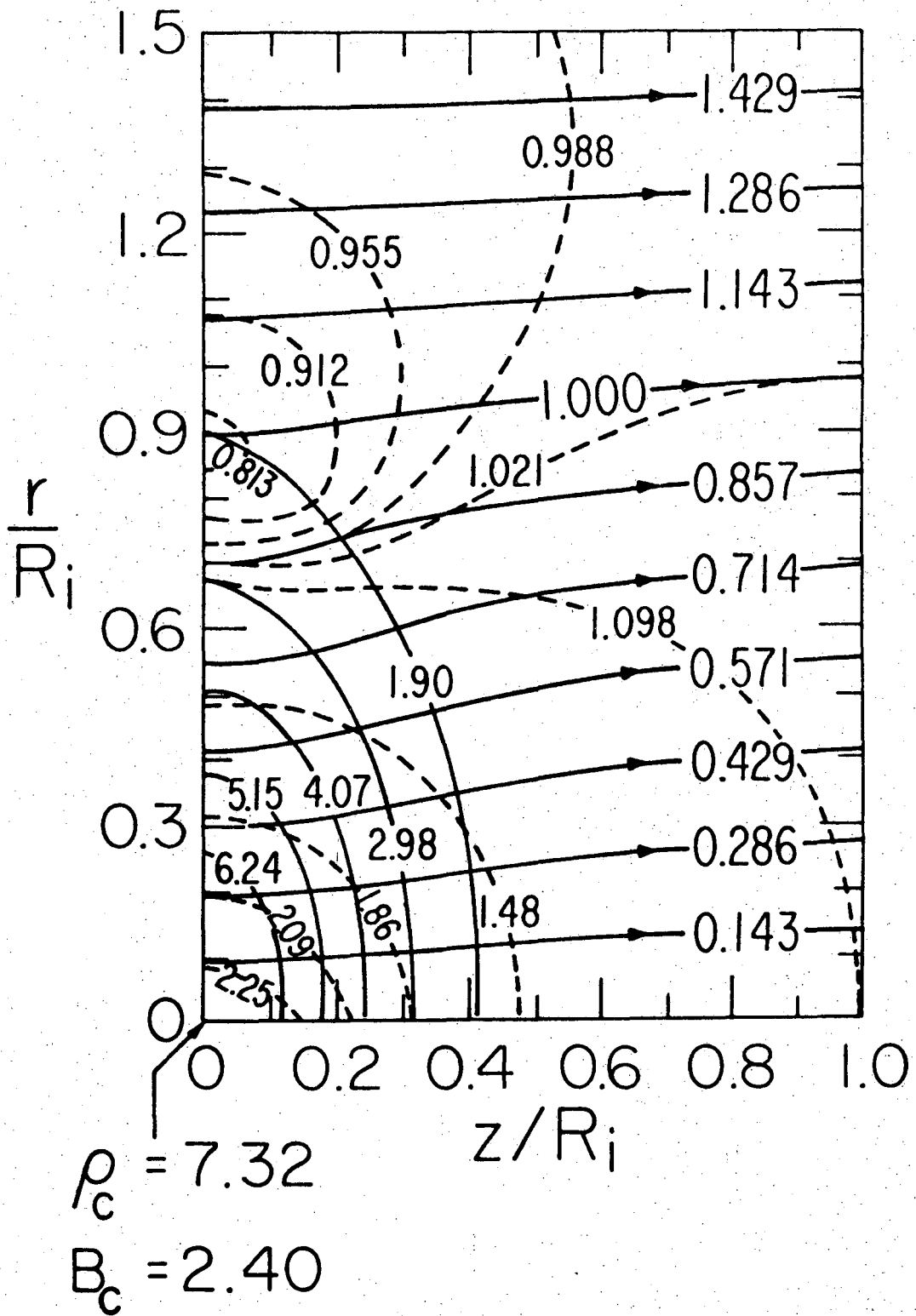


Fig. 11a

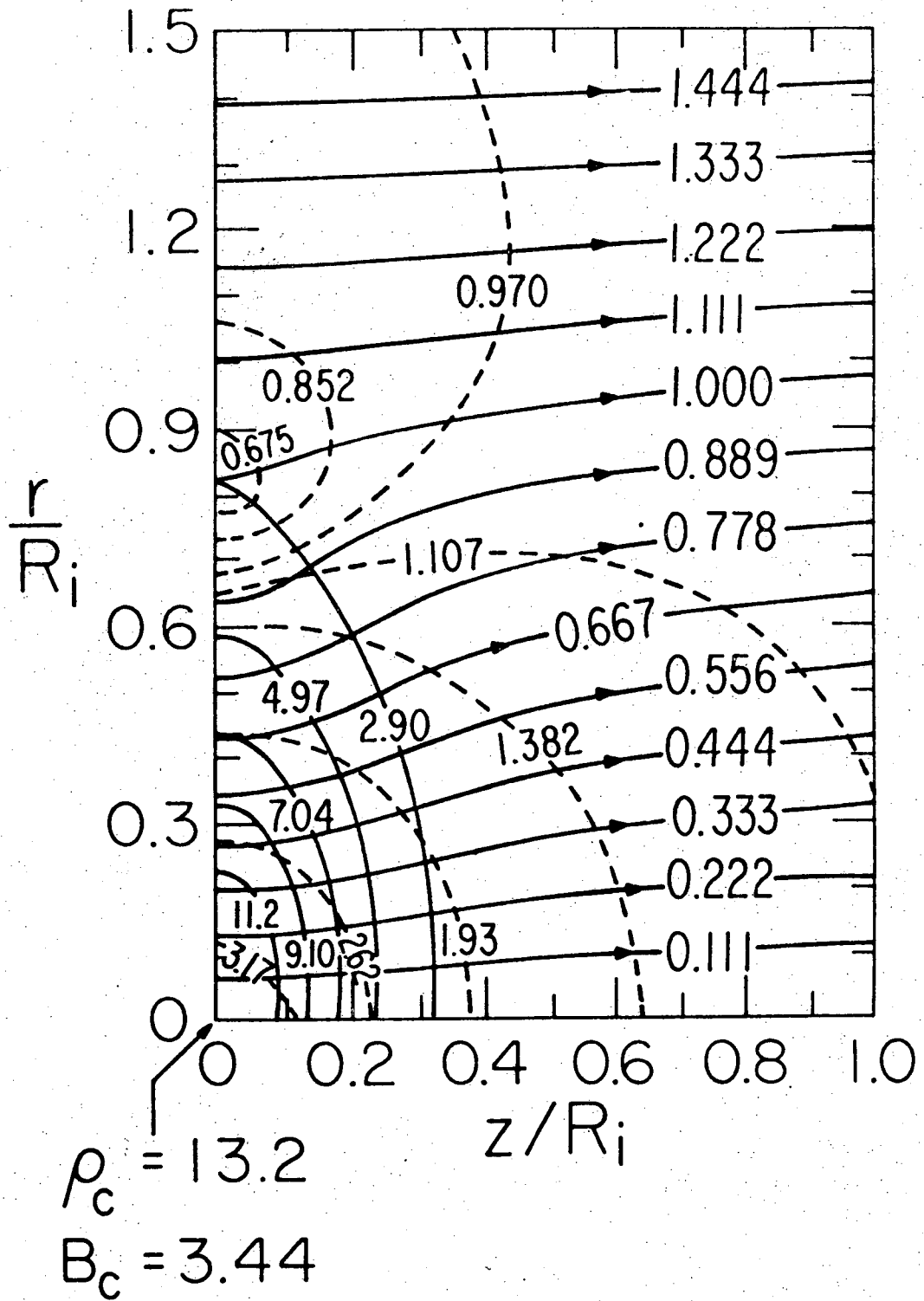


Fig. 11b

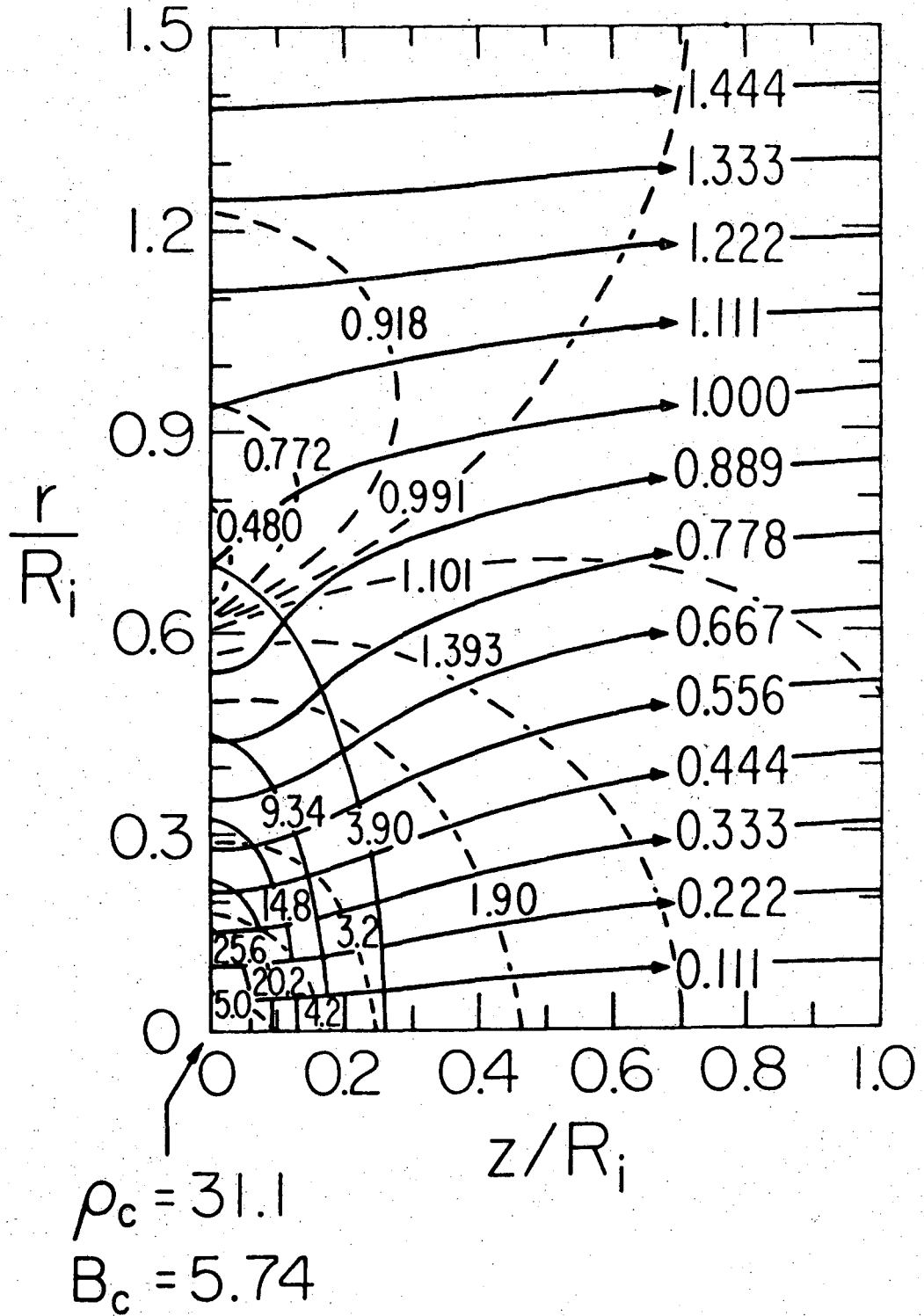


Fig. 11c

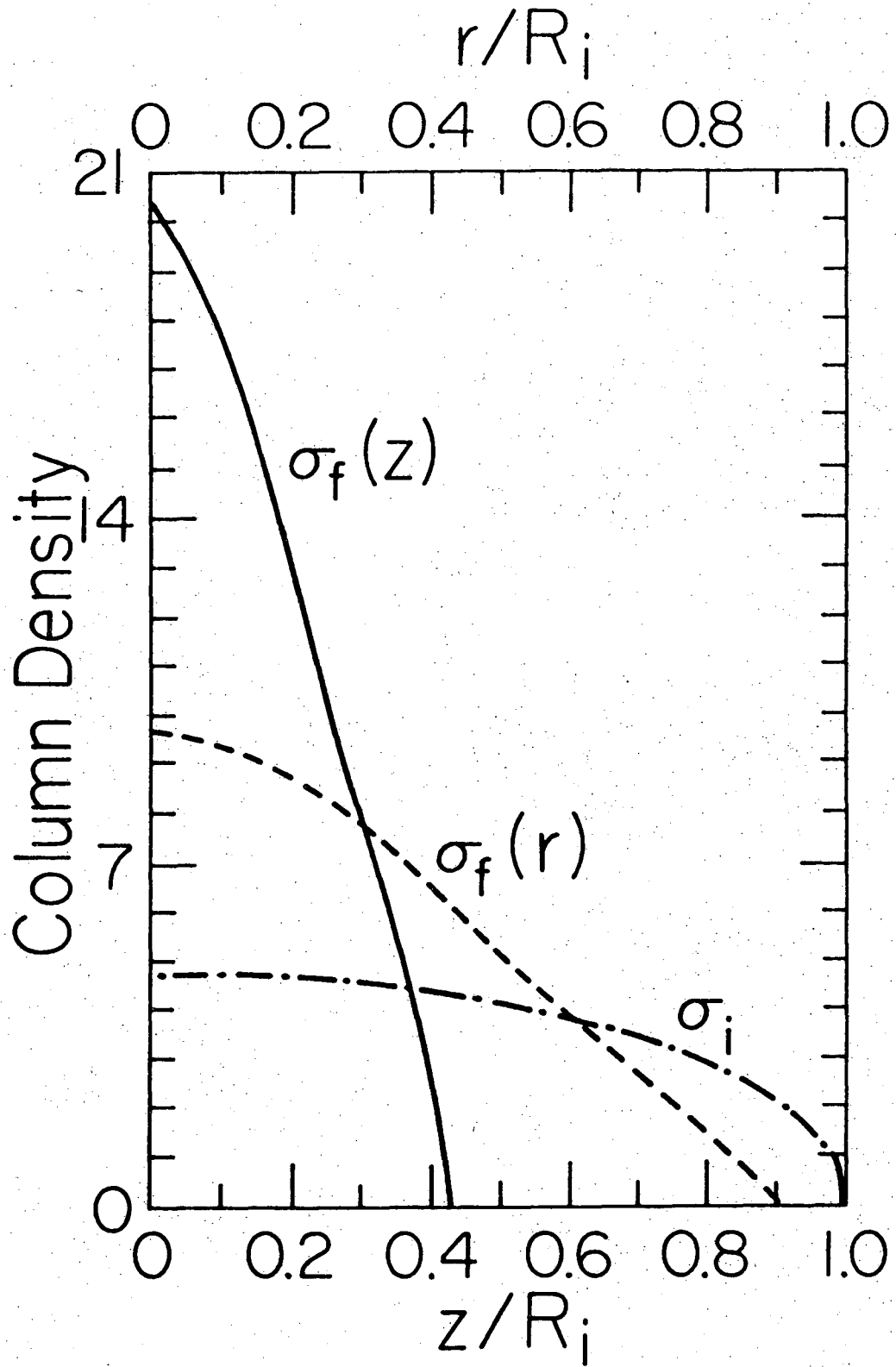


Fig. 12a

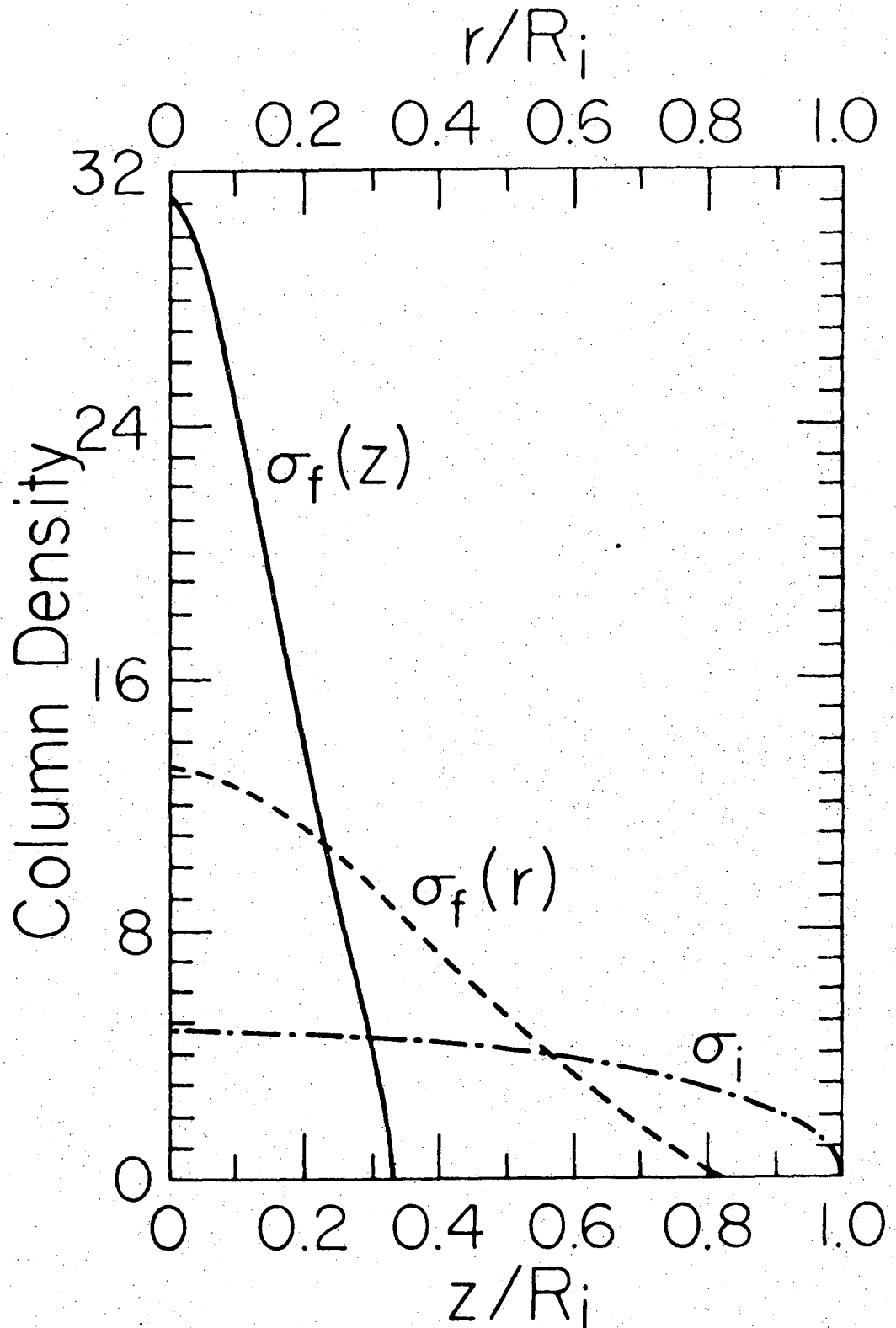


Fig. 12b

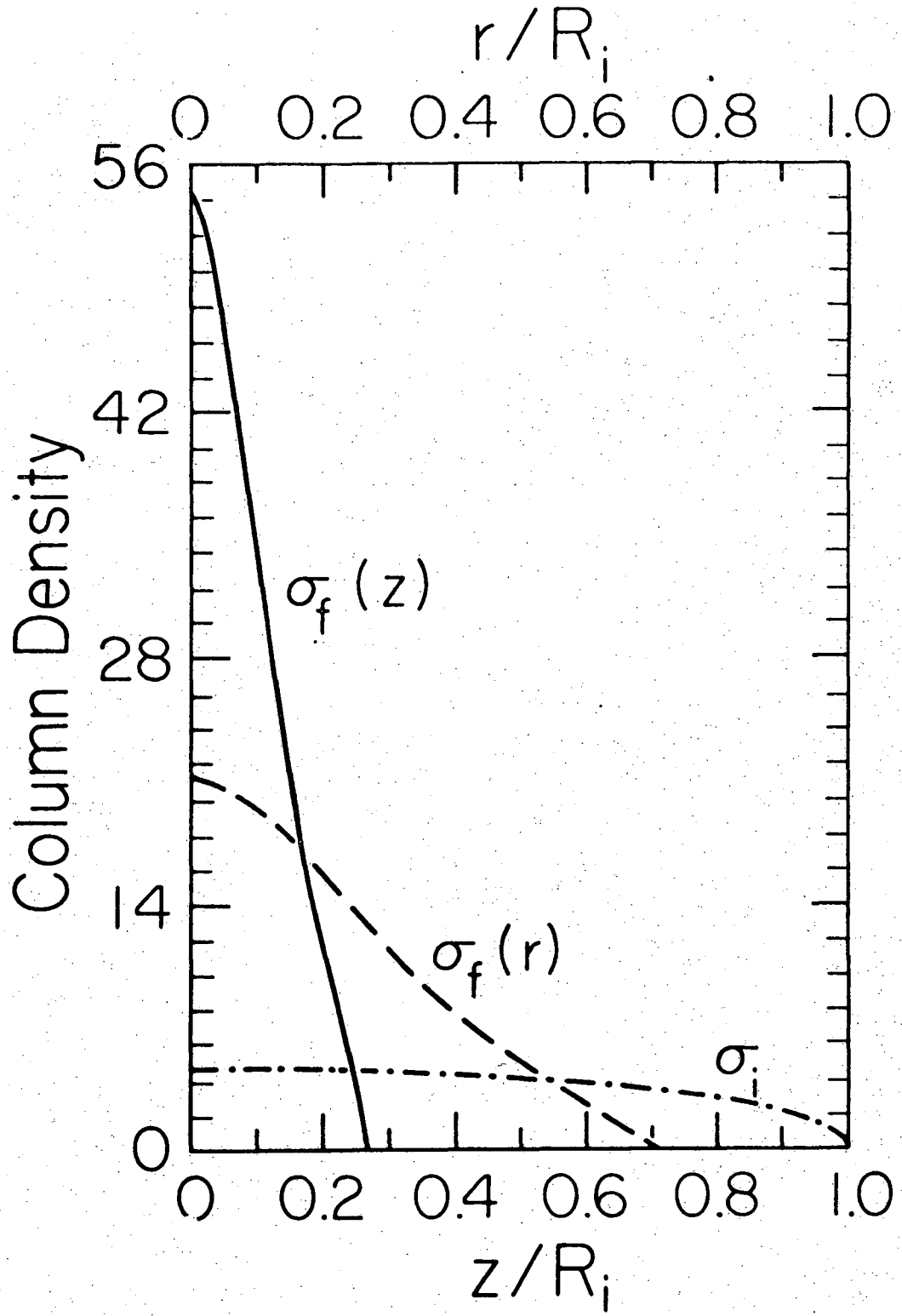


Fig. 12c

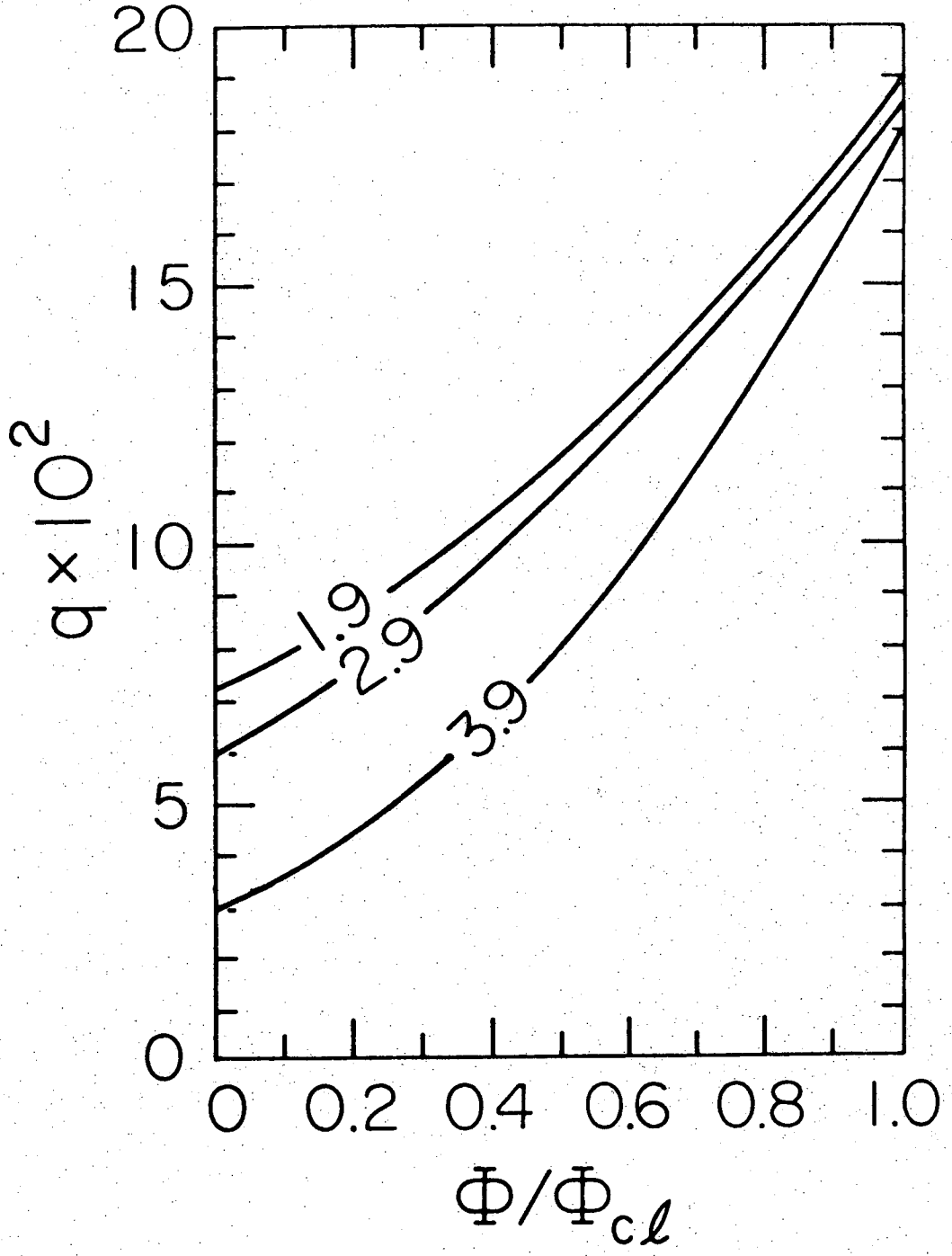


Fig. 13



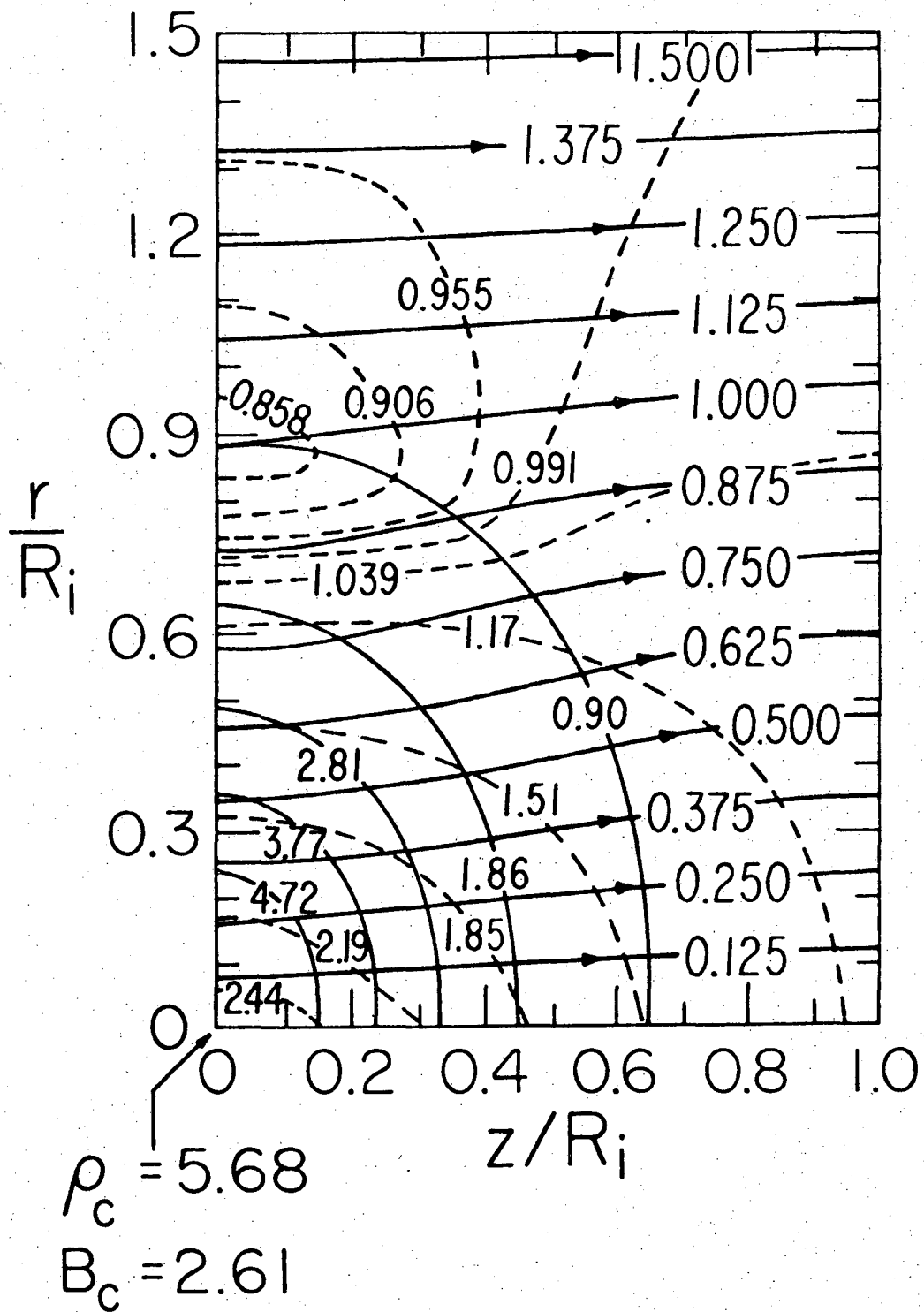


Fig. 14a

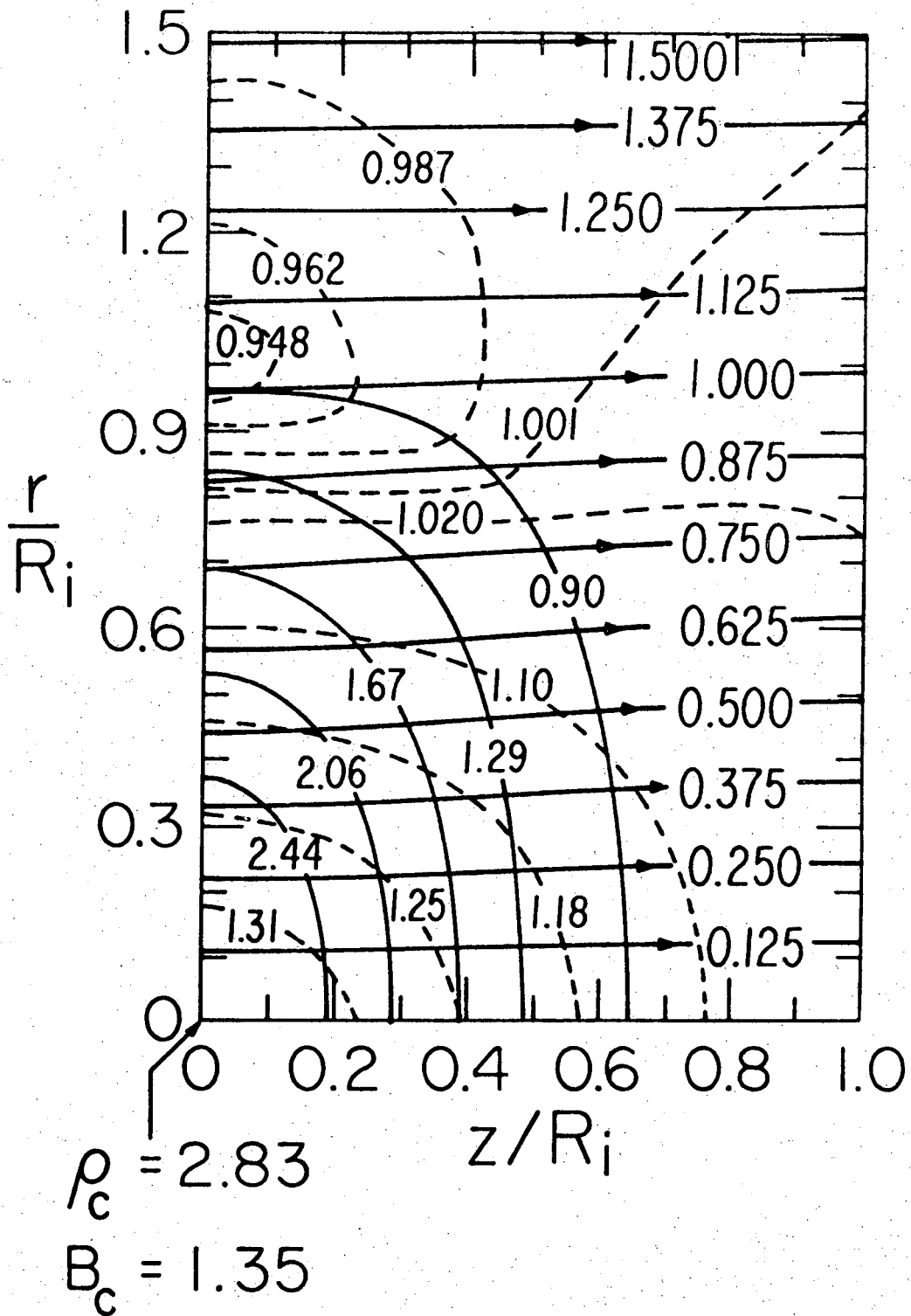


Fig. 14b

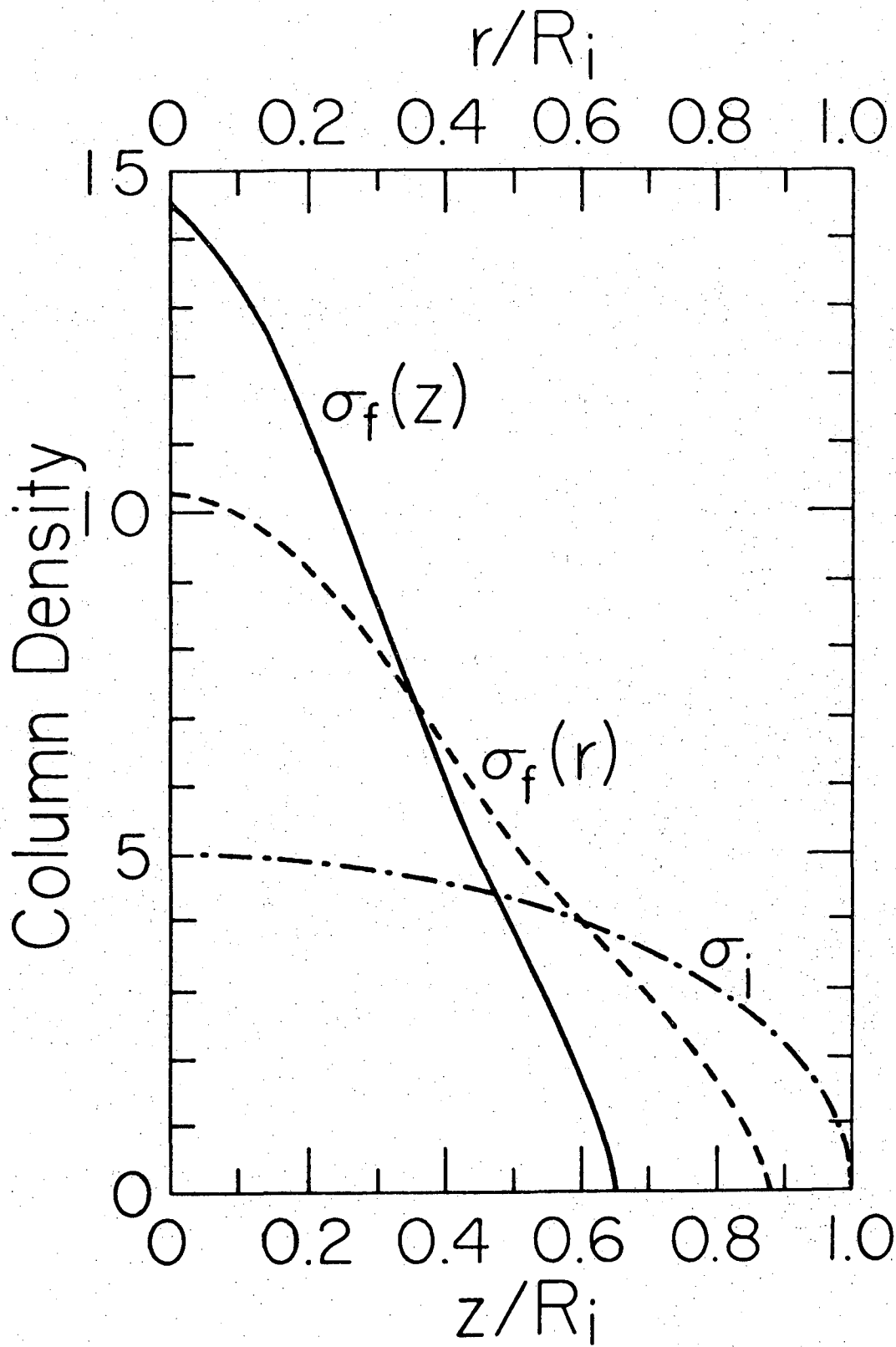


Fig. 15a

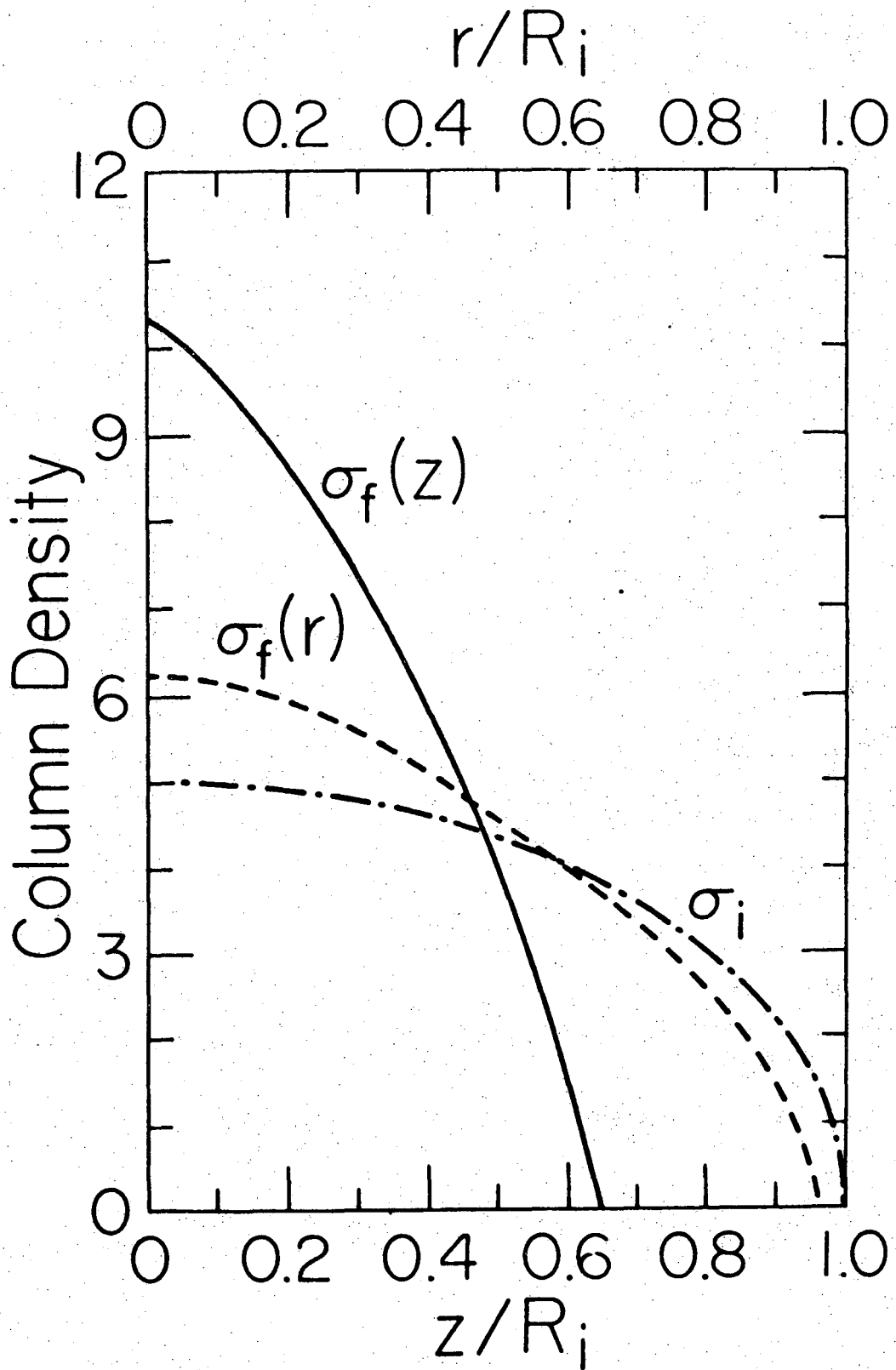


Fig. 15b

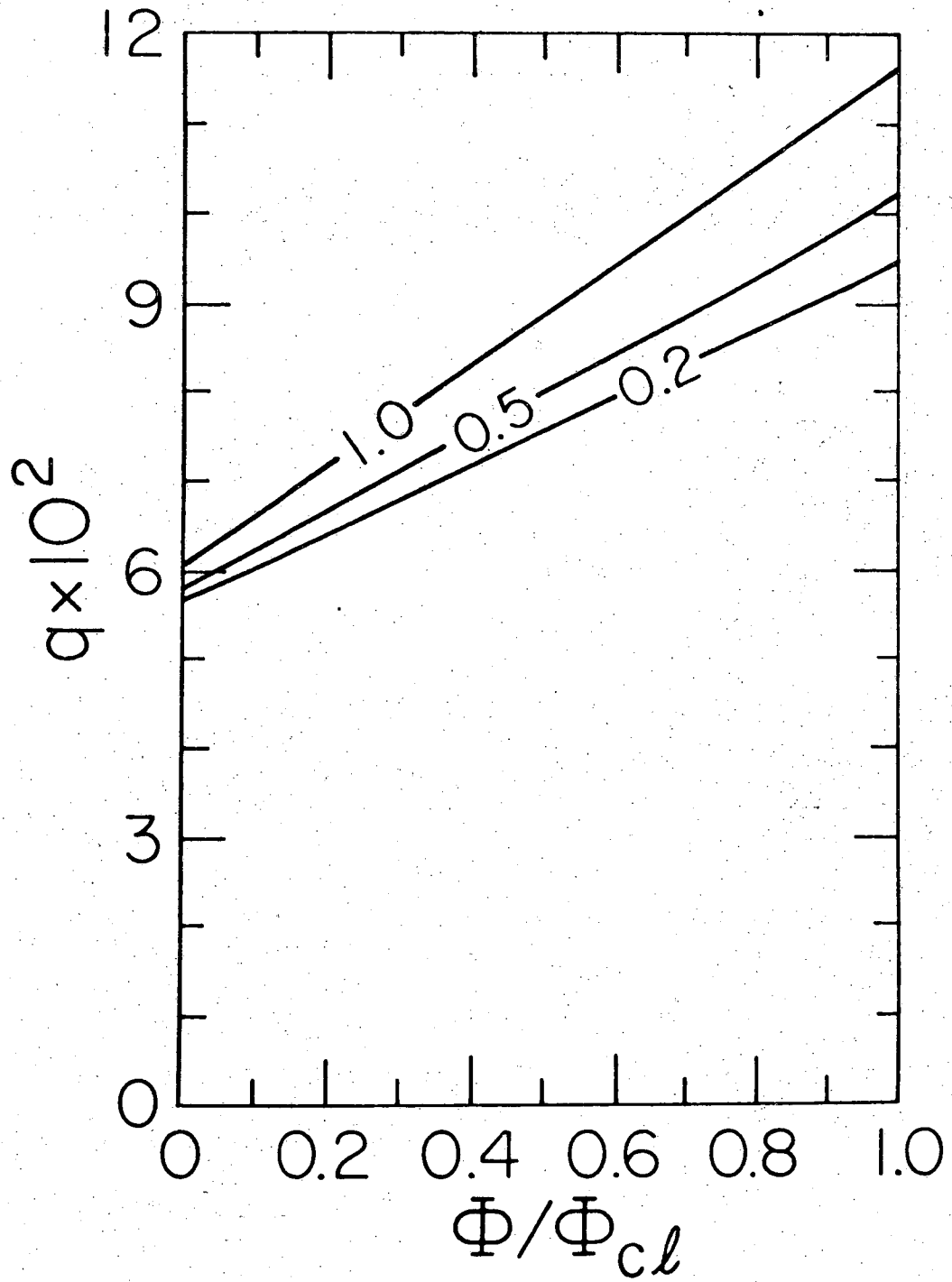


Fig. 16

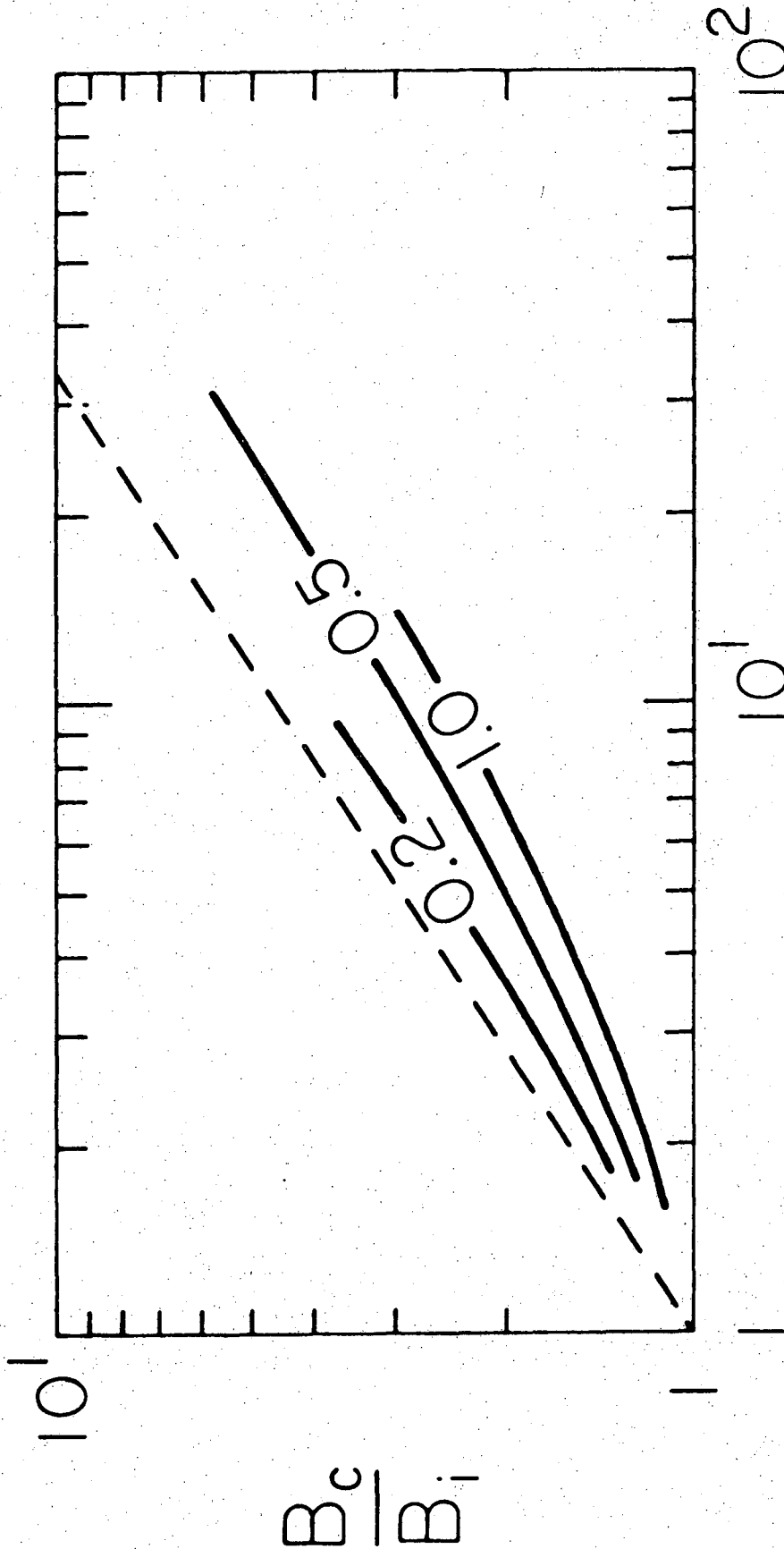


Fig. 17  
 $\rho_c/\rho_i$

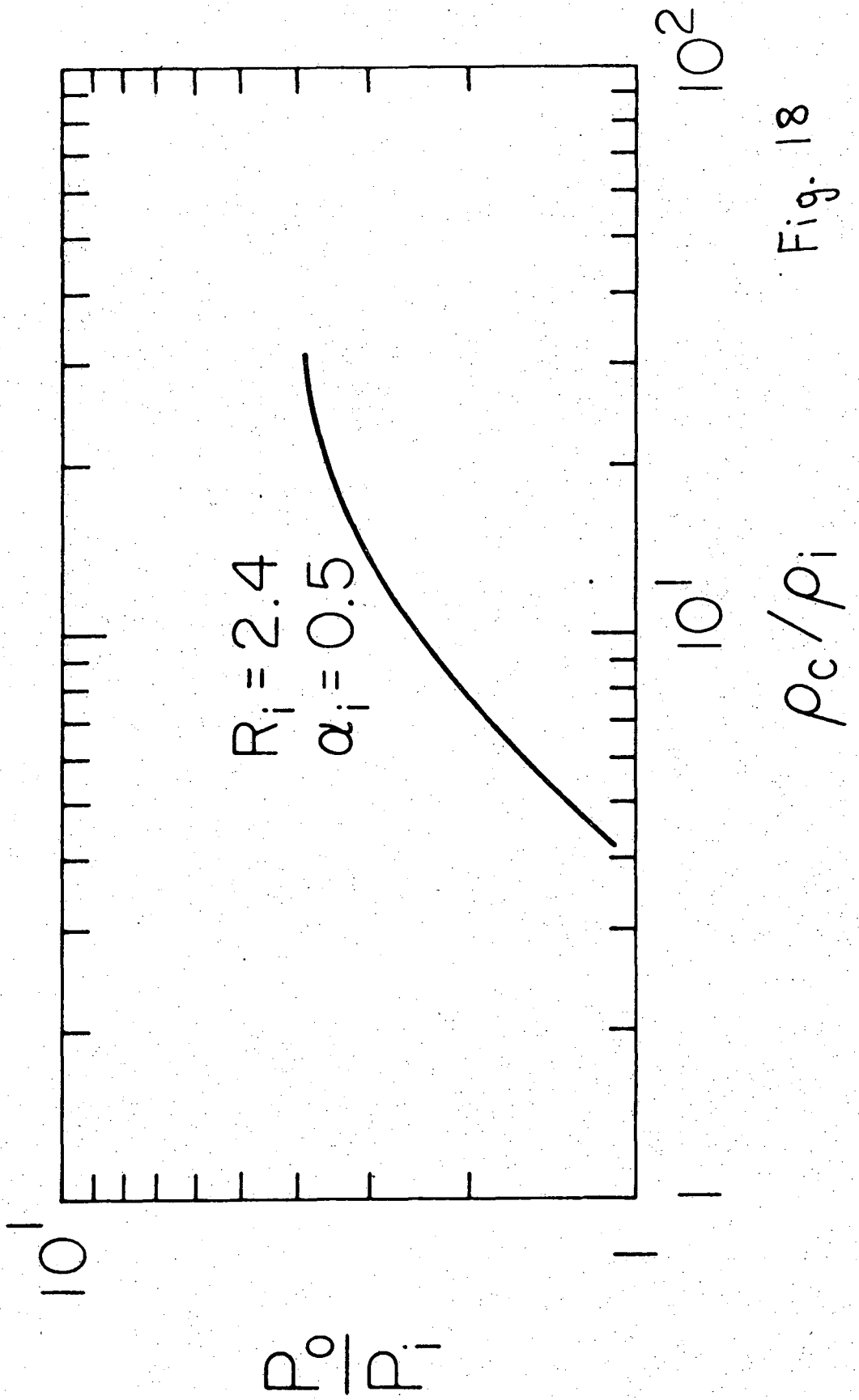


Fig. 18

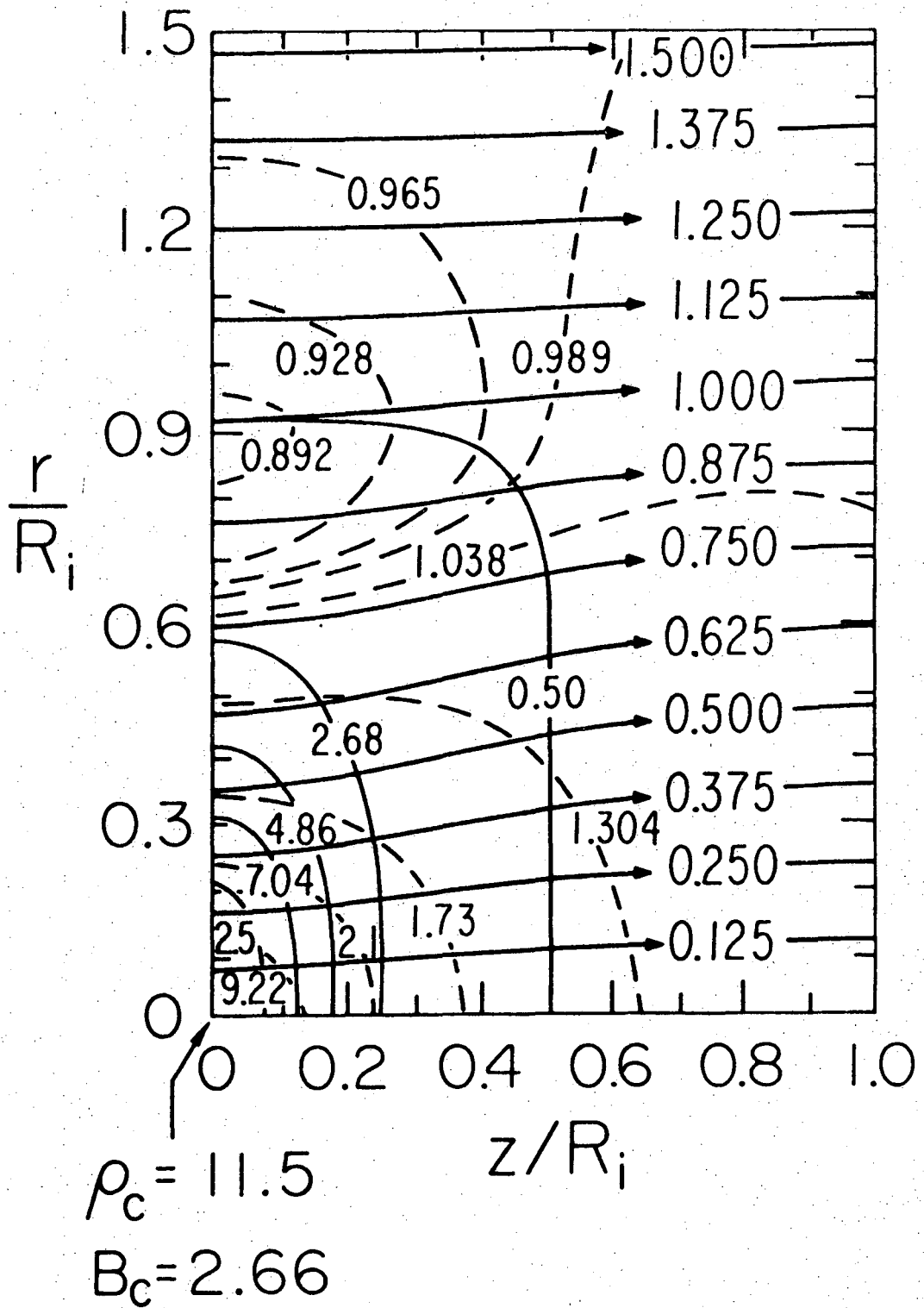


Fig. 19a



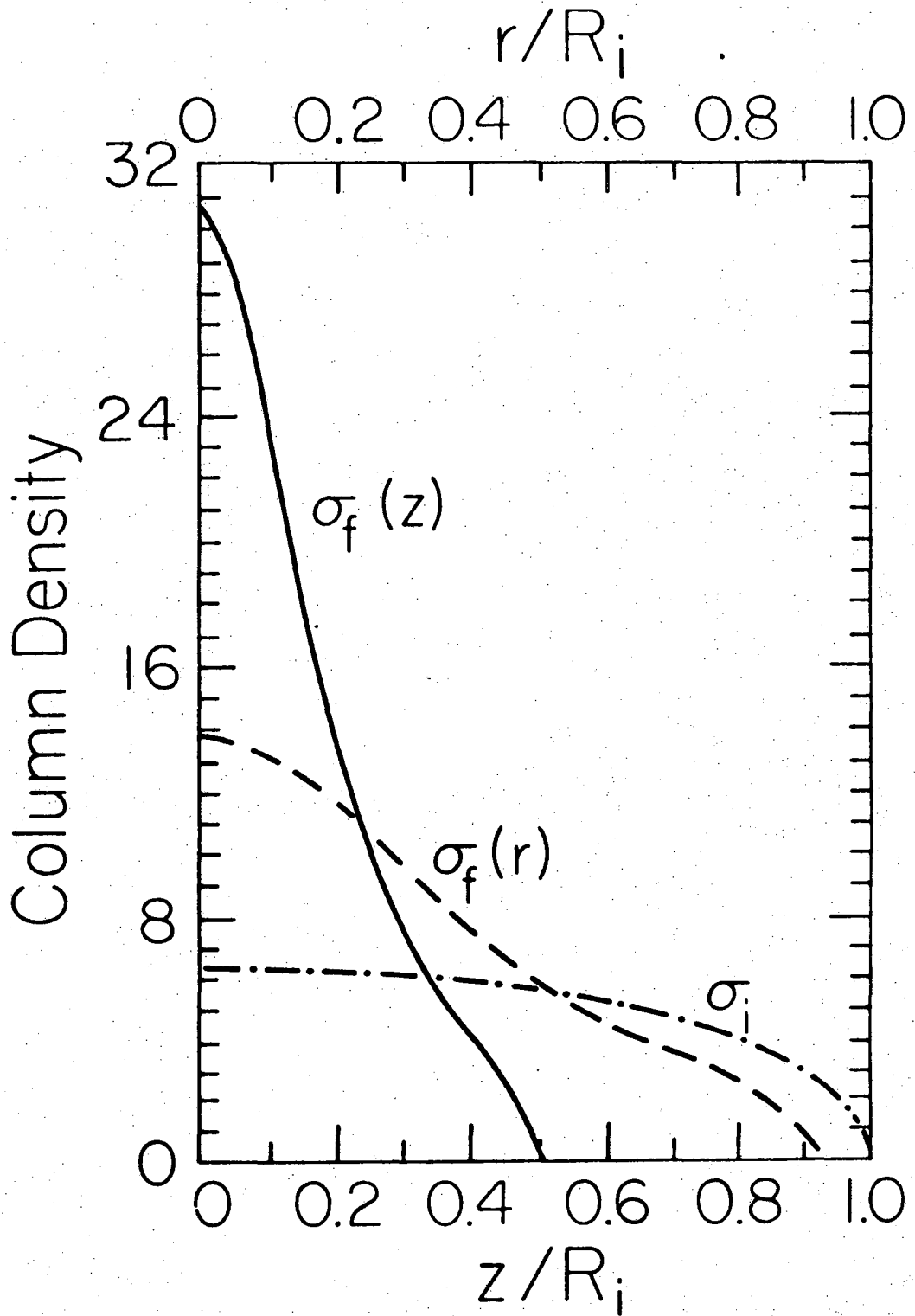


Fig. 19b

## APPENDIX A

## METHOD OF SOLUTION

A Triple-Relaxation Iterative Procedure (TRIP)

We write eqs. (177) and (178) formally as

$$F(A) = Q(r, \phi, \psi; \alpha_i, R_i) \quad (A1)$$

and

$$L(\psi) = \rho(\phi, \psi), \quad (A2)$$

where  $\phi(r, z) \equiv rA(r, z)$ . In eqs. (A1) and (A2),  $F$  and  $L$  are linear differential operators, and  $Q$  and  $\rho$  are nonlinear algebraic operators. Both  $Q$  and  $\rho$  vanish outside the cloud, whose boundary is defined by

$$\rho[\phi(r, z), \psi(r, z)] = P_0 = \text{a constant}. \quad (A3)$$

The boundary conditions on  $A$  and  $\psi$  are specified by eqs. (182a) - (182h). We note that  $A(r, z)$  satisfies Dirichlet boundary conditions on three sides of the rectangle (the "large cylinder" of § VIIA5), whose corners are  $(0, 0)$ ,  $(0, Z)$ ,  $(R, Z)$ ,  $(R, 0)$ , and Neumann on the fourth. The potential  $\psi(r, z)$  satisfies Dirichlet conditions on two adjacent sides and Neumann on the opposite two.

Since each equation is formally similar (but not identical) to eq. (C1) of Appendix C of Paper I, we used a similar procedure to obtain a solution. The complication now is that eqs. (A1) and (A2) must be solved simultaneously. In addition, since neither  $\phi$  nor  $\psi$  are known before a solution is at hand, the location of the cloud boundary (see eq. [A3]) cannot be determined until the problem is actually solved. It must, therefore, be treated as a free boundary.

We start with an initial guess  $A^{(0)}$ ,  $\psi^{(0)}$  and a cloud boundary

specified by a function  $Z_{cl}^{(0)}(\phi^{(0)}, \rho^{(0)})$  -- see fig. 7 -- which does not necessarily satisfy condition (A3). Note that  $\rho^{(0)}$  is equal to unity inside the cloud and zero outside if the cloud boundary is initially spherical. We define a sequence of iterates by the recursion relations

$$L(\psi_*^{(n+1)}) = \rho^{(n+1)}(\phi^{(n)}, \psi^{(n)}) \quad (A4)$$

$$\psi^{(n+1)} = \phi^{(n)} \psi^{(n)} + (1 - \phi^{(n)}) \psi_*^{(n+1)}, \quad 0 \leq \phi^{(n)} < 1 \quad (A5)$$

and

$$F(A_*^{(n+1)}) = Q(r, \phi^{(n)}, \psi^{(n+1)}; \alpha_i, R_i) \quad (A6)$$

$$A^{(n+1)} = \theta^{(n)} A^{(n)} + (1 - \theta^{(n)}) A_*^{(n+1)}, \quad 0 \leq \theta^{(n)} < 1, \quad (A7)$$

where  $n = 0, 1, 2, \dots$ . The quantities  $A_*^{(n+1)}$  and  $\psi_*^{(n+1)}$  are provisional iterates and  $\phi^{(n)}, \theta^{(n)}$  are the relaxation parameters at the  $n$ th iteration. Note that the right-hand side of eq. (A6) contains the latest iterate,  $\psi^{(n+1)}$ . We discovered that large oscillations of the cloud boundary during the first few iterations (a consequence of a bad initial guess) can be avoided and convergence be speeded up considerably if we also underrelaxed the boundary itself by taking

$$Z_{cl}^{(n+1)} = \chi^{(n)} Z_{cl}^{(n)} + (1 - \chi^{(n)}) Z_{cl*}^{(n+1)}, \quad 0 \leq \chi^{(n)} < 1, \quad (A8)$$

where we have simplified the notation by omitting the arguments; a subscript \* on  $Z_{cl}$  means that the arguments are the starred quantities  $A$  and  $\psi$  in the indicated iteration. The physical meaning of eq. (A8) is that a slight violation of the conservation of the mass-to-flux ratio is allowed during the first few iterations. Without eq. (A8), this conservation law is imposed exactly through eqs. (179) and (180). If, instead of choosing

$$\begin{aligned} \rho^{(0)} &= 1, & \text{inside the cloud;} \\ &= 0, & \text{outside the cloud} \end{aligned}$$

and a spherical cloud boundary, we chose an elliptical cloud boundary with semi-major axis equal to  $R_i$  and semi-minor axis  $Z_i < R_i$ , convergence was further speeded up. In such a case, of course,  $\rho^{(0)}$  must be multiplied by  $R_i/Z_i$  in order to maintain a mass-to-flux ratio appropriate to the spherical reference state.

We say that a solution is reached if the conditions

$$\frac{|A_*^{(n+1)} - A^{(n)}|}{A_*^{(n+1)}} < \epsilon_1, \quad (\text{A9})$$

$$\frac{|\psi_*^{(n+1)} - \psi^{(n)}|}{\psi_*^{(n+1)}} < \epsilon_2 \quad (\text{A10})$$

and

$$|Z_{cl}^{(n+1)} - Z_{cl}^{(n)}| < \epsilon_3(z) \quad (\text{A11})$$

are satisfied simultaneously. The quantities  $\epsilon_1$  and  $\epsilon_2$  are small positive constants that can be chosen at will to achieve desired levels of accuracy. Similarly for  $\epsilon_3$ , except that it depends on the local mesh size -- we employ a nonuniform mesh; see below.

As in the problem solved in Paper I, we chose a set of field lines (15 - 30 within the cloud and at least 10 in the intercloud medium),  $\{\phi_i\}$ ,  $i = 1, 2, \dots, I$ , and we followed them from iteration to iteration until they settled down and the solution criterion (A9) - (A11) was satisfied. We usually found solutions within a number of iterations varying from 3 to about 50 (each taking less than 0.5 seconds of CPU time on the CDC 7600 computer), depending on our initial guess and solution criteria.

However, we often forced the program to continue for over 100 iterations in order to determine its asymptotic convergence properties. We determined that, with  $\epsilon_1 = \epsilon_2 = 0.01 - 0.02$  and  $\epsilon_3(z) \leq$  (half the local mesh size) and the additional requirement that eqs. (A9) - (A11) be satisfied by several successive iterations (usually 10), a solution was within one percent of that obtained with much stricter solution requirements, which necessitated a number of iterations usually two or three times larger.

Since any rapid variation of the functions in our equations is expected to occur within the cloud or in its immediate neighborhood, we employed a nonuniform mesh such that at least 15 mesh points existed within the r-extent and at least 10 within the z-extent of a cloud in the equilibrium state (not just the initial guess). On the other hand, as few as 10 mesh points would represent a region of the intercloud medium ten times larger than the initial radius ( $R_1$ ) of the cloud with practically the same accuracy as 30 mesh points, because of the smooth and very slow variation of the various functions there. It was essential, however, that the transition between the fine mesh and the coarse mesh be smooth. A smooth transition often made the difference between obtaining a solution within a relatively small number of iterations and not finding a solution at all.

The calculation of the right-hand side of eq. (A1) was done in much the same way as that of the right-hand side of eq. (C1) of Paper I. Once that is done, the right-hand side of eq. (A2) is obtained by simple multiplications and exponentiations (see eq. [178]). With  $Q$  and  $\rho$  known, the Poisson equation for  $\psi$  and the Poisson-like equation for  $A$  are solved by a fast direct method developed by Swarztrauber (1972). Since, in obtaining  $Q$  we used substantially the same routines as in Paper I, the

accuracy may be expected to be comparable with that shown in Table 3, Paper I. That cannot, of course, be taken for granted. To test the accuracy of the present program we used values of  $R_1$  small enough for self-gravity to be unimportant (we avoided large values of  $P_0$  that would bring gravitational forces into play by compressing the cloud) and we compared the numerical solution with one that can be obtained very easily under these conditions through analytical means. They agreed to within one percent. This does not necessarily reflect the accuracy of solutions obtained with a large  $R_1$ , or a large  $P_0$ . Since no exact equilibrium solutions are known in the general case, we could only use as an indication of the accuracy of our program the following criteria.

(i) Doubling the number of mesh points in each direction changed a typical solution by at most one percent.

(ii) Varying the values of  $R$  and  $Z$  (see § VIIA5) by a factor of 2 produced changes of less than one percent in a solution.

(iii) Forcing the program to continue for over 100 iterations altered a solution by at most 4 percent in the value of the central density (it depends exponentially on  $\psi$ ; see eq. [128]) while all other functions exhibited considerably smaller changes.

(iv) A slight change in the values of the relaxation parameters changed the number of iterations required to reach a solution, but the solution itself changed by less than 2 percent. When this test was performed on a critical state, it sometimes collapsed because of numerical noise.

The accompanying chart shows the flow of calculations in the program. Each "box" contains the function calculated at that point. The basic process or equation needed for that calculation is indicated by

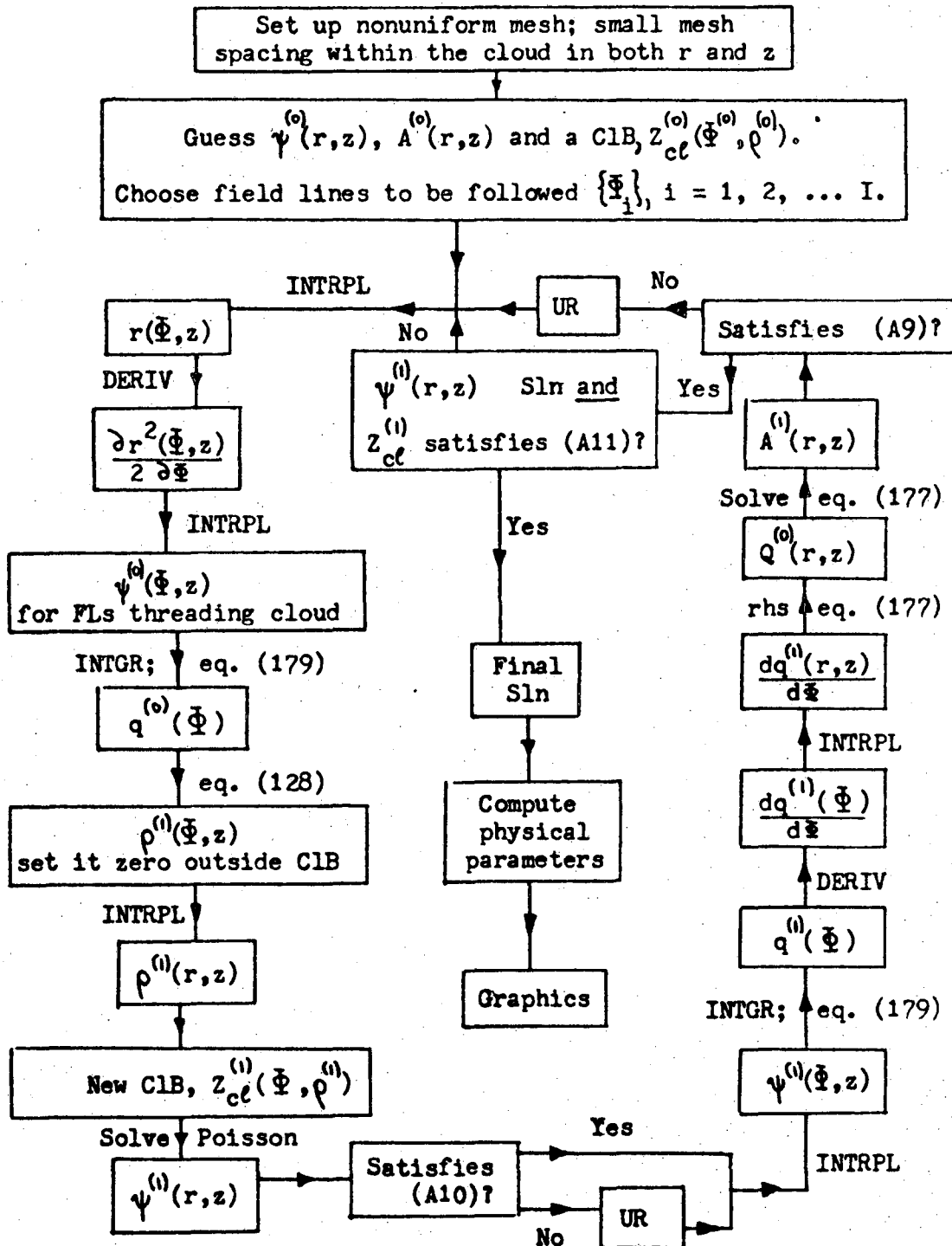
information written by the arrows. When the arguments of a function are  $r$  and  $z$ , the values of the function are known at the mesh points. When an argument is  $\phi$ , the function is known along field lines. We found it both expedient and essential to use two interwoven meshes and to switch back and forth, through interpolations, at crucial points in the program. One mesh  $(r, z)$  is fixed. The second mesh  $(\phi, z)$  is defined at each iteration by the current position of the field lines. In the chart we use the following abbreviations for economy of space:

FL = field line  
INTRPL = interpolate  
CIB = Cloud Boundary  
UR = underrelax  
Sln = Solution  
DERIV = take derivative  
INTGR = integrate  
rhs = right-hand side.

We note that as long as  $Q$  and  $\rho$  are given whatever values they may inside the cloud and set equal to zero outside, eqs. (A1) and (A2) are solved over the "large cylinder" without additional regard to the location of the cloud boundary. Continuity of all physical quantities that must exhibit such property across the cloud boundary was proven in § VIIA4.

(NOTE: Flow Chart is found on the following page)

Program Flow Chart





APPENDIX B

Reprint of "Paper I" which is referenced in the text.

## STATIC EQUILIBRIA OF THE INTERSTELLAR GAS IN THE PRESENCE OF MAGNETIC AND GRAVITATIONAL FIELDS: LARGE-SCALE CONDENSATIONS\*

TELEMACHOS CH. MOUSCHOVIAS

Physics Department, University of California, Berkeley; and Harvard College Observatory, Cambridge, Massachusetts

Received 1974 February 5; revised 1974 March 11

### ABSTRACT

We present equilibrium states of the interstellar gas, which has run down the perturbed magnetic field lines of a stratified, isothermal initial state under the action of a vertical galactic gravitational field. The final states are lower in total energy than the corresponding initial states. Their properties depend quantitatively on the horizontal (but not so much on the vertical) wavelength of the initial perturbation. A striking feature of the final states is that the scale height of the gas increases (decreases) where the gas density increases (decreases). A connection between initial and final states is made by conserving the mass-to-flux ratio in each flux tube. Thus, although we determine final equilibrium states by solving a time-independent problem, in a time-dependent problem our final states can be reached from the corresponding initial states through continuous deformations of the field lines. The final states are consistent with observations in the solar neighborhood. We treat the interesting case of the magnetic pressure being initially comparable to the pressure of the thermal gas.

We show that the isothermal gas-field-gravity system possesses an "energy integral." An effective potential energy is identified, and an "energy principle" follows as a corollary. The iterative procedure used in order to solve the magnetohydrostatic equations is outlined, and upper limits on the numerical errors are given. We also extend our formalism so that it can apply to the case of a general (rather than an isothermal) equation of state.

*Subject headings:* hydromagnetics — instabilities — interstellar matter — magnetic fields — plasmas

### I. INTRODUCTION

The dimensions of many condensations of the interstellar gas are so large and the condensations themselves are so closely associated with the interstellar magnetic field that one may conclude that these large-scale condensations could be produced by very long-wavelength hydromagnetic disturbances. Parker (1966), using linear stability analysis, showed that the interstellar gas, which is partially supported by magnetic and cosmic-ray pressures against the Galactic gravitational field, could be unstable with respect to deformations of the field lines. Lerche (1967*a*) determined a final state for the interstellar gas and field system, in which Parker's magnetogravitational instability had developed. Since he ignored the pressure of the gas, the final state consisted of infinitesimally thin sheets of matter that extended perpendicular to the galactic plane. This state is unstable with respect to small horizontal displacements of the gas elements (Lerche 1967*b*). Parker (1968*a*) found a different equilibrium state, but at the same time he pointed out the very special nature of his solution because of a simplifying mathematical assumption made (see § II*a* below).

In this paper we assume strict flux-freezing and we derive a general nonlinear, elliptic, second-order, partial differential equation, a subset of whose solutions properly describes equilibrium states of the interstellar gas and field system in a galactic gravita-

tional field (§ II*a*). In § II*b*, by making use of constants of the motion, we remove an arbitrariness that would otherwise exist in the source term of this equation. This allows us to make a connection between initial and final states, even though we solve a time-independent problem. The boundary conditions and the assumed initial state are presented in § III. In § IV we obtain and discuss an "energy integral" of the isothermal gas-field-gravity system and we endeavor to anticipate what energy changes will take place as the system makes a transition from an initial to a final state. The physics corresponding to each step of the method of solution is explained in § V*a*. Indications for the physical stability of the final states are discussed in § V*b*. We present three typical final states in § VI; important features and observational predictions are discussed in some detail. In § VII we make a few concluding remarks and a semiquantitative comparison with observations in the solar neighborhood. Mathematical derivations that would interrupt the continuity of an argument, together with a description of our iterative scheme, are left for the appendices. The generalization of our formalism, so that it can apply to equations of state  $P = P(\rho)$ , is also left for an appendix.

### II. HYDROSTATIC EQUILIBRIUM INCLUDING FLUX-FREEZING

#### a) Reduction to One Equation

Consider a conducting gas of density  $\rho$  and pressure  $P$  in hydrostatic equilibrium in a magnetic field  $\mathbf{B}$  and a gravitational field  $\mathbf{g}$ , derivable from a potential  $\psi$ .

\* This work was supported mainly by the National Science Foundation under grant GP-36194X, and in part by the Lawrence Berkeley Laboratory under the auspices of the U.S. Atomic Energy Commission.

Denoting the current density by  $j$ , we may write the magnetohydrostatic force equation as

$$-\nabla P - \rho \nabla \psi + j \times B/c = 0, \quad (1)$$

where  $c$  is the speed of light in vacuum. The quantities  $B$  and  $j$  are related by Maxwell's equation

$$c \nabla \times B = 4\pi j. \quad (2)$$

The equation of state is

$$P = \rho C^2, \quad (3)$$

where  $C$  is the isothermal speed of sound in the gas. In this paper we take  $C = \text{constant}$ . If a magnetic vector potential,  $A$ , is defined by

$$B = \nabla \times A, \quad (4)$$

then Maxwell's equation

$$\nabla \cdot B = 0 \quad (5)$$

is satisfied identically.

Following previous authors, we assume that all quantities are independent of  $z$  (2D geometry) and that  $B_z = 0$ . Then  $B_x = +\partial A/\partial y$ ,  $B_y = -\partial A/\partial x$ , and the magnetic vector potential can be written as  $A = e_z A(x, y)$ . Since  $B = -e_z \times \nabla A$ , it follows that  $B \cdot \nabla A = 0$ , so that  $A$  is constant on a field line. Assuming flux-freezing, one can show ~~that  $\nabla A = 0$ , so~~ that  $A$  is a constant of the motion in the flow associated with Parker's instability. Each field line, therefore, retains its initial value of  $A$ .

We define a scalar function of position,  $q(x, y)$ , by

$$q = P \exp(\psi/C^2), \quad (6)$$

and we write equation (1) in terms of  $A$  and  $q$  as

$$j \nabla A/c = \exp(-\psi/C^2) \nabla q. \quad (7)$$

Decomposing equation (7) in directions parallel and perpendicular to field lines and recalling that  $A$  is constant on a field line, we can show that

$$P \exp(\psi/C^2) \equiv q = \text{constant on a field line} = q(A); \quad (8)$$

and that

$$\begin{aligned} \frac{j}{c} \exp(\psi/C^2) &= \text{constant on a field line} \\ &= \frac{dq}{dA}. \end{aligned} \quad (9)$$

The quantity  $q$ , being a function of  $A$  at hydrostatic equilibrium, expresses the fact that, since magnetic forces act only perpendicular to the field lines, pressure gradients exactly balance the gravitational forces along a field line. The meaning of equation (9) is as follows. If a magnetic vector potential  $A^*(x, y)$  [and therefore a magnetic field  $B^*(x, y)$ ] is given, and if matter is

distributed among field lines so that the forces parallel to field lines are in exact balance [i.e.,  $q^* = q^*(A^*)$ ], then we can balance the forces in a direction perpendicular to the field lines by calculating a current density  $j^*$  from equation (9). However,  $B^*$  and  $j^*$  will not be consistent with each other unless they have satisfied equation (2), which may be written in terms of  $A$ , with  $j$  eliminated in favor of  $q$ , as

$$\nabla^2 A = -4\pi \frac{dq}{dA} \exp\left(-\frac{\psi}{C^2}\right). \quad (10)$$

So far, equation (10) differs from an equation derived by Dungey (1953) only in that our  $\psi$  is any gravitational potential. For example,  $\psi$  can be the gravitational potential of the Galaxy as a whole, or that of a dense cloud in the interstellar medium. In the former case,  $\psi$  can be obtained from Schmidt's (1965) model of the Galaxy; in the latter case, a Poisson equation for  $\psi$  has to be considered simultaneously with equation (10) in order to obtain a self-consistent solution. In this paper we take  $\psi$  to be due to the Galaxy as a whole.

Let the gas and field system be in some initial state, in which Parker's (1966) magnetogravitational instability develops with wavelengths  $\lambda_x$  and  $\lambda_y$  in the  $x$ - and  $y$ -directions, respectively. We take the system to be periodic in  $x$  (along the galactic plane) and we assume that the pair of (unstable) wavelengths ( $\lambda_x, \lambda_y$ ) is the same everywhere in the Galaxy. Moreover, we assume that the magnetic field is frozen in the matter. In order

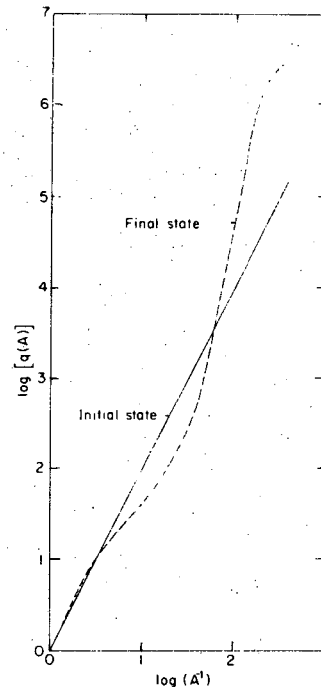


FIG. 1.—The dependence of the function  $q$  on  $A$  in the stratified initial state ( $\alpha = 1$ ) and in a typical final state (that of fig. 2c). Both  $q$  and  $A$  are normalized to their values on the  $x$ -axis in the initial state.

$$* (\vec{\nabla} \cdot \vec{\nabla}) \vec{A} + \vec{\nabla} \times \vec{B} = 0$$

to find a final equilibrium state for this system we must solve equation (10); and for this task we need to calculate  $q(A)$ . Parker (1968a) assumed that  $q(A)$  is either a linear or a quadratic function of  $A$ , and he solved the resulting linear equation (10) for the case in which the gravitational potential  $\psi$  is proportional to the vertical distance  $y$ . We find below that, for the plane-parallel initial state proposed by Parker (1966), the function  $q$  varies as an *inverse* power of  $A$  (see eq. [15]). In the final states as well,  $q$  varies as some inverse power of  $A$  (see fig. 1). Although  $q$  is a function of  $A$  alone at hydrostatic equilibrium, it is *not* a constant of the motion. Consequently, we are not permitted to calculate (or to specify)  $q(A)$  in some initial state and then proceed to determine a final state characterized by the same  $q(A)$ .

### b) Calculation of the Function $q(A)$

In general,  $q(A)$  can be calculated as follows. With  $X \equiv \lambda_x/2$ , the mass ( $\delta m$ ) in a flux tube between field lines characterized by  $A$  and  $A + \delta A$  is, by definition,

$$\delta m(A) = \int_{-X}^{+X} dx \int_{y(x,A)}^{y(x,A+\delta A)} dy(x,A) \rho[x, y(x,A)]. \quad (11)$$

It is natural to consider  $x$  and  $A$  as the independent variables. Since the integration over  $y$  in equation (11) is performed keeping  $x$  fixed, we may write  $dy = dA(\partial y/\partial A)$  and effect the change of variables from  $y$  to  $A$ . We eliminate  $\rho$  in favor of  $A$  by using equations (8) and (3), and we expand the integrand of the resulting equation in a Taylor series about  $A$  keeping only first-order terms. (The neglect of higher-order terms is justified *a posteriori*.) We then solve for  $q(A)$  to obtain

$$q(A) = \frac{C^2}{2} \frac{dm}{dA} \int_0^X dx \frac{\partial y(x,A)}{\partial A} \exp \left[ -\frac{\psi(x,A)}{C^2} \right]. \quad (12)$$

The quantity  $y(x,A)$  refers to the  $y$ -coordinate of the field line  $A$  at  $x$ .<sup>1</sup>

If  $dm/dA$  is given,  $q(A)$  follows from equation (12) for any proposed configuration. In particular, both  $q$  for the initial and  $q$  for the final states can be calculated using the *same*  $dm/dA$ , since conservation of both mass and flux implies that  $dm/dA$  is a *constant of the motion*.

Note that  $q(A)$  depends on the shape of the field lines, which are originally unknown. Hence, in general, one must solve equations (10) and (12) simultaneously for any given  $dm/dA$ . The initial state of the gas and field system is not known in reality, for it depends on the mechanism which creates the magnetic flux. Here we take it to be the plane-parallel system proposed by Parker (1966). This defines  $dm/dA$  for the final state as well. We emphasize, however, that the only information needed in order to determine a final state is the mass-to-flux ratio in each flux tube. If the distribution

of mass among the various flux tubes is obtained from observations, we can determine a final equilibrium state without reference to any particular initial state.

### III. THE INITIAL STATE: BOUNDARY CONDITIONS

As an initial state we consider the stratified equilibrium state of the interstellar gas and magnetic field in a gravitational field  $\mathbf{g} = -e_y g(y)$ , where  $g(y) = -g(-y)$  is a positive constant. Following Parker (1966), we assume that the ratio of the magnetic to gas pressures,

$$\alpha \equiv B^2/8\pi P, \quad (13)$$

is constant in the initial state. For this state we find

$$A_i(y) = -2HB_i(0) \exp(-y/2H), \quad (14)$$

$$q_i(A_i) = \rho_i(0)C^2[-2HB_i(0)/A_i]^{2\alpha} \quad (15)$$

and

$$\frac{dm}{dA} = \frac{2X\rho_i(0)}{B_i(0)} \left[ -\frac{A}{2HB_i(0)} \right], \quad (16)$$

where  $X \equiv \lambda_x/2$  and  $H$  is the combined scale height of the gas and field given by

$$H \equiv (1 + \alpha)C^2/g. \quad (17)$$

The quantities  $B_i(0)$  and  $\rho_i(0)$  are, respectively, the values of  $B_i$  and  $\rho_i$  at  $y = 0$ . The subscript  $i$  signifies the initial state. In equation (16)  $A$  is not subscripted because, as explained in § 11b,  $dm/dA$  is the same function of  $A$  in the initial and final states.

The boundary conditions are as follows. Since the  $x$ -axis is taken to coincide with the galactic plane and the system is assumed periodic in  $x$ , there is reflection symmetry about both the  $x$ - and  $y$ -axes. The former symmetry implies that the field line originally coinciding with the  $x$ -axis remains undeformed, i.e.,

$$A(x, y = 0) = -2HB_i(0) = \text{constant}. \quad (18)$$

Periodicity in  $x$  is expressed by

$$\left. \frac{\partial A(x, y)}{\partial x} \right|_{x=0, \pm X} = 0. \quad (19)$$

Boundedness at infinity and conservation of the total magnetic flux imply

$$\begin{aligned} A(x, y) &= 0, & y &= +\infty; \\ &= -4HB_i(0), & y &= -\infty. \end{aligned} \quad (20)$$

Because of the symmetries, equation (10) may be solved in the rectangle  $0 < x < X$ ,  $0 < y < \infty$ . In fact, this semi-infinite rectangle may be replaced by a finite one without affecting the solution very much, provided only that the extent of the finite rectangle in the  $y$ -direction is much larger than  $H$  (see § VI d). So, we set the upper boundary at  $y = Y \gg H$  and we replace equation (20) by

$$A(x, Y) = A_i(Y), \quad (21)$$

<sup>1</sup> In Appendix A we generalize the definition of  $q$  (eq. [6]) to apply to any equation of state,  $P = P(\rho)$ . We also derive equations, which are generalizations of equations (10) and (12).

where  $A_i(Y)$  is the initial value of  $A$  at  $y = Y$ . If one recalls that the perturbations which Parker (1966, Appendix III) showed to be unstable always leave some field lines of the initial state undeformed, equation (21) is equivalent to taking the upper boundary at the position of the first undeformed field line of the initial state.

Before solving equations (10) and (12), we wrote them in a dimensionless form (see Appendix C1). Thus,  $\alpha$  of the initial state is the only free parameter in the equations (see eq. [C1], Appendix C).

#### IV. ENERGY CONSIDERATIONS

##### a) An Energy Principle

In Appendix B we show that the magnetohydrodynamic equations possess an "energy integral," and we identify an effective potential energy  $W$  of the isothermal gas-field-gravity system which is given by

$$W = W_p + W_m + W_g, \quad (22)$$

where

$$W_p = \int P \ln PdV, \quad (23)$$

$$W_m = \int (B^2/8\pi)dV \quad \text{and} \quad W_g = \int \rho\psi dV. \quad (24), (25)$$

One can show directly that the force equation (1) follows from the requirement that the first variation of  $W$  vanish under an arbitrary displacement  $\xi$  of the plasma elements, provided that (i) mass is conserved; (ii) flux is conserved; (iii) the temperature is constant. In the case of a system periodic in one direction ( $x$ ), one needs the additional assumption that (iv) no mass is transferred from one period to the next during the infinitesimal plasma displacements. This demonstration rigorously qualifies  $W$  as a potential energy and allows one to study the stability of an equilibrium state by investigating the sign of the potential energy associated with small deviations from the assumed equilibrium.

##### b) The Meaning of $W_p$

In equation (22), the magnetic energy  $W_m$  and the gravitational energy  $W_g$  are given by familiar expressions. Note, however, that the quantity  $P \ln P$  has replaced the usual term  $P/(\gamma - 1)$ . The meaning of  $P \ln P$  becomes transparent, if we examine the first law of thermodynamics (for an ideal gas in the absence of any fields). This is

$$dQ = du + Pd(\rho^{-1}). \quad (26)$$

The quantities  $Q$  and  $u$  are, respectively, the heat supplied to the gas and the internal energy of the gas; both  $Q$  and  $u$  are measured in units of energy per unit mass. For an isothermal process,  $du$  vanishes and  $dQ$  is an exact differential.

Letting  $\theta$  denote the heat per unit volume supplied to the gas (i.e.,  $\theta = \rho Q$ ), we may write equation (26) as

$$d\theta = (\theta/P - 1)dP. \quad (27)$$

A straightforward integration yields  $\theta$  as a function of  $P$ ; this is further integrated over volume to obtain

$$\begin{aligned} \Theta &\equiv \int \theta dV \\ &= - \int P \ln PdV + b \int PdV \\ &= -W_p + b \int PdV, \end{aligned} \quad (28)$$

where  $b$  is a constant of integration. The second term on the right-hand side of equation (28) is the same for all states, because the total mass is fixed and the gas is isothermal. Therefore, the heat ( $\Delta\Theta$ ) supplied to the gas in going from one state to another is simply given by

$$\Delta\Theta = -\Delta W_p. \quad (29)$$

Since  $\Delta W_p$  was derived from the second term on the right-hand side of equation (26), it represents the work done by the gas against pressure forces in making a transition between two states along an isothermal path. If  $\Delta W_p > 0$ , heat is released by the gas. Note, also, that for a reversible isothermal process, the change in the entropy (denoted by  $\Delta S$ ) is given by

$$\Delta S = \Delta\Theta/T = -\Delta W_p/T. \quad (30)$$

Hence,  $W_p$  provides a measure of the entropy and it is equal to the Helmholtz free energy of the gas, to within an additive constant.

##### c) Expected Energy Changes

When Parker's instability develops, compression occurs in some parts of the system and expansion in others. Consequently, one cannot anticipate what the net changes in  $W_m$  and  $W_p$  will be when a final state is reached. Compression (expansion) tends to increase (decrease)  $W_m$  and  $W_p$ . This is obvious in the case of  $W_m$ . It is so for  $W_p$  as well, because when gas is being compressed it tends to heat up; for the temperature to remain constant (an assumption in our model), heat has to be released. Typical cooling times are of the order of  $10^5$  years in the interstellar medium and become shorter as the gas density increases (Spitzer 1968). Since this time is smaller than the  $e$ -folding time of the instability ( $10^7$  years), the gas has enough time to cool down.

The gravitational energy ( $W_g$ ) is expected to decrease, since gas drains down the perturbed field lines under the action of the galactic gravitational field. The "fact" that the expanding field lifts some matter to higher altitudes is not expected to produce a net increase in the gravitational energy, for field lines can expand only because gas is being "unloaded" from their raised portions.

#### V. METHOD OF SOLUTION AND PHYSICAL STABILITY

##### a) The Physics behind the Method of Solution

To obtain a simultaneous solution of the equilibrium equations (10) and (12) we developed and followed the

procedure outlined in Appendix C. The physics behind that iterative procedure is as follows. (i) Guess a set of field lines (and, therefore, a magnetic field), which satisfy the periodicity and symmetry conditions discussed in § III. (ii) Distribute the total mass among the various flux tubes in such a way that the mass-to-flux ratio in each flux tube is equal to the mass-to-flux ratio in the corresponding flux tube of the initial state. (iii) Allow mass to slide up or down along field lines (without transferring any mass from one tube to another) until pressure gradients and gravitational forces are in exact balance *along* field lines. (iv) From the magnetic field obtained in step (i) and the mass distribution achieved in step (iv), calculate the current density necessary to balance all forces in a direction *perpendicular* to the field lines. (v) Check whether the just calculated current density is consistent with the magnetic field of step (i); if it is not, use this current density to calculate a new ("better") magnetic field and go to step (ii) to repeat the process until consistency is achieved. The introduction of an underrelaxation parameter in the iterative scheme provides a measure of *how much* "better" (or "worse"!) the magnetic field of one iteration is, compared with that of the previous iteration.

### b) Stability

The stratified initial state is unstable only if the horizontal and vertical wavelengths of the applied perturbation simultaneously exceed some critical values (see Parker 1966), namely,

$$\lambda_x > \Lambda_x \equiv 4\pi H(2\alpha + 1)^{-1/2}, \quad \alpha \neq 0, \quad (31)$$

and

$$\lambda_y > \Lambda_y(\lambda_x) \equiv \Lambda_x(1 - \mu^2)^{-1/2}. \quad (32)$$

The quantities  $\alpha$  and  $H$  are defined by equations (13) and (17), respectively, and  $\mu = \Lambda_x/\lambda_x < 1$ . Parker's dispersion relation implies that, for a fixed  $\lambda_x > \Lambda_x$ , the growth rate of the perturbation increases as  $\lambda_y (> \Lambda_y)$  increases. In addition, for a fixed  $\lambda_y > \Lambda_y$ , the growth rate first increases and then decreases as  $\lambda_x$  increases. The maximum growth rate is reached when  $\lambda_x \leq 2\Lambda_x$  and  $\lambda_y = \infty$ . For typical parameters of the interstellar medium, the inverse of the maximum growth rate is approximately  $10^7$  years. This is smaller than the time required for one galactic rotation (approximately  $10^8$  years).

Starting from the stratified initial state, we applied a perturbation (in the form of a deformation of the field lines) characterized by a *stable* pair of wavelengths  $(\lambda_x, \lambda_y)$ . Our iterative scheme always converged to the initial state, no matter how large the amplitude of the perturbation was and regardless of the particular values of  $\lambda_x$  and  $\lambda_y$ , as long as they were stable. On the other hand, our iterative scheme never converged to the initial state in the case that the perturbation was characterized by an *unstable* pair of wavelengths, even if the amplitude of the perturbation was as small as 1 percent. This is an indication (although not a proof)

that *the iterative scheme cannot converge to solutions representing physically unstable states.*

For a fixed unstable pair of wavelengths, we obtained convergence to one and the same solution (distinct from the initial state) for a wide range of amplitudes of the initial perturbation. When perturbations were applied to this solution, the iterative scheme always converged back to it. This, in conjunction with the properties of the iterative scheme described in the preceding paragraph, *suggests* that our solutions represent states of the gas-field-gravity system which are physically stable, at least in a local sense. The class of perturbations applied to a final state was such that each wavelength of the final state contained an integral number of perturbation wavelengths. This prohibits mass transfer from one period of the equilibrium state to the next. Of course, for a definitive statement on the nature of an equilibrium state, one must consider all arbitrary perturbations. We make additional comments on stability in § VIc.

## VI. FINAL STATES

We chose several pairs of unstable wavelengths  $(\lambda_x, \lambda_y)$  for the perturbation applied to the initial state (see § III), and for each such pair we found a final equilibrium state. Figures 2a, 2b, and 2c represent typical final states, produced by perturbations that had the same vertical but different horizontal wavelengths. Ten field lines (*solid curves*) and three isodensity contours (*dashed lines*) are shown. The field lines are chosen so that the amount of magnetic flux contained between any two consecutive ones is constant. Thus, the spacing between consecutive field lines is inversely proportional to the mean strength of the magnetic field in the interval. The ratio  $\alpha$  in the initial state (the only free parameter in the equations) was taken equal to unity.

### a) Dependence on $\lambda_x$

A comparison of figures 2a, 2b, and 2c reveals that, as the horizontal wavelength increases, so does the deformation of the field lines. It is the case that the more deformed the field lines are, the more effective the gravitational field is in "unloading" the gas from their inflated portions. Therefore, the gas density at the midplane of the condensation ( $x = 0, y > 0$ ) is expected to increase as  $\lambda_x$  increases. This is borne out in figure 3, which exhibits the dependence of the "emission measures" (EM) on  $x$ , in these three final states.<sup>2</sup> The horizontal distance  $x$  is measured from the center of each condensation. In the final state characterized by  $X = 15$ , we note that

$$\text{EM}(x = 0) \simeq 3 \text{EM}(x = 15), \quad (33)$$

$$\text{EM}(x = 0) = 2.2 \text{EM}_i. \quad (34)$$

<sup>2</sup> We define the emission measure of a final state at a particular  $x$  by  $\text{EM}(x) = \int \rho_f^2(x, y) dy$ , and we normalize it to that of the initial state,  $\text{EM}_i = \int \rho_i^2(y) dy$ . The subscripts  $f$  and  $i$  denote final and initial states, respectively.

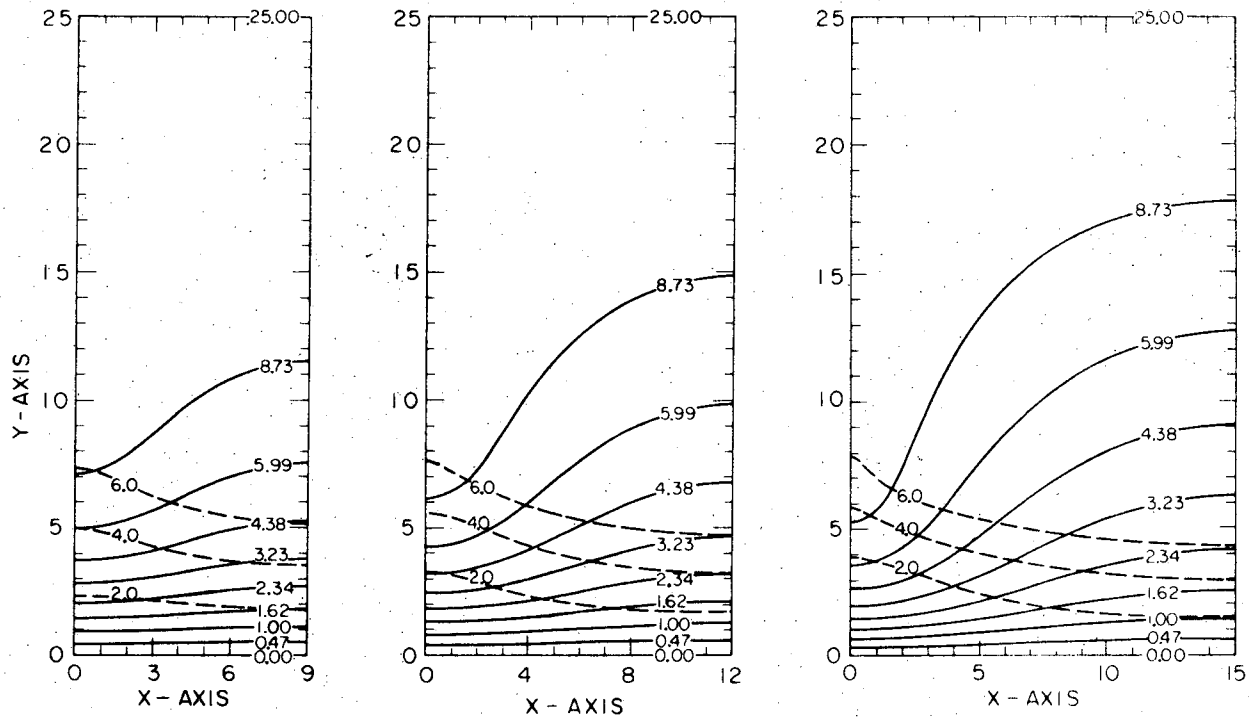


FIG. 2a (left), 2b (center), and 2c (right).—Final equilibrium states of the interstellar gas-field system in a galactic gravitational field  $\mathbf{g} = -e_y g(y)$ , where  $g(y) = -g(-y)$  is a positive constant. Distance is measured in units of  $C^2/g$ , where  $C$  is the isothermal speed of sound in the gas. The dimensions of each graph are equal to half a wavelength in the  $x$ - and half a wavelength in the  $y$ -direction. Half the critical wavelength in the  $x$ -direction is equal to 7.26. Field lines (solid curves) are chosen so that the magnetic flux between any two consecutive ones is constant. The isodensity contours (dashed curves) represent the points at which the density decreases to  $e^{-1}$ ,  $e^{-2}$ , and  $e^{-3}$  its value on the  $x$ -axis. The number on each curve is the  $y$ -coordinate of that curve in the initial state, in which  $\alpha = 1$ .

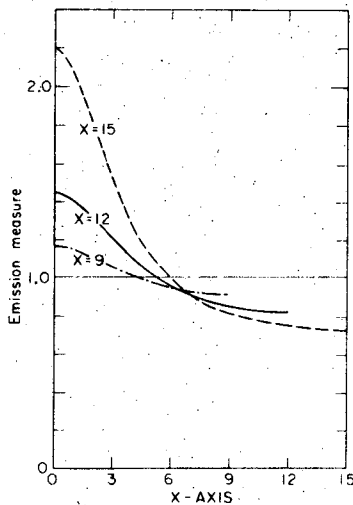


FIG. 3.—The emission measure (normalized to its value in the stratified initial state) as a function of  $x$  in the three final states of figure 2. The unit of length is  $C^2/g$ . The number ( $X$ ) labeling each curve is equal to half of the horizontal wavelength of the corresponding final state. The curves  $X = 9$  and  $X = 12$  could also represent the normalized column density in the corresponding final states to within a few percent. Similarly, the curve  $X = 15$  could represent the corresponding column density to within 18%.

In this final state the column density of the gas as a function of  $x$ ,  $N_H(x)$ , differs from  $EM(x)$  by at most 18 percent; in the other two final states presented,  $EM(x)$  and  $N_H(x)$  differ by only a few percent.

A striking feature of the final states is the fact that, compared with the initial scale height, the scale height of the gas increases at the position of the magnetic field "valleys" and decreases at the "wings" of the condensations, where the field lines have expanded. At the midplane of the condensations, moreover, while the gas density increases with increasing  $\lambda_x$ , the scale height of the gas increases as well (compare the lowest isodensity contours of figs. 2a, 2b, and 2c). This implies that the gas density increases not so much because of compression in the vertical direction, but because of a very efficient drainage of the gas from the inflated field lines. The additional fact that in the "wings" the gas density and the scale height decrease as  $\lambda_x$  increases precludes the explanation that gas observed at high altitudes in the Galaxy is gas that has been lifted by the expanded field lines. In fact, if the magnetogravitational instability is to be invoked to explain the high-altitude gas, one should concentrate on the identification of that gas with the rise of the isodensity contours at the position of magnetic field "valleys" (see fig. 2).

The ratio of the magnetic to gas pressures, an

TABLE 1  
ALPHA AND THE GAS DENSITY IN THREE FINAL STATES\* AT SOME POINTS

(x, y)	$\alpha(x, y)$			$\rho(x, y)$		
	a	b	c	a	b	c
(0, 0).....	1.2	1.4	2.0	1.0	1.0	1.0
(0, 22).....	0.1	0.05	0.03	$8.8 \times 10^{-5}$	$2.1 \times 10^{-4}$	$4.2 \times 10^{-4}$
(X, 0)†.....	0.9	0.7	0.6	1.0	1.0	1.0
(X, 22).....	$1.6 \times 10^2$	$7.1 \times 10^3$	$9.0 \times 10^4$	$1.8 \times 10^{-6}$	$1.8 \times 10^{-7}$	$4.1 \times 10^{-8}$

\* The columns headed a, b, and c refer to the final states of figures 2a, 2b, and 2c.

† Recall that X ( $\equiv \lambda_x/2$ ) is different in each state; it increases as we go from state a to state c.

interesting quantity in itself, constitutes another indicator of the efficiency with which gas drains down the inflated field lines, and of the dependence of this efficiency on  $\lambda_x$ . Table 1 exhibits the values of  $\alpha(x, y)$  (see eq. [13]) in the final states of figures 2a, 2b, and 2c (henceforth referred to as states a, b, and c) at some key points (x, y). The gas density is also shown at the same points; it is normalized to its initial value on the x-axis. In addition to the information supplied in table 1, we remark that both the gas density and the magnetic field are monotonically decreasing functions of y at a fixed x. At the two values of y used in table 1, the normalized density in the initial state is  $\rho_i(0) = 1.0$  and  $\rho_i(22) = 1.8 \times 10^{-5}$ . The final density along the x-axis is always uniform (and equal to unity to within a few percent) because of the requirement that there be reflection symmetry about the x-axis (see eq. [18]). No pressure gradients can be sustained along the x-axis, because the x-component of the gravitational field is assumed to vanish, and because magnetic forces do not act along field lines.

The fact that at  $x = 0$  alpha decreases monotonically as y increases, and the fact that at  $x = X$  alpha increases monotonically with y, are different expressions of the same conclusion stated above, namely: *the increase of the gas density in the magnetic field "valleys" is due primarily to efficient drainage along field lines, rather than to compression perpendicular to the galactic plane.* This drainage is more efficient the larger  $\lambda_x$  is. In addition, the computed low densities at  $x = X$  and large y's, in conjunction with the large values of  $\alpha$  in the same region, indicate that the magnetic field is nearly a vacuum field at the raised portions of the upper field lines.

The absolute "horizontal width" of the condensation (denoted by D and defined as the distance from the center of the condensation to the point x, at which the normalized emission measure becomes equal to unity) shows an increase with increasing  $\lambda_x$  (see fig. 3). However, the ratio  $D/\lambda_x$  decreases as  $\lambda_x$  increases; it is equal to 0.47 in state a and drops to 0.38 in state c. We should bear in mind that the above definition of D uses as a reference the stratified initial state, which, as emphasized in § IIb, is needed only to provide a mass-to-flux ratio in each flux tube of the system. In external galaxies seen face-on, one can observe the contrast between regions of high and low gas density. Thus, the relevant quantity is the ratio  $EM(x=0)/EM(x=X)$

for each of the states of figure 3. This contrast becomes more pronounced as  $\lambda_x$  increases.

### b) Energy Changes

In making a transition from an initial to a corresponding final state, the system alters its magnetic and gravitational energies. In addition, while remaining isothermal, the gas does work (positive or negative) against pressure forces, thus releasing or absorbing heat (see eq. [29]). The net reduction of each of the three forms of energy is shown in table 2 in the case of the final states a, b, and c. In each state all numbers are normalized to the internal energy U of the gas which is given by

$$U = \int \frac{3}{2} PdV. \quad (35)$$

The quantity U is constant because of the isothermal equation of state and because of conservation of total mass.

Starting with the heat term, we note that more heat is given off as  $\lambda_x$  increases. Since heat is released by compressed gas and absorbed by expanded gas, the amount of heat released may be taken as a rough measure of the net compression suffered by the gas. Thus, the entries in the second column of table 2 confirm that the larger  $\lambda_x$  is, the more efficiently the gas is compressed.

In spite of the large expansion suffered by field lines in the "wings" of each condensation, the reduction in magnetic energy is small compared with that of the other energy terms. The relatively weak compression of the magnetic field [that takes place primarily along

TABLE 2  
ENERGY REDUCTION FOR THREE FINAL STATES

FINAL STATE	ENERGY RELEASED*		
	Heat ( $\times 10^2$ )	Magnetic ( $\times 10^2$ )	Gravitational ( $\times 10^2$ )
a.....	2.32	0.00	2.37
b.....	5.73	0.90	5.50
c.....	11.8	2.67	12.9

\* In each state, the energy released has been normalized to the internal energy of the gas,  $(3/2) \int PdV$ .



the midplane ( $x = 0, y > 0$ ) almost cancels the effect of the large expansion in the "wings." This is not surprising, since the field lines that suffer the greatest expansion are those at intermediate and high altitudes, where the magnetic energy content is small in the first place. The increase in the amount of magnetic energy released at larger  $\lambda_x$  may be due to the availability of a larger volume, in which field lines can expand.

The gravitational energy behaves as anticipated in § IVc. It is interesting to note that the heat released keeps pace with the decrease in gravitational energy, since both quantities reflect the accumulation of gas in magnetic field "valleys."

### c) Which Is The Final State?

Over horizontal distances that are larger than twice the critical wavelength  $\Lambda_x$ , given by equation (31), the possibility of two "final" states (one having a wavelength equal to twice that of the other) arises. Merely on energy considerations, the state with the longer wavelength is a more likely final state, since it is lower in total energy. We chose  $Y = 25$  and  $X = 18$ , and we applied a perturbation to the stratified initial state that had a wavelength  $\lambda_x = X$  (rather than the usual  $\lambda_x = 2X$ ).<sup>3</sup> Furthermore, we imposed no condition whatsoever at  $x = X/2$ . The final state obtained in this manner exhibited the characteristic double "hump," as expected. Its field lines differed from those of figure 2a by less than three parts in 1000 at all points. When perturbations were applied to this state, the iterative scheme converged back to it. Only when the amplitude of the "perturbation" was so large that it erased the double "hump" did the iterative scheme pick out the state that has twice as large a horizontal wavelength. This leads us to believe that both states represent local potential wells and that it takes a finite amount of energy to push the system out of the state with the shorter wavelength and down the potential hill into the lower energy state, characterized by the longer wavelength. If perturbations that can provide the necessary energy are available, the interstellar gas condensations discussed so far may tend to coalesce into larger (and denser) condensations, separated by a larger mean distance.

Suppose, now, that a disturbance in the initial state consists of a superposition of many wavelengths. Under these conditions, which final state will be reached? A perturbation with initial growth rate  $n$  grows in time as  $\exp(nt)$ . Because of the exponential dependence on  $n$ , the amplitudes of two perturbations, which differ in their growth rates by a small amount, will be very different after some time has elapsed. So, given a spectrum of wavelengths for the initial perturbation, that final state is more likely to be reached that has a wavelength corresponding to the maximum growth rate. In all cases presented, we have fixed  $Y = 25$ . Since we also took  $\alpha = 1$ , this implies that

<sup>3</sup> Whenever numbers are given, the unit of length is  $C^2/g$ , where  $C$  is the isothermal speed of sound in the gas and  $g$  is the magnitude of the vertical gravitational field of the Galaxy (assumed to be a constant; see § III).

the maximum growth rate occurs at approximately  $X = 12.4$ . The solution of figure 2b is close to this final state.

In summary, then, the factors deciding which final state will be reached are as follows. (i) If the initial perturbation is monochromatic, its wavelength alone determines the final state. (ii) If a spectrum of wavelengths is initially available, that final state will be reached which corresponds to the wavelength of maximum relative growth rate. (iii) If disturbances continue to be present during the transition of the system, the amplitudes of these disturbances may also play a role in determining the final state. A definitive statement must await exact calculations.

### d) Dependence on $\lambda_y$

Unlike the horizontal wavelength, the vertical wavelength does not affect a solution very much, provided only that  $\lambda_y \gg H$ . For a fixed (unstable)  $\lambda_x$  we found that, by changing  $\lambda_y$  by almost a factor of 2, a typical solution changed by much less than 1 percent at small  $y$ 's, and by a few percent at intermediate  $y$ 's. One could anticipate this insensitive dependence of a solution on  $\lambda_y$ , since more than 90 percent of the energy (per unit length along  $x$ ) of the initial state resides under the altitude  $y \simeq 7$ , and more than 50 percent of the energy is under  $y \simeq 2.5$ . We further observed that the shape of the field lines at very large  $y$ 's depends on  $\lambda_y$ , if  $\lambda_y \sim \lambda_x (\gg H)$ .<sup>4</sup> In the case that  $\lambda_y \gg \lambda_x \sim H$ , this effect becomes negligible altogether.

## VII. CONCLUDING REMARKS AND COMPARISON WITH OBSERVATIONS

We have determined final equilibrium states for a model of the interstellar gas and field in the galactic gravitational field. Our solutions represent *large-scale* isothermal condensations of the interstellar gas in magnetic-field "valleys." They should *not* be identified with "standard clouds," which could be produced by the magnetogravitational instability only if  $\alpha \gg 1$  (corresponding to a cold gas and a critical wavelength of the instability which is only a fraction of the scale height). We find that the boundaries of the large-scale isothermal condensations are fairly diffuse. This is to be expected, since we have not allowed any "phase transitions" to occur in the manner described by Field, Goldsmith, and Habing (1969). The thermal instability (Field 1965), which we have not considered here, could produce only *small-scale* (less than 1 pc) structure within the large-scale condensations, which the magnetogravitational instability initiates.

A distinctive feature of the final states is that condensation occurs not so much because of compression in the direction of  $g$ , as because of drainage of the gas along field lines, especially at intermediate and high altitudes. As a consequence, at the midplane of the condensation, the scale height of the gas in a final

<sup>4</sup> Although this is insignificant for the problem at hand because of the energy argument just cited, the shape of field lines at high altitudes may be important in the context of cosmic-ray propagation.

state is larger (by a factor of  $\sim 2$ ) than the scale-height in the corresponding stratified initial state; at the "wings" of the condensation the opposite is true. Thus, the observed gas at high galactic altitudes cannot be interpreted as gas lifted by expanding field lines. If at all, it should be identified with the rise of the isodensity contours in magnetic field "valleys." As a corollary, it is unlikely that any substantial *material* galactic halo can form by inflated field lines. A *radio* halo could indeed form, however, by cosmic rays and expanding field lines in the manner described by Parker (1968b).

To compare with observations one needs to know the characteristic wavelength of a typical final state. A lower limit to this wavelength is, of course, the critical wavelength for the instability,  $\Lambda_x$  (see eq. [31]). Care should be taken, however, not to identify  $H$ , in the expression for  $\Lambda_x$ , with the observed scale height of the gas *today*. The observed scale height is representative of the final state, rather than the initial one, since the growth-time of the instability is only  $10^7$  years. Realizing that  $\alpha$  is a point function and that it cannot therefore be obtained by averaging either  $B$  or  $\rho$  over large distances, in order to make a semi-quantitative comparison with observations we assume that  $\alpha \sim 1$ . Then, since the observed scale height is of the order of  $10^2$  pc, we expect gas condensations produced by Parker's instability to be separated by at least a few (3 or 4) hundred parsecs. Unless  $\alpha$  is unexpectedly large, gas condensations separated by smaller distances than this cannot be attributed to this instability. Because Parker's instability is associated with very long wavelengths, final condensations involving up to  $10^6 M_\odot$  could be produced. (Note that a gas element travels only a fraction of the horizontal wavelength in going from an initial to a final state.) Also, because of the large scales that could be involved (up to a few kiloparsecs), *we view this instability as providing the stage on which small-scale processes in the interstellar medium* (e.g., dark cloud formation and cloud collapse, star formation and supernova explosions etc.) *act out their individual roles.*

Both the nicely displayed, recent 21-cm observations by Heiles and Jenkins (1973), as well as the compilation of 21-cm observations by Fejes and Wesselius (1973), when combined with the starlight polarization measurements by Mathewson and Ford (1970), reveal an intimate association between the interstellar gas and the interstellar magnetic field. In fact, enormous gas condensations coincide with magnetic-field "valleys." At the position of the field "valleys" the gas extends high above the plane and it does so in directions parallel to the magnetic field. The most prominent condensation is centered at about  $l = 40^\circ$ ; it is a few tens of degrees wide and extends above (and below) the plane by at least as much as  $60^\circ$ . Field lines emanating from this condensation form arches above the Sun's location and return to the plane in the general direction  $l = 250^\circ$ , where another condensation is located. The "edge" of the condensation at  $l = 40^\circ$  may be as close as 100 pc, and that at  $l = 250^\circ$  as close as 200 pc. However, the starlight-polarization maps of Mathewson and Ford show that most of the contribu-

tion to polarization comes from the distance range 200–400 pc in each of these directions. Moreover, contribution to polarization is also made by gas extending out to about 600 pc in each direction. Therefore, the separation between the "centers" of the two condensations may be as large as 600 pc. Not only is this separation within the range of unstable wavelengths for the magnetogravitational instability, but it may also be close to the wavelength corresponding to the maximum growth rate.

Below the galactic plane, two prominent condensations that are centered at  $l \simeq 40^\circ$  and  $l \simeq 190^\circ$ , respectively, are similar in size and in separation to the ones just discussed. They are located in magnetic field "valleys" and they are joined by field lines that arch high below the plane. They too may constitute evidence that the magnetogravitational instability has occurred in the solar neighborhood.

If the Jeans instability were responsible for the formation of these condensations, then (i) they would be more centrally condensed, and (ii) the long dimension of each condensation would certainly *not* be along the magnetic field. When self-gravitation becomes important, three-dimensional calculations (that incorporate the assumption of flux-freezing rigorously) show that the equilibrium states exhibit flattening *along* the magnetic field (Mouschovias 1974).

The observed symmetry of high- and low-density regions about the galactic plane is understood in the context of the magnetogravitational instability. Whatever the mechanism that triggers the instability (spiral density shock waves?), it certainly must act coherently over a region larger than the critical wavelength for the onset of the instability (several hundred parsecs). Since the interstellar gas forms a thin disk having thickness of a few hundred parsecs *today*, the perturbation that triggers the instability can influence the gas above and below the galactic plane in a similar manner. Therefore, if the initial distribution of the gas was symmetric about the plane, the final state is expected to retain this symmetry. Smaller-scale deviations from this symmetry may be attributed to local phenomena (e.g., depletion of gas by star formation, ionization by nearby stars, sweeping of gas by supernova shocks, etc.).

Observations of the motion of the interstellar gas in the solar neighborhood show a flow pattern in which gas falls down toward the galactic plane and flows out in the general direction of the galactic center *and* that of the anticenter (Erickson, Helfer, and Tatel 1959; Helfer 1959; Weaver 1973). The velocities observed are a few kilometers per second. This particular flow pattern is consistent with a picture in which gas is still sliding down the expanding field lines joining the two condensations referred to above, which are located at  $l \simeq 40^\circ$  and  $l \simeq 250^\circ$ .

Observations of external galaxies provide further evidence for the magnetogravitational instability. This (and some consequences of the assumption that the instability is triggered by a spiral density shock wave) will be discussed in another publication (Mouschovias, Shu, and Woodward 1974).

It is with much appreciation that I recall the problematizing discussions which I have shared with Professor George B. Field. I am also thankful to Dr. Paul Concus for his advice on numerical matters in general, and for his help in estimating the asymptotic convergence-rate of the iterative scheme, in particular. Professor Frank H. Shu's criticism is much appre-

ciated. Without the generosity of the Theoretical Physics Group of the Lawrence Berkeley Laboratory who provided me with time on the excellent LBL computing facilities, this project would not have been completed. I am also indebted to the Mathematics and Computing Group of LBL for their support.

## APPENDIX A

GENERALIZATION OF THE FUNCTION  $q$  TO EQUATIONS OF STATE  $P = P(\rho)$ 

Even if the isothermal equation of state is replaced by a general equation of state

$$P = P(\rho), \quad (\text{A1})$$

a connection between initial and final states may still be made. For this purpose we define  $q(x, y)$  by

$$q = \exp \left( \int \frac{dP}{\rho} + \psi \right). \quad (\text{A2})$$

Following the same procedure that we did in § II, we can still show that

$$q = q(A) \quad (\text{A3})$$

and that equations (10) and (12) now become, respectively,

$$\nabla^2 A = -4\pi\rho \frac{d \ln q(A)}{dA} \quad (\text{A4})$$

and

$$q(A) = \frac{1}{2} \frac{dm}{dA} \int_0^x dx \frac{\partial y(x, A)}{\partial A} \left[ \frac{dq}{dP} - q(A) \frac{d\psi}{dP} \right]^{-1}. \quad (\text{A5})$$

In equation (A4)  $\rho$  is eliminated by using equation (A2), i.e.,

$$\rho = q(A) \left[ \frac{dq}{dP} - q(A) \frac{d\psi}{dP} \right]^{-1}. \quad (\text{A6})$$

In practice, the derivatives appearing in the right-hand sides of equations (A5) and (A6) are calculated in a straightforward fashion by using the chain rule. We obtain

$$\begin{aligned} \frac{dq}{dP} &= \frac{dq}{dA} \frac{dA}{dP} \\ &= \frac{dq}{dA} \left( \frac{\partial A}{\partial x} \frac{\partial x}{\partial \rho} + \frac{\partial A}{\partial y} \frac{\partial y}{\partial \rho} \right) \left( \frac{dP}{d\rho} \right)^{-1} \end{aligned} \quad (\text{A7})$$

and

$$\frac{d\psi}{dP} = \left( \frac{\partial \psi}{\partial x} \frac{\partial x}{\partial \rho} + \frac{\partial \psi}{\partial y} \frac{\partial y}{\partial \rho} \right) \left( \frac{dP}{d\rho} \right)^{-1}. \quad (\text{A8})$$

The price that we have paid, in order to replace the isothermal equation of state with the general equation of state (A1), is that the iterative procedure over the single function  $A$  must now be replaced by an iterative procedure over all three functions  $A$ ,  $q$ , and  $\rho$ . The solution of this general problem is feasible.

## APPENDIX B

## AN "ENERGY INTEGRAL" FOR AN ISOTHERMAL PLASMA

Bernstein *et al.* (1958) state that the equations of magnetohydrodynamics

$$\frac{dv}{dt} = -\nabla P - \rho \nabla \psi + \frac{j}{c} \times B \quad (\text{B1})$$

$$\frac{\partial \rho}{\partial t} + \nabla \cdot (\rho v) = 0, \quad (\text{B2})$$

$$E + (v/c) \times B = 0, \quad (\text{B3})$$

$$\frac{d}{dt} (P\rho^{-\gamma}) = 0, \quad (\text{B4})$$

$$\nabla \times E = -\frac{1}{c} \frac{\partial B}{\partial t}, \quad (\text{B5})$$

$$\nabla \times B = (4\pi/c)j, \quad (\text{B6})$$

$$\nabla \cdot B = 0, \quad (\text{B7})$$

possess the energy integral

$$\int dV \left( \frac{1}{2} \rho v^2 + \frac{B^2}{8\pi} + \rho \psi + \frac{P}{\gamma - 1} \right) = \text{a constant}, \quad (\text{B8})$$

where the integration is extended over all space. The operators  $\partial/\partial t$  and  $d/dt$  denote Eulerian and comoving time-derivatives, respectively.

Here we show that, even in the case that the plasma is isothermal (i.e.,  $\gamma = 1$ ), an "energy integral" still exists; it is identical with that of equation (B8), except for the fact that the term  $P/(\gamma - 1)$  is replaced by  $P \ln P$ . We proceed in the usual manner to take the dot product of both sides of equation (B1) with  $v$ ; then, by using equations (B2)–(B7), we write each term as follows:

$$v \cdot \frac{j}{c} \times B = -\nabla \cdot \left( \frac{c}{4\pi} E \times B \right) - \frac{\partial}{\partial t} \left( \frac{B^2}{8\pi} \right), \quad (\text{B9})$$

$$-\rho v \cdot \nabla \psi = -\nabla \cdot (\rho \psi v) - \frac{\partial}{\partial t} (\rho \psi). \quad (\text{B10})$$

Also,

$$-v \cdot \nabla P = -\nabla \cdot (Pv) + P \nabla \cdot v. \quad (\text{B11})$$

But, by judiciously adding and subtracting the quantity  $P \ln P \nabla \cdot v$ , we can show that the last term in equation (B11) may be written as

$$P \nabla \cdot v = - \left[ \frac{\partial}{\partial t} (P \ln P) + \nabla \cdot (P \ln P v) \right]. \quad (\text{B12})$$

Collecting all terms, we obtain

$$\begin{aligned} & \frac{\partial}{\partial t} \left( \frac{1}{2} \rho v^2 + \frac{B^2}{8\pi} + \rho \psi + P \ln P \right) \\ & + \nabla \cdot \left[ \frac{1}{2} \rho v^2 v + \frac{c}{4\pi} E \times B + \rho \psi v + P \ln (P/e) v \right] = 0. \end{aligned} \quad (\text{B13})$$

In equation (B13),  $e$  is the natural-logarithm base. If the plasma extends over all space, being periodic in  $x$  (with a wavelength  $\lambda_x$ ) and symmetric about the  $x$ -axis, we may integrate equation (B13) over one period of the system in  $x$ , and over the upper half-plane in  $y$ .<sup>5</sup> The

<sup>5</sup> As in the main text, the geometry is taken to be two-dimensional, although this is not necessary for this argument.

divergence term yields a surface integral with all the terms vanishing, if there is no mass transfer from one period to the next, or across the  $x$ -axis, and if either the magnetic field or the velocity vanishes at  $y = \infty$ . Formally these conditions are

$$\hat{n} \cdot v = 0 \quad \text{at} \quad \begin{cases} (x, y = 0) \\ (x = \pm X, y) \end{cases} \quad (\text{B14})$$

and either

$$B(x, y = \infty) = 0, \quad \text{or} \quad v(x, y = \infty) = 0. \quad (\text{B15})$$

The unit normal to the "surface" of a period is denoted by  $\hat{n}$ , and  $X$  is equal to  $\lambda_x/2$ . Thus, the result of the integration is

$$\int dV \left( \frac{1}{2} \rho v^2 + \frac{B^2}{8\pi} + \rho \psi + P \ln P \right) = \text{a constant}. \quad (\text{B16})$$

The first term in this integral is the kinetic energy of the fluid. The sum of the other three terms acts as an effective potential energy of the isothermal plasma. This point and the meaning of  $P \ln P$  are discussed in the main text (see § IV). Here we only remark that  $P \ln P$  is not the internal energy density of the fluid; the latter is always equal to  $3P/2$ .

## APPENDIX C

### METHOD OF SOLUTION

#### I. THE DIMENSIONLESS PROBLEM

We measure the magnetic vector potential and the gas density in units of their initial values on the  $x$ -axis, i.e.,  $-2HB_i(0)$  and  $\rho_i(0)$ , respectively. The unit of length is taken as  $C^2/g$ , and the unit of time is fixed by choosing the unit of velocity as  $C$ , the isothermal speed of sound in the gas. With the gravitational field chosen as in § III, we may write the dimensionless form of equation (10) as

$$\nabla^2 A(x, y) = Q(y, A; \alpha), \quad (\text{C1})$$

where

$$Q(y, A; \alpha) = -\frac{1}{8\alpha(1+\alpha)^2} \frac{dq(A)}{dA} \exp(-y). \quad (\text{C2})$$

The parameter  $\alpha$  is characteristic of the initial state (see eq. [13]). Similarly, equation (12) becomes

$$q(A) = \frac{1}{2} \frac{dm}{dA} \int_0^x dx \frac{\partial y(x, A)}{\partial A} \exp[-y(x, A)], \quad (\text{C3})$$

where

$$\frac{dm}{dA} = -4X(1+\alpha)A, \quad (\text{C4})$$

and  $X$  is defined by  $X \equiv \lambda_x/2$ . The dimensionless form of the boundary conditions is

$$A(x, y = 0) = 1, \quad (\text{C5})$$

$$\left. \frac{\partial A(x, y)}{\partial x} \right|_{x=0, \pm X} = 0, \quad (\text{C6})$$

and

$$\begin{aligned} A(x, y) &= 0, \quad y = +\infty; \\ &= 2, \quad y = -\infty. \end{aligned} \quad (\text{C7})$$

The approximate boundary condition that replaces equation (C7) is

$$A(x, Y) = A_i(Y), \quad (\text{C8})$$

with  $A_i(y)$  given by

$$A_i(y) = \exp[-y/(2\alpha + 2)]. \quad (\text{C9})$$

#### II. OUTLINE OF THE NUMERICAL SCHEME

In equation (C1)  $\nabla^2$  is a linear differential operator and  $Q$  is a nonlinear algebraic operator. We solved equation (C1) numerically by an underrelaxation iterative procedure. The premise was that, if we can

calculate  $Q$  as a function of  $x$  and  $y$  (rather than  $A$  and  $y$ ), we could easily solve the resulting Poisson equation by any one of the many available fast techniques (see Dorr 1970). We know  $Q$  as a function of  $x$  and  $y$ , however, only if a solution  $A(x, y)$  is at hand; hence the necessity of an iterative scheme.

Starting from an initial guess  $A^{(0)}(x, y)$ , we define a sequence of iterates by the recursion relations

$$\nabla^2 A_*^{(n+1)} = Q(y, A^{(n)}; \alpha), \quad n = 0, 1, 2, \dots, \quad (C10)$$

$$A^{(n+1)} = \theta^{(n)} A^{(n)} + (1 - \theta^{(n)}) A_*^{(n+1)},$$

$$0 \leq \theta^{(n)} < 1. \quad (C11)$$

The quantity  $A_*^{(n+1)}$  is a provisional iterate and  $\theta^{(n)}$  is the relaxation parameter at the  $n$ th iteration. We say that a solution is reached if the following condition is satisfied at all points  $(x, y)$ :

$$\frac{|A_*^{(n+1)} - A^{(n)}|}{A_*^{(n+1)}} < \epsilon. \quad (C12)$$

In equation (C12), absolute values are denoted by the vertical bars. (Recall that the dimensionless  $A$  is always positive.) The quantity  $\epsilon$  is a small positive number and can be chosen at will to achieve desired levels of accuracy.

We chose some field lines of the initial state (the number varied from 65 to 129), we introduced perturbations most often having the form

$$\delta A(x, y) = -A_i(y)\mu \sin(\pi y/Y) \cos(\pi x/X), \quad (C13)$$

where  $\mu$  is a fixed positive number less than unity, and we followed these field lines from iteration to iteration until they settled down. Although we found solutions (to within 1 or 2%) in a number of iterations varying from 6 to 22, we forced the program to continue for as many as 97 iterations in order to make a detailed error analysis. Thus, we computed the asymptotic convergence rate and demonstrated that, at any one interior point, our solutions are accurate to within 0.5 percent.

In more detail, the steps involved in the iterative scheme are the following.

i) Define a uniform mesh over the region of interest having  $J$  points in the  $y$ -direction and  $K$  points in the  $x$ -direction:

$$y_j = (j - 1)\Delta y, \quad j = 1, 2, \dots, J; \quad (C14)$$

$$x_k = (k - 1)\Delta x, \quad k = 1, 2, \dots, K; \quad (C15)$$

where  $\Delta y = Y/(J - 1)$  and  $\Delta x = X/(K - 1)$ . [Note that, a mesh having been defined, all functions of one (two) variables become one- (two-) dimensional arrays.]

ii) Choose a set of field lines of the initial state which we shall follow. Let this set be  $\{A_i\}$ ,  $i = 1, 2, \dots, I$ .

iii) Guess an  $A^{(0)}(x, y)$ .

iv) For each  $x$ , interpolate to find  $y(A_i, x)$ ,  $i = 1, 2, \dots, I$ . That is, obtain  $y$  as a function of  $x$  along each field line chosen in step (ii).

v) For each  $x$ , differentiate  $y(A_i, x)$  with respect to  $A$  to obtain  $\partial y/\partial A$ .

vi) Perform the integration in equation (C3) for each  $A_i$ .

vii) Obtain  $q(A_i)$  from equation (C3), since  $dm(A_i)/dA$  is always given by equation (C4).

viii) Perform the differentiation with respect to  $A$  to find  $h(A_i) \equiv dq(A_i)/dA$ .

ix) Since  $h(A_i)$  is known along the field lines, whose position was determined in step (iv), interpolate to obtain  $h$  at the mesh points. This interpolation is done, for each  $x$ , by using  $y(A_i, x)$  as old abscissae and  $y_j$  as new abscissae; the subscripts  $i$  and  $j$  span their respective ranges.

x) With the right-hand side known as a function of  $x$  and  $y$ , the Poisson equation (C1) is solved to find  $A^{(1)}(x, y)$ .

xi) If  $A^{(1)}$  and  $A^{(0)}$  satisfy the criterion given by equation (C12), then  $A^{(1)}$  is a solution. If they do not, underrelax  $A$  as in equation (C11) and go back to step (iv) to repeat the process.

Numerical integrations, differentiations, and interpolations are performed so many times in the program that, although the routines performing each operation are very accurate, their combined effect in the calculation of the right-hand side of equation (C1) cannot be predicted. To study this effect we searched for a function  $\bar{A}(x, y)$ , which would (i) correspond to field lines having the desired wavy shape; (ii) satisfy the appropriate boundary conditions; and (iii) allow us to calculate the right-hand side of equation (C1) analytically! If such an  $\bar{A}(x, y)$  is known, then the calculated  $Q(y, \bar{A}; \alpha)$  can be compared with the  $Q$  computed by the program and the net numerical errors be determined. Such an  $\bar{A}$  is obtained by solving the quadratic

$$\exp[-y/(2\alpha + 2)] = (1 - \bar{A})(\bar{A} - A_0)w(x) + \bar{A}, \quad (C16)$$

where

$$w(x) = \kappa \cos(\pi x/X), \quad |\kappa| < 1, \quad (C17)$$

and  $A_0$  is the value of  $A$  in the initial state at  $y = Y$ .

It is remarkable that we found that the maximum error in the computation of  $dq(\bar{A})/dA$  occurs at the upper boundary (where all physical quantities are very

TABLE 3  
MAXIMUM COMPUTATIONAL ERRORS

Function	Maximum Error (%)	Location
$y(\bar{A}, x)$ .....	0.320	$i = 2, k = 2$
$\partial y(\bar{A}, x)/\partial A$ .....	0.060	$i = 65, k = 15$
$f(\bar{A})^*$ .....	0.098	$i = 1$
$q(\bar{A})$ .....	0.445	$i = 65$
$dq(\bar{A})/dA$ .....	0.770	$i = 64$
$dq[\bar{A}(x, y)]/dA$ .....	0.91	$j = 64, k = 45$

\* The function  $f(\bar{A})$  is defined as the integral in the denominator of equation (C3).

small compared with their values on the  $x$ -axis) and is equal to 0.91 percent. Table 3 exhibits the maximum errors in the computation of the various quantities and the points at which these errors occur. The mesh was uniform in each direction; the number of mesh points in the  $y$ -direction was 65, and that in the  $x$ -direction was 63. This is the smallest number of mesh points used to obtain any one of our solutions. Thus, the

errors given in table 3 are the largest that we may expect. The indices  $j$  and  $k$  denote mesh points in the  $y$ - and  $x$ -directions, respectively (see eqs. [C14] and [C15]). The index  $i$  denotes field lines, the lowest field line having  $i = 1$  and the one at  $y = Y$  having  $i = 65$ . Note that the maximum errors occur at the boundaries. In fact, the errors at interior points are much less than those given in table 3.

## REFERENCES

- Bernstein, I. B., Frieman, E. A., Kruskal, M. D., and Kulsrud, R. M. 1958, *Proc. Roy. Soc. (London)*, **A244**, 17.  
 Dorr, F. W. 1970, *SIAM Review*, **12**, No. 2, 248.  
 Dungey, F. W. 1953, *M.N.R.A.S.*, **113**, 180.  
 Erickson, W. C., Helfer, H. L., and Tatel, H. E. 1959, *Proceedings IAU Symposium 9*, ed. R. N. Bracewell (Stanford: Stanford University Press), p. 390.  
 Fejes, I., and Wesselius, P. R. 1973, *Astr. and Ap.*, **24**, No. 1, 1.  
 Field, G. B. 1965, *Ap. J.*, **142**, 531.  
 Field, G. B., Goldsmith, D., and Habing, H. J. 1969, *Ap. J. (Letters)*, **155**, L149.  
 Heiles, C., and Jenkins, E. 1973, papers presented at 139th and 140th meeting of the AAS, and IAU Sympo. No. 60.  
 Helfer, H. L. 1959, *A.J.*, **64**, 128.  
 Lerche, I. 1967a, *Ap. J.*, **149**, 395.  
 ———. 1967b, *ibid.*, p. 553.  
 Mathewson, D. S., and Ford, V. L. 1970, *Mem. R.A.S.*, **74**, 143.  
 Mouschovias, T. Ch. 1974, in preparation.  
 Mouschovias, T. Ch., Shu, F. H., and Woodward, P. R. 1974, submitted to *Astr. and Ap.*  
 Parker, E. N. 1966, *Ap. J.*, **145**, 811.  
 ———. 1968a, *ibid.*, **154**, 57.  
 ———. 1968b, in *Stars and Stellar Systems*, Vol. 7, *Nebulae and Interstellar Matter*, ed. B. Middlehurst and L. H. Aller (Chicago: University of Chicago Press), pp. 707-754.  
 Schmidt, M. 1965, in *Stars and Stellar Systems*, Vol. 5, *Galactic Structure*, ed. A. Blaauw and M. Schmidt (Chicago: University of Chicago Press), pp. 513-530.  
 Spitzer, L., Jr. 1968, *Diffuse Matter in Space* (New York: Interscience).  
 Weaver, H. 1973, paper presented at the IAU Joint Discussion No. 3, Sydney, Australia.

TELEMACHOS CH. MOUSCHOVIAS

Department of Physics, University of California, Berkeley, CA 94720

**LEGAL NOTICE**

*This report was prepared as an account of work sponsored by the United States Government. Neither the United States nor the United States Energy Research and Development Administration, nor any of their employees, nor any of their contractors, subcontractors, or their employees, makes any warranty, express or implied, or assumes any legal liability or responsibility for the accuracy, completeness or usefulness of any information, apparatus, product or process disclosed, or represents that its use would not infringe privately owned rights.*

TECHNICAL INFORMATION DIVISION  
LAWRENCE BERKELEY LABORATORY  
UNIVERSITY OF CALIFORNIA  
BERKELEY, CALIFORNIA 94720